1998

Hole burning with pressure and electric field: a window on the electronic structure and energy transfer dynamics of bacterial antenna complexes

Hsing-Mei Wu
Iowa State University

Hole burning with pressure and electric field: A window on the electronic structure and energy transfer dynamics of bacterial antenna complexes

by

Hsing-Mei Wu

A dissertation submitted to the graduate faculty

in partial fulfillment of the requirements for the degree of

DOCTOR OF PHILOSOPHY

Major: Physical Chemistry

Major Professor: Gerald J. Small

Iowa State University

Ames, Iowa

1998

Graduate College
Iowa State University

This is to certify that the Doctoral dissertation of

Hsing-Mei Wu

has met the dissertation requirements of Iowa State University

Signature was redacted for privacy.

Major Professor

Signature was redacted for privacy.

For the Major Program

Signature was redacted for privacy.

For the Graduate College

TABLE OF CONTENTS

ACKNOWLEDGMENTS vii

ABSTRACT viii

CHAPTER 1. INTRODUCTION TO LIGHT-HARVESTING COMPLEXES 1
1.1 General Introduction to Photosynthesis 1
1.1.1 Reaction centers 3
1.2 Light-Harvesting Complexes 5
1.2.1 Crystal structure of LH2 from *Rps. acidophila* (strain 10050) 7
1.2.2 A comparison of LH2 structures from *Rps. acidophila* and *Rs. molischianum* 16
1.2.3 Projection structure of LH1 complex from *Rhodospirillum rubrum* 17
1.2.4 Organization of photosynthetic complexes in the membrane of purple bacteria 18
1.3 Application of Hole Burning Spectroscopy to Light-Harvesting Complexes 19
1.3.1 Marriages of non-photochemical hole burning spectroscopies with high pressure and electric field 19
1.4 Thesis Organization 20
1.5 Other Published Work of the Candidate 21
1.6 References 22

CHAPTER 2. MECHANISMS FOR EXCITATION ENERGY TRANSFER AND RELAXATION 26
2.1 Introduction 26
2.1.1 Energy transfer in photosynthesis 27
2.2 Förster Energy Transfer 28
2.2.1 Conventional Förster theory 28
2.2.2 Implications and validity of assumptions made in conventional Förster energy transfer 31
2.2.3 Kolaczkowski-Hayes-Small (KHS) theory for weak coupling energy transfer 33
2.3 Energy Transfer via Electron Exchange Interactions 36
2.4 Molecular Excitons 38
2.4.1 Mott-Wannier and Frenkel excitons 38
2.4.2 An excitonically coupled dimer — A simple example 42
2.4.3 Extension from the dimer to molecular crystals and circular aggregates 47

2.4.4 Exciton-phonon coupling 48
2.4.5 Inter-exciton level relaxation processes — Beyond the Condon approximation 52
2.5 References 53

CHAPTER 3. FEMTOSECOND AND HOLE BURNING STUDIES OF B800'S EXCITATION ENERGY RELAXATION DYNAMICS IN THE LH2 ANTENNA COMPLEX OF *RHODOPSEUDOMONAS ACIDOPHILA* (STRAIN 10050) 57
Abstract 57
Introduction 58
Experimental 62
Femtosecond studies 62
Hole burning studies 64
Materials 65
Results 65
Femtosecond studies (ambient pressure) 65
Hole burning studies (ambient pressure) 69
High-pressure-hole burning of chromatophores 71
Discussion 72
Förster B800 → B850 energy transfer 73
Conclusions 84
Acknowledgments 86
References and Notes 86
Tables 89
Figure Captions 92
Figures 94

CHAPTER 4. COMPARISON OF THE LH2 ANTENNA COMPLEXES OF *RHODOPSEUDOMONAS ACIDOPHILA* (STRAIN 10050) AND *RHODOBACTER SPHAEROIDES* BY HIGH PRESSURE-ABSORPTION, -HOLE BURNING AND TEMPERATURE-DEPENDENT ABSORPTION SPECTROSCOPIES 105
Abstract 105
Introduction 106
Experimental 113
Results 114
Temperature dependence studies 116
Pressure dependence studies 118
Discussion 120
Temperature dependencies of the LH2 absorption spectrum 121
Pressure dependencies of the LH2 absorption spectrum 126
Exciton and vibrational structure in the absorption spectrum

of the LH2 complex 131
Concluding Remarks 134
Acknowledgments 137
References and Notes 138
Table 143
Figure Captions 144
Figures 147

CHAPTER 5. EXCITON LEVEL STRUCTURE AND ENERGY DISORDER OF THE B850 RING OF THE LH2 ANTENNA COMPLEX 157
Abstract 157
Introduction 158
Background on Electronic Structure of LH2 Complexes 161
Results and Discussion 164
Energy disorder and the B850 ring 165
Satellite hole structure associated with burning of the B850 band 174
Concluding Remarks 179
Acknowledgments 182
References and Notes 182
Table 185
Figure Captions 186
Figures 189

CHAPTER 6. SYMMETRY-BASED ANALYSIS OF THE EFFECTS OF RANDOM ENERGY DISORDER ON THE EXCITONIC LEVEL STRUCTURE OF CYCLIC ARRAYS: APPLICATION TO PHOTOSYNTHETIC ANTENNA COMPLEXES 198
Abstract 198
Introduction 199
Theoretical Background 201
Coupling selection rules 204
The participation number N 204
Results and Discussion 206
Localization or extendedness 209
C_8 and C_{16} ring systems 212
Diagonal vs off-diagonal random energy disorder 212
Energy disorder and the Stark effect 213
Concluding Remarks 215
Acknowledgments 218
References and Notes 219
Tables 222
Figure Captions 225

Figures 227

CHAPTER 7. STARK HOLE-BURNING STUDIES OF THREE PHOTOSYNTHETIC COMPLEXES 235
Abstract 235
Introduction 236
Experimental 240
Results and Analysis 241
BChl *a* antenna complex of *Cb. tepidum* 243
LH1 only mutant chromatophores 245
LH1 of wild-type chromatophores from *Rb. sphaeroides* 246
B800 band of *Rps. acidophila* and *Rs. molischianum* 246
Discussion 247
825 nm band of the FMO complex 247
LH1 and LH2 antenna complexes 253
Stark hole-burning and classical modulation spectroscopies 257
Acknowledgments 259
References and Notes 260
Tables 265
Figure Captions 268
Figures 269

CHAPTER 8. CONCLUSIONS 274

APPENDIX. SYMMETRY ADAPTED BASIS DEFECT PATTERNS FOR ANALYSIS OF THE EFFECTS OF ENERGY DISORDER ON CYCLIC ARRAYS OF COUPLED CHROMOPHORES 278

ACKNOWLEDGMENTS

I would like to take this opportunity to express my genuine thanks to those who assisted me during of my graduate research.

I am indebted to my research advisor, Professor Gerald Small, for his guidance, patience and numerous discussions in the past few years. I am fortunate to benefit from his knowledge and insights in various subjects.

Dr. Raja Reddy and Dr. Margus Rätsep deserve my sincere appreciation and much credit for the work presented in this dissertation. I am especially grateful to Dr. Ryszard Jankowiak for his assistance and expertise. I also would like to acknowledge Dr. John Hayes and Dr. Tõnu Reinot for providing their invaluable advice and experience.

I would like to extend my thanks to Kathy Fitzgerald and all the group members, past and present, for the fun and jokes. I am particularly thankful to Nick Milanovich and Kenny Roberts who spent hours proofreading my writing.

My thanks also goes to Derek Brammeier for the laughter we shared during the course of writing this dissertation.

Most of all, I would like to thank my parents and my brother. It was their constant love, support and understanding that kept me focused on completing my graduate studies.

ABSTRACT

Light-harvesting (LH) complexes of cyclic (C_n) symmetry from photosynthetic bacteria are studied using absorption and high pressure- and Stark-hole burning spectroscopies. The B800 absorption band of LH2 is inhomogeneously broadened while the B850 band of LH2 and the B875 band of the LH1 complex exhibit significant homogeneous broadening due to ultra-fast inter-exciton level relaxation. The B800→B850 energy transfer rate of $(\sim 2\ ps)^{-1}$ as determined by hole burning and femtosecond pump-probe spectroscopies, is weakly dependent on pressure and temperature, both of which significantly affect the B800-B850 energy gap. This resilience is theoretically explained in terms of a modified Förster theory with the spectral overlap provided by the B800 fluorescence origin band and weak vibronic absorption bands of B850. Possible explanations for the additional sub-picosecond relaxation channel of B800 observed with excitation on the blue side of B800 are given. Data from pressure and temperature dependent studies show that the B800 and B850 bacteriochlorophyll *a* (BChl *a*) molecules are weakly and strongly excitonically coupled, respectively, which is consistent with the X-ray structure of LH2. The B875 BChl *a* molecules are also strongly coupled. It is concluded that electron-exchange, in addition to electrostatic interactions, is important for understanding the strong coupling of the B850 and B875 rings. The large linear pressure shifts of $\sim -0.6\ cm^{-1}$/MPa associated with B850 and B875 can serve as important benchmark for electronic structure calculations. The high pressure data obtained for the B800 band, which lead to compressibility values, indicate that the packing of the α, β-polypeptides in the LH2 complex of *Rhodobacter* (*Rb.*) *sphaeroides*, for which a structure is unknown, is looser than for *Rhdopseudomonas* (*Rps.*) *acidophila* whose LH2 structure has been determined. The looser packing is supported by temperature dependent data obtained for the B850 bands. Temperature dependent spectra establish that both the LH2 and LH1 complexes undergo a quite subtle and non-denaturing change near

150 K. Theoretical analysis leads to the conclusion that the nearest neighbor couplings of the B850 and B875 rings are stronger by about 40% for the low temperature structure. Zero-phonon hole action spectroscopy is used to resolve and characterize the lowest energy exciton level (B870) of the B850 ring of A symmetry. The action spectrum indicates that B870 lies 200 cm^{-1} lower in energy than the E_1 level which determines the position of the B850 band maximum. The B870 exciton level, which is forbidden in the absence of energy disorder, carries 3-5% of the total absorption intensity of the B850 ring. A novel theory for analyzing the effects of energy disorder on the exciton level structure of cyclic arrays is presented and used to interpret the experimental results on B870. The theory employs symmetry-adapted basis defect patterns (BDP) which constitute a complete basis set. It is shown that the effects of energy disorder, either diagonal or off-diagonal, on the exciton levels which contribute to the B850 band (including B870) can be largely understood in terms of a single BDP of e_1 symmetry. Relative to "brute force" procedures for analyzing the effects of energy disorder, the new theory simplifies computations and, more importantly, provides far more physical insight. The first Stark hole burning results for photosynthetic complexes are presented. The dipole moment changes ($f \cdot \Delta\mu$) associated with $S_1(Q_y) \leftarrow S_0$ transitions of B800 and B870 of LH2, B896 (the lowest exciton level) of LH1 and B825 of Fenna-Matthews-Olson (FMO) complexes studied fall in the range ~ 0.5-1.2 D. Weak dependencies on laser polarization and burn frequency are observed. That all complexes investigated show linear Stark broadening implies there is a random contribution to $\Delta\mu$ from the "outer shell" of the protein matrix. The presence of Stark splitting, which is only observed in holes burned in B825 of FMO complex, suggests that there is well-defined contribution associated with the "inner shell" of the protein to $\Delta\mu$. Discussion about the consistently larger $f \cdot \Delta\mu$ from classical Stark modulation spectroscopies (it is 3-4 times larger in the case of B850 and B875), as well as the differences between the two Stark techniques, is given. An explanation for the small hole-burning values of $f \cdot \Delta\mu$ for the B870 and B896 levels associated with cyclic arrays of

strongly coupled BChl dimers is given based on structural, symmetry and energy disorder considerations.

CHAPTER 1. INTRODUCTION TO LIGHT-HARVESTING COMPLEXES

1.1 General Introduction to Photosynthesis

The beauty and complexity of photosynthesis go beyond what is indicated by the deceptively simple generalization of CO_2 fixation given by [1, 2]

$$nCO_2 + 2nH_2A + h\nu \rightarrow n(CH_2O) + 2nA + nH_2O. \quad (1.1)$$

Here, A is either oxygen or sulfur. Photosynthesis, which takes place in chloroplasts of higher plants and membranes of prokaryotes, involves delicate interplay between many proteins and pigments; the majority of pigments are either chlorophylls (Chls) or bacteriochlorophylls (BChls). (Figure 1.1 shows the structure of Chl *a* and BChl *a*.) After excitation by light, certain Chls (BChls) are able to initiate charge transfer; electrons are transferred to acceptors and subsequently an electrochemical potential across the photosynthetic membrane is created which drives the reactions which produce energy-rich compounds such as ATP and NADPH.

The classic experiment by Emerson and Arnold in 1932 showed that production of *every* O_2 molecule needed the presence of ~2500 Chls in *Chlorella* cells under saturated illumination [3]. Their observation led to the concept of the *photosynthetic unit* (PSU) in which light is first absorbed by hundreds of Chls or BChls (the *light-harvesting* or *antenna* complexes), as well as other minor pigments such as carotenoids. The excitation energy is then transferred to a specialized non-covalently bounded dimer of Chls (BChls) of the reaction center (RC), the so-called *special pair*, which initiates the electron transfer process after excitation [2, 4, 5]. For purple bacteria, a typical ratio of antenna BChl molecules per special pair ranges from about 100 to 250. That the Chls of RCs lie lower in energy than the light-harvesting (antenna) pigments enables efficient energy funneling to the RC trap. The

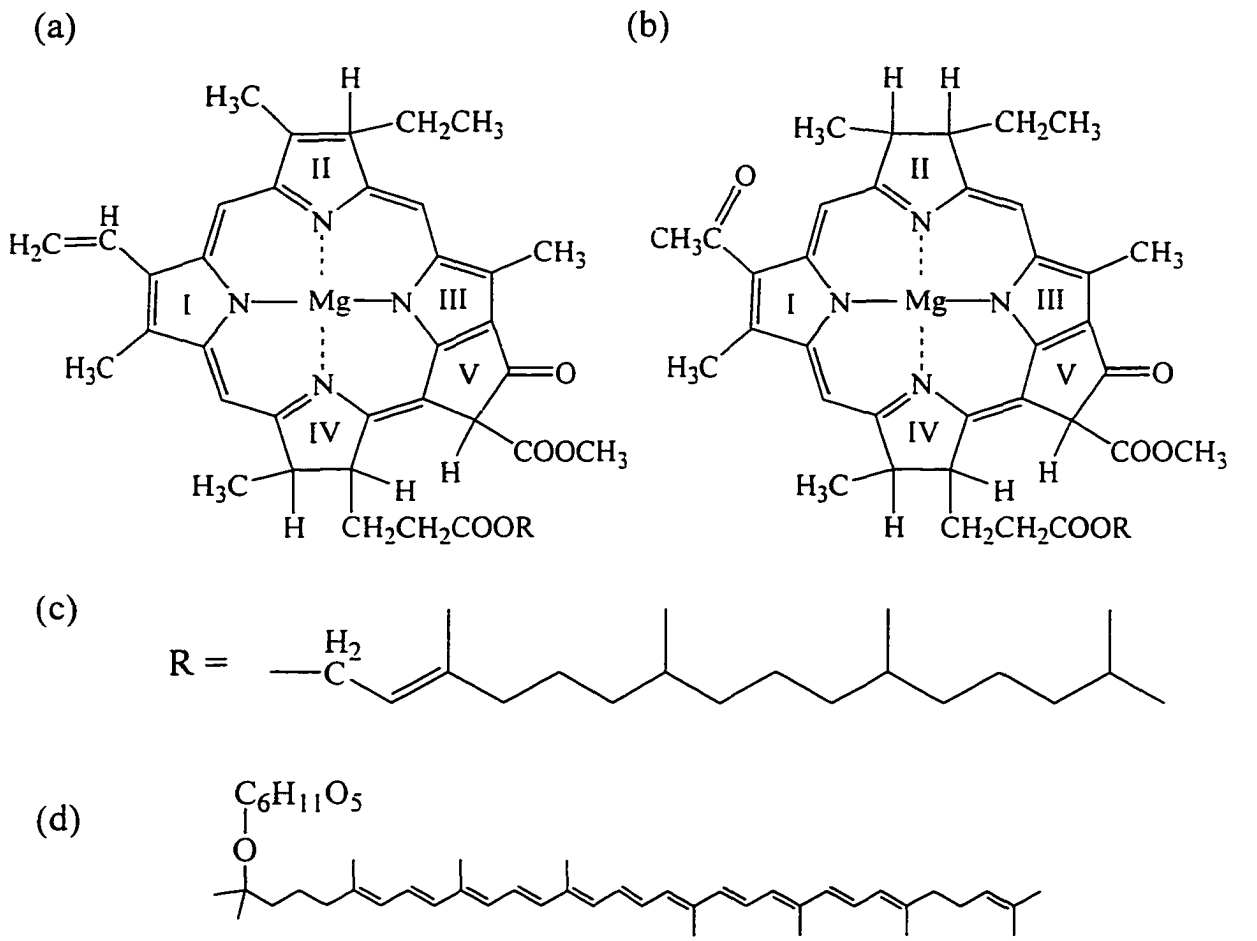

Figure 1.1 Structures of (a) chlorophyll *a*, (b) bacteriochlorophyll *a*, (c) the phytyl chain and (d) rhodopin glucoside. Rhodopin glucoside is the main carotenoid molecules found in light-harvesting complex 2 of purple bacteria *Rhodopseudomonas acidophila*. The phytyl chain is abbreviated as R in structures (a) and (b). The Roman numbers I to V label the rings of Chl and BChl adopted from the IUPAC system. On ring I, Chl *a* has a vinyl group while BChl *a* has acetyl. Furthermore, Chl *a* have one more unsaturated bonds located on ring II than BChl *a*, which contributes to the difference between their absorption band positions. Chl *b* or BChl *b* has one different side chain attached to ring II from Chl *a* or BChl *a*. Pheophytin or bacteriopheophytin molecules are also found in photosynthetic organisms. Their structures are the same as their corresponding Chl or BChl except that the central magnesium is replaced by two protons bonded to rings I and III.

existence of light-harvesting pigments not only broadens the wavelength range of the light absorbed, but also keeps RCs running at an optimal rate. RCs are capable of cycling at a rate of 1000 Hz, while chlorophyll molecules can only absorb photons at a rate ranging from 0.1 Hz in dim light to 10 Hz under direct illumination [5, 6].

1.1.1 Reaction Centers

An important milestone in photosynthesis research in the previous decade was the determination of the high-resolution crystal structure of the RC of the purple bacteria *Rhodopseudomonas viridis* and *Rhodobacter sphaeroides* [7-12] (see Refs. [13, 14] for recent reviews). These structures represent one of the few obtained for membrane proteins which have been solved at atomic resolution. The essential components of the bacterial RC are two protein subunits (L and M) which are approximately related by C_2 symmetry and bind the cofactors. In the bacterial RC, there are the special pair (the primary electron donor), two accessory BChls, two bacteriopheophytin (BPh) molecules and two quinone (Q) molecules which serve as secondary and tertiary electron acceptors, see Figure 1.2. Due to their Q_y absorption band maximum in nanometers, the special pairs of *Rb. sphaeroides* and *Rps. viridis* are named P870 and P960, respectively (P stands for pigments). The former contains BChl *a*, while the latter consists of BChl *b* as the main pigments. The initial electron transfer steps in photosynthesis takes place at very fast rate. The excited P870* transfers an electron to BPh in 3 ps to form $P870^{+}BPh^{-}$. The electron then moves to Q_A, and subsequently to Q_B, in 200 ps and 60 μs, respectively, to further stabilize the charge separation (Q_A and Q_B are the quinone molecules associated with the L and M branches, respectively, see Figure 1.2). $P870^{+}$ becomes active, again, after being reduced by a cytochrome. The same electron transfer process, beginning with excitation of P870, repeats till the fully reduced Q_B^{-2} is formed to combine with protons from cytosol to generate neutral quinol molecules (QH_2). The re-oxidation of QH_2 and electron flow back to P870 via the cytochrome-bc_1 and *c*-type cytochrome complex drive protons outward across the cell membrane, and hence produce

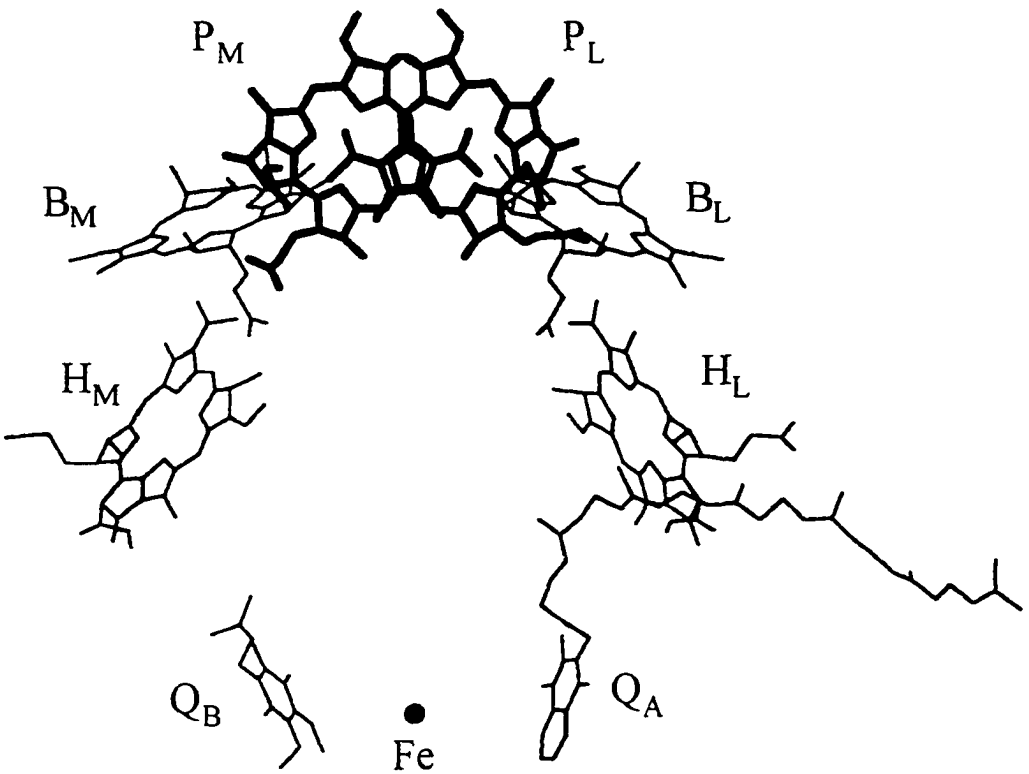

Figure 1.2 Structure of the RC of *Rhodopseudomonas viridis* [7, 8]. P, B, H and Q label the special pair, the accessory BChl, bacteriopheophytin and quinone molecules, respectively. L and M denote the protein branches with which P, B, H are associated. For clarity, the phytyl chains of BChls and bacteriopheophytin molecules are not shown. Q_A and Q_B are the secondary and tertiary electron acceptors, respectively. Fe is a nonheme iron atom present in the reaction center. The figure was generated using the program RasMol [15].

a transmembrane electrochemical potential gradient. ATP synthase utilizes this proton gradient to form ATP. The entire electron flow process is cyclical [16,17]. Though the L and M branches are homologous, the binding and orientations of their associated pigments are slightly different. Electron transfer occurs predominately along the L branch [18]. The aforementioned electron transfer steps also apply to BChl *b* containing P960 from *Rps. viridis*.

In plants and cyanobacteria, there are two types of RC, photosystem II (PS II) and photosystem I (PS I) which work in series (Z scheme, proposed by Hill and Bendall in 1960 [2]), in contrast to only one RC in purple bacteria [2]. Similar to P870 or P960 in bacteria, the primary electron donors of PS I and PS II are referred to as P700 and P680 due to the location in nm of their Q_y absorption bands. Currently, only medium resolution crystal structure (~4.5 Å) of PS I RC is available [19], but protein sequence and other experimental data reveal that PS I and PS II share certain common structural characteristics with RCs of purple bacteria [8, 20]. The strong oxidant produced by excited P680 is used to evolve O_2 from water, while the electron is transferred in several steps to $P700^+$ to re-activate it. The excitation of P700 leads to the formation of NADPH. See, for example, Ref. [21] for more details.

1.2 Light-Harvesting Complexes

As mentioned in the previous section, light-harvesting complexes broaden the range of solar wavelengths used and make the most of the fast RC cycling rate. Recently, advances in obtaining high resolution crystal structure have attracted a lot of research interest in understanding the structure and excitation transfer dynamics of antenna complexes and in developing applications such as artificial antenna and bio-sensors.

To understand the mechanism of the efficient light harvesting and energy transfer processes of antenna complexes, it is essential to know the structures of the protein

complexes, the arrangements and bindings of the pigments in the complexes. The structure provides guidelines for quantum chemical calculations and interpretations of experimental data. Nevertheless, technically speaking it is non-trivial to purify and obtain high-quality, non-denatured 3-D crystals exhibiting good diffraction.

In the mid-1970s, the water-soluble BChl *a* protein from green sulfur bacterium *Prosthecochloris aestuarii* (also known as the FMO complex), which transfers excitation energy from chlorosome to the core antenna of the RC, was shown by X-ray crystallography to contain three protein-pigments subunits arranged with a C_3 symmetry. In each subunit there are seven symmetry-inequivalent BChl *a* [22]. Recently, the structure of the same type of complex from *Chlorobium tepidum* was solved at a resolution of 2.2 Å [23]. It was found that the main structural features of the FMO complex from *Prosthecochloris aestuarii* are conserved. As for plants and green algae, the structure of the isolated Chl *a/b* light-harvesting complex 2 trimers associated with PS II has been determined at a resolution of 3.4 Å, but this level of resolution was not sufficient to allow for differentiation between the Chl *a* and Chl *b* molecules [24].

Of all the photosynthetic protein complexes, antenna and RC complexes of purple non-sulfur bacteria have attracted the most attention due to their overall less congested spectral features. For purple non-sulfur bacteria, there are generally two types of antenna complexes, light-harvesting complexes 1 and 2 (abbreviated as LH1 and LH2). Due to their Q_y absorption maxima in nanometers at room temperature, they are also referred to as B875 and B800-850, respectively. Under different growth conditions, some bacteria, such as *Rhodopseudomonas acidophila*, are capable of having one additional type of antenna, LH3 (B800-820), which absorbs at approximately 800 and 820 nm. Each and every RC is accompanied by one LH1 (B875), while the growth conditions, such as light intensity and temperature, will affect the amount of LH2 per RC. At room temperature, electronic excitation transfer from B800 to B850 occurs in 0.7 ps and is followed by ultra-fast inter-

exciton level relaxation processes within B850 which occur on a ~ 100 fs time scale. B850 → B875 energy transfer occurs in about 3 ps. Following inter-exciton level relaxation within B875, the excitation energy is finally transferred to P870 RC in 50 ps. Figure 1.3 shows the low-temperature absorption spectrum of B800-850 and B875 and a summary of the excitation transfer dynamics. An exciting advance in photosynthesis research was the recently determined X-ray structure of LH2 from *Rps. acidophila* (strain 10050) at 2.5 Å resolution [25, 26]. The structure shown in Figure 1.4 has nine pairs of transmembrane spanning α, β-polypeptides arranged with a C_9 symmetry. Each pair binds two BChl *a* near the periplasmic side which give rise to a Q_y-absorption band at ~ 850 nm, while one BChl *a* bound near the cytoplasmic side absorbs near 800 nm, Figures 1.5 to 1.7. LH2 from another purple bacterium *Rhodospirillum molischianum* was shown to have similar cyclic arrangement [27], except it exhibits C_8 instead of C_9 symmetry.

1.2.1 Crystal Structure of LH2 from *Rps. acidophila* (Strain 10050)

The building block of LH2 is the α, β-polypeptide pairs, Figure 1.5. While the α apoprotein contains 53 amino acids, the β apoprotein consists of 41. Related to each other by C_9 symmetry with the rotational axis perpendicular to the membrane surface, the nine pairs of the polypeptides are arranged in two concentric cylinders with radii of 18 Å for the α and 34 Å for the β apoproteins, Figure 1.4. Both α and β helix axes run nearly parallel to the membrane normal, 2° and 15° respectively. A protomer, the smallest repeating unit of the LH2 structure, is defined as a radially related α, β pair and the associated pigments, which includes three BChl *a* and two carotenoid molecules (rhodopin glucoside, see Figure 1.1(d) for its structure) [25].

The so-called B850 molecules, which are 18 BChl *a* coordinated to histidine residues of the polypeptide pairs (His31 of the α and His30 of the β), form a circle in the space between the α and the β cylinders (Figures 1.5 to 1.7). The molecular planes of those BChl *a* are parallel to the membrane normal and the central magnesium atoms are approximately

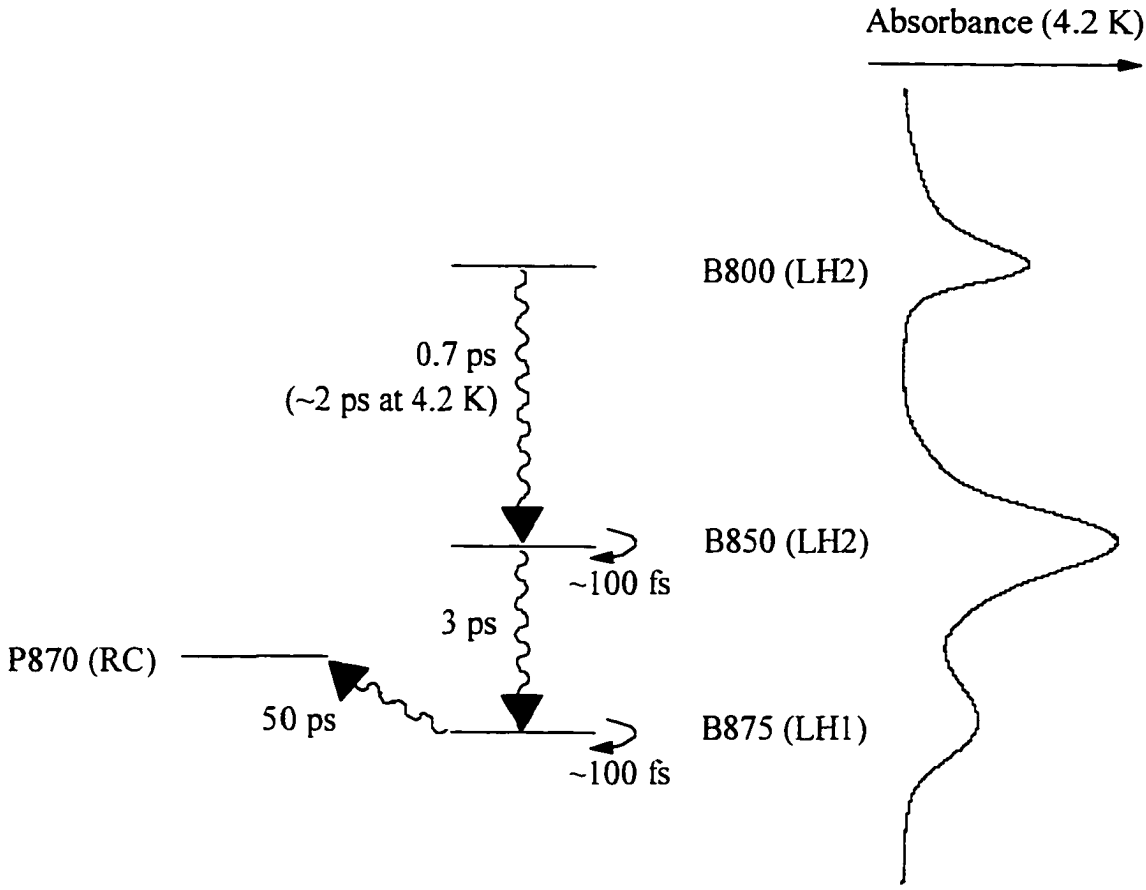

Figure 1.3 Low temperature absorption spectrum of chromatophores of *Rps. acidophila*. At 4.2 K, the B800, B850 and B875 bands are at 12445 cm^{-1} (804 nm), 11495 cm^{-1} (870 nm) and 11055 cm^{-1} (905 nm), respectively. At room temperature, the B850 and B875 bands are not resolved and lead to a single band at 11590 cm^{-1} (863 nm). While the locations of the B850 and B875 bands depend strongly on temperature, the position of B800 is temperature independent. A simple energy level diagram is included on the left to show the transfer times (at room temperature) of different energy transfer steps from B800 to P870 RC. See text.

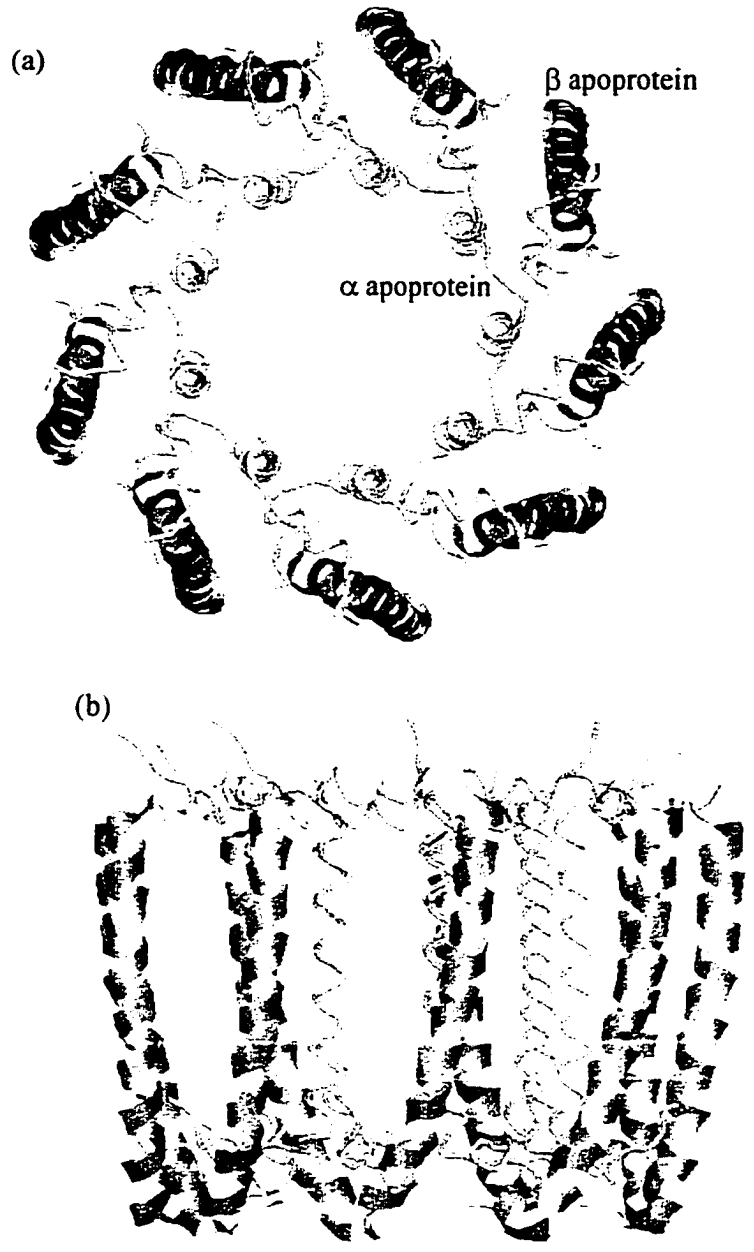

Figure 1.4 The cyclically arranged α, β-polypeptides of the LH2 complex from *Rps. acidophila* (strain 10050) [25, 26]. α polypeptides are on the inner circle with a radius of 18 Å (lighter gray tubes) while β are on the outer circle with a radius of 34 Å (darker gray ribbons). Part (a) shows the view looking down on the membrane from the periplasmic side. Part (b) is a view perpendicular to that of part (a) showing the helices going across the membrane. See text for more details. The figures were generated according to the crystallography coordinates using the RasMol program [15].

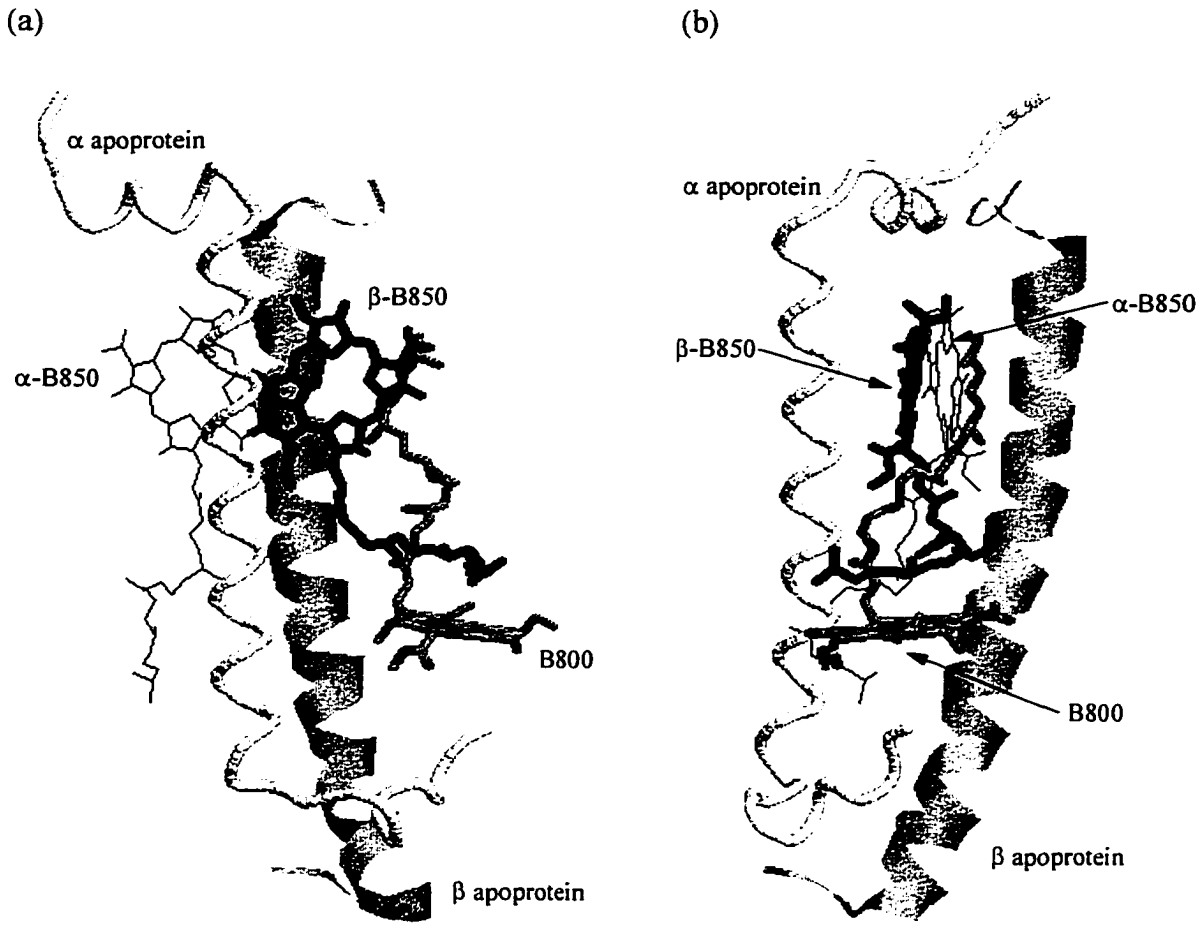

Figure 1.5 Two different views of the protomer (excluding the carotenoid molecules) of the LH2 complex from *Rps. acidophila*, which is the repeating unit of the C_9 complex. As in Figure 1.4, the lighter tube is the α-polypeptide, while the darker gray ribbon is the β-polypeptide. Figure (a) is a view from the C_9 cylinder center. Near the cytoplasmic side (bottom of the figure) is the monomer-like B800 molecule (shown with gray sticks). Near the other side of the membrane, there are two strongly coupled B850 molecules (shown as black wires and sticks respectively). Figure (b) is the side view of (a) with B800 and β-B850 in the foreground and α-B850 in the background. The figures were plotted with RasMol [15].

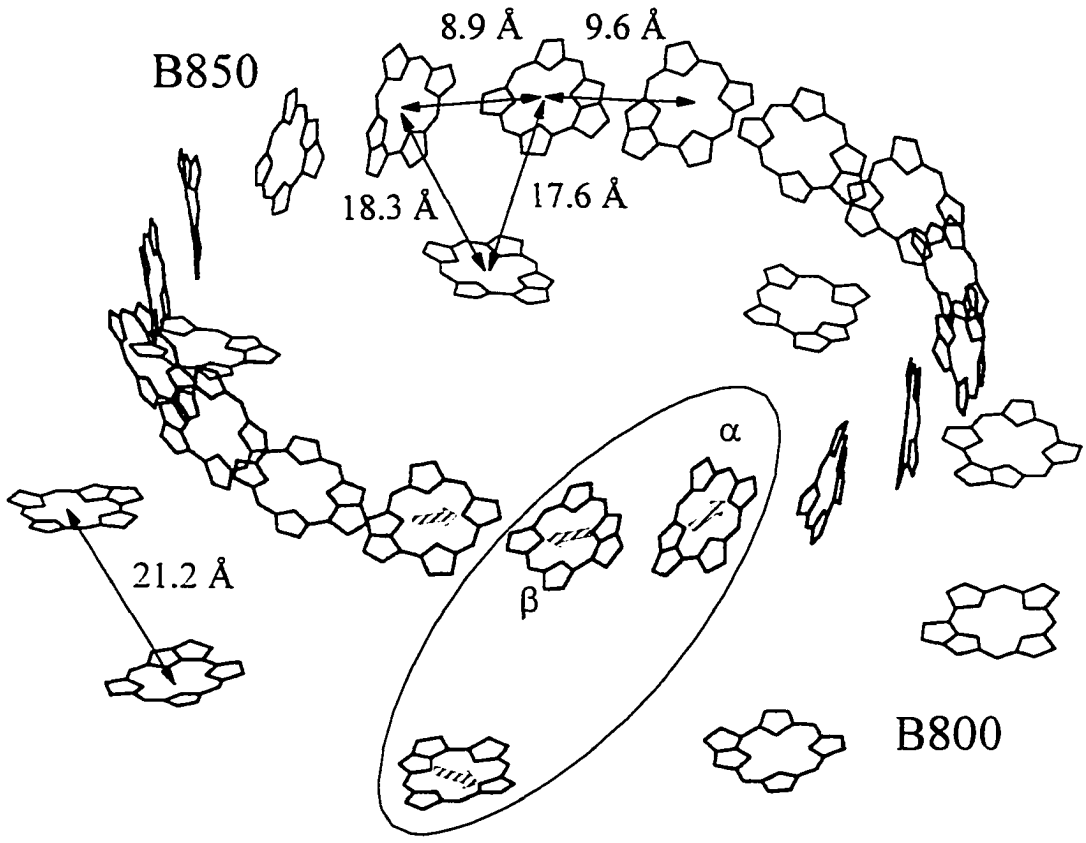

Figure 1.6 Arrangement of the 27 BChls in LH2 of *Rps. acidophila*. The upper ring contains 18 B850 molecules, while the lower ring contains 9 B800 molecules. For clarity, all the side chains on BChls are omitted. The oval encloses the BChls belonging to the same polypeptide pair and the two B850 molecules are labeled by α and β to denote the polypeptides to which they bind. Double-headed arrows mark the Mg...Mg distances between BChls. Note the alternating distances between B850 molecules around the ring. The shaded arrows are drawn to show the directions of Q_y-transition dipole moments of the BChls. See text for more details. This figure was modified from the one made by the RasMol program [15].

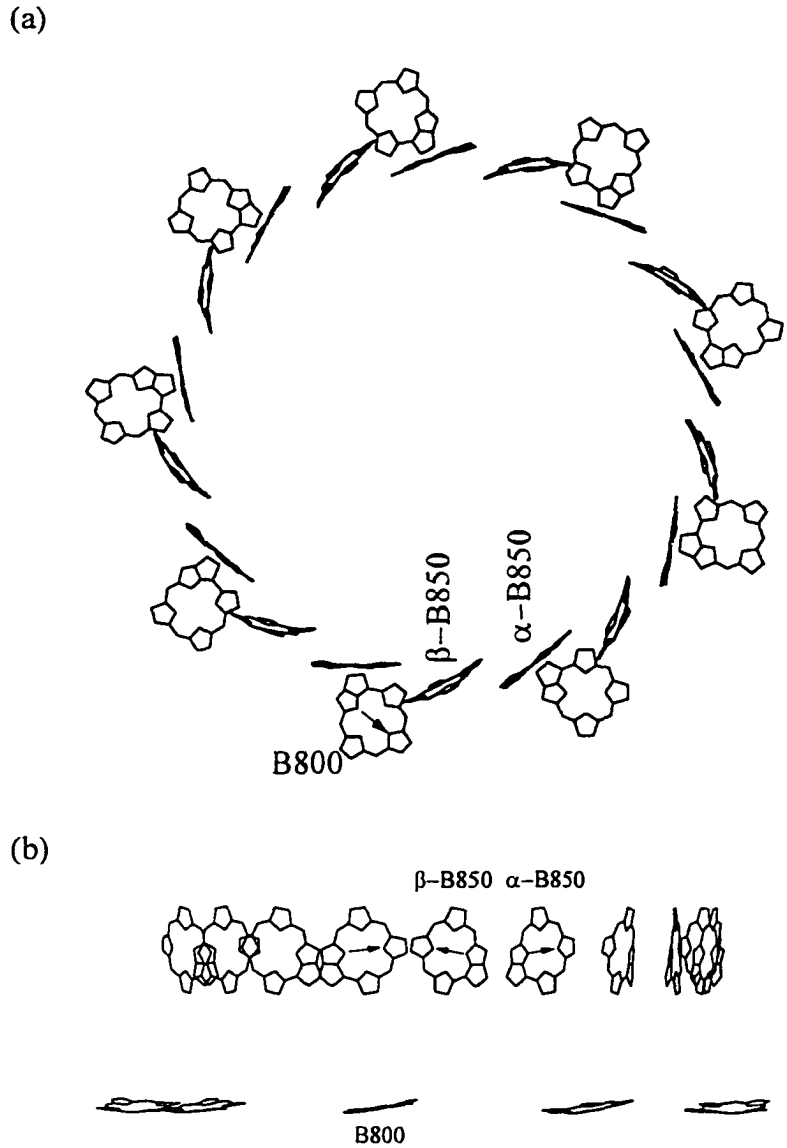

Figure 1.7 (a) Arrangement of the 27 BChl *a* molecules in LH2 of *Rps. acidophila* viewed from the periplasmic side of the membrane. Figure (b) shows the BChls associated with five α, β polypeptide pairs in the lower part of (a) when viewed perpendicular to the C_9 axis. All the side chains on BChls are omitted. In (a) and (b), the arrows show the Q_y-transition dipole moments of B800 and B850 molecules , respectively. The direction of the Q_x-transition dipoles, which is perpendicular to Q_y-transition dipoles by pointing from the nitrogen atom on ring II to that of ring IV, is not shown . For clarity, B800, α-B850 and β-B850 are used to label the three comformationally different BChl *a* molecules associated with one of the polypeptide pairs. The figures were generated by RasMol [15].

10 Å from the presumed periplasmic membrane surface. The Mg...Mg distances for BChl are either 9.6 Å or 8.9 Å with the former being within the protomer, Figure 1.6. Within one protomer, B850 molecules overlap at rings III and V, while between adjacent protomers they overlap at rings I. Due to the C_9 symmetry and the alternating distances, B850 can be viewed as a 9-mer of heterodimers [25, 26, 28-31]. The relative orientation of the transition dipoles of the B850 molecules gives rise to strong Coulombic interactions. The angle between end-to-end Q_y dipoles of B850 within one protomer is 14° and it increases to 26° for neighboring B850 belonging to different protomers (Figures 1.6 and 1.7). The larger angle, however, is compensated by a shorter Mg...Mg distance of 8.9 Å when calculating transition dipole-dipole excitonic coupling which varies inversely as the third power of the distance. Such a short distance of ~ 9 Å and the head-to-head arrangement results in strong Q_y-Q_y coupling interactions (V ~ +300 cm^{-1}) between neighboring BChl molecules [32].

The absorption band at ~ 800 nm is caused by the Q_y-transition of the nine BChl *a* located between β apoproteins, Figures 1.5 to 1.7. Those pigments are held in place by the central magnesium ligated to the carboxyl oxygen of the N-terminal formylmethionine belonging to the α polypeptide [25, 26]. The bacteriochlorin planes are parallel to the cytoplasmic membrane surface which is ~ 11 Å away. As shown in Figures 1.6 and 1.7, the Q_x and Q_y transition dipoles of B800 molecules deviate from the radius and tangent of the nonameric ring by an angle of 15°. The Mg...Mg distance of 21.2 Å makes B800 molecules monomer-like with relatively weak interaction of ~ −25 cm^{-1} as suggested by spectroscopic studies [30, 32-34].

The Mg...Mg distances between B800 and the nearest B850 molecules are either 17.6 Å (with the B850 from the α of the neighboring protomer) or 18.3 Å, see Figure 1.6. The angles of the B800 and the B850 Q_y-transition dipoles corresponding to these two distances are 43° and 105°, respectively. With a separation of ~ 18 Å and the unfavorable

angle, the largest B800-B850 interaction is 27 cm^{-1} [32], which is comparable to the weak B800-B800 coupling mentioned above.

The much stronger couplings between B850 molecules are responsible, in part, for the red shift of the B850 absorption band relative to B800, but there are other factors which contribute to the different band positions [35]. The environment around B800 and B850 molecules is quite different with the former in a relatively polar region and the latter in a hydrophobic region [25]. Besides, B800, α-B850 and β-B850 (the prefixes α- and β- label the polypeptides to which the B850 molecules are bound) distort to different extent and in different ways, which can cause Q_y-energy shift of up to several tens of nanometers [36, 37]. α-B850 molecules show significant hybrid ruffling. Both B800 and β-B850 molecules adopt a standard, slightly bowed conformation with the latter being more planar [26]. In addition, the ligation to Mg^{2+} of B800 molecule is on the opposite face when compared with both types of B850 molecules [35]. There are hydrogen bonds formed between the acetyl oxygen of ring I of all BChls and the polypeptides. B800 has hydrogen bond to the β-Arg20 residue, while the two B850 are hydrogen bonded to α-Trp45 and α-Tyr44, respectively [35].

In addition to BChl *a*, there are also carotenoids which harvest photons in the region from 450 to 570 nm where there is no strong BChl absorption. The most important role played by carotenoids is to serve as the photo-protective agent by quenching the BChl excited triplet state. It is known that this triplet state can readily react with oxygen to produce singlet oxygen whose strong oxidizing power is destructive to the photosynthetic organisms [38, 39].

The carotenoids found in LH2 of *Rps. acidophila* is rhodopin glucoside, see Figure 1.1(d) for its structure. Half of the carotenoid molecules have their glucoside head groups in the hydrophilic pocket in the cytosol region of the membrane, while the others start from the periplasmic side [26]. Their long conjugated hydrocarbon chains extend across the membrane, passing through the B800 and B850 region and making many close contacts with either the phytyl side chains or the main BChl planes, see Figure 1.8. Several contact

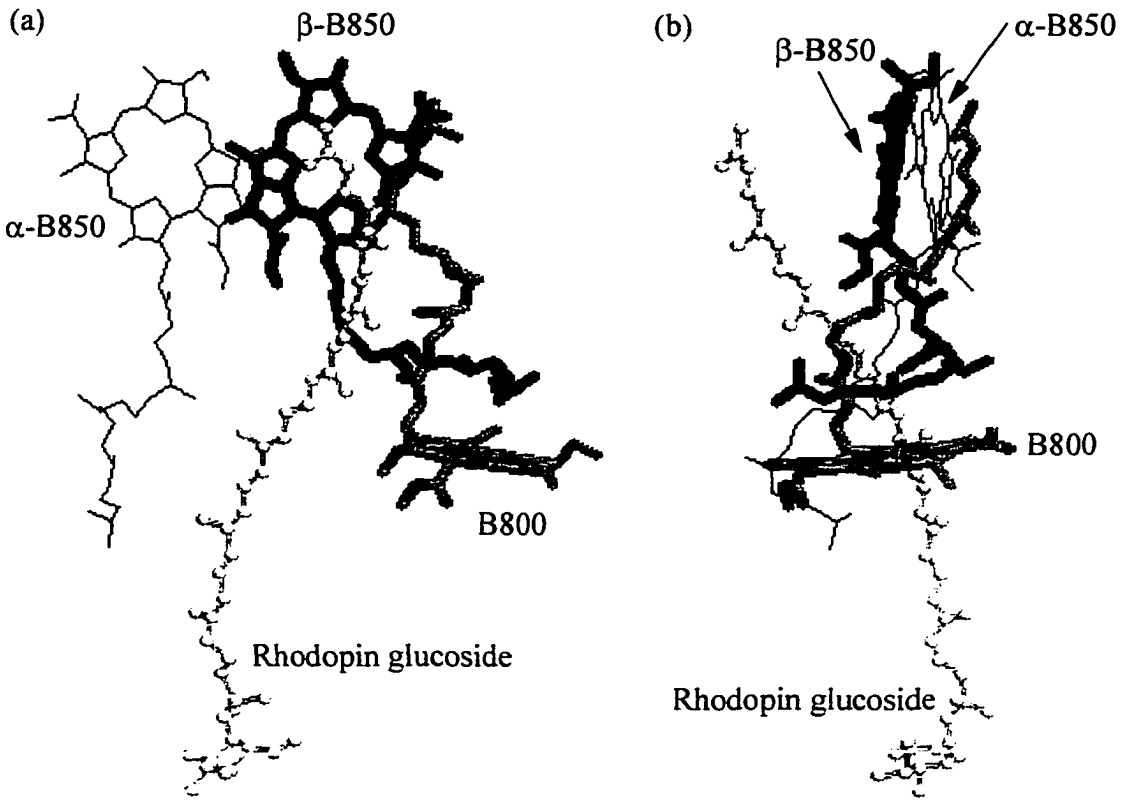

Figure 1.8 The spatial arrangements of rhodopin glucoside, B800 and B850 molecules. The above figures correspond to Figure 1.5(a) and (b), respectively, except that the polypeptide pairs are omitted and the carotenoid molecules are included in Figure 1.8. See text. The other carotenoid revealed in more recent analysis of the crystal structure was not shown in the figure [26]. The images were generated using the program RasMol [15].

distances are as short as ~ 3.5 Å, which may provide for a contribution to B800 → B850 energy transfer from the electron exchange mechanism [26]. As pointed out by Freer *et al.* [26], the presence of carotenoids running across the membrane and making many close contacts with B800 and B850 pigments introduces additional binding stability into the LH2 skeleton.

1.2.2 A Comparison of LH2 Structures from *Rps. acidophila* and *Rs. molischianum*

Shortly after the success of Freer *et al.* [26], a 2.4 Å resolution crystal structure of LH2 from another purple non-sulfur bacterium, *Rs. molischianum,* was determined by molecular replacement using X-ray diffraction [27]. The architectural principles of the two LH2, i.e. the cyclic arrangement of protein pairs and the pigments, are conserved. The major difference is that instead of possessing C_9 symmetry, LH2 from *Rs. molischianum* is a C_8 arrangement of 8 polypeptide pairs [27]. As a result, the B800 and B850 rings of LH2 from *Rs. molischianum* are 8-mer of monomers and heterodimers, respectively. The overall construction of LH2 from *Rs. molischianum* appears to be more tightly packed. The diameters of the inner and outer cylinders formed by the α and β helices are 31 and 62 Å, respectively. The α apoprotein consisting of 27 amino acids deviates from the membrane normal by 2°, while the 34-residue-long β apoprotein is tilted away from the membrane normal by about 10°. As in *Rps. acidophila*, BChl *a* molecules are the major light absorbing pigments. For *Rs. molischianum*, however, lycopene and rhodopin are found to be the major and minor carotenoids, respectively [27, 40]. The B800 BChl molecules sandwiched between β polypeptides are separated from each other by a Mg...Mg distance of 22 Å. The Mg...Mg distances between nearest neighbor B850 molecules are 9.2 Å within the protomer and 8.9 Å between nearest protomers, as compared with 9.6 and 8.9 Å in *Rps. acidophila*. The Mg...Mg distances between B800 and the nearest B850 molecules are either 19.1 Å (with the B850 from the α of the neighboring protomer) or 20.2 Å. The angles between the Q_y-transition dipole moments of B800 and the nearest B850 molecules are 13.1° and 151.5°,

respectively. The longer B800-B850 distances observed in LH2 of *Rs. molischianum* are less favored for Förster energy transfer than *Rps. acidophila* , but are compensated by larger κ^2 values, see Eqs. (2.3) and (2.4).

The most apparent difference between these two LH2 complexes is associated with B800 binding and orientation. B800 molecules of *Rs. molischianum* are bound to an aspartate residues of the α-apoprotein, instead of formylmethionine residues as observed for *Rps. acidophila*. For LH2 of *Rs. molischianum*, the B800 macrocycles deviate from the membrane surface by 38° (though the Q_y-transition dipole moments are parallel to the membrane plane to within 10°), which is nearly twice the angle (18°) observed in *Rps. acidophila*. From the superposition of the α, β pairs from these two LH2 [27], a roughly 90° rotation has to be applied in order to overlap the projection of Q_y-transition dipoles on the membrane. Consequently, for *Rs. molischianum* and *Rps. acidophila*, the Q_y-transition dipole of the B800 molecule is approximately parallel and perpendicular to that of the α-B850 molecule in the same protomer, respectively.

Although the binding and the orientation of B800 molecules in *Rs. molischianum* and *Rps. acidophila* are quite different, the absorption properties and B800 → B850 energy transfer time are very similar, see Refs. [30, 41].

1.2.3 Projection Structure of LH1 Complex from *Rhodospirillum rubrum*

In 1995, Karrasch *et al.* reported a projection map of the LH1 (B875) complex of purple non-sulfur bacterium *Rhodospirillum rubrum* at a resolution of 8.5 Å [42]. LH1 is the only antenna complex of *Rs. rubrum*. The data indicate that the cyclic arrangements seen in LH2 exist in LH1 but LH1 possesses a larger ring size than LH2. The building block is an α, β-polypeptide pairs with 52 (α) and 54 (β) amino acid residues. 16 polypeptide pairs aggregate to form a C_{16}-ring with an outer diameter of 116 Å and an inner diameter of 68 Å, which is large enough to house RC within. LH1 complex exhibits a single Q_y-absorption band at 880 nm which exhibits significantly homogeneous broadening due to inter-exciton

level relaxation processes [42]. The locations of pigments in the complex are not clearly resolved due to the limited resolution of 8.5 Å. Based on the LH2 structure, the conserved histidine residues and spectroscopic properties , the BChls which contribute to the 880-nm band are believed to lie edge-on between α and β polypeptides as in the case of the B850 molecules of LH2. The density observed in the projection map suggests that B875 BChls are strongly interacting with neighboring B875 with an estimated nearest Mg...Mg separation of ~ 7.5 Å [42], which is also similar to B850 molecules.

1.2.4 Organization of Photosynthetic Complexes in the Membrane of Purple Bacteria

It is generally accepted that RC is located inside the LH1 ring. However, the exact arrangement of the LH2 complexes around the LH1-RC unit in the natural membrane is unknown. Several models have been proposed. For example, Monger and Parson proposed a clustered model with an aggregate of several LH1-RC surrounded by LH2 [43]. Recently, Papiz *et al.* suggested a building unit of one LH1-RC enclosed by eight cyclically arranged LH2 complexes [44]. They argued that their model has the flexibility of accommodating other membrane proteins and it can give an ordered and hexagonally-packed units of sixfold symmetry in accordance with the low resolution electron microscopic data [45]. See Ref. [44] for further discussion.

Recently, Hu and Schulten [46] employed molecular dynamics simulations and energy minimization to model the structure of LH1 of *Rb. sphaeroides* with its RC located inside the ring. Taking advantage of the high degree of homology of the α, β-polypeptide pairs of LH1 of *Rb. sphaeroides* to those of LH2 of *Rs. molischianum*, the structure of the former complex is modeled as a 16-mer by using the C_8 arrangement of the latter as a template. The conserved histidine residues, α-His32 and β-His39, are the binding sites for B875 BChl *a* molecules. The shortest Mg...Mg distance between B875 BChl *a* molecules and the RC special pair (P_L or P_M) is 42 Å, while it is 35 Å between the B875 and accessory BChl molecules. The planes of tryptophan residues in the LH1-RC complex and the LH2

complex are used to align the pigment-protein complexes of the basic PSU, which is one LH2 complex in contact with one LH1-RC unit. The B850 BChls of LH2 and the B875 BChls of LH1 are exactly coplanar, which is the optimal arrangement for excitation energy transfer to the RC. See Ref. [46] for more details.

1.3 Application of Hole Burning Spectroscopy to Light-Harvesting Complexes

This dissertation presents the results of the candidate's original studies on light-harvesting complexes by high pressure- and Stark-hole burning as well as theoretical results on the effects of energy disorder using symmetry-adapted basis defect patterns.

1.3.1 Marriages of Non-Photochemical Hole Burning Spectroscopies with High Pressure and Electric Field

After the pioneering works of Kharlamov, Personov, and Bykovskaya [47] and Gorokhovskii, Kaarli and Rebane [48] in 1974, persistent spectral hole burning in crystalline and amorphous solids has proven to be one of the most powerful frequency-domain spectroscopies. Excellent general reviews on hole burning may be found in Refs. [49-51]. Later, non-photochemical hole burning proved to be an unrivaled frequency-domain tool for the study of photosynthetic protein complexes since it provides information on Q_y-electronic structure, structural heterogeneity and inhomogeneous spectral broadening, distributions of donor-acceptor energy gap values, electron-protein phonon coupling, Chl (BChl) vibrational frequencies/Franck-Condon factors and transport dynamics from zero-point level. See Refs. [52, 53] and references listed in Ref. [51].

Following the success of Small and coworkers [54, 55] in applying hole burning with high pressure to study photosynthetic reaction centers and the FMO complex, the same combination is further employed to investigate antenna complexes from purple bacteria, which is the main focus of the candidate's work. The beauty of the high pressure experiment is the ability to continuously tune spectroscopic properties via the pressure-induced changes

in relative orientations of pigments and their separation as well as changes in pigment-protein distances. In a sense, a new "*mutant*" of the complex is obtained at every pressure. Thus, a much more systematic approach to understanding electronic structure and transport dynamics becomes available.

Recently, Stark hole burning was performed successfully for the first time on photosynthetic antenna complexes [56, 57]. Information such as the dipole moment changes associated with the transitions from the ground to excited states and charge transfer interactions can be extracted from the data. Due to the narrowness of zero-phonon holes, only moderate electric field strength is required for Stark hole burning as compared with the classical Stark modulation experiment performed on the whole absorption band.

Hole burning, high pressure, and Stark experimental setups are given in Refs. [58], [54] and [57], respectively, as well as in the related chapters of this dissertation.

1.4 Thesis Organization

Chapter 1 gives a general background on photosynthesis and light-harvesting complexes. The emphasis is placed on the description of high resolution crystal structures of antenna complexes from purple bacteria. Chapter 2 is a short review on mechanisms of excitation energy transfer and relaxation including theories of Förster energy transfer, electron exchange and molecular excitons. Chapter 3 to 7 are selections of published or accepted papers of the candidate. In Chapter 3, high-pressure hole burning and femtosecond pump-probe spectroscopies are used to study B800→B850 energy transfer kinetics of LH2 complex from *Rps. acidophila* (strain 10050). Comparisons of LH2 from *Rps. acidophila* and *Rb. sphaeroides* are given in Chapter 4 using different combinations of absorption or hole burning spectroscopies with temperature or pressure. The studies related to the effects of energy disorder on the B850 exciton level structure and spectroscopic properties are contained in Chapters 5 and 6. The former is aimed towards understanding B850's exciton

level structure by using symmetry-adapted basis defect patterns to account for the experimentally observed oscillator strength and energy splittings of the exciton levels. The latter deals with the effects of energy disorder on exciton level localization and the implications of localization on the interpretation of Stark hole burning data. Chapter 7 describes and discusses the Stark hole burning results obtained for three types of antenna complexes from photosynthetic bacteria. The shortcomings of classical Stark modulation spectroscopies are also discussed in Chapter 7. General conclusions are given in Chapter 8. The appendix provides detailed derivations of the theoretical equation used in Chapters 5 and 6.

1.5 Other Published Work of the Candidate

The following are titles of papers not included in this dissertation in chronological order:

- High Pressure Studies of Excitonically Coupled Photosynthetic Antenna Complexes [59].
- Pressure Dependence of Energy and Electron Transfer in Photosynthetic Complexes [60].
- High Pressure Studies of Energy Transfer and Strongly Coupled Bacteriochlorophyll Dimers in Photosynthetic Protein Complexes [34].
- A Comparison of the LH2 Antenna Complex of Three Purple Bacteria by Hole Burning and Absorption Spectroscopies [41].
- Direct Observation and Hole Burning of the Lowest Exciton Level (B870) of the LH2 Antenna Complex of *Rhodopseudomonas acidophila* (Strain 10050) [28].
- Symmetry Adapted Basis Defect Patterns for Analysis of the Effects of Energy Disorder on Cyclic Arrays of Coupled Chromophores [29].
- Stark Hole Burning Spectroscopy of a Photosynthetic Complex: LH2 of Purple Bacteria [56].

- Hole Burning and Absorption Studies of the LH1 Antenna Complex of Purple Bacteria: Effects of Pressure and Temperature [61].

1.6 References

[1] Stryer, L. *Biochemistry,* 3rd Ed.; Freeman and Company: New York, 1988; Chapter 22.

[2] Zubay, G. *Biochemistry,* 3rd Ed.; Wm. C. Brown Publishers: Dubuque, 1993; Chapter 16.

[3] Emerson, R.; Arnold, W. *J. Gen. Physiol.* **1932**, *16*, 191.

[4] Duysens, L. N. M. *Transfer of Excitation Energy in Photosynthesis*, Ph. D. Thesis. State University of Utrecht, 1952.

[5] Mauzerall, D.; Greenbaum, N. L. *Biochim. Biophys. Acta*, **1989**, *974*, 119.

[6] van Grondelle, R.; Sundström, V. In *Photosynthetic Light-Harvesting Systems*, Scheer, H. Ed.; Walter de Gruyter & Co.: Berlin, New York, 1988: p 403.

[7] Deisenhofer, J.; Epp. O.; Miki, K.; Huber, R.; Michel, H. *J. Mol. Biol.* **1984**, *180*, 385.

[8] Deisenhofer, J.; Epp. O.; Miki, K.; Huber, R.; Michel, H. *Nature*, **1985**, *318*, 618.

[9] Allen, J. P.; Feher, G.; Yeates, T. O.; Rees, D. C.; Deisenhofer, J.; Michel. H.; Huber, R. *Proc. Natl. Acad. Sci. U. S. A.* **1986**, *83*, 8593.

[10] Arnoux, B.; Decruis, A. Reiss-Husson, F.; Lutz, M.; Norris, J.; Schiffer, M.; Chang. C. H. *FEBS Lett.* **1989**, *258*, 47.

[11] El-Kabbana, O.; Chang, C. H.; Tiede, D.; Norris, J.; Schiffer, M. *Biochem.* **1991**, *30*, 5361.

[12] Deisenhofer, J. Epp. O.; Sinning, I; Michel, H. *J. Mol. Biol.* **1995**, *246*, 429.

[13] Lancaster, C. R. D.; Ermler, U.; Michel, H. In *Anoxygenic Photosynthetic Bacteria*, Blankenship. R. E.; Madigan, M. T.; Bauer, C. E. Ed.; Kluwer Academic Publishers: Dordrecht, 1995: Chapter 23.

[14] Deisenhofer, J.; Michel, H. In *Chlorophylls*, Sheer, H. Ed.; CRC Press: Boca Raton, 1991, p. 617.

[15] Sayle, R.; Milner-White, E. J. *Trends Biochem. Sci.* **1995**, *20*, 374.

[16] Pierson, B. K. *Arch. Microbiol.* **1985**, *143*, 260.

[17] Zannoni, D.; Ingledew, W. J. *Febs. Lett.* **1985**, *193*, 93.

[18] Michel-Beyerle, M. E.; Plato, M.; Deisenhofer, J.; Michel, H.; Bixon, M.; Jortner, J. *Biochim. Biophys. Acta*, **1988**, *932*, 52.

[19] Fromme, P.; Witt, H. T.; Schubert, W.-D.; Klukas, O.; Saenger, W.; Krauss, N. *Biochim. Biophys. Acta* **1996**, *1275*, 76.

[20] Rochaix, J. D.; Dron, M.; Rahire, M.; Malnoe, P. *Plant Mol. Biol.* **1984**, *3*, 363.

[21] Mathis, P.; Rutherford, A. W. *New Comprehensive. Biochem.* **1987**, *15*, 63.

[22] Tronrud, D. E.; Schmid, M. F.; Matthews, B. W. *J. Mol. Biol.* **1986**, *188*, 443.

[23] Li, Y.-F.; Zhou, W.; Blankenship, R. E.; Allen, J. P. *J. Mol. Biol.* **1997**, *271*, 456.

[24] Kühlbrandt, W.; Wang, D. N. Fujiyoshi, Y. *Nature*, **1994**, *367*, 614.

[25] McDermott, G.; Prince, S. M.; Freer, A. A.; Hawthornthwaite-Lawless, A. M.; Papiz, M. Z.; Cogdell, R. J.; Isaacs, N. W. *Nature* **1995**, *374*, 517.

[26] Freer, A.; Prince, S; Sauer, K.; Papiz, M.; Hawthornthwaite-Lawless, A.; McDermott, G.; Cogdell, R.; Isaacs, N. W. *Structure* **1996**, *4*, 449.

[27] Koepke, J.; Hu, X.; Muenke, C.; Schulten, K. Michel, H. *Structure*, **1996**, *4*, 581.

[28] Wu, H.-M.; Reddy, N. R. S.; Small, G. J. *J. Phys. Chem. B* **1997**, *101*, 651.

[29] Wu, H.-M.; Small, G. J. *Chem. Phys.* **1997**, *218*, 225.

[30] Chapter 4; Wu, H.-M.; Ratsep, M.; Jankowiak, R.; Cogdell, R. J.; Small, G. J. *J. Phys. Chem. B* **1997**, *101*, 7641.

[31] Chapter 5; Wu, H.-M.; Ratsep, M.; Lee, I.-J.; Cogdell, R. J.; Small, G. J. *J. Phys. Chem. B* **1997**, *101*, 7654.

[32] Sauer, K.; Cogdell, R. J.; Prince, S. M.; Freer, A. A.; Isaacs, N. W.; Scheer, H. *Photochem. Photobiol.*, **1996**, *64*, 564.

[33] Cogdell, R. J.; Scheer, H. *Photochem. Photobio.* **1985**, *42*, 669.

[34] Reddy, N. R. S.; Wu, H.-M.; Jankowiak, R.; Picorel, R.; Cogdell, R. J.; Small, G. J. *Photosynth. Res.* **1996**, *48*, 277.

[35] Prince, S. M.; Papiz, M. Z.; Freer, A. A.; McDermott, G.; Hawthornwaite-Lawless, A. M.; Cogdell, R. J.; Isaacs, N. W. *J. Mol. Biol.* **1997**, *268*, 412.

[36] Gudowska-Nowak, E.; Newton, M. D.; Fajer, J. *J. Phys. Chem.* **1990**, *94*, 5795.

[37] Gentemann, S.; Nelson, N. Y.; Jaquinod, L.; Nurco, D. J.; Leung, S. H.; Medforth, C. J.; Smith, K. M.; Fajer, J.; Holten, D. *J. Phys. Chem. B* **1997**, *101*, 1247.

[38] Sietermann, D. *Biochim. Biophys. Acta* **1985**, *811*, 325.

[39] Cogdell, R. J.; Frank, H. A. *Biochim. Biophys. Acta* **1987**, *895*, 63.

[40] Germeroth, L; Lottspeich, F.; Robert, B.; Michel, H. *Biochem.* **1993**, *32*, 5615.

[41] Wu, H.-M.; Reddy, N. R. S.; Cogdell, R. J.; Muenke, C.; Michel, H.; Small, G. J. *Mol. Cryst. Liq. Cryst.* **1996**, *291*, 163.

[42] Karrasch, S.; Bullough, P. A.; Ghosh, R. *EMBO J.* **1995**, *14*, 631.

[43] Monger, T. G.; Parson, W. P. *Biochim. Biophys. Acta* **1977**, *460*, 393.

[44] Papiz, M. Z.; Prince, S. M.; Hawthornthwaite-Lawless, A. M.; McDermott, G.; Freer, A. A.; Isaacs, N. W.; Cogdell, R. J. *Trends in Plant Sci.* **1996**, *1*, 198.

[45] Miller, K. R. *Nature* **1982**, *300*, 53.

[46] Hu, X.; Schulten, K. *Biophys. J.* submitted.

[47] Kharlamov, B. M.; Personov, R. I.; Bykovskaya, L. A. *Opt. Commun.* **1974**, *12*, 191.

[48] Gorokhovskii, A. A.; Kaarli, R. K.; Rebane, L. A. *JETP Lett.* **1974**, *20*, 216.

[49] Moerner, W. E. Ed. *Persistent Spectral Hole Burning: Science and Applications*; Springer-Verlag: Berlin, 1988.

[50] Völker, S. In *Relaxation Processes in Molecular Excited States*, Fünfschilling, J. Ed.; Kluwer: Dordrecht, 1989; p. 113.

[51] Jankowiak, R.; Hayes, J. M.; Small, G. J. *Chem. Rev.* **1993**, *93*, 1471.

[52] Köhler, W.; Friedrich, J.; Fischer, R.; Scheer, H. *J. Chem. Phys.* **1988**, *89*, 871.

[53] van der Laan, H.; Schmidt, Th.; Visschers, R. W.; Visscher, K. J.; van Grondelle, R.; Völker, S. *Chem. Phys. Lett.* **1990**, *170*, 231.

[54] Reddy, N. R. S.; Jankowiak, R.; Small, G. J. *J. Phys. Chem.* **1995**, *99*, 16168.

[55] Chang, H.-C.; Jankowiak, R.; Reddy, N. R. S.; Small, G. J. *Chem. Phys.* **1995**, *197*, 307.

[56] Rätsep, M.; Wu, H.-M.; Hayes, J. M.; Small, G. J. *Spectrochim Acta A*, in press.

[57] Chapter 7; Rätsep, M.; Wu, H.-M.; Hayes, J. M.; Blankenship, R. E.; Cogdell, R. J.; Small, G. J. *J. Phys. Chem. B* **1998**, in press.

[58] Lyle, P. A.; Kolaczkowski, S. V.; Small, G. J. *J. Phys. Chem.* **1993**, *97*, 6924.

[59] Reddy, N. R. S.; Wu, H.-M.; Jankowiak, R.; Small, G. J. In *High Pressure Science and Technology, Proceedings of the Joint XV AIRAPT & XXXIII EHPRG International Conference*, Trzeciakowski, W. Ed.; Warsaw, Poland, 1996, p 878.

[60] Reddy, N. R. S.; Chang, H.-C.; Wu, H.-M.; Jankowiak, R.; Small, G. J. In *Proceedings of Third Feldafing International Workshop on Reaction Center of Photosynthetic Bacteria: Structure and Dynamics*, M. E. Michel-Beyerle, Ed.; Springer-Verlag, 1996, p 255.

[61] Wu, H.-M.; Rätsep, M.; Jankowiak, R.; Cogdell, R. J.; Small, G. J. *J. Phys. Chem. B*, **1998**, in press.

CHAPTER 2. MECHANISMS FOR EXCITATION ENERGY TRANSFER AND RELAXATION

2.1 Introduction

Understanding electronic excitation energy transfer in photosynthetic antenna complexes is of very considerable importance. It is the process which precedes primary charge separation process in RC. Energy transfer is often treated in two limits, strong and weak coupling between the donor (D) and acceptor (A) molecules (states). An important criterion for weak coupling is that the interaction between D and A is small relative to their electronic energy gap. When this gap is small, the homogeneous broadenings of the D and A levels due to dephasing must be small relative to the D-A energy gap. The Förster theory of electronic energy transfer [1, 2] is a weak coupling theory developed to understand energy transfer between donor and acceptor molecules in liquids. The interaction between D and A was taken to be of the transition dipole-dipole type. Later, Dexter extended the theory to include exchange coupling involving two-electron exchange integrals and higher multipole interactions [3]. Nevertheless, the Förster-Dexter theory is a weak coupling theory whose energy transfer rate expression stems from the Fermi-Golden rate expression with the "trigger" being the static intermolecular potential energy. Furthermore, the theory was not designed for solids such as photosynthetic complexes whose optical absorption and fluorescence transitions suffer from significant inhomogeneous broadening, *vide infra*.

Förster-Dexter theory, which has been widely applied in photosynthesis, is inapplicable when one is confronted with an array of strongly coupled and identical (chemically) Chl molecules [4, 5]. Strong coupling means that the nearest neighbor Chl-Chl interactions are much larger than the homogeneous width of the Chl optical transition. Strong coupling, with static lattice approximation, means that the Hamiltonian which determines the excitonic wavefunctions and energies already includes the static

intermolecular potential energy. Thus, relaxation between exciton levels is induced by phonons which modulate the intermolecular pigment-pigment interactions. The B850 and B875 rings of BChl molecules are prime candidates for such a situation, although the effects of energy disorder from structural heterogeneity must be taken into account. That is, if the disorder-induced splittings between the exciton levels are much larger than the nearest neighbor coupling, the exciton levels will no longer be delocalized on individual molecules. In this case, weak coupling energy transfer theory would become applicable and energy transfer thought of as an incoherent hopping process [6].

As discussed in Chapter 3, the interactions between the B800 and B850 molecules of the LH2 complex are weak enough for B800 → B850 transfer to be describable by a modified Förster theory which takes into account structural heterogeneity, *vide infra.*

2.1.1 Energy Transfer in Photosynthesis

Energy transfer consistent with the Förster mechanism has been observed in various types of donor-acceptor systems in solutions or solids. Of particular relevance to this dissertation is the mechanism for B800 → B850 transfer in the LH2 complex which has been extensively studied by ultrafast pump-probe and hole burning spectroscopies [7-13]. The LH2 structure which yields a nearest neighbor B800-B850 distance of 17.6 Å and a dipole-dipole orientation factor κ of 0.78 [14] results in a weak coupling of 27 cm^{-1} [15]. This favors Förster-type energy transfer. The Dexter-type electron exchange mechanism for B800 → B850 transfer is unimportant because of the large separation distances. However, it provides the route for both the deactivation of triplet BChl, which is harmful to the bacteria, by a triplet carotenoid state [16, 17] as well as symmetry-forbidden singlet-singlet energy transfer from the 2^1A_g state of carotenoid to the BChl *a* Q_y state [2, 18-20]. The nearly co-linear arrangement of adjacent B850 Q_y-transition dipoles (κ =1.67 and 1.19) and the short nearest neighbor B850-B850 separation distance (~ 9 Å) gives rise to a strong excitonic interaction, ~ 300 cm^{-1} according to Sauer *et al.* [15]. Hole-burning studies have indicated a

fast relaxation among exciton levels (~ 100 fs) and have been used to characterized the spectroscopic properties of the lowest exciton level of strongly-coupled B850 BChl *a* molecules [11, 21-24].

The three types of energy transfer mechanisms mentioned above are discussed separately in the remaining part of this chapter. In addition, a modified Förster theory for energy transfer developed by Small and coworkers [25] which is based on the Fermi-Golden rule is also presented. This theory has been successfully applied to explain the resilience of B800 → B850 energy transfer rates to pressure and temperature [13, 26] as well as to species and mutations which changes the B800-B850 energy gap by several hundred wavenumbers [27, 28].

2.2 Förster Energy Transfer

2.2.1 Conventional Förster Theory

Förster transfer between the excited state, D*, of donor molecules and acceptor molecules (A) in dilute solids or liquids where the average D-A separation distance is $\gtrsim$ 20 Å has been thoroughly studied [1]. (The trivial mechanism of reabsorption by A of the photon emitted by D* is easily distinguished from Förster transfer since it does not lead to a shortening of D*'s lifetime [29].)

In the limit of weak coupling between D and A molecules, the transition rate from the initial state $|D^*A\rangle$ to the final state $|DA^*\rangle$ is given by the Fermi-Golden rule [30]:

$$k_{ET} = \frac{2\pi}{\hbar}\left|\langle D^* A|V|DA^*\rangle\right|^2 \rho(E), \tag{2.1}$$

where V is the molecular interaction between D and A and $\rho(E)$ is the density of final states isoenergetic with the initial D* levels. $\rho(E)$ is referred to as the Franck-Condon factor weighted density of states associated with vibrations when the Condon approximation is employed, which is an excellent approximation for strongly allowed electronic transitions.

Strictly speaking, $\rho(E)$ depends on temperature. Förster theory assumes that thermalization of the molecular vibrations and bath phonons occurs on a faster time scale than energy transfer. V can be expressed by a multipole expansion [2, 31]. In Förster theory, the dipole-dipole approximation is employed so that the matrix element in Eq. (2.1) is

$$V_{dd} = \kappa |\vec{\mu}_D||\vec{\mu}_A| / R^3, \tag{2.2}$$

where $R \equiv |\vec{\mathbf{R}}_{DA}|$ is the distance from the center of molecule D to that of molecule A and $\vec{\mu}_D$ and $\vec{\mu}_A$ are the electronic transition dipoles of D and A, respectively. κ is the orientation factor defined as $\kappa \equiv \hat{\mu}_D \cdot \hat{\mu}_A - 3(\hat{\mu}_D \cdot \hat{\mathbf{R}}_{DA})(\hat{\mathbf{R}}_{DA} \cdot \hat{\mu}_A)$, which can range from –2 to 2. The circumflex symbol ^ denotes the unit vector associated with its corresponding vector, $\vec{\mu}_D$, $\vec{\mu}_A$ and $\vec{\mathbf{R}}_{DA}$, respectively. Figure 2.1 shows several relative $\hat{\mu}_D$-$\hat{\mu}_A$ orientations and the corresponding κ values. For a random distribution of dipole moments, $\kappa^2 = 2/3$. The neglect of higher order multipole interaction terms is justified except when the electronic transitions of D and A are only weakly allowed.

Förster showed that Eq. (1) can be expressed as [1, 29]

$$k_{ET} = \tau_f^{-1}(\overline{R}_0 / R)^6, \tag{2.3}$$

where τ_f is the empirical fluorescence lifetime of the non-interacting donor. $\overline{R}_0$ is the critical molecular separation defined by Förster [29] as

$$\overline{R}_0^6 = \frac{9000 \ln 10 \kappa^2 \eta_D^0}{128 \pi^6 n^4 N} \int_0^\infty f_D(\nu) \varepsilon_A(\nu) \frac{d\nu}{\nu^4}. \tag{2.4}$$

Here, η_D^0 is the quantum yield of the donor, n is the refractive index of the solvent, N is the Avogadro's number, ν is frequency in wavenumber, $f_D(\nu)$ is the spectral distribution of the donor fluorescence and $\varepsilon_A(\nu)$ is the molar decadic extinction coefficient of the acceptor. The integral in Eq. (2.4) defines the spectral overlap between the donor's fluorescence and the acceptor's absorption, which is equal to 1 for perfect overlap. When R equals $\overline{R}_0$, energy transfer time equals the fluorescence lifetime of D*. Based on experimental data, Duysens

$$\kappa \equiv \hat{\mu}_D \cdot \hat{\mu}_A - 3(\hat{\mu}_D \cdot \hat{\mathbf{R}}_{DA})(\hat{\mathbf{R}}_{DA} \cdot \hat{\mu}_A)$$

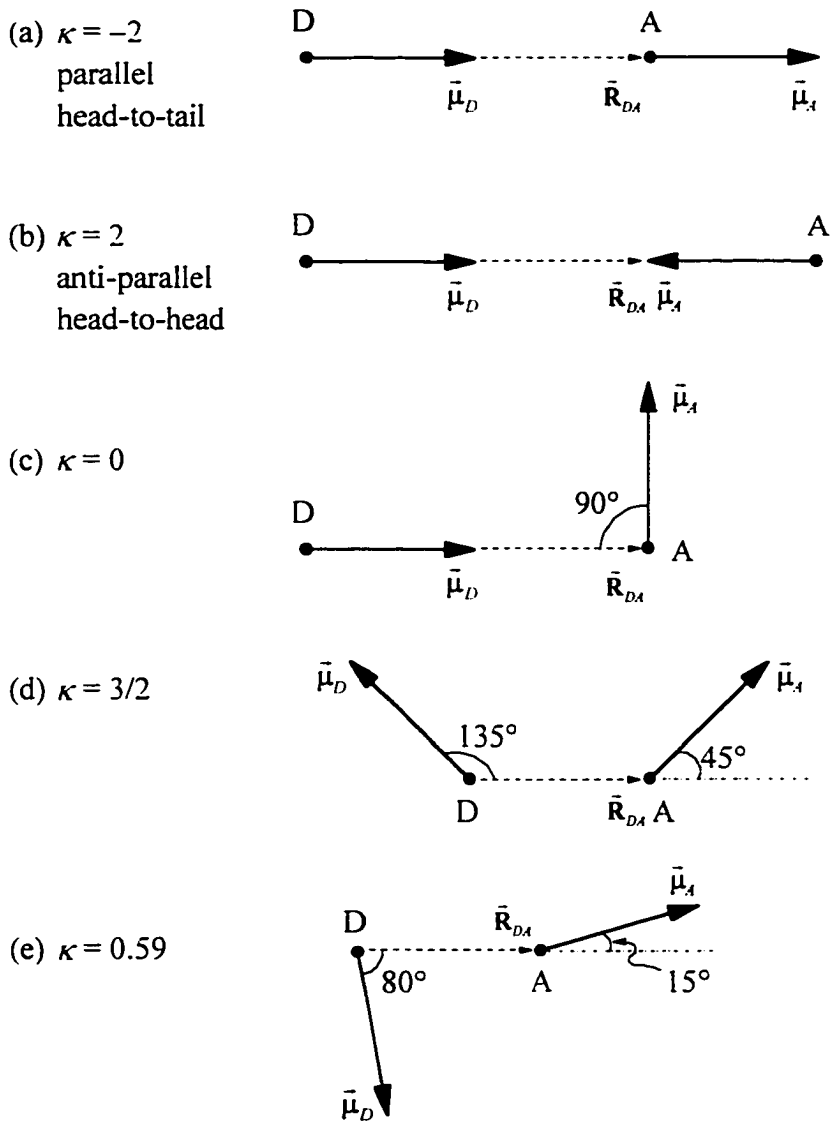

Figure 2.1 Examples of donor-acceptor arrangements and their corresponding orientation factors κ, which ranges from −2 to 2. The solid straight lines are the vectors of transition dipole moments ($\vec{\mu}_D$ and $\vec{\mu}_A$), while the dashed lines shows the vector ($\vec{\mathbf{R}}_{DA}$) connecting the donors and the acceptors (marked by the solid circles at one end of $\vec{\mu}_D$ or $\vec{\mu}_A$ vectors). Here $\vec{\mu}_D$, $\vec{\mu}_A$ and $\vec{\mathbf{R}}_{DA}$ are assumed to be in the same plane for illustration purpose, however, this assumption does not generally hold in real systems.

[32] reported that $\overline{R}_0 \sim 60$ Å for chlorophyll *a*, which is generally larger than the values (10 to 50 Å) for typical dye molecules in solution.

2.2.2 Implications and Validity of Assumptions Made in Conventional Förster Energy Transfer

Förster-type energy transfer for weakly coupled D and A molecules is expected to be dominant when the transitions involved are dipole-allowed. Due to the dipole-dipole nature of the coupling, the transfer rate is inversely proportional to the sixth power of the donor-acceptor distance R, Eq. (2.3). (Spin-flip energy transfer is not taken into account in Förster theory.) Fulfilling of the *co-linear* and the *resonance* conditions will optimize the transfer rate. The former condition is easily understood by examining Figure 2.1 and Eq. (2.4), which is proportional to κ^2. When the transition dipole moments of the donor and the acceptor are in line, either head-to-head or head-to-tail configuration, κ^2 is the largest with a value of 4. The meaning of *resonance* condition is demonstrated in Figure 2.2. The value of the spectral overlap integral, which defines the magnitude of overlap between donor fluorescence and acceptor absorption spectra, ranges from 0 to 1. The value of 1, which is the optimal value for Förster transfer, corresponds to perfect overlap. Since Förster theory assumes that the "hot" excited donor must undergo vibrational relaxation before energy transfer, the best spectral overlap will occur when the excitation energy transfers downhill from donor to acceptor, Figure 2.2 (a). That is, the energy transferred from D* to A is less than $h\nu$, the excitation energy of D. The difference in energy is lost in the thermalization process with the surrounding medium.

Long-distance energy transfer, however, has been observed in systems with forbidden transitions, either resulting from symmetry- or spin-forbiddenness. These transitions can become weakly allowed by mixing with proper molecular vibrations and with states having different multiplicities, respectively.

If the system has allowed-donor and forbidden-acceptor transitions, $\overline{R}_0$ will be small

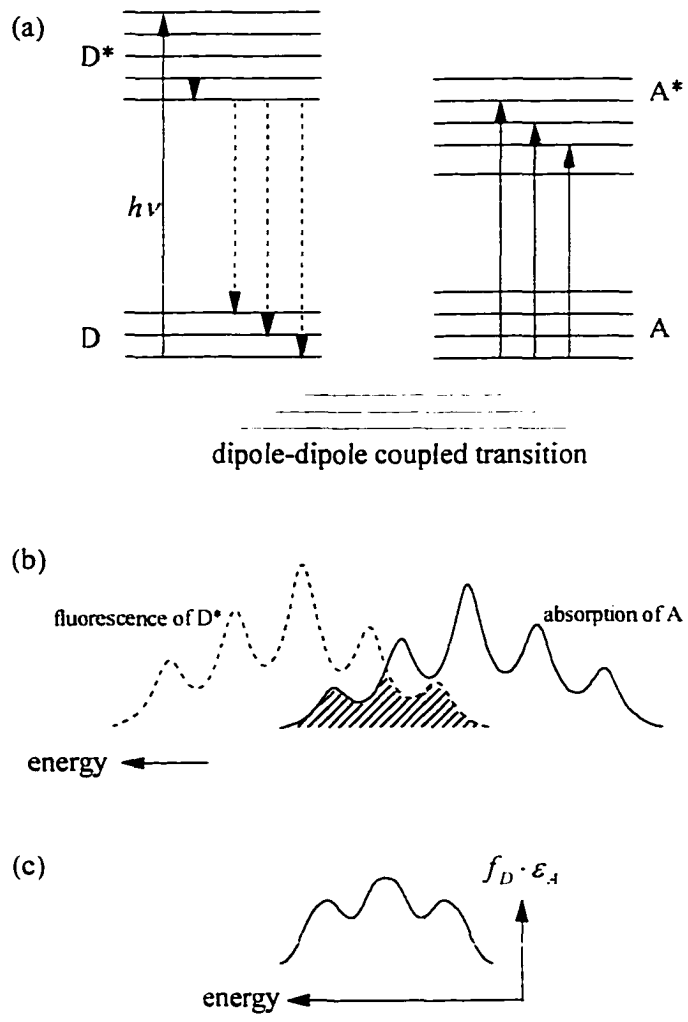

Figure 2.2 (a) A simplified energy level diagram showing the fulfillment of the *resonance* condition between the donor and acceptor. Following the excitation of energy $h\nu$. the donor molecule undergoes vibrational relaxation with the surrounding medium as shown by the wavy arrows. The energy is transferred to the acceptor which is in *resonance* with D* via the dipole-dipole coupling. For easy comparison, the ground states of D and A are offset to the same energy. (b) An illustration of the resonance condition by the spectral overlap (shaded area) between the donor's fluorescence (dashed line) and the acceptor's absorption (solid line). (c) A plot of the spectral overlap from (b). Due to the partial overlap as demonstrated in the figure, the value of the spectral overlap integral is between 0 and 1.

and energy transfer can be triggered by higher-order Coulombic coupling terms. As the donor-acceptor distance R decreases, the higher-order interactions plays more and more important role in the donor-acceptor coupling. As demonstrated by Dexter [3], to describe the energy transfer dynamics for this situation it is now necessary to include terms such as the dipole-quadrupole interaction which results in an inverse eighth power dependence on R. This type of energy transfer may be observed in systems which have dipole-forbidden transitions and R larger than the van der Waals radius (When the donor and the acceptor are within the van der Waals contact, energy transfer usually occurs via electron exchange, which is described in Section 2.3).

In Förster theory, after the donor is optically excited, vibrational relaxation, which takes place in ~ 1 ps, occurs prior to the transfer of energy to the acceptor. This assumption is not valid for energy transfer processes which occur on a sub-picosecond time scale. Again, Förster-Dexter theory is questionable for strongly coupled arrays of chromophores. As already mentioned, Förster theory is not applicable to systems in which the D and A optical transitions suffer from significant inhomogeneous broadening from structural heterogeneity. The structural heterogeneity leads to a distribution of D-A energy gap values which can result in dispersive (non-single exponential) kinetics for the $D^* \rightarrow A$ energy transfer process, see the following subsection. For example, the inhomogeneous broadenings of the Q_y-absorption transitions of photosynthetic complexes are ~ 100-200 cm^{-1}. (For example, the B800 and B850 bands of LH2 from *Rps. acidophila* exhibit an inhomogeneous broadening of 120 cm^{-1} at 4.2 K [21].)

2.2.3 Kolaczkowski-Hayes-Small (KHS) Theory for Weak Coupling Energy Transfer

In 1994, Small and coworkers developed a theory (KHS) which takes into account dispersive kinetics of energy transfer [25]. They took into account both the inhomogeneous and homogeneous broadening of the optical transitions in order to properly describe the excitation transfer kinetics observed in photosynthetic protein complexes. The theory allows

for calculation of energy transfer rates without having to resort to experimental spectra for the spectral overlap factor of Förster theory which, in any event, is a questionable thing to do when the spectral bands are inhomogeneously broadened. What is required for calculations with KHS theory are experimental values of Franck-Condon factors for pigment intramolecular vibrations and protein phonons, the width of the distribution of D-A energy gap values and the homogeneous and inhomogeneous contributions to the widths of the relevant spectral transitions. The electronic coupling matrix element must be calculated. The theory is valid for finite temperature. KHS theory has been shown to be in good agreement with electron transfer rates in photosystem II [33], energy transfer in light-harvesting complexes 2 from bacteria [13, 26, 27]. For brevity, only key equations involved in the derivation are included in this section. One can start by writing down the rate constant for adiabatic energy transfer as [34, 35]

$$k_{DA}(\Omega) = V^2 \int_{-\infty}^{\infty} e^{-i\Omega t} f(t)\, dt, \tag{2.5}$$

where Ω and V are the adiabatic electronic energy gap and the appropriate electronic coupling matrix element between the donor and the acceptor states. Note that circular frequency is chosen to be the energy unit here. The kernal $f(t)$ has the form of

$$f(t) = \int d\Omega\, G(\Omega) e^{i\Omega t}. \tag{2.6}$$

In Eq. (2.6), $G(\Omega)$ is the thermally averaged nuclear factor and its form depends on whether the phonon is localized or delocalized‡. By working within the Condon approximation and being guided by hole burning data, the appropriate form of $f(t)$ for delocalized phonons is

$$f(t) = \exp(-\tilde{S}) \exp\{S \exp(-\sigma^2 t^2/2)[(2\bar{n}+1)\cos(\omega_m t) + i \sin(\omega_m t)]\}, \tag{2.7}$$

---

‡ If the participation of high-frequency intramolecular vibrations is required due to a large donor-acceptor gap, the phonon contribution to the nuclear factor retains the form of Eq. (3) of Ref. [25] as for the delocalized phonons.

where $\bar{n} = [\exp(\hbar\omega_m / kT) - 1]^{-1}$ is the mean thermal occupation number for the phonons. In arriving at Eq. (2.7), a Gaussian function carrying a width of $\sim 2\sigma$ is used to approximate the one-phonon profile having a mean frequency of ω_m. S is the Huang-Rhys factor at 0 K which characterizes the electron-phonon coupling strength. In the mean phonon frequency approximation employed,

$$\tilde{S} = S \,\mathrm{ctnh}(\hbar\omega_m / 2kT). \tag{2.8}$$

The Franck-Condon factor for the zero-phonon process is in fact $\exp(-\tilde{S})$. $f(t)$ is further approximated by expanding Eq. (2.7) in terms of t and anything higher than quadratic terms is neglected. This approximation is valid for $(\omega_m t_{1/2})^2 < 1$ where $t_{1/2} = \omega_m^{-1}[2S(2\bar{n}+1)]^{1/2}$, and it is expected not to break down at temperatures much lower than ~ 50 K (see the argument presented in Ref. [25]). As discussed in Ref. [25], the zero-phonon process only plays a minor role in energy transfer for inhomogeneously broadened systems such as photosynthetic protein complexes. As a result, it will be of little consequence if the contribution from zero-phonon lines is deleted by introducing the multiplicative factor $[1 - \exp(-\tilde{S})]$ into $f(t)$. By taking the Fourier transform, the expression for energy transfer rate is obtained as

$$k_{DA}(\Omega, T) = 2\pi V^2 (1 - e^{-\tilde{S}})[(2\pi\tilde{S}(\sigma^2 + \omega_m^2))^{-1/2} e^{-(\Omega - S\omega_m)^2 / 2\tilde{S}(\sigma^2 + \omega_m^2)}] \tag{2.9}$$

where the electronic energy gap $\Omega = \omega_D - \omega_A > 0$.

Since the system considered is inhomogeneously broadened, it is necessary to average Eq. (2.9) with a proper distribution function f_Ω for Ω to address the problem of dispersive kinetics. If f_Ω adopts a Gaussian form, the averaged rate becomes

$$\langle k_{DA}(T) \rangle = 2\pi V^2 (1 - e^{-\tilde{S}})[2\pi(\Gamma^2 + \tilde{S}(\sigma^2 + \omega_m^2))]^{-1/2} e^{-(\Omega_0 - S\omega_m)^2 / 2[\Gamma^2 + \tilde{S}(\sigma^2 + \omega_m^2)]}. \tag{2.10}$$

Here Γ^2 is the variance for f_Ω. As pointed out in Refs. [25, 36], Γ^2 and $\tilde{S}(\sigma^2 + \omega_m^2)$ are, respectively, associated with inhomogeneous and homogeneous broadening. If the following condition

$$S(\sigma^2 + \omega_m^2) >> \Gamma^2 \tag{2.11}$$

is satisfied, $\langle k_{DA}(T) \rangle \approx k_{DA}(\Omega = \Omega_0, T)$. That is, the energy transfer kinetics is non-dispersive.

Eq. (2.9) and (2.10) can be modified to account for the electronic dephasing by substituting, everywhere, $\tilde{S}(\sigma^2 + \omega_m^2)$ by $\Sigma^2(T) \equiv (\tilde{\Gamma}/2)^2 + \tilde{S}(\sigma^2 + \omega_m^2)$. Here $\tilde{\Gamma}$ denotes the homogeneous broadening contribution from dephasing. Therefore, Eq. (2.10) is now

$$\langle k_{DA}(T) \rangle = 2\pi V^2 (1 - e^{-\tilde{S}})[2\pi(\Gamma^2 + \Sigma^2)]^{-1/2} e^{-(\Omega_0 - S\omega_m)^2/2(\Gamma^2 + \Sigma^2)}. \tag{2.12}$$

Analogous to Eq. (2.11), the criterion for non-dispersive kinetics becomes

$$\Sigma^2 = (\tilde{\Gamma}/2)^2 + \tilde{S}(\sigma^2 + \omega_m^2) >> \Gamma^2. \tag{2.13}$$

There are experimental data indicating that high frequency Franck-Condon modes can play significant roles in energy transfer by fulfilling the necessary spectral overlap requirement of Förster theory [13, 26]. Eq. (2.12) of KHS theory may be modified to include the contributions from intramolecular vibrations by writing it as

$$\langle k_{DA}(T) \rangle = 2\pi V^2 (1 - e^{-\tilde{S}})(2FC_{loc})[2\pi(\Gamma^2 + \Sigma^2)]^{-1/2} e^{-(\Omega_0 - \omega_{loc} - S\omega_m)^2/2(\Gamma^2 + \Sigma^2)}, \tag{2.14}$$

where ω_{loc} and FC_{loc} are the frequency and Franck-Condon factor for the intra-molecular vibration modes involved in the energy transfer [13, 26].

2.3 Energy Transfer via Electron Exchange Interactions

When the donor-acceptor separation is small, there will be an appreciable charge distribution overlap. Multipole expansion in the interaction energy V, which is used to evaluate the matrix elements in the Fermi-Golden Rule expression, Eq. (2.1), is no longer a good approach. The matrix element part in Eq. (2.1) has to be replaced by

$$\left| \sum_{i,j} \langle D^* A | \frac{q_i q_j}{r_{ij}} | DA^* \rangle \right|^2, \tag{2.15}$$

where the summation is carried out over all pairs of charges on D and A. By substituting the antisymmetrized spin-orbital functions into expression (2.15) and simplifying using the Condon-Slater rules and assuming that the ground and excited states on the donor molecule differ by only one spin-orbital ($u_n \neq u'_n$), and similarly for the acceptor molecule ($v_n \neq v'_n$), one obtains

$$\begin{aligned}
&\sum_{i,j}\langle D^* A|\frac{q_i q_j}{r_{ij}}|DA^*\rangle \\
&=\sum_{i,j}\langle u_1 u_2 u_3 \ldots u_n; v_1 v_2 v_3 \ldots v_m|\frac{q_i q_j}{r_{ij}}|u_1 u_2 u_3 \ldots u'_n; v_1 v_2 v_3 \ldots v'_m\rangle \\
&=\langle \phi_n(1)\phi_m(2)|\frac{1}{r_{12}}|\phi'_n(1)\phi'_m(2)\rangle\langle \sigma_n(1)|\sigma'_n(1)\rangle\langle \sigma_m(2)|\sigma'_m(2)\rangle \\
&-\langle \phi_n(2)\phi_m(1)|\frac{1}{r_{12}}|\phi'_n(1)\phi'_m(2)\rangle\langle \sigma_m(1)|\sigma'_n(1)\rangle\langle \sigma_n(2)|\sigma'_m(2)\rangle
\end{aligned} \tag{2.16}$$

where each spin-orbital function u_k or v_k equals the product of a space function ϕ_k and a spin function σ_k (either as spin up α or spin down β). The numbers 1 and 2 are dummy indices denoting the positions of the two electrons. The two terms in Eq. (2.16) represent the matrix elements resulting from the *Coulombic* and the *exchange* couplings. The former reduces to Förster theory in the dipole-dipole coupling approximation. The conservation of spins on both donor and acceptor molecules in Förster energy transfer is clear by examining Eq. (2.16), since the Coulombic term will vanish unless $\sigma'_n = \sigma_n$ and $\sigma'_m = \sigma_m$. Nevertheless, for exchange coupling, both $\sigma'_m = \sigma_n$ and $\sigma'_n = \sigma_m$ have to be satisfied during the energy transfer. Thus, energy transfer by electron exchange can occur when the spins of the donor and the acceptor are interchanged simultaneously during the process. This provides the mechanism for the triplet-triplet energy transfer, such as the deactivation of excited triplet BChl *a* by triplet carotenoid molecules.

The distance (R) dependence of $\langle \phi_n(2)\phi_m(1)|1/r_{12}|\phi'_n(1)\phi'_m(2)\rangle$ is rather complicated, but generally speaking it dies off rapidly as R increases. Following Dexter [3], the energy transfer rate can be expressed as

$$k_{ET} = K \cdot J \cdot \exp(-2R/L). \tag{2.17}$$

Here K is a constant related to the specific interaction involved, J is the normalized spectral overlap between D and A and L is a constant of the order of the molecular size.

Figure 2.3 is a simple pictorial diagram showing the Dexter energy transfer via electron exchange, as well as the diagram for energy transfer via Coulombic interactions. As shown in Figure 2.3 (a), the exchange interaction induces the simultaneous jumps of electrons 1 from D* to A* and 2 from A to D, which is different from Figure 2.3 (b) for Coulombic coupling where electrons remain in the same molecules. Actually the electron exchange coupling is a pure quantum mechanical property which rises from the *indistinguishability* of electrons in the presence of appreciable wavefunction overlap. Unlike Förster energy transfer which is feasible with R as large as tens of angstrom, Dexter type can only occur when the donor and the acceptor are in close contact (usually $\lesssim$ 5 Å).

2.4 Molecular Excitons

2.4.1 Mott-Wannier and Frenkel Excitons

As mentioned in Section 2.1, the excitation is delocalized in the strong coupling limit and is often referred to as an *exciton*, which is a term now widely used in photosynthesis. The term *exciton*, which originally derives from solid state physics, is introduced to denote its quasi-particle nature — the wave-like properties of delocalization and the particle-like properties of effective mass, definite momentum and energy.

The *Mott-Wannier exciton*, which is commonly observed in covalent solids such as Ge, Si and CdS and ionic crystals with large dielectric constants (such as Cu_2O), is actually an electron-hole pair weakly bound by an attractive electrostatic force, see Figure 2.4 (a).

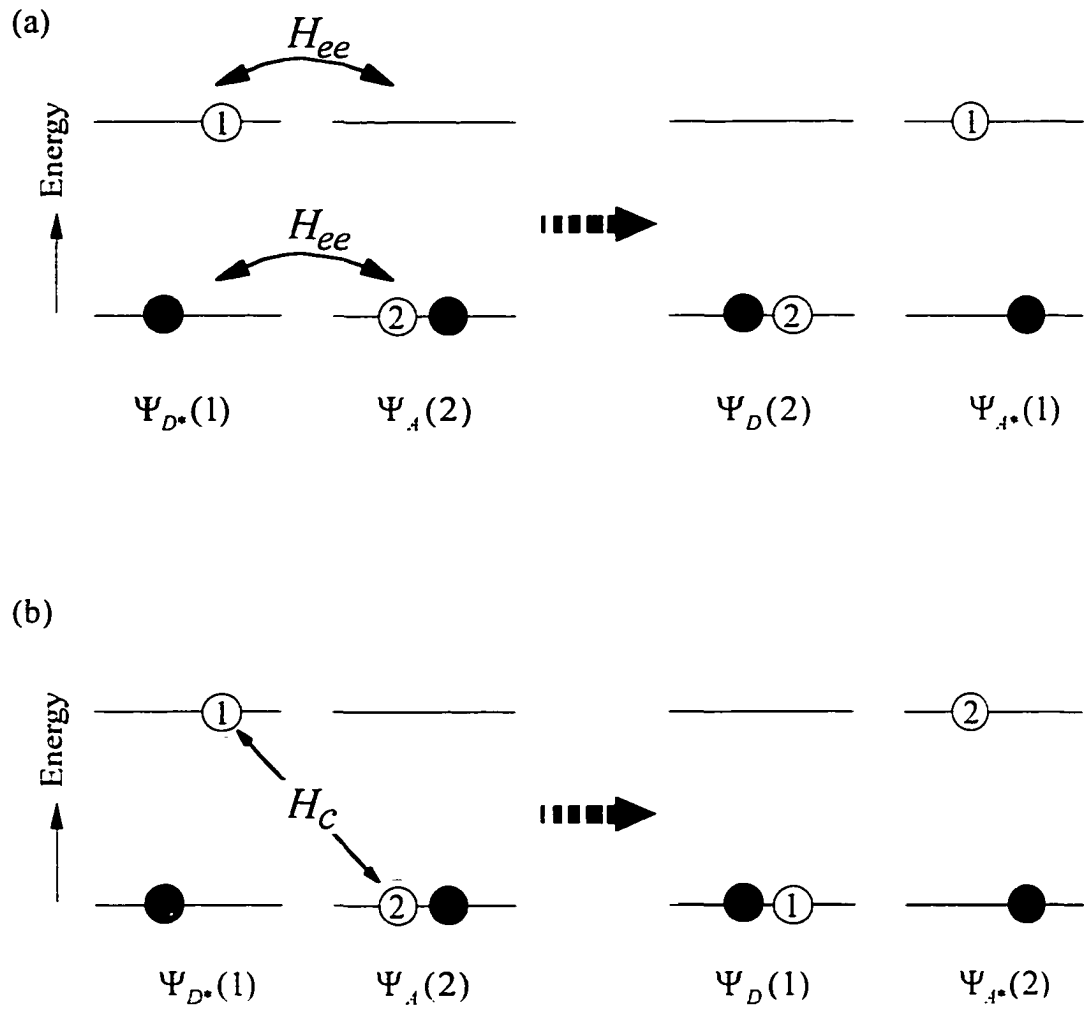

Figure 2.3 Schematic representation of excitation energy transfer via (a) electron exchange H_{ee} and (b) coulombic interactions H_c. The orbitals of the donor and the acceptor are depicted qualitatively by two-level systems with two electrons in each molecule. The *active* electrons are shown by open circles labeled as 1 and 2. The solid circles represent the *inactive* electrons whose interactions with others are nearly unaffected by the energy transfer processes. As shown in (a), exchange coupling induces simultaneous jumps of electrons 1 and 2 to the other molecules. In (b), the coulombic interaction makes electron 1 to return to the ground state and electron 2 is excited to the higher state.

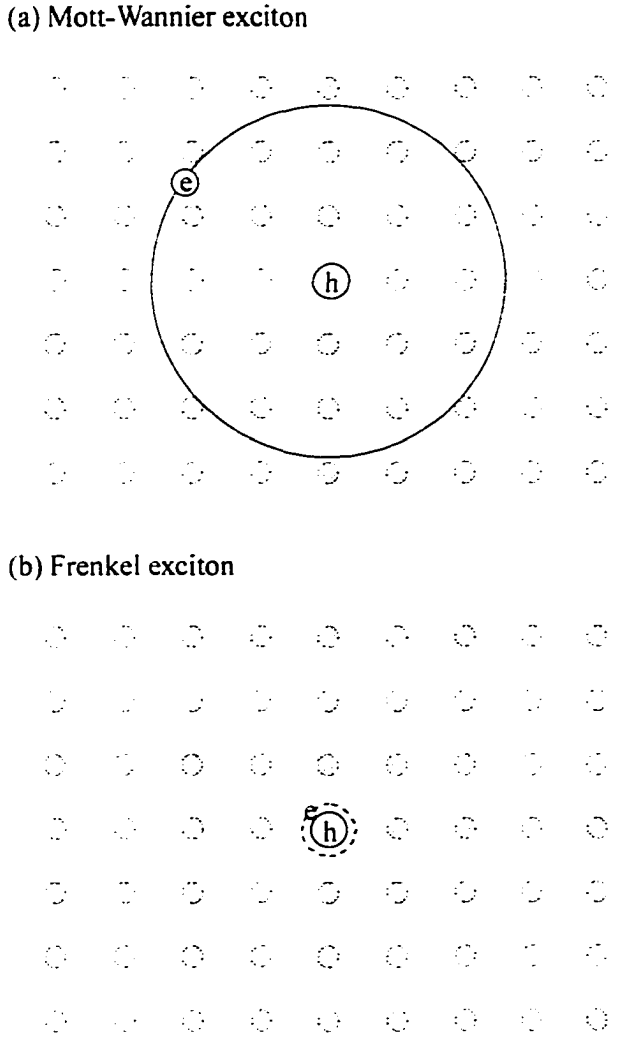

Figure 2.4 Conceptual illustration of Mott-Wannier exciton (a) and Frenkel exciton (b). The shaded circles shows the lattice molecules, while e and h label electrons and holes, respectively. In (a), the exciton is a bound electron-hole pair which moves as a unit in the crystal. The electron-hole separation is large relative to the lattice constant. In (b), it depicts a tightly bounding electron-hole pair confined within one molecule, which corresponds to an excited molecule. Due to the coupling with other molecules, this Frenkel exciton is not localized on one molecule. To correctly describe it quantum mechanically, it is necessary to use a superposition of wavefunctions of the entire lattice (i.e. in the Bloch wave form) due to the fact that there is equal probability for each molecule to be associated with the exciton.

The electron-hole separation is large compared with the lattice constant. Mott-Wannier excitons can propagate in the crystal to transport energy, but not electricity, due to the fact that they are charge-neutral. Readers interested in Mott-Wannier excitons may consult Refs. [4, 37-39] for further information.

Now consider the *tightly-bound* exciton which has the electron and the hole confined within one molecule. Actually, this essentially pictures an excited state of a single molecule, Figure 2.4 (b). Due to the coupling interactions between molecules in the crystal, the excitation energy will be passed from molecule to molecule like a wave instead of being localized on one site. This type of exciton is a collective electronic excitation of molecules, the *Frenkel exciton*, which has been thoroughly studied in molecular crystals such as naphthalene and anthracene. In a "perfect" crystal with no defects or phonons which undergo scattering with the exciton (meaning $T \rightarrow 0$ K), the Frenkel exciton is a perfectly delocalized state with a Bloch-type wavefunction. Every molecule in the crystal has an equal probability of being excited and for every level of the exciton band there is a definite phase relationship defined by the coefficients of the Bloch wavefunction. Thus, the concept of energy transfer loses its meaning. Of course, creation of a perfect Frenkel exciton in the laboratory is another matter, e.g. crystals have surfaces and there is no such thing as a perfect crystal. Nevertheless, exciton theory allows one to calculate band structures which can be used to calculate the group velocities (v_g) of exciton wavepackets with well-defined $\underline{\mathbf{k}}$, where $\underline{\mathbf{k}}$ is the wavevector. One can then define the exciton coherence length $l_{coh} = v_g/\gamma$, where γ is the scattering frequency (via defects or phonons) of the wavepacket. When l_{coh} >> a unit cell length, the exciton is referred to as delocalized. When l_{coh} is comparable to a unit cell length it is referred to as localized and energy transfer can then be treated as an incoherent hopping process [40, 41].

In recent years the term exciton has been widely used by workers interested in the nature of the excited electronic states of photosynthetic antenna complexes such as the cyclic

C_n LH2 and LH1 complexes of purple bacteria. With reference to earlier discussion of these complexes, it is clear that one is dealing with nano-excitons and, therefore, that the concepts of wavepacket velocity and coherence length are quite ill-defined. All that is implied by a "perfect" exciton of LH1 or LH2 is that it is completely delocalized with each BChl *a* molecules of the ring having an equal probability of being excited. The problem becomes more interesting when one realizes that proteins are glass-like, meaning that they are nothing like perfect crystals. Thus, the effects of energy disorder (diagonal or off-diagonal) become very important as discussed in Chapters 5 and 6. In the case of diagonal energy disorder, the exciton levels become localized in the limit of very strong disorder which is defined by the disorder-induced couplings between the zero-order exciton levels being much larger than the zero-order splittings between the exciton levels. As shown in Chapter 6, the B850 and B875 rings of LH2 and LH1, respectively, fall in the category of weak disorder, meaning that the exciton levels are neither perfectly localized or delocalized.

The following two subsections, 2.4.2 and 2.4.3 are a review of the Frenkel exciton theory in the static lattice approximation, meaning that exciton-phonon coupling is neglected as well as the effects of energy disorder.

2.4.2 An Excitonically Coupled Dimer — A Simple Example

Consider an isolated molecule with the eigenfunction φ^i and the eigenenergies E^i defined by the Hamiltonian H

$$H\varphi^i = E^i\varphi^i, \tag{2.18}$$

where $i = g$ or e denote the ground and excited states. Now introduce one more identical molecule into the system which couples with the other via the intermolecular potential energy V. The total wavefunction and energy for the system with both molecules in the ground state may be written as

$$\psi^g = \varphi_1^g\varphi_2^g \tag{2.19a}$$

$$\left\langle \psi^g \left| H_1 + H_2 + V \right| \psi^g \right\rangle = 2E^g + D^g, \tag{2.19b}$$

where the subscripts 1 and 2 denote the two molecules and $D^g \equiv \left\langle \psi^g \left| V \right| \psi^g \right\rangle$. The presence of the term D^g is the so-called *van der Waals interaction* or *dispersion energy* for the ground state.

The wavefunctions for the electronically excited dimer may be written as

$$\Psi(\pm) = 2^{-1/2}(\psi_1^e \pm \psi_2^e), \tag{2.20}$$

The coefficient $2^{-1/2}$ holds with the neglect of overlap between the two monomers. ψ_1^e and ψ_2^e are the wavefunctions describing excitation localized on molecules 1 and 2, respectively. That is,

$$\psi_1^e = \varphi_1^e \varphi_2^g \tag{2.21a}$$

$$\psi_2^e = \varphi_1^g \varphi_2^e. \tag{2.21b}$$

Eq. (2.20) gives the delocalized basis set (wavefunctions) for the excited dimer, while Eq. (2.21a-b) defines the localized states. The energy of the excited dimer is given by

$$\left\langle \Psi(\pm) \left| H_1 + H_2 + V \right| \Psi(\pm) \right\rangle = E^g + E^e + D^e \pm M, \tag{2.22}$$

where D^e and V are defined as followed

$$D^e \equiv \left\langle \psi_1^e \left| V \right| \psi_1^e \right\rangle = \left\langle \psi_2^e \left| V \right| \psi_2^e \right\rangle \tag{2.23a}$$

$$M \equiv \left\langle \psi_1^e \left| V \right| \psi_2^e \right\rangle = \left\langle \psi_2^e \left| V \right| \psi_1^e \right\rangle. \tag{2.23b}$$

Similar to D^g, D^e is the van der Waals interaction or dispersion energy but for the excited dimer. M, the *resonance transfer integral*, determines the resonance energy transfer time and the *dimer* (*exciton*) *splitting*. The relative orientation of the two molecules determines the sign of M. Figure 2.5 shows several examples of M with different monomer orientations in the dipole-dipole approximation. $(D^e - D^g)$ is the so-called *solvent shift* in the excitation energy between the isolated and coupled monomers. Usually, molecules in the excited state interact more strongly than in the ground state. As a result, the solvent shift causes a decrease in the excitation energy. See Figure 2.6 for an illustration of D^g, D^e and M. As

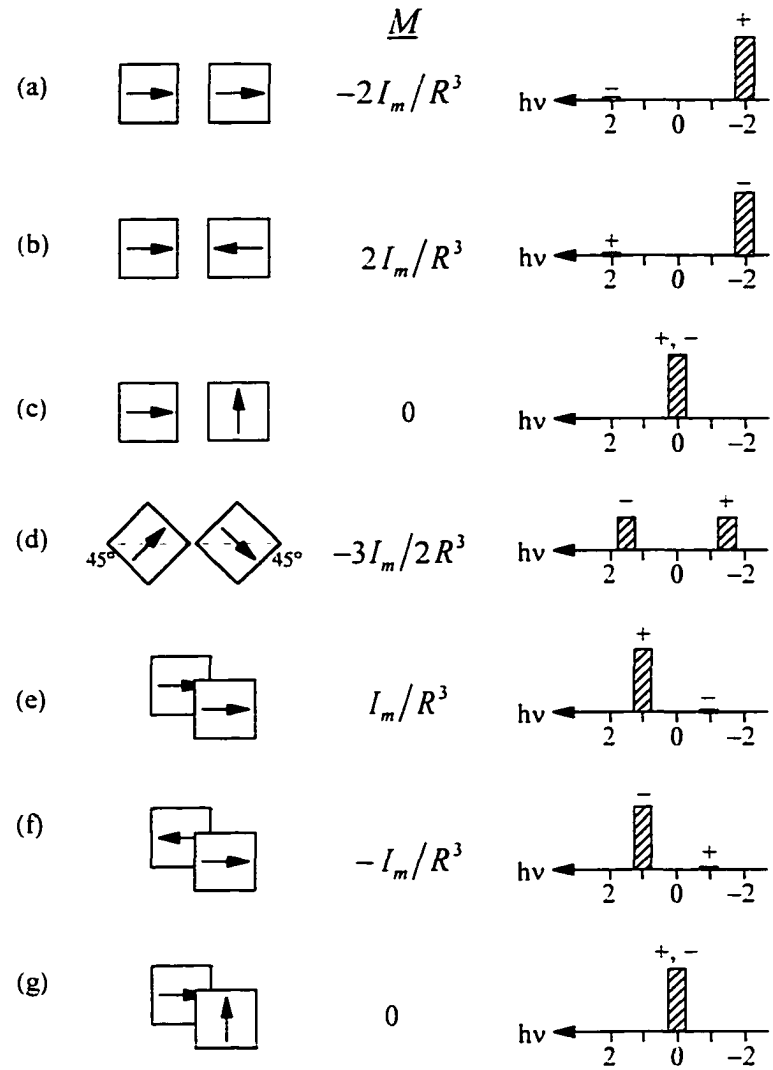

Figure 2.5 Schematic representations of seven dimer arrangements with their dimer splittings M, Eq. (2.23b), and their redistribution of oscillator strength. Although the squares and the associated arrows are meant to show the BChl (Chl) molecular planes and their Q_y transition dipole moments, they are applicable to other molecules with in-plane transition dipoles. Geometries (a) through (d) are co-planar, while (e) through (g) are stacked. The dimer splittings are calculated within the dipole-dipole approximation (Eq. (2.2)), i.e. $M = \kappa I_m/R^3$ where $I_m = |\vec{\mu}_1||\vec{\mu}_2| = |\vec{\mu}_1|^2 = |\vec{\mu}_2|^2$ is the transition dipole strength of the monomer. The right-most column qualitatively shows the spectra of the dimer with the energy ($h\nu$) in units of I_m/R^3 and the excitation energy of a monomer is defined as zero. + and – signs are used to label the wavefunctions $\Psi(+)$ and $\Psi(-)$. See text for further explanation.

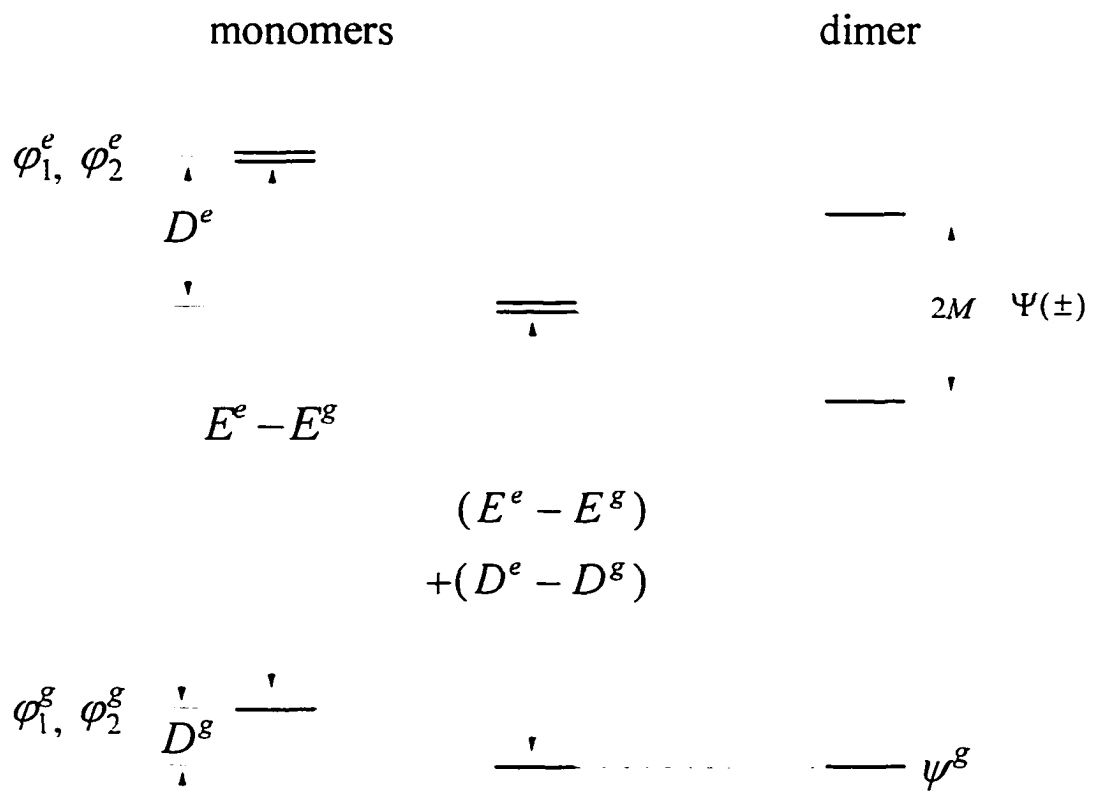

Figure 2.6 Energy level diagram of two isolated monomers and an excitonically coupled dimer. φ_i^g and φ_i^e (i = 1, 2) are the ground and the excited state wavefunctions for monomer i, respectively. For the dimer, ψ^g is the wavefunction for the ground state, while $\Psi(\pm)$ are the dimer (exciton) wavefunctions. The dispersion interaction between monomers introduced a decrease of $D^e - D^g$ in excitation energy, which is often referred to as the solvent shift. The exciton levels are further split by an energy of $2M$. The geometric arrangement of the two monomers determines which of the exciton wavefunctions $\Psi(\pm)$ will have higher energy, see Figure 2.5, as well as the magnitude and the sign of M. See text for further explanation.

indicated in Eq. (2.22), Figures 2.5 and 2.6, $\Psi(+)$ and $\Psi(-)$ are not degenerate, but are separated by a splitting of $2M$. The splitting of excited states is an important characteristic of excitonic behavior. In addition to this splitting, the formation of exciton is often accompanied with a redistribution of oscillator strength, which is described below.

The transition dipole strength of the dimer $I_d(\pm)$ from ψ^g to $\Psi(\pm)$ can be expressed in terms of I_m, the transition dipole strength of the isolated molecules

$$I_d(\pm) = \left| \langle \psi^g | \underline{\mu}_1 + \underline{\mu}_2 | \Psi(\pm) \rangle \right|^2 = I_m(1 \pm \cos\theta), \tag{2.24}$$

where θ is the angle between the transition dipole moments of the two monomers. $\underline{\mu}_1$ and $\underline{\mu}_2$ are the dipole moment operators for the two molecules. The right-most column of Figure 2.5 shows how $I_d(\pm)$, the transition dipole strength, varies with the angle θ.

In Figure 2.5(a), the head-to-tail arrangement having a κ value of -2 gives a negative M equal to $-2I_m / R^3$. According to Eq. (2.22), $\Psi(+)$ and $\Psi(-)$ are the lower and upper dimer states, respectively. Since $\theta = 0°$, I_d is $2I_m$ for $\Psi(+)$ and 0 for $\Psi(-)$, see Eq. (2.24). That is, the upper dimer component is transition forbidden. Similarly, one can generate the qualitative pictures as shown in Figure 2.5(b) through (g). Note that cases (a) and (b) are indistinguishable from a spectral point of view (only the lower dimer state is transition allowed). In (a) the lower dimer state is $\Psi(+)$, while in (b) it is $\Psi(-)$. In contrast to (a) and (b), where the transition dipoles lie in the same plane, (e) and (f) of the stacked configurations illustrate the situation where only the upper dimer components are transition allowed. In Figure 2.5(d), the two split dimer components are transition allowed and both carry a transition dipole strength equal to I_m. The dimer arrangements shown in Figure 2.5(c) and (g) have M values of zero and do not result in splitting or a redistribution of the transition dipole strength.

When the dimer states, $\Psi(+)$ and $\Psi(-)$, are spectrally well-resolved one can excite either of them selectively to initially create delocalized dimer states. The excitation energy

undergoes coherent oscillation between the two monomers with a frequency of M, with M in the unit of circular frequency. Strictly speaking, this oscillation does not represent energy transfer since it does not alter the initially excited level. For real energy transfer to occur, the excitation ultimately needs to be localized on one of the two monomers. Such localization could result from self-trapping due to exciton-phonon coupling or energy disorder when the dimer is imbedded in a bath. It is possible to initially create a state with excitation localized on one of the two monomers if the frequency width of the excitation pulse is wider than $2M$.

2.4.3 Extension from the Dimer to Molecular Crystals and Circular Aggregates

The aforementioned exciton for a Frenkel-like dimer can be easily extended to cover molecular aggregates and crystals. For a system containing n molecules, the wavefunction for the excitation energy localized on molecule α located at position $\underline{\alpha}$ is

$$\psi_{\alpha}^{e} = \varphi_{\alpha}^{e} \prod_{\alpha=0(\beta\neq\alpha)}^{n-1} \varphi_{\beta}, \tag{2.25}$$

where φ_{β} is the ground state wavefunction for molecule β and φ_{α}^{e} is the excited state wavefunction for molecule α. Eq. (2.25) is analogous to Eq. (2.21). Let H_{α} be the energy operator for the α-th molecule and $V_{\alpha\beta}$ be the interaction between molecules α and β. The Hamiltonian for the exciton states is

$$H = \sum_{\alpha} H_{\alpha} + \sum_{\alpha,\beta}{}' V_{\alpha\beta}. \tag{2.26}$$

A general solution to Eq. (2.26) is

$$\Psi(\underline{\mathbf{k}}) = n^{-1/2} \sum_{\alpha} \exp(i\underline{\mathbf{k}} \cdot \underline{\alpha})\, \psi_{\alpha}^{e}. \tag{2.27}$$

$\underline{\mathbf{k}}$ is the wavevector and is determined from the boundary conditions. Eq. (2.27) is of Bloch-wave form and is only true for the system with one molecule per unit cell. (Consult Ref. [5] for the analogous exciton wavefunction of Eq. (2.27) for crystals with more than one translationally inequivalent molecule per unit cell.) For a 3-dimensional crystal with only one molecule per unit cell,

$$\underline{\mathbf{k}} = \sum_{p=1}^{3} \frac{2\pi}{N_p} q_p \underline{\mathbf{b}}_p \,, \tag{2.28}$$

where $\underline{\mathbf{b}}_p$ (p = 1, 2 and 3) are the reciprocal lattice vectors defined according to the direct lattice vectors $\underline{\mathbf{a}}_{p'}$ as $\underline{\mathbf{b}}_p \cdot \underline{\mathbf{a}}_{p'} = \delta_{pp'}$. q_p is an integer confined within the range $-N_p/2 \le q_p \le N_p/2$. N_p satisfies the relation $n \equiv N_1 N_2 N_3$ when the crystal is assumed to be parallelepiped. For more details, see Ref. [5]. The delocalized basis set in the form of Eq. (2.27) for a cyclically coupled array, which is relevant to the light-harvesting complexes of purple bacteria, is given in the Appendix, Eq. (A.3). The Hamiltonian for a linear aggregate has been diagonalized and the expression for the exciton wavefunctions can be found in Refs. [42, 43].

As in the case of dimer, the degeneracy of the excited energy levels will be lifted to produce an exciton band. However, the band will span a range of ~ $4M$ for molecular crystals or circular aggregates (in the nearest neighbor approximation) instead of $2M$ as shown earlier for dimers.

2.4.4 Exciton-Phonon Coupling

So far in the discussion of excitons, it has been assumed that the molecules are fixed rigidly at the lattice points. In this section, the consequences of the molecular displacements from equilibrium positions in connection to excitons are discussed. This formulation was outlined for excitons in molecular crystals by Davydov [5].

To proceed, the Hamiltonian of the exciton is conveniently written in terms of the localized basis representation as

$$H_{ex}(\underline{\mathbf{R}}) = \sum_n [\varepsilon + \sum_m{}' D_{nm}(\underline{\mathbf{R}})] B_n^+ B_n + \sum_{n,m}{}' M_{nm}(\underline{\mathbf{R}}) B_m^+ B_n, \tag{2.29}$$

where ε is the free-molecule excitation energy for the transition of interest and B_n and B_n^+ are the annihilation and creation operators for the nth site, respectively. D_{nm} and M_{nm} are, respectively, the dispersion and resonance-energy transfer matrix elements between sites n and m. The term containing the summation of D_{nm}, which corresponds to D^e in Eq. (2.23a)

for a dimer, is the total interaction of the excited molecule with all of the ground-state molecules. The term M_{nm} governs the excitation energy transfer from molecule n to m. Similar to M of Eq. (2.23b), M_{nm} results in delocalization of the excitation energy and the exciton band. The presence of the D_{nm} and M_{nm} terms introduces the dependence on the lattice configuration $\underline{\mathbf{R}}$ into the Hamiltonian $H_{ex}(\underline{\mathbf{R}})$. Eq. (2.29) may be expanded in a Taylor series about $\underline{\mathbf{R}} = 0$, the equilibrium position, and all the terms higher than the linear term are discarded. Therefore, it becomes

$$H_{ex}(\underline{\mathbf{R}}) = H_{ex}(0) + H^{(1)}_{ex-ph} + H^{(2)}_{ex-ph}, \tag{2.30}$$

where

$$H_{ex}(0) = \sum_{n}[\varepsilon + \sum_{m}{}' D_{nm}(0)]B_n^{+}B_n + \sum_{n,m}{}' M_{nm}(0)B_m^{+}B_n \tag{2.31}$$

is the Hamiltonian for the non-deformed lattice which yield the crude adiabatic energies for the exciton levels. $H^{(1)}_{ex-ph}$ and $H^{(2)}_{ex-ph}$ are linear exciton-phonon coupling terms given by

$$H^{(1)}_{ex-ph} = \sum_{n,m}{}' B_n^{+}B_m \sum_{j=1}^{6}[R_n^j(\frac{\partial M_{nm}}{\partial R_n^j})_0 + R_m^j(\frac{\partial M_{nm}}{\partial R_m^j})_0] \tag{2.32a}$$

$$H^{(2)}_{ex-ph} = \sum_{n,m}{}' B_n^{+}B_n \sum_{j=1}^{6}[R_n^j(\frac{\partial D_{nm}}{\partial R_n^j})_0 + R_m^j(\frac{\partial D_{nm}}{\partial R_m^j})_0]. \tag{2.32b}$$

In these two equations, $j = 1, 2, 3, \ldots, 6$ denote the six (three translational and three rotational) degrees of freedom of the molecule. To see the physics behind $H^{(1)}_{ex-ph}$ and $H^{(2)}_{ex-ph}$ better, it is more convenient to express them in terms of the creation and annihilation operators $b^{+}_{s,\underline{\mathbf{q}}}$ and $b_{s,\underline{\mathbf{q}}}$ for an sth branch phonon of wavevector $\underline{\mathbf{q}}$ and the delocalized basis set operators $B^{+}(\underline{\mathbf{k}})$ and $B(\underline{\mathbf{k}})$. The Hamiltonian for the phonons in the absence of excitons is

$$H^{0}_{ph} = \sum_{s,\underline{\mathbf{q}}} \hbar\omega_s(\underline{\mathbf{q}})(b^{+}_{s,\underline{\mathbf{q}}}b_{s,\underline{\mathbf{q}}} + 1/2). \tag{2.33}$$

$B^{+}(\underline{\mathbf{k}})$ and $B(\underline{\mathbf{k}})$ are in the delocalized representation which diagonalize $H_{ex}(0)$ and are related to B_n by

$$B_n = N^{-1/2}\sum_{\underline{k}} B(\underline{k})\exp(i\underline{k}\cdot\underline{n}). \tag{2.34}$$

Now $H_{ex-ph}^{(1)}$ and $H_{ex-ph}^{(2)}$ become

$$H_{ex-ph}^{(1)} = N^{-1/2}\sum_{\underline{k},\underline{q},s} F_s(\underline{k},\underline{q})\, B^{+}(\underline{k}+\underline{q})\, B(\underline{k})(b_{s,\underline{q}} + b_{s,-\underline{q}}^{+}) \tag{2.35a}$$

$$H_{ex-ph}^{(2)} = N^{-1/2}\sum_{\underline{k},\underline{q},s} \chi_s(\underline{q})\, B^{+}(\underline{k})\, B(\underline{k})(b_{s,\underline{q}} + b_{s,-\underline{q}}^{+}). \tag{2.35b}$$

$F_s(\underline{k},\underline{q})$ and $\chi_s(\underline{q})$ characterize the exciton-phonon coupling strength which are given by

$$F_s(\underline{k},\underline{q}) = \sum_{j,m(\neq 0)} e_s^j(\underline{q})\beta_s^j(\underline{q})\left[\left(\frac{\partial M_{0m}}{\partial R_0^j}\right)_0 + e^{i\underline{q}\cdot\underline{m}}\left(\frac{\partial M_{0m}}{\partial R_m^j}\right)_0\right]e^{i\underline{k}\cdot\underline{m}} \tag{2.36a}$$

$$\chi_s(\underline{q}) = \sum_{j,m(\neq 0)} e_s^j(\underline{q})\beta_s^j(\underline{q})\left[\left(\frac{\partial D_{0m}}{\partial R_0^j}\right)_0 + e^{i\underline{q}\cdot\underline{m}}\left(\frac{\partial D_{0m}}{\partial R_m^j}\right)_0\right], \tag{2.36b}$$

respectively. $e_s^j(\underline{q})$ is the jth component of a unit polarization vector for the sth phonon branch with wavevector $\underline{q}$, while $\beta_s^j(\underline{q})$ is the *rms* amplitude of the corresponding motion [5, 44]. For more details regarding the derivation, see Refs. [5, 45-47].

The connecting bridges of Eqs. (2.35a-b) in the delocalized basis set and Eqs. (2.32a-b) in the localized basis set are the unitary-transformation-related Eq. (2.34) and

$$B(\underline{k}) = N^{-1/2}\sum_{n} B_n \exp(-i\underline{k}\cdot\underline{n}). \tag{2.37}$$

Section IV.A.4 of Ref. [47] provides a nice discussion relating the choice between delocalized and localized representations.

Let us proceed to examine the physical meanings behind $H_{ex-ph}^{(1)}$ and $H_{ex-ph}^{(2)}$. The former relates to the inter-site coupling terms M. When the lattice vibrates about its equilibrium positions, the interactions between molecules change accordingly. F_s in fact characterizes the coupling strength between the phonon modes and the inter-site interactions. $H_{ex-ph}^{(1)}$ is the term responsible for the elastic and inelastic scattering of the excitons from one $\underline{k}$ value to another. During the process, the total number of excitons remains the same while that of phonons changes. The simple diagrams in Figure 2.7 depict this scattering process.

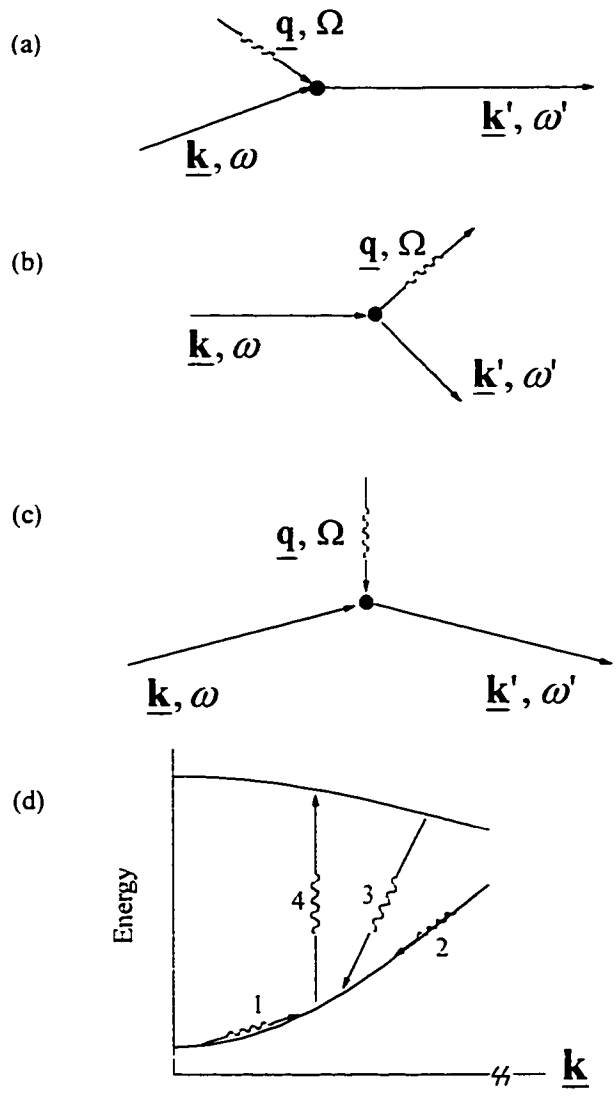

Figure 2.7 Vector diagrams (a-c) and a dispersion curve (d) showing examples of exciton-phonon scattering events (a-c). The exciton (solid arrows) having the wavevector $\underline{\mathbf{k}}$ and the frequency ω is scattered to an exciton state of $\underline{\mathbf{k}}'$ and ω'. The phonon (wavy arrows) absorbed or emitted in the process has a wavevector of $\bar{\mathbf{q}}$ and a frequency of Ω. Both the energy and the momentum conservation must be fulfilled in the scattering events. Processes (a), (c), 1 and 4 show phonon-absorption processes, while (b), 2 and 3 are for phonon-emission. Intra- and inter-exciton band scattering processes are depicted in 1-2 and 3-4, respectively. For crystals with more than one molecule per unit cell, inter-exciton band scattering may occur with no change in $\underline{\mathbf{k}}$ (governed by the coupling term Eq. (2.36b)), such as the process 4 in (d).

The term $H^{(2)}_{ex-ph}$. is diagonal in the delocalized representation and it is associated with the dispersion term D. The lattice vibration results in a fluctuation of the center of gravity of the exciton bands. χ_S characterizes how strong the change in exciton energy is with respect to the phonons. $H^{(2)}_{ex-ph}$ will shift the equilibrium configuration of the intermolecular coordinates to a new position, i.e. it causes a lattice deformation over the region the exciton excitation is distributed. If the lattice deformation is very large, the exciton will become localized. The name *polaron*† is introduced to refer to the exciton plus its accompanying lattice deformation under the influence of $H^{(2)}_{ex-ph}$.

Since $H^{(1)}_{ex-ph}$ and $H^{(2)}_{ex-ph}$ arises from different properties of the molecular crystals, their relative magnitude varies from system to system and depends on the electronic excitation of the same sample.

2.4.5 Inter-Exciton Level Relaxation Processes — Beyond the Condon Approximation

When the excitonic level splittings associated with the chromophores are large relative to the dephasing of the levels (i.e. in the strong coupling limit), the Condon approximation, which assumes that the electronic coupling is independent of the phonon coordinates, is no longer valid. In this strong coupling regime, the excitonic wavefunctions are determined by the Hamiltonian which already includes the static intermolecular potential energy. This is the potential that into Fermi-Golden rule expression of the Förster theory, see Section 2.2.1. The spectral density is a Franck-Condon factor weighted density of the final states of the energy transfer process. For strongly excitonically coupled systems such as the B850 molecules of LH2 and the B875 molecules of LH1, relaxation between exciton levels is induced by phonons which modulate the intermolecular pigment-pigment interactions. We refer to those phonons as promoting modes with coordinates Q_p (frequency ω_p). With V_{int} the interchromophore interaction, $(\partial V_{\text{int}} / \partial Q_p)_0 Q_p$ is the term that enters the Fermi-Golden rule

---

† The term polaron also often refers to an electron plus its lattice deformation in solid state physics.

when linear coupling in the phonon coordinate Q_p is assumed. One obtains for the downward inter-exciton level relaxation rate:

$$\frac{2\pi}{\hbar}\left|\left\langle \Psi^f \left|\left(\frac{\partial V_{\text{int}}}{\partial Q_p}\right)_0\right|\Psi^i\right\rangle\left\langle n_p+1\left|Q_p\right|n_p\right\rangle\right|^2 \rho(\Omega), \tag{2.38}$$

where Ψ^i and Ψ^f are the wavefunctions of the initial and final exciton levels, and Ω is the energy gap between the two levels. The phonon coordinate of the promoting mode can be expressed in terms of the creation and annihilation operators b^+ and b:

$$Q_p = (\hbar / 2\omega_p)^{1/2}(b_p + b_p^+). \tag{2.39}$$

Thus, Eq. (2.38) becomes

$$\frac{\pi}{\omega_p}(\bar{n}_p+1)\left|\left\langle \Psi^f \left|\left(\frac{\partial V_{\text{int}}}{\partial Q_p}\right)_0\right|\Psi^i\right\rangle\right|^2 \rho(\Omega-\omega_p), \tag{2.40}$$

where the argument of the spectral density ρ indicates that the effective energy gap has been reduced by one quantum of the promoting mode. $\rho(\Omega-\omega_p)$ is still a weighted density of states involving other phonons which are Franck-Condon active. Note that promoting modes need not be Franck-Condon active. In Eq. (2.40), $\bar{n}_p$ is the thermal occupation number, $[\exp(\hbar\omega_p / kT)-1]^{-1}$. In the high temperature limit, $(\bar{n}_p+1) \propto T$.

A more detailed treatment [5, 47] reveals that the electronic matrix element in Eq. (2.40) describes how the resonance energy transfer matrix elements associated with the excitonically coupled chromophores vary with Q_p.

2.5 References

[1] Förster, Th. *Ann. Physik* **1948**, *2*, 55.

[2] Struve, W. S. In *Anoxygenic Photosynthetic Bacteria*: Blankenship, R. E.; Madigan, M. T.; Bauer, C. E. Eds.; Kluwer: Dordrecht, 1995; Chapter 15.

[3] Dexter, D. L. *J. Chem. Phys.* **1953**, *21*, 836.

[4] Knox, R. S. *Theory of Excitons*, Academic Press: New York, 1963.

[5] Davydov, A. S. *Theory of Molecular Excitons*; Plenum Press: New York, 1971.

[6] Pearlstein, R. M. In *Photosynthesis*, Vol. 1; Govindjee Ed.; Academic Press: New York, 1982; Chapter 7.

[7] van der Laan, H.; Schmidt, Th.; Visschers, R. W.; Visscher, K. J; van Grondelle, R.; Völker, S. *Chem. Phys. Letts.* **1990**, *170*, 231.

[8] Shreve, A. P.; Trauman, J. K.; Frank, H. A.; Owens, T. G.; Albrecht, A. C. *Biochim. Biophys. Acta.* **1991**, *973*, 93.

[9] Reddy, N. R. S.; Small, G. J.; Seibert, M.; Picorel, R. *Chem. Phys. Letts.* **1991**, *181*, 391.

[10] Reddy, N. R. S.; Small, G. J. *J. Chem. Phys.* **1991**, *94*, 7545.

[11] Reddy, N. R. S.; Cogdell, R. J.; Zhao, L. Small, G. J. *Photochem. Photobiol.* **1993**, *57*, 35.

[12] Monshouwer, R.; de Zarate, I. O.; van Mourik, F.; van Grondelle, R. *Chem. Phys. Lett.* **1995**, *246*, 341.

[13] Chapter 3; Wu, H.-M.; Savikhin, S.; Reddy, N. R. S.; Jankowiak, R.; Cogdell, R. J.; Struve, W. S.; Small, G. J. *J. Phys. Chem.* **1996**, *100*, 12022.

[14] Koepke, J.; Hu, X.; Muenke, C.; Schulten, K. Michel, H. *Structure*, **1996**, 4, 581.

[15] Sauer, K.; Cogdell, R. J.; Prince, S. M.; Freer, A. A.; Isaacs, N. W.; Scheer, H. *Photochem. Photobiol.*, **1996**, *64*, 564.

[16] Sietermann, D. *Biochim. Biophys. Acta* **1985**, *811*, 325.

[17] Cogdell, R. J.; Frank, H. A. *Biochim. Biophys. Acta* **1987**, *895*, 63.

[18] Shreve, A. P.; Trautman, J. K.; Frank, H. A.; Owens, T. G.; Albrecht, A. C. *Biochim. Biophys. Acta* **1991**, *1058*, 280.

[19] Frank, H. A.; Farhoosh, R.; Aldema, M. L.; DeCoster, B.; Christensen, R. L.; Gebhard, R.; Lugtenburg, J. *Photochem. Photobiol.* **1993**, *57*, 49.

[20] Hu, X.; Ritz, T.; Damjanovic, A.; Schulten, K. *J. Phys. Chem. B* **1997**, *101*, 3854.

[21] Wu, H.-M.; Reddy, N. R. S.; Small. G. J. *J. Phys. Chem. B* **1997**, 101, 651.

[22] Reddy, N. R. S.; Picorel, R.; Small, G. J. *J. Phys. Chem.* **1992**, *96*, 6458.

[23] Wu, H.-M.; Reddy, N. R. S.; Cogdell, R. J.; Muenke, C.; Michel, H.; Small, G. J. *Mol. Cryst. Liq. Cryst.* **1996**, *291*, 163.

[24] Chapter 4; Wu, H.-M.; Ratsep, M.; Jankowiak, R.; Cogdell, R. J.; Small, G. J. *J. Phys. Chem. B* **1997**, *101*, 7641.

[25] Kolaczkowski, S. V.; Hayes, J. M.; Small, G. J. *J. Phys. Chem.* **1994**, *98*, 13418.

[26] Reddy, N. R. S.; Wu, H.-M.; Jankowiak, R.; Picorel, R.; Cogdell, R. J.; Small, G. J. *Photosynth. Res.* **1996**, *48*, 277.

[27] van der Laan, H.; De Caro, C.; Schmidt, Th.; Visschers, R. W.; van Grondelle, R.; Fowler, G. J. S.; Hunter, C. N.; Völker, S. *Chem. Phys. Letts.* **1993**, *212*, 569.

[28] Fowler, G. J. S.; Hess, S.; Pullerits, T.; Sundström, V.; Hunter, C. N. *Biochem.* **1997**, *36*, 11282.

[29] Förster, Th. *Discuss. Faraday Soc.* **1959**, *27*, 7.

[30] Atkins, P. W. *Molecular Quantum Mechanics*, 2nd Ed., Oxford: London, 1983, p.198.

[31] Hirschfelder, J. O.; Meath, W. J. *Adv. Chem. Phys.* **1967**, *12*, 3.

[32] Duysens, L. N. M. *Prog. Biophys.* **1964**, *14*, 48.

[33] Chang, H.-C.; Jankowiak, R.; Reddy, N. R. S.; Small, G. J. *Chem. Phys.* **1995**, *197*, 307.

[34] Kubo, R.; Toyozawa, Y. *Prog. Theor. Phys.* **1955**, *13*, 160.

[35] Englman, R. *Nonradiative Decay of Ions and Molecules in Solids*; North-Holland: Amsterdam, 1979.

[36] Small, G. J.; Hayes, J. M.; Silbey, R. J. *J. Phys. Chem.* **1992**, *96*, 7499.

[37] Dresselhaus, G. *Phys. Chem. Solids* **1956**, *1*, 14.

[38] Elliott, R. J. *Phys. Rev.* **1957**, *108*, 1384.

[39] Sturge, M. D. In *Excitons*, Rashba, E. I.; Sturge, M. D. Eds., North-Holland Publishing: Amsterdam, 1982, p.5.

[40] Silbey, R. *Annu. Rev. Phys. Chem.* **1976**, *27*, 203.

[41] Knox, R. S. *Top. Photosynth.* **1977**, *2*, 55.

[42] Hochstrasser, R. M.; Whiteman, J. D. *J. Chem. Phys.* **1972**, *56*, 5945.

[43] Fidder, H.; Knoester, J.; Wiersma, D. A. *J. Chem. Phys.* **1991**, *95*, 7880.

[44] Craig, D. P.; Dissado, L. A. *Chem. Phys.* **1976**, *14*, 89.

[45] Venkataraman, G.; Sahni *Rev. Mod. Phys.* **1970**, *42*, 409.

[46] Burland, D. M.; Zewail, A. H. *Adv. Chem. Phys.* **1979**, *40*, 369.

[47] Johnson, C. K.; Small, G. J. In *Excited States*: Lim, E. C. Ed.; Academic Press: New York, 1982; Vol. 6, p.97.

CHAPTER 3 FEMTOSECOND AND HOLE BURNING STUDIES OF B800'S EXCITATION ENERGY RELAXATION DYNAMICS IN THE LH2 ANTENNA COMPLEX OF *RHODOPSEUDOMONAS ACIDOPHILA* (STRAIN 10050)

A paper published in the *J. Phys. Chem.* **1996**, *100*, 12022.

H.-M. Wu, S. Savikhin, N. R. S. Reddy, R. Jankowiak, R. J. Cogdell,
W. S. Struve and G. J. Small

Abstract

One- and two-color pump/probe femtosecond and hole burning data are reported for the isolated B800-850 (LH2) antenna complex of *Rhodopseudomonas acidophila* (strain 10050). The two-color profiles are interpretable in terms of essentially monophasic B800→ B850 energy transfer with kinetics ranging from 1.6 to 1.1 ps between 19 and 130 K for excitation at or to the red of the B800 absorption maximum. The B800 zero-phonon hole profiles obtained at 4.2 K with burn frequencies located near or to the red of this maximum yielded a transfer time of 1.8 ps. B800 hole burning data (4.2 K) are also reported for chromatophores at ambient pressure and pressures of 270 and 375 MPa. At ambient pressure the B800-B850 energy gap is 950 cm^{-1} while at 270 and 375 MPa it is close to 1000 and 1050 cm^{-1}, respectively. However, no dependence of the B800→B850 transfer time on pressure was observed, consistent with data for the B800-850 complex of *Rhodobacter sphaeroides*. The resilience of the transfer rate to pressure-induced changes in the energy gap and the weak temperature dependence of the rate are consistent with the model that has the spectral overlap (of Förster theory) provided by the B800 fluorescence origin band and weak vibronic absorption bands of B850. However, both the time domain and hole burning data establish that there is an additional relaxation channel for B800 which is observed when

excitation is located to the blue of the B800 absorption maximum. Several explanations for this faster channel are considered including that it is due to intra-B800 energy transfer or a manifestation of coupling of B800 with quasi-degenerate upper exciton levels of the B850 molecules. The data indicate that it is not due to vibrational relaxation.

1. INTRODUCTION

The LH1 and LH2 light harvesting complexes of the purple bacterium *Rhodobacter sphaeroides* have proven to be excellent systems for the study of the excited state (Q_y) electronic structure and energy transfer dynamics of photosynthetic antennae. Progress in recent years has been especially impressive, due to the application of femtosecond and spectral hole burning spectroscopies (for a recent review see Sundström and van Grondelle [1]).

The LH1 complex (which appears to encircle the reaction center) and the distal LH2 complex of *Rb. sphaeroides* and *Rhodopseudomonas acidophila* are also referred to as B875 and B800-850 because they respectively give rise to bacteriochlorophyll *a* (BChl *a*) absorption bands at 875, 800 and 850 nm (room temperature wavelengths). Low temperature (4.2 K) absorption spectra of samples of the chromatophores and isolated B800-850 complexes used in this work are shown in Fig. 1. That the B800, B850 and B875 bands are well-resolved is but one reason why the two antenna complexes have received so much attention. This paper is concerned mainly with the B800-850 complex, specifically that of *Rps. acidophila* (strain 10050).

Structural models for LH2 put forth during the middle to late 1980s have in common an α,β polypeptide pair which binds one and two BChl *a* molecules at the cytoplasmic and periplasmic sides of the membrane, respectively (for a recent review see Zuber and Cogdell [2]). The former and latter BChl *a* molecules are associated with B800 and B850, respectively. There was general agreement that some type of cyclic arrangement of the α,β

pairs constituted the basic cell of LH2's two-dimensional lattice [2-5] and that pair-wise excitonic interactions between B850 molecules are considerably stronger than those between B800 molecules. Very recently, the X-ray structure of the B800-850 complex of *Rps. acidophila* (strain 10050) was reported at a resolution of 2.5 Å [6]. The structure revealed that this complex is a cyclic 9-mer of α,β pairs, meaning that B800 and B850 can be viewed as cyclic 9-mers of BChl *a* monomers and dimers, respectively. In this paper the B850 dimer referred to is the one with the shortest Mg...Mg distance (8.7 Å) between BChl molecules. Details of the structure will be considered in section IV. Suffice it to say now that the structure is entirely consistent with the excitonic interactions between B800 molecules (separated by 21 Å) being weak relative to those between B850 molecules.

Energy transfer from B800 to B850 molecules is rapid and occurs on a picosecond time scale, even in the low temperature limit. The nearest neighbor B800-B850 distance is 17.6 Å (Mg...Mg) [6]. Time domain studies with ~ 100 fs resolution led to B800→B850 transfer times of 0.7 ps and 1.2 ps at room temperature [7] and 77 K [8], respectively, for the isolated B800-850 complex of *Rb. sphaeroides*. van der Laan et al. [9] and Reddy et al. [10] used persistent nonphotochemical hole burning to arrive at a transfer time of 2.4 ps at liquid helium temperatures. The former and latter experiments were performed on the isolated complex from *Rb. sphaeroides* and chromatophores of the NF57 mutant of *Rb. sphaeroides* (which is devoid of B875), respectively. Reddy et al. [11] also reported that the B800→B850 transfer time for chromatophores of *Rb. sphaeroides* is 2.4 ps at 4.2 K. Later, they reported that the B800→B850 transfer time for the isolated LH2 complex of *Rps. acidophila* (strain 10050) is about 2 ps at 4.2 K [12].

The above works established that the temperature dependence of B800→B850 transfer kinetics is weak. As pointed out in ref. 10, this temperature sensitivity hinges, in part, on the nature of the broadening of the B800 and B850 bands (cf. Fig. 1). The B800 zero-phonon hole burning data of van der Laan et al. [9] and Reddy et al. [10] established that

at liquid He temperatures the B800 spectrum is largely inhomogeneously broadened due to the intrinsic "glass-like" structural disorder of proteins [13,14]. Such broadening is ubiquitous in chromophore-containing protein complexes and can be understood in terms of subtle differences in structure between members of the ensemble of protein particles being studied. In sharp contrast, the hole spectra of the B800-850 complex of *Rb. sphaeroides* [10] and *Rps. acidophila* [12] established that B850 is dominated by homogeneous broadening (Γ_h) with $\Gamma_h \sim 200$ cm^{-1}. Reddy et al. [10,12] attributed the homogeneous broadening to the excitonic level structure of B850 and ultra-fast inter-exciton level relaxation processes, an interpretation which is consistent with the X-ray structure of the B800-850 complex of *Rps. acidophila* [6] and recent femtosecond data [15,16]. They noted that because the homogeneous broadening is comparable to kT at room temperature, a weak temperature dependence for the B800→B850 energy transfer rate for *Rb. sphaeroides* might be expected. They proposed that the mechanism for B800→B850 transfer in *Rb. sphaeroides* is of the Förster type with spectral overlap provided mainly by Franck-Condon active BChl *a* vibrational modes near 750 and 920 cm^{-1}. They also concluded that, at low temperatures, spectral overlap between the B800 fluorescence origin or (0,0) band and the B850 absorption origin band makes a negligible contribution to the transfer rate. This is evident from the absorption spectra in Fig. 1 (especially for *Rps. acidophila*) when it is noted that the Stokes shift of the fluorescence associated with the B800 origin band is very small ~ 10 cm^{-1} at 4.2 K. The Stokes shift due to phonons is given by $\sim 2S\omega_m$ where S is the so-called Huang-Rhys factor and ω_m is the mean frequency of the phonons which couple to the optical transition [17]. For B800, S ~ 0.3 and $\omega_m \sim 30$ cm^{-1} [10] as will be discussed in section 4. Such weak electron-phonon coupling ($S\omega_m$ is the optical reorganization energy) and concomitant small Stokes shift for the Q_y-state is generally observed for chlorophylls imbedded in antenna proteins [13,14]. Stokes shifts of $\lesssim 10$ cm^{-1} have been measured for the LHC II complex of photosystem II [17] and the BChl *a* antenna complex of *P. aestuarii*

[18]. The fact that a protein is a solid eliminates the solvatochromic contribution of about 100 cm^{-1} to the Stokes shift seen for chlorophylls in solvents at room temperature [19].

In an interesting set of experiments, van der Laan et al. [20] determined that the B800→B850 transfer rate of *Rb. sphaeroides* in the low temperature limit is only weakly affected by mutations which reduce the energy gap to as small a value as 450 cm^{-1}. (The gap in Fig. 1 is 780 cm^{-1}.) This is consistent with the results of high resolution line narrowing experiments which showed that there is considerable Franck-Condon activity at 340 and 560 cm^{-1} [21,22]. These authors also presented an analysis of their results that provides some support for the aforementioned energy transfer model of Reddy et al. Very recently, Reddy et al. [23] reported on the effect of high pressure on the B800→B850 transfer rate of the NF57 mutant of *Rb. sphaeroides* at 4.2 K. The rate at a hydrostatic pressure of 680 MPa, which increases the B800-B850 energy gap to 900 cm^{-1}, was observed to be the same as that at ambient pressure, where the gap is 750 cm^{-1}. This resilience against pressure was explained in terms of the above model of Reddy et al. using the theory of Kolaczkowski et al. [24] together with the structure of the B800-B850 complex [6] and previously determined values for the parameters that enter into the Förster-type rate expression. Furthermore, the calculations yielded a transfer time of ~ 1 ps at room temperature (ambient pressure) and a weak temperature dependence (a factor of ~ 3 diminution in rate as the temperature is decreased from 300 to 4 K). It should be noted that these calculations took into account the homogeneous and inhomogeneous broadenings of the B800 and B850 absorption bands and circumvented the problem of measuring spectral overlap associated with weak vibronic transitions. However, they were incomplete in the sense that they ignored the details of the excitonic level structure of the B850 ring and assumed perfect cyclic symmetry. This assumption means, for example, that the dimers of B850 are energetically equivalent which, given the structure of the complex [6], means that only one exciton level carries significant absorption intensity [25,26].

As mentioned, femtosecond and hole burning data have indicated that ~ 200 fs relaxation processes among exciton levels of B850 do occur. Interestingly, the recent hole burning results of De Caro et al. [27] for B800 of the isolated *Rb. sphaeroides* complex indicate that an additional decay channel for excited B800 molecules appears when excitation occurs to the blue of the B800 band maximum. Earlier it had been reported that the zero-phonon hole burning efficiency significantly decreases for burn frequencies to the blue of the band maximum [9,10]. For frequencies to the red of the B800 band maximum, the zero-phonon hole width is constant, yielding the aforementioned 2.4 ps B800→B850 transfer time, while at 200 cm^{-1} to the blue of the maximum the relaxation time decreases to 0.90 ps [20]. The one-color femtosecond data (77 K) of Monshouwer et al. [8] also indicate the existence of an additional relaxation channel. Both works attribute the relaxation to some type of intra-B800 energy transfer process.

In this paper we report femtosecond pump-probe (one- and two-color) and hole burning data for the isolated B800-850 complex of *Rps. acidophila* (strain 10050). Ambient and high pressure hole burning data for chromatophores are also presented. The objectives of the experiments were to better characterize the B800→B850 energy transfer process, including its temperature and pressure dependences, and to determine whether or not the just mentioned additional decay channel for B800 exists for the above complex. The results establish that it does. Several models for this channel are considered.

2. EXPERIMENTAL

2.1. Femtosecond Studies

Femtosecond experiments were restricted to the isolated LH2 (B800-850) complex of *Rps. acidophila* (strain 10050) at ambient pressure.

The self-mode-locked Ti:sapphire laser and pump-probe optics have been described previously [28]. The existing radio-frequency (RF) multiple modulation scheme was

replaced with a new system, in which the probe beam detector photodiode was incorporated into an RLC prefiltering loop tuned to the RF detection frequency [29]. LH2 samples were housed between optical flats spaced by 0.5 mm in a window assembly in thermal contact with a 2.25 cm diameter Cu cold finger in an Air Products (Allentown, PA) DE202 closed-cycle He expander module. The sample temperature was directly monitored at the center of the LH2/glass medium using a calibrated Cu-constantan (type T) thermocouple. The pump and probe beams entered the sample through a low-birefringence quartz window, and exited through a sapphire window that contacted the Cu window assembly through an In foil gasket. The temperature differential between the center of the sample and the cold finger was 6 K when the cold finger was cooled to 13 K. The lowest temperature achieved was thus 19 K. LH2 samples were diluted in 0.1% LDAO buffer, and then mixed with glycerol in 1:2 proportions. In low-temperature experiments, samples were rapidly cooled to 140 K, then slowly (~ 10 minutes) to 130 K, and then rapidly to 19 K; this protocol yielded glasses with good optical quality.

In two-color pump-probe experiments, the Ti:sapphire laser was operated without an intracavity birefringent tuning filter, yielding output pulses with ~ 40 nm bandwidth. The pump and probe spectra were shaped using bandpass interference filters (CVI Corporation, Albuquerque, NM) with transmission curves nominally centered at 790, 800, 810, 830, 850, 860, 870 and 880 nm. The true center wavelengths for the transmitted pump and probe pulses were typically 788, 804, 812, 830, 851, 860, 866 and 880 ± 1 nm, with bandwidths ranging from 5.2 to 6.7 nm fwhm. Representative pump and probe pulse spectra are superimposed on LH2 19 K steady-state absorption spectrum in Fig. 2. While many combinations of pump and probe wavelengths could thus be studied, our ultrafast work focused on B800→B850 energy transfer kinetics, in order to make direct comparisons with the spectral hole burning component of this paper. The laser cross-correlation function between pump and probe pulses was simultaneously measured with each absorption

difference profile using a zero-background $LiIO_3$ crystal; the cross-correlations for most wavelength combinations were 210-250 fs fwhm.

2.2. Hole Burning Studies

Hole burning (non-photochemical) experiments at ambient pressure were performed on chromatophores and the isolated B800-850 complex of *Rps. acidophila* at 4.2 K. High pressure - hole burning experiments were performed with chromatophores at 4.2 K.

The hole burning apparatus has been discussed in detail [30]. Briefly, a Bruker HR 120 Fourier transform spectrometer was used for recording of pre-burn and post-burn absorption spectra. All spectra reported were obtained after a 100 scan average, at a resolution of 1 cm^{-1}. Zero-phonon holes (ZPH) burned into B800 were periodically measured at a resolution of 0.5 cm^{-1} and found to be no sharper than those recorded at a resolution of 1 cm^{-1} (as expected from previous studies [12] which showed that the homogeneous width of the B800 ZPH is in the range of 5-6 cm^{-1}). The burn laser was a Coherent CR 899-21 Ti:sapphire laser (linewidth of 0.07 cm^{-1}) pumped by a 15 W Innova Ar-ion laser. For ambient pressure experiments a Janis 8-DT convection cooling liquid helium cryostat was used. Samples were dissolved in a glycerol:water (0.1% LDAO, 2:1 by volume) glass-forming mixture and the solutions contained in a polypropylene tube.

The high pressure apparatus has been described in detail [30,31]. Briefly, hydrostatic pressures were generated by a three-stage hydraulic compressor (model U11, Unipress Equipment Division, Polish Academy of Sciences, Warsaw, Poland) using helium gas as the pressure transmitting medium. Pressure is delivered to a specially designed cell (Unipress) which is housed in a model 11 DT cryostat (Janis Research Co., Wilmington, MA). The high pressure cell cavity (7 mm diameter and 8 mm height) houses the sample which is contained in a double nested gelatin capsule. Details concerning measurement of pressure and

temperature and the procedure used to generate high pressures at low temperatures are given in ref. 31.

Burn intensities and times are given in the figure captions or text.

2.3 Materials

Isolated B800-850 complexes and chromatophores of *Rps. acidophila* and *Rb. sphaeroides* were prepared as described in Cogdell and Hawthornthwaite [32]. The isolation procedure is the same as that used in the work which led to the X-ray diffraction structure of the B800-850 complex of *Rps. acidophila*. The absorption spectra shown in Fig. 1 are the sharpest yet reported at 4.2 K; see, for example, those given in refs. 9-12. Thus, structural heterogeneity of the samples studied can be viewed as relatively minimal. It should also be noted that the bandwidths for the isolated B800-850 complexes are narrower than those of the chromatophores, suggesting that the isolation procedure was not disruptive.

3. RESULTS

3.1. Femtosecond Studies (ambient pressure)

Figure 3 shows a two-color LH2 absorption difference profile obtained at 19 K using the pump and probe wavelengths 805 and 880 nm. This pump wavelength excites at the B800 band maximum, while the probe wavelength lies to the red of the B850 band maximum at ~ 870 nm. The negative-going signal in Fig. 3 is dominated at all times by photobleaching and stimulated emission (PB/SE). This profile is well simulated by biexponential kinetics, with 1.60 ps PB/SE risetime and 188 ps decay time. Given the short time window in this figure (which highlights the early-time kinetics relevant to B800→B850 energy transfer), the slow PB/SE decay kinetics are not accurately determined here. χ^2 is not improved in a triexponential fit, which yields the PB/SE rise component 1.60 ps and the decay components 24 ps (major) and 416 ps (minor). Table 1 lists optimized parameters for multiexponential

fits to all of the two-color time-resolved profiles in this work. The 1.60 ps lifetime is associated with the B800→B850 energy transfer kinetics at this temperature. This lifetime has an uncertainty of ~ 0.20 ps.

Biexponential analysis of a two-color profile (not shown) obtained at 19 K using the pump wavelength 812 nm (at the red edge of the B800 band) and 880 nm probe wavelength in an 8 ps time window yields a 1.47 PB/SE rise component and a 316 ps decay component. The former lifetime component falls within error of the 1.60 ps kinetics in the 805→880 nm profile. The 805→880 nm profile differs from the 812→880 nm profile in that the latter shows a noticeably larger prompt PB/SE rise component (Table 1), and hence a smaller PB/SE component with finite risetime. Thus, the prompt PB/SE spectrum of B800 pigments directly excited at 812 show more intensity at 880 nm than pigments excited at 805 nm.

Figure 4 shows a set of 19 K two-color profiles obtained by exciting LH2 complexes at 810 nm and probing at the sequence of wavelengths 850, 859 and 866 nm. The *rise* behaviors of all three profiles are well simulated with single-exponential kinetics, with lifetimes 1.51, 1.60 and 1.62 ps, respectively (Table 1). Within our experimental uncertainty the differences in these values cannot be viewed as significant. The principal difference among these profiles is that, while the absorption difference signal is dominated throughout by PB/SE when the probe wavelength is 866 nm (and 880 nm, cf. Fig. 3), it is dominated by excited state absorption (ESA) for the probe wavelengths 850 and 859 nm. Since the rise kinetics are so similar in all cases, the profiles in Fig. 4 are attributable to formation of a B850 excited state(s) whose absorption difference spectrum exhibits an ESA → PB/SE zero-crossing point between 859 and 866 nm. Such a bipolar absorption difference spectrum qualitatively resembles the one observed for BChl *a* monomers in polar solvents [19]; however, the LH2 absorption difference spectrum may be complicated by the presence of 1-exciton → 2-exciton transitions.

The temperature dependence of our time-resolved B800→B850 energy transfer kinetics is summarized in Fig. 5, which superimposes 810→866 nm two-color profiles for the temperatures 19, 51 and 130 K. As at 19 K, the signal remains dominated at all times by PB/SE; the rise kinetics are accelerated at higher temperature. The PB/SE rise kinetics are well described using single-exponential components with lifetimes 1.62, 1.50 and 1.14 ps at 19, 51 and 130 K (Table 1). The rise amplitudes are similar for all three temperatures.

In Fig. 6, we show absorption difference spectra at fixed delays, assembled from two-color profiles excited at 783 nm (at the blue edge of the B800 band) and probed at ~ 5 nm intervals from 780 to 815 nm at 19 K. The spectral evolution during the first 400 fs are shown in the top portion of Fig. 6. The absorption difference spectrum at zero time is dominated by a major PB/SE peak near 800 nm, but it also displays a PB/SE shoulder at 785-795 nm that is not apparent in the steady-state absorption spectrum (cf. Fig. 2). During the first 400 fs, the major PB/SE peak increases slightly in intensity and red-shifts to ~ 805 nm, while the PB/SE shoulder between 785 and 795 nm declines. The cumulative effect resembles redistribution of PB/SE signal from the shoulder to wavelengths slightly to the red of the prompt PB/SE peak at ~ 800 nm. Analysis of a 783→795 nm two-color profile in a 24 ps window (one of the profiles used to assemble Fig. 6, not shown) reveals a 400 fs PB/SE decay component, while analysis of a 783→810 nm profile in the same window shows a 380 fs PB/SE rise component. At later times (400 fs to 8 ps, bottom of Fig. 6), the 805 nm PB/SE peak undergoes little spectral shifting, but decays in magnitude as electronic excitation leaves the B800 antenna. Concomitantly, the apparent baseline of the absorption difference signal between 780 and 815 nm grows more positive, due to growth of B850 ESA during B800→ B850 energy transfer. Analysis of individual two-color profiles used in compiling Fig. 6 typically shows ESA rise components of 1.8-1.9 ps for probe wavelengths between 800 and 815 nm. This is, within experimental uncertainty, the same value as stated earlier for the B800→B850 energy transfer time. The overall spectral evolution during the first 400 fs (top

of Fig. 6) is clearly not well described by hole (transient)-broadening. It is not consistent with the spectral evolution expected for vibrational cooling or IVR in pigments with small intramolecular Huang-Rhys factors ($S \leq 0.05$); in such a case, the PB/SE band maximum is not expected to red-shift [33]. It similarly appears unlikely that the 400 fs kinetics arise from dielectric relaxation since the required large amplitude protein motions are frozen out at 19 K. However, the spectral evolution qualitatively resembles that which would be observed in the case of energy transfer among diagonally disordered B800 pigments. In this picture, 783 nm preferentially excites pigments near the blue edge of the B800 spectrum, producing a PB/SE spectrum peaking near 800 nm (Fig. 6). Downhill energy transfers to lower-lying B800 pigments would then yield a red-shifted absorption difference spectrum, exhibiting diminished PB/SE from 785 to 795 nm and a Stokes-shifted band maximum. Such an interpretation raises questions about how subpicosecond energy transfers can occur among B800 pigments that are presumably weakly coupled. Alternatively, the spectral evolution can be viewed as uniform photobleaching of the B800 steady-state spectrum, with an SE spectrum that red-shifts during the first few hundred femtoseconds.

In Fig. 7, we show individual two-color profiles for the B800 antenna pumped at eight different wavelengths from 778 to 810 nm, and probed at the fixed wavelength 808 nm at 19 K. The profiles obtained using the pump wavelengths 778 through 800 nm can be qualitatively understood in terms of the absorption difference spectra in Fig. 6. Analyses of the profiles for pump wavelengths ≤ 797 nm yield substantial 400-480 fs PB/SE rise components of varying amplitude, and a 1.8-1.9 ps ESA rise component. Again, the latter is attributed to B800→B850 energy transfer. Anomalies occur when the pump and probe spectra overlap significantly, i.e. for the pump wavelengths 805 and 810 nm. In this case, the profiles appear to be perturbed by electronic coherence and oscillations, with the result that the 810→808 PB/SE decay profile becomes convex. This example emphasizes the potentially misleading kinetics that may be derived from one-color profiles.

The femtosecond components in Figs. 6-7 are not easily rationalized in terms of recent exciton model simulations of B800-850 electronic structure, based on the known crystallographic structure [6] of the LH2 complex from *Rps. acidophila* (see section IV). While the spectral evolution in Fig. 6 suggests that they could arise from intra-B800 processes, we searched for evidence of components with lifetimes in the hundreds of femtoseconds in B800→B850 two-color experiments. In particular, a 789→846 nm profile (not shown; excited at the blue edge of the B800 spectrum, and probed in the B850 absorption region), was analyzed using several alternative models. Like the 810→859 and 810→850 profiles in Fig. 4, this profile was dominated by ESA at all times. An analysis using *freely varied* lifetime and amplitude parameters yielded a ESA rise component with ~ 30 fs (i.e. essentially prompt) lifetime. A slightly poorer fit could be achieved by fixing this lifetime at 400 fs, but only at the expense of introducing a ~ 90 fs shift in the time origin. Such a shift is unphysically large, given the group velocity dispersion in our pump-probe apparatus. We conclude that the maximum risetime of the "prompt" component in our B800 →B850 two-color experiments is ~100 fs (probably lower), and that there is no component in these energy transfers analogous to the ~400 fs processes observed in the B800 spectral evolution.

3.2. Hole Burning Studies (ambient pressure)

In this and the following subsection the uncertainty in the reported zero-phonon hole (ZPH) widths (FWHM) is ± 0.4 cm^{-1}. This uncertainty in width leads to a ± 0.2 ps uncertainty in the reported relaxation times. ZPH of $\lesssim$ 10% depth were used.

Results are presented first for the isolated B800-850 complex of *Rps. acidophila*. The arrows (a-f) in the 4.2 K B800 absorption profile shown in Fig. 8 locate the burn wavelengths used. The B800 absorption maximum lies at 802 nm (12,465 cm^{-1}). The inset shows 1 cm^{-1} resolution scans of ZPH a and e over a 50 cm^{-1} range. The energies of the burn wavelengths

(in cm^{-1}) and the ZPH widths are given in the caption. The data show that the widths for holes a-d are the same within our experimental uncertainty. Averaging of these four widths leads to a B800→B850 transfer time of 1.8 ± 0.2 ps [12] which is within experimental uncertainty equal to the value of 1.6 ps at 19 K given in the preceding subsection. However, holes e and f, which lie 30 and 65 cm^{-1} to the blue of the B800 absorption maximum, carry larger widths of 8.3 and 10.2 cm^{-1}. The latter width would correspond to a depopulation relaxation time of 1.0 ps. This time is longer than the ~ 400 fs relaxation time (19 K) deduced from the femtosecond two-color experiments of the preceding subsection, but the pump frequency used there is 160 cm^{-1} to the blue of hole f.

Figure 9 shows the 4.2 K B800 absorption profile peaking at 804 nm (12,445 cm^{-1}) for *Rps. acidophila* chromatophores with burn wavelengths indicated by arrows a-h. ZPH widths, %- hole depths and burn fluences are given in Table 2. As was the case for the isolated complex, the ZPH width remains constant until the burn frequency is located to the blue of the B800 maximum. The average of the widths for holes a-d yields a B800→B850 transfer time of 2.3 ± 0.2 ps, which is 30% longer than for the isolated complex. That the data suggest that the width may begin to increase at hole e is not convincing given our stated experimental uncertainty. The widths of holes g and h, located 80 and 105 cm^{-1} to the blue of the B800 maximum are, however, significantly larger but are given only as > 10 cm^{-1} because of poor signal to noise. Hole g, after significant smoothing, is shown in the inset along with hole b. The unsmoothed profiles for holes g and h (not shown) indicate that their widths are no wider than 12 cm^{-1}. Inspection of the %-hole depths and burn fluences given in Table 2 reveals that the hole burning efficiencies for holes g and h are about a factor of 7 lower than for holes a-c. Taking the width of hole g as 10 cm^{-1} and that of holes a-c as 4.7 cm^{-1} one would predict, under the assumption that the rate constant for nonphotochemical hole burning is constant over the burn frequency range, that [34] the efficiency for hole g should be about a factor of 5 lower with half of the diminution due to the reduction in

induced absorption rate and the other half due to a reduction in nonphotochemical hole burning quantum yield. Given our experimental uncertainty this predicted factor is viewed as being in reasonable agreement with the experimental value of 7. We add that the procedure used here and in ref. 34 to determine the hole burning efficiency is not the most accurate. One needs to monitor the hole growth kinetics at each burn frequency in real time as described in ref. 34. Preliminary results from such experiments have been obtained and confirm the very significant decrease in burning efficiency as the burn frequency is tuned to the blue of the B800 absorption maximum.

In summary, the time-resolved and hole burning data (ambient pressure) indicate that an additional relaxation channel exists for B800 molecules whose excitation energies lie to the blue of the B800 absorption maximum by $\gtrsim$ 50 cm^{-1}.

3.3. High Pressure - Hole Burning of Chromatophores

Figure 10 shows the absorption profile of B800 at a pressure of 270 MPa, 4.2 K. Relative to its value at ambient pressure, the B800 maximum has shifted 25 cm^{-1} to the red. This, together with the small pressure broadening of 15 cm^{-1}, is consistent with the detailed high pressure data reported in ref. 23 for the isolated B800-850 complex of *Rb. sphaeroides* and its chromatophores. At 270 MPa the B800-B850 energy gap, relative to its value of 950 cm^{-1} at ambient pressure, is increased to 990 cm^{-1} (an increase which is also consistent with the results of ref. 23). The burn wavelengths used at 270 MPa are indicated by arrows a-f in Fig. 10. The inset of Fig. 10 shows the profiles for holes b and d. Results analogous to those in Table 2 are given in Table 3. The widths for the two lowest energy holes are, within experimental uncertainty, the same as those obtained for holes a and b in Fig. 9, see Table 2. Thus, increasing the B800-B850 energy gap to 990 cm^{-1} does not have a significant effect on the B800$\rightarrow$B850 energy transfer rate for excitation to the red of the B800 maximum. An increase in holewidth occurs for higher energy burn frequencies, beginning at hole c (width

of 7.7 cm^{-1}). This hole is located at the B800 maximum, 12,420 cm^{-1}. Inspection of the %-hole depths and burn fluences in Table 3 suggests again that the increase in holewidth with increasing burn frequency may be related to decreasing hole burning efficiency. The efficiencies for holes b-f are a factor of about 3, 5, 6, 10 and 14 lower than that of hole a. Comparison of the data in Tables 2 and 3 indicates that a pressure of 270 MPa causes the onset of the additional B800 decay channel, measured relative to the B800 maximum, to be shifted about 50 cm^{-1} to the red relative to its value at ambient pressure. We believe this observation may be important for understanding the decay mechanism, cf. following section. Finally, hole burning was performed on a different sample from the same batch at a pressure of 375 MPa. At this pressure the B800-B850 energy gap is 1050 cm^{-1}. Results analogous to those in Tables 2 and 3 are given in Table 4. The B800 absorption maximum lies at 12,415 cm^{-1}. The burn frequencies range from near the maximum and to the red since we were primarily interested in seeing whether the B800→B850 energy kinetics associated with excitation on the red side of B800 would be different. Comparison of the widths of the ZPH in Table 4 with those of holes a-d in Table 2 and a and b of Table 3 indicates that, within the experimental uncertainty of ± 0.4 cm^{-1} (± 0.2 ps), pressures up to 375 MPa have, at most, a weak effect on the kinetics of B800→B850 transfer.

4. DISCUSSION

The hole burning and femtosecond data presented speak to two problems associated with energy relaxation dynamics of the B800-850 complex. We refer to the first as the Förster B800→B850 energy transfer problem because, for many years, this transfer has been attributed to some type of Förster-based mechanism, i.e. the coupling between B800 and B850 molecules was taken to be weak. The X-ray structure of the B800-850 complex of *Rps. acidophila*, calculations based on the coordinates [26] and hole burning data [12] provide support for the assumption of weak coupling. The second problem is that of the additional

B800 relaxation channel whose existence is confirmed here both for the chromatophores and the isolated complex of *Rps. acidophila* (strain 10050). That this channel exists in chromatophores is important because, otherwise, it could be suggested that it is a consequence of the procedure used to isolate the B800-850 complex.

4.1. Förster B800→B850 Energy Transfer

Based on the room temperature absorption spectra of the B800-850 complex it would not be unreasonable to suggest that the transfer stems from spectral overlap between the tails of the B800 origin fluorescence and B850 origin absorption bands. However, the fact that the kinetics for transfer in the low temperature limit are only about a factor of 3 slower than at ambient temperature and 4.2 K spectra of the type shown in Fig. 1 establish that this "electronic resonance" mechanism is not viable, cf. Introduction. Rather, and as pointed out by Reddy et al. [10], Förster transfer appears to occur by virtue of intramolecular BChl *a* vibrations with frequencies in the vicinity of the B800-B850 energy gap. In addition, and as discussed in ref. 10, utilization of the Förster spectral overlap criterion is invalid when spectral bands suffer from significant inhomogeneous broadening (one of the assumptions of Förster theory is that spectral bands are homogeneously broadened). This problem and that associated with the measurement of spectral overlap associated with weak vibronic transitions can be circumvented provided the relevant Franck-Condon factors for intramolecular and protein phonon modes and homogeneous and inhomogeneous broadenings of spectral bands are known. Reddy et al. [23] used the following rate expression, based on the theory of ref. 24, for analysis of the pressure dependence of the B800→B850 energy transfer kinetics in *Rb. sphaeroides*:

$$< k_{DA} > = 2\pi n^{-4} V^2 \left(1 - e^{-\tilde{S}}\right) (2FC_{loc}) \left[2\pi\left(\Gamma^2 + \Sigma^2\right)\right]^{-1/2}$$
$$\times \exp - \left[(\Omega_o - \omega_{loc} - S\omega_m)^2 / 2\left(\Gamma^2 + \Sigma^2\right)\right]. \quad (1)$$

Here, V is the electronic coupling (unit of circular frequency), ω_{loc} and FC_{loc} are the frequency and Franck-Condon factor for the BChl acceptor mode, Γ^2 is the variance of the donor-acceptor electronic energy gap, Σ^2 is the variance of a homogeneous broadening factor, Ω_o is the average value of the D-A energy gap and n is the refractive index. $\tilde{S}(T)$ is S ctnh($\hbar\omega_m$/2kT), where ω_m is the mean frequency of the low frequency phonons involved as acceptor modes and S is the Huang-Rhys factor for the phonons. Σ is also temperature dependent:

$$\Sigma^2(T) \sim \tilde{S}(T)\left(\sigma^2 + \omega_m^2\right) + \left(\Gamma_h / 2\right)^2 , \quad (2)$$

where σ^2 is the variance of the frequency distribution of phonons that couple to the energy transfer process and Γ_h is the homogeneous broadening of the B850 band. The term $\left(1 - \exp(-\tilde{S})\right)$ is the Franck-Condon factor for the phonons. Discussion of Eq. (1) is given in refs. 24 and 35. We note only that $2\Sigma(T)$ is approximately the width of the homogeneous spectral density associated with the transfer process while 2Γ is the width of the distribution of D-A electronic energy gap values due to structural heterogeneity. As in ref. 23, we use the following spectroscopically determined values for S, σ, ω_m, $FC_{loc}(\omega_{loc} = 750\ cm^{-1})$, $FC_{loc}(\omega_{loc} = 920\ cm^{-1})$, the refractive index n, Γ_h and Γ: 0.3; 14 cm^{-1}; 20-30 cm^{-1}; 0.05; 0.05; 1.5; 200 cm^{-1}; and 80 cm^{-1}. The value of Γ_h is slightly smaller than that used in ref. 23 because the widths of B800 and B850 shown in Fig. 1 for *Rps. acidophila* are about 20% narrower than those of the *Rb. sphaeroides* (NF57 mutant) samples used in ref. 23. From Fig. 1, $\Omega_o = 950\ cm^{-1}$ (ambient pressure, low temperature). Because of the large values of Γ_h

and Γ we also include BChl *a* modes of frequency higher than 920 cm^{-1}. We do so approximately (using the high resolution vibronic data for the Q_y-transition of BChl *a* from refs. 21 and 22) by lumping modes near 1200 cm^{-1} together as one mode with a Franck-Condon factor of 0.05. Finally, we use the calculated value of V = – 80 cm^{-1} from ref. 23 for coupling between a B800 molecule and either of its two nearest neighbor B850 dimers. We note that the X-ray structure shows that the Q_y-dipoles of the monomers of the B850 dimer ($R_{Mg...Mg}$ = 8.7 Å) lie nearly in the membrane plane and are close to anti-parallel. Thus, only the lowest energy dimer component carries high intensity with a transition dipole magnitude close to twice that of a BChl monomer. For this component in the presence of perfect C_9-symmetry, only the E_1 doubly degenerate exciton level of the B850 ring is allowed in absorption. The value of V = – 80 cm^{-1} corresponds to the interaction between the transition dipole of the strongly allowed B850 dimer level and that of the nearest B800 monomer and was obtained using the structure in ref. 6 and a monomer BChl dipole strength of 39 D^2 [4,36]. Calculated B800→B850 transfer times for several temperatures are given in Table 5 for a B800-B850 energy gap of 950 cm^{-1} and ω_m = 30 cm^{-1}. For comparison the experimental energy transfer times at 4.2, 19, 51, 130 and 300 K are 1.8, 1.6, 1.5, 1.1 and ~ 0.7 ps. The calculated values are in reasonable agreement with experiment at any temperature and the predicted temperature dependence is weak. However, the predicted onset of a measurable change in transfer time above 4.2 K occurs at too low a temperature. Hole burning studies had shown no measurable temperature dependence for T $\lesssim$ 30 K in *Rb. sphaeroides* [9]. The onset seen in Table 5 is determined by the Franck-Condon factor for phonons, $1-\exp(-\tilde{S})$. Thus, it is possible that Eq. (1) overemphasizes the importance of phonons in the transfer process at lower temperatures. Increasing the mean phonon frequency from 30 to ~ 50 cm^{-1} would lead to improved agreement but we are reluctant to do so since such a high frequency has not been observed by hole burning in any protein-chlorophyll complex. As discussed in ref. 23, application of Eq. (1) to this energy transfer

problem assumes that the B850 band can be viewed as being due to a single exciton level of the C_9-ring that carries the homogeneous width (~ 200 cm^{-1}) of the B850 absorption band. Ignored, then, is that several exciton levels may lie within the B850 band and that the dipole-forbidden levels can acquire oscillator strength due to imperfections in the ring structure [37,38]. In our opinion, a better understanding of the B800→B850 transfer process must await an improved understanding of B850's exciton level structure, including the effects of diagonal and off-diagonal energy disorder.

Results for Ω_0 = 1000 and 1050 cm^{-1} (values of the energy gap at p = 270 and 375 MPa) and T = 4.2 K are also given in Table 5. There is little difference between the energy transfer times for Ω_0 = 1000 or 1050 cm^{-1} and 950 cm^{-1} (ambient pressure value), as is observed. It should be noted that the calculations do not take into account weaker modes near 1050 cm^{-1} [21,22]. Their inclusion would lead to better agreement with experiment.

In summary, the Förster energy transfer model presented in ref. 10 and here provides a basis for understanding the weak temperature dependence of B800→B850 energy transfer as well as the resilience of its kinetics to substantial variations in the electronic energy gap (see, also, the Introduction). The success of the model arises mainly because it takes into account the large homogeneous broadening of the B850 band and the fact that the $S_0 \rightarrow Q_y$ spectrum of chlorophylls is characterized by a forest of weak vibronic transitions involving modes between ~ 300 and 1300 cm^{-1} [21,22]. No mode has a Franck-Condon factor larger than ~ 0.05 but, nevertheless, such a value suffices for picosecond energy transfer dynamics for reasonable value of V (~ – 80 cm^{-1}).

We conclude this section with discussion of the additional B800 decay channel identified here for *Rps. acidophila* and for *Rb. sphaeroides* in refs. 12 and 27. A key result from the two-color femtosecond experiments of this work is that at 19 K pumping sufficiently to the blue of the B800 maximum leads to photobleaching of B800 near its band maximum in ~ 400 fs. Furthermore, such pumping does not produce a corresponding 400 fs

component in the PB/SE of B850 (results A). Key hole burning results from this work and ref. 12 are that the holewidth is constant for frequencies (ω_B) $\lesssim$ that of the B800 band maximum and increases substantially for ω_B located sufficiently to the blue of the band maximum (result B). Other relevant results (C) from this work on *Rps. acidophila* is that the hole burning efficiency at ambient pressure is constant for $\omega_B \lesssim$ that of the B800 band maximum but decreases significantly for ω_B greater than the frequency of the band maximum and pressure causes the onset (measured relative to the B800 maximum) of the decrease in hole burning efficiency to shift to the red. From Tables 2 and 3 one sees, for sufficiently large ω_B, that the efficiency decreases by over a factor of 5 relative to its value on the red-side of the B800 band maximum. From the theory of hole profiles [39,40] one might suggest that this decrease in the efficiency for the ZPH is simply the result of the electron-phonon coupling which leads to a decrease in the Franck-Condon factor of the zero-phonon line (accompanied by an increase of the Franck-Condon factor of the broad phonon-sideband) as one tunes the burn frequency through B800 from red to blue. The calculated hole profiles (solid) shown in Fig. 11 argue against this possibility based on the weakness of the electron-phonon coupling. This weakness is evident in the left most inset of Fig. 11 which shows a 30% (OD change) experimental ZPH (of B800) along with its accompanying phonon sideband hole. The integrated intensity of the ZPH relative to the sideband hole yields a Huang-Rhys factor (S) of 0.35, cf. caption. The mean phonon frequency is 30 cm^{-1}. The dashed curve in Fig. 11 is the calculated B800 absorption obtained with S = 0.3, ω_m = 30 cm^{-1} and an inhomogeneous broadening of 130 cm^{-1}. The calculated width of the band is in good agreement with those of the B800 band of *Rps. acidophila* shown in Fig. 1. The solid profiles in Fig. 11 are those of the ZPH calculated with a constant burn fluence that provides a Δ OD change of 0.1 for the red-most hole. The profile of the ZPH as a function of burn frequency represents the so-called ZPH-action spectrum introduced by Reddy et al. [38]. One sees that this profile is a reasonable mirror image of the absorption profile, a

consequence of weak electron-phonon coupling. In this paper we have reported data for the %-hole depth as a function of burn fluence. The %-hole depth is Δ OD/OD where OD is the optical density at the burn frequency prior to the burn. From the right-most inset one sees, for S = 0.35 (experimental value), that the %-hole depth or burning efficiency decreases by only a factor of 2 in tuning from – 100 to + 100 cm^{-1}. A much higher value of S is required to increase this factor to 5 or more. It should also be noted that the %-hole depth varies little from – 100 cm^{-1} to the band maximum at 0 cm^{-1}, in agreement with experiment. The results of Fig. 11 indicate that the significant decrease in hole burning efficiency is most likely related to the additional B800 relaxation channel.

In what follows we consider four possible explanations for the above channel. Not considered is that it is due to vibrational relaxation of B800 BChl *a* modes excited in absorption since at low temperatures the B800 band is too sharp (see Fig. 1 caption) for it to be contributed to (at the burn wavelengths used) by low frequency modes. To see this we note that the broad and weak absorption feature at ~ 13,200 cm^{-1} in Fig. 1 for *Rps. acidophila* corresponds to a B800 BChl *a* mode(s) near 750 cm^{-1}. As pointed out earlier, hole burned spectra yielded a value of 0.05 for its Franck-Condon factor. The intensity of the feature at 13,200 cm^{-1} relative to that of the B800 (origin) band is consistent with this value. It was also determined that intramolecular modes with a frequency < 260 cm^{-1} are extremely weak with Franck-Condon factors $\lesssim 10^{-4}$ [21,22]. Thus, the contributions from these modes to the main part of the B800 band is negligible. The four explanations considered for the additional channel are that it is associated with: vibrational relaxation of directly excited BChl *a* modes which build on B850 and lie to the blue of the B800 maximum (i); B800 excitonic level structure and inter-exciton level relaxation (ii); coupling of B800 with upper exciton levels of B850, a possibility recently suggested by Reddy et al. [23] (iii); and intra-B800 energy transfer under the assumption that excitonic delocalization within B800 molecules is negligible (iv). These possibilities are considered in the order just presented.

The viability of mechanism (i) involving relaxation of directly excited vibrational modes of B850 can be assessed, in part, in terms of chlorophyll Franck-Condon factors [21,22] and the vibronic satellite hole structure of B850 reported in ref. 10. A key point is that the largest Franck-Condon factor for chlorophyll modes is ~ 0.05, which means that the maximum intensity of a B850 vibronic transition in the vicinity of B800 is one-twentieth that of the intensity near the B850 band maximum, cf. Fig. 1. Furthermore, the hole burning results of ref. 10 for *Rb. sphaeroides* show the existence of comparable vibronic activity on the blue and red sides of the B800 absorption maximum. Reddy et al. [10] concluded that the maximum contribution of B850 vibronic transitions to the B800 absorption profile at ~ ± 100 cm^{-1} of the B800 maximum is no greater than 10%. The %-contribution at the B800 maximum itself would be significantly smaller. To explain the hole burning result B, *vide supra*, in terms of mechanism (i) one would have to assume that the ZPH on the blue side of B800 are primarily associated with weak B850 vibronic transitions while those on the red side are associated with B800. (The latter assumption is viewed as valid given the good agreement reported here between the two-color femtosecond and hole burning values for the B800→B850 energy transfer rate for excitation at and to the red of the B800 absorption maximum.) Mechanism (i) is suspect also since the additional decay channel is observed for both *Rb. sphaeroides* and *Rps. acidophila* even though their B800-B850 energy gaps differ by nearly 200 cm^{-1} at low temperatures. We conclude that mechanism (i) is not a plausible explanation for the additional decay channel of B800.

Considered next is mechanism (ii) which has the additional decay channel due to the excitonic level structure of B800 and inter-exciton level structure relaxation. For consideration of this mechanism we present the results of calculations which neglect non-nearest neighbor coupling between B800 molecules, a reasonable assumption given the C_9-symmetry of B800 and nearest neighbor Mg...Mg distance of 21 Å. Under C_9-symmetry, the energies of the exciton levels are given by

$$E_j = 2Vn^{-2}\cos(2\pi j / N) \qquad (3)$$

with N = 9 and j = 0,1,...8 and n the refractive index. With C_9-symmetry and the X-ray structure of the B800-850 complex of *Rps. acidophila*, only the degenerate j = 1/8 levels are expected to carry significant absorption intensity (polarized perpendicular to the C_9 axis, which is perpendicular to the membrane plane in chromatophores). For V we use the calculated (dipole-dipole approximation) value of – 37 cm^{-1} from ref. 23 and a value of 1.5 for the refractive index, n. (The value of Vn^{-2} = 16 cm^{-1} is about 30% smaller than that calculated by Sauer et al. [26] using the coordinates of the complex [6] and point monopoles.) In units of $|V|n^{-2}$, the relative disposition of the exciton levels of the non-degenerate j = 0 and doubly degenerate j = 1/8, 2/7, 3/6 and 4/5 levels are – 1.00, – 0.77, – 0.17, + 0.50 and 0.94. The energy range spanned by the exciton levels is only 32 cm^{-1}. Note that the strongly allowed j = 1/8 (E_1) levels lie only 4 cm^{-1} above the bottom of the exciton manifold and, therefore, that the B800 absorption maximum would essentially define the average energy of the bottom of the manifold (assuming that deviation from C_9-symmetry is not so pronounced as to endow the other exciton levels with significant dipole strength). Since the levels above j = 1/8 are forbidden under C_9-symmetry (the j = 0 level may carry some absorption strength due to slight tilting of the Q_y-transition dipoles out of the membrane plane) the hole burning result B, *vide supra*, cannot be explained in terms of mechanism (ii). Furthermore, |V| is considerably smaller than the inhomogeneous width (145 cm^{-1}) of the B800 absorption band, suggesting that delocalized exciton states are unlikely to figure importantly, even in the low temperature limit where phase memory loss is slow. Allowance for structural deviation of the complex from C_9-symmetry, which would introduce diagonal and off-diagonal energy disorder into the excitonic Hamiltonian, would

mix the zero-order delocalized states [37,38]. However, such disorder within any given single complex would tend to localize the excited states.

Mechanism (iii) has the additional decay channel being a manifestation of coupling between B800 and the upper exciton level(s) of B850 which lie close in energy to B800. The calculations of Sauer et al. [26], which utilize the coordinates for the B800-850 complex at room temperature, place the upper excitonic levels in the near vicinity of B800. The levels which are weakly allowed (~ 0.05 of the absorption intensity of B850) are predicted to lie near 780 nm. Because of the assumptions made in the calculation there is some uncertainty in the value of 780 nm; the point, however, is that the possibility that upper exciton levels are placed in the near vicinity of B800 is distinct. This is interesting because the weakly allowed levels might provide for a fast quasi-resonant (electronic) Förster mechanism for B800→ B850 transfer [23,41]. Such transfer provides a plausible explanation for hole burning results B and C under the assumption that upper exciton levels of B850 yield an effective spectral density onsetting some tens of cm^{-1} to the blue of the B800 maximum. However, it is inconsistent with results A of the two-color femtosecond experiments (see also Fig. 6). A related but different possibility is that the upper B850 exciton levels which lie to the blue of the B800 band maximum (Sauer et al. [26] predict five such levels on the blue side of B800) are quite strongly coupled (quasi-resonant) to (with) certain B800 molecules so that excitation on the blue side creates mixed states which subsequently undergo relaxation. Indeed. the 0-fs Δ-absorbance spectrum of Fig. 6, which shows that the levels pumped at 783 nm produce photobleaching just to the blue of the B800 maximum, is consistent with this scenario. One relaxation route would be direct population of the lower exciton levels of B850 but, again, this route is not in accord with result A of the femtosecond experiments as well as those of Fig. 6. A second route, which is in accord, is downward relaxation to levels within the B800 band which are much more localized on B800 molecules. In consideration of this model one should keep in mind that the B800 absorption band is inhomogeneously

broadened and that considerable energetic inequivalence (*vide infra*) between B800 molecules in any given ring should be expected. This model is consistent with results B and C. For example, it provides an explanation for the redshift of the onset of decreasing hole burning efficiency (and increasing holewidth) with increasing pressure. From ref. 23 the linear pressure shifts of B800 and B850 of *Rb. sphaeroides* are – 0.08 and – 0.28 cm^{-1}/MPa (values confirmed in this work on *Rps. acidophila*). According to the analysis of Reddy et al., the pressure shift for the upper exciton levels of B850 should be very similar to those of the lower exciton levels which are responsible for the B850 band. Accordingly, at a pressure of 270 MPa the upper exciton levels should shift 54 cm^{-1} further to the red than the B800 levels. This shift is close in value to the ~ 50 cm^{-1} redshift observed at 270 MPa for the onset of decreasing hole burning efficiency. It appears, therefore, that the somewhat counter-intuitive model just presented is not at odds with our experimental data. It remains to be seen whether or not the model is capable of withstanding detailed theoretical analysis.

If the Q_y-states of the B800 ring are localized, intra-B800 energy transfer between individual BChl molecules of the ring may be responsible for B800's additional decay channel (mechanism iv). With this mechanism one views the inhomogeneously broadened B800 absorption band as due to an ensemble average (which takes into account statistical fluctuations in structure from complex to complex), of individual complexes within which the BChl molecules can have different Q_y-state energies. The width of the B800 absorption band, 145 cm^{-1}, sets a reasonable upper limit for the energetic differences. Since the additional channel is observed for isolated complexes, mechanism (iv) can be scrutinized in terms of a single B800 9-mer subject to Q_y-diagonal energy disorder. The donor-acceptor gaps cannot be significantly larger than the width of the B800 band. Therefore, intramolecular BChl *a* modes cannot serve as acceptor modes in the transfer process, since the Franck-Condon factors for modes with frequency lower than 260 cm^{-1} are $\lesssim 10^{-4}$

[21,22]. Thus, and as discussed in ref. 24, protein phonons would have to serve as the acceptor modes. The expression then used for calculation of k_{DA} is [24]

$$k_{DA} = 2\pi n^{-4} V^2 (1 - e^{-\tilde{S}}) (2\pi \Sigma^2)^{-1/2} \times \exp -\left[(\Omega_o - S\omega_m)^2 / 2\Sigma^2\right], \quad (4)$$

where $\tilde{S}$ is defined following Eq. (1) and Σ^2 is given by Eq. (2), except that the Γ_h term is deleted. As before, we set S = 0.3, ω_m = 30 cm^{-1}, σ = 14 cm^{-1}, and n = 1.5. The value of $|V|$ used is 37 cm^{-1}, *vide supra*. Results for the D-A energy gap (Ω_0) equal to 80, 60, 50, 40, 30 and 20 cm^{-1} (T = 4.2 and 77 K) are given in Table 6. The results are telling. First, for $\Omega_0 \gtrsim 40$ cm^{-1} the energy transfer rate does not compete with B800→B850 transfer in the low temperature limit. For Ω_0 = 80 cm^{-1} (close to the half-width of the B800 absorption band) the energy transfer time is very long, ~ 1.2 ns. Second, the intra-B800 transfer mechanism carries a very strong temperature dependence for $\Omega_0 \gtrsim 40$ cm^{-1}. For Ω_0 = 60 cm^{-1}, k_{DA} increases by a factor of ~ 25 as the temperature is increased to 77 K. Comparison of the 1.2 K hole burning results of De Caro et al. [27] and the 77 K femtosecond data of Monshouwer et al. [8] reveals that the temperature dependence of the additional B800 decay channel is weak. Monshouwer et al. report a decay time of 500 fs for excitation 65 cm^{-1} to the blue of the B800 maximum for *Rb. sphaeroides* at 77 K while ~ 400 fs is reported here at 19 K for excitation 250 cm^{-1} to the blue of the maximum (*Rps. acidophila*). In addition, it is difficult to reconcile hole burning result B in terms of the results of Table 6 since a small (~ 30 cm^{-1}) D-A energy gap is required to achieve transfer in 1 ps in the low temperature limit. Put another way, the results of Table 6 indicate that a variation in holewidth should also be seen for burn frequencies located to the red of the B800 absorption maximum which is not observed. However, the calculations were performed under the assumption that the B800 ring of BChl *a* molecules is not subject to significant distortion from C_9 -symmetry. We are not able to exclude this possibility although the

distortion would have to satisfy several conditions in order to be consistent with our data. For example, the distortion would have to lead to a significant increase in coupling between certain nearest neighbor B800 molecules in order to account for the 400 fs kinetics of the additional decay channel. In this regard, theoretical modeling studies are planned.

CONCLUSIONS

The femtosecond and hole burning results presented for the LH2 (B800-850) complex of *Rps. acidophila* (strain 10050) identity two excitation energy relaxation channels for B800. The first is B800→B850 energy transfer which dominates relaxation when excitation is near or to the red of the B800 absorption maximum. Both the time domain and hole burning data reveal that the kinetics of this process are insensitive to such excitation frequencies. The femtosecond data show that the kinetics are monophasic for the early times of interest. They show further that the kinetics exhibit a weak temperature dependence, consistent with earlier work. This weakness, together with the resilience of the kinetics to substantial pressure-induced changes of the B800-B850 energy gap, were shown to be explicable in terms of the Förster-type energy transfer model of Reddy et al. [10] that has the required spectral overlap provided by the B800 fluorescence origin band of B800 and vibronic absorption transitions of B850. When results for the B800-B850 complex of *Rb. sphaeroides* (including mutants) are taken into account, one is led to the conclusion that the kinetics for B800→B850 transfer change little as the energy gap is varied from ~ 450 to 1050 cm^{-1}. This, perhaps, surprising result is consistent with the above model as demonstrated by the theoretical calculations presented here and in ref. 23. Such a consistency would have been impossible to demonstrate in the absence of previously determined values for chlorophyll intramolecular Franck-Condon factors as well as the homogeneous and inhomogeneous broadening contributions to the B800 and B850 absorption bands.

The second B800 relaxation channel is observed at ambient pressure for excitation frequencies located to the blue of the B800 absorption maximum. This channel is about a factor of 4 faster than the first channel which occurs in ~ 1.8 ps in the low temperature limit. The rate constant for the second channel is ~ $(400\ fs)^{-1}$ when excitation is located sufficiently to the blue of the B800 absorption band maximum. Several explanations for the second channel were considered. Eliminated as plausible was vibrational relaxation occurring following direct excitation of either B800 or B850 vibronic transitions. Another possibility considered was that it is due to B800 inter-exciton level downward relaxation. This possibility was argued to be unlikely on the basis of excitonic calculations and the large inhomogeneous broadening of the B800 absorption band. A model in which excited B800 molecules decay into weakly absorbing upper exciton levels of B850 which lie to the blue of the B800 band maximum (but still within the B800 band) was also considered. Electronic structure calculations of the B800-850 complex indicate that this model is plausible. The hole burning data obtained at ambient and high pressures are consistent with this model. However, the two-color pump-probe femtosecond results are not, i.e. no corresponding ~ 400 fs photobleaching of B850 was observed following excitation to the blue of the B800 band maximum. A related model was proposed in which upper exciton levels of B850 are quasi-resonant and, therefore, quite strongly coupled with B800 molecules that absorb on the blue side of the B800 band. Excitation to the blue of the B800 maximum is envisaged as creating mixed B800-B850 states which subsequently relax to states of lower energy within the B800 band which are characterized by a high degree of localization on B800 molecules. Qualitatively, this model appears to be consistent with both the femtosecond and hole burning data (including high pressure). Finally, the results of calculations were presented which, together with certain of our data, indicate that the additional ~ 400 fs channel is not due to intra-B800 band energy transfer under the assumption of C_9-symmetry. Nevertheless,

the possibility that a significant distortion of the B800 ring from C_9-symmetry is responsible for the additional channel cannot be excluded at this time.

ACKNOWLEDGMENTS

Research at the Ames Laboratory was supported by the Division of Chemical Sciences, Office of Basic Energy Sciences, US Department of Energy. Ames Laboratory is operated for USDOE by Iowa State University under contract W-7405-Eng-82. Research at the University of Glasglow was supported by SERC. We thank K. Sauer for useful discussions and a preprint of his paper on the calculation of optical spectra for the LH2 complex.

REFERENCES AND NOTES

1. Sundström, V.; van Grondelle, R. In *Anoxygenic Photosynthetic Bacteria*, Blankenship, R. E.; Madigan, M. T.; Baller, C. E., Eds.; Kluwer Academic Publishers: Dordrecht, 1995; p. 349.

2. Zuber, H.; Cogdell, R. In *Anoxygenic Photosynthetic Bacteria*, Blankenship, R. E., Madigan, M. T., Bauer, C. E., Eds.; Kluwer Academic Publishers: Dordrecht, 1995; p. 315.

3. Scherz, A.; Parson, W. W. *Photosynth. Res.* **1986**, *9*, 21.

4. Scherz, A.; Rosenbach-Belkin, V. In *The Photosynthetic Bacterial Reaction Center, Structure and Dynamics*, Breton, J. and Vermeglio, A., Eds.; Plenum Press, New York, 1988; p. 295.

5. Braun, P.; Scherz, A. *Biochem.* **1991**, *30*, 5177.

6. McDermott, G.; Prince, S. M.; Freer, A. A.; Hawthornthwaite-Lawless, A. M.; Papiz, M. Z.; Cogdell, R. J.; Isaacs, N. W. *Nature* **1995**, *374*, 517.

7. Shreve, A. P.; Trauman, J. K.; Frank, H. A.; Owens, T. G.; Albrecht, A. C. *Biochim. Biophys. Acta.* **1991**, *973*, 93.

8. Monshouwer, R.; de Zarate, I. O.; van Mourik, F.; van Grondelle, R. *Chem. Phys. Lett.* **1995**, *246*, 341.

9. van der Laan, H.; Schmidt, Th.; Visschers, R. W.; Visscher, K. J; van Grondelle, R.; Volker, S. *Chem. Phys. Letts.* **1990**, *170*, 231.

10. Reddy, N. R. S.; Small, G. J.; Seibert, M.; Picorel, R. *Chem. Phys. Letts.* **1991**, *181*, 391.

11. Reddy, N. R. S.; Small, G. J. *J. Chem. Phys.* **1991**, *94*, 7545.

12. Reddy, N. R. S.; Cogdell, R. J.; Zhao, L. Small, G. J. *Photochem. Photobiol.* **1993**, *57*, 35.

13. Jankowiak, R.; Hayes, J. M.; Small, G. J. *Chem. Rev.* **1993**, *93*, 1471.

14. Reddy, N. R. S.; Lyle, P. A.; Small, G. J. *Photosyn. Res.* **1992**, *31*, 167.

15. Savikhin, S.; Struve, W. S. *Chem. Phys.* **1996**, *210*, 91.

16. Savikhin, S.; Struve, W. S. *Biophys. J.* **1994**, *67*, 2002.

17. Reddy, N. R. S.; van Amerongen, H.; Kwa, S. L. S.; van Grondelle, R.; Small, G. J. *J. Phys. Chem.* **1994**, *98*, 4729.

18. Johnson, S. G.; Small, G. J. *J. Phys. Chem.* **1991**, *95*, 471.

19. Becker, M.; Nagarajan, V.; Parson, W. W. *J. Am. Chem. Soc.* **1991**, *113*, 6840.

20. van der Laan, H.; de Caro, C.; Schmidt, Th.; Visschers, R. W.; van Grondelle, R.; Fowler, G. J. S.; Hunter, C. N.; Volker, S. *Chem. Phys. Letts.* **1993**, *212*, 569.

21. Renge, I.; Mauring, K.; Avarmaa, R. *J. Lumn.* **1987**, *37*, 207.

22. Gillie, J. K.; Small, G. J.; Golbeck, J. H. *J. Phys. Chem.* **1989**, *93*, 1620.

23. Reddy, N. R. S.; Wu, H.-M.; Jankowiak, R.; Picorel, R.; Cogdell, R. J.; Small, G. J. *Photosyn. Res.* **1996**, *48*, 277.

24. Kolaczkowski, S. V.; Hayes, J. M.; Small, G. J. *J. Phys. Chem.* **1994**, *98*, 13418.

25. Pearlstein, R. M.; Zuber, H. In *Antennas and Reaction centers of Photosynthetic Bacteria*, Springer series in Chemical Physics 42; Michel-Beyerle, M. E., Ed.; Springer -Verlag: Berlin, 1985; p. 53.

26. Sauer, K.; Cogdell, R. J.; Prince, S. M.; Freer, A. A.; Isaacs, N. W.; Scheer, H. *Photochem. Photobiol.* **1996**, *64*, 564.

27. De Caro, C.; Visschers, R. W.; van Grondelle, R.; Völker, S. *J. Phys. Chem.* **1994**, *98*, 10584.

28. Savikhin, S.; Struve, W. S. *Biochem.* **1994**, *33*, 11200.

29. Savikhin, S. *Rev. Sci. Instrum.* **1995**, *66*, 4470.

30. Chang, H.-C.; Jankowiak, R.; Reddy, N. R. S.; Small, G. J. *Chem. Phys.* **1995**, *197*, 307.

31. Reddy, N. R. S.; Jankowiak, R.; Small, G. J. *J. Phys. Chem.* **1995**, *99*, 16168.

32. Cogdell, R. J.; Hawthornthwaite, A. M. In *The Photosynthetic Reaction Center*, Deisenhofer, J., and Norris, J. R., Eds.; Academic Press, San Diego, Vol. 1, 1993; p. 23.

33. Struve, W. S. *Biophys. J.* **1995**, *69*, 2739.

34. Kenney, M. J.; Jankowiak, R.; Small, G. J. *Chem. Phys.* **1990**, *146*, 47.

35. Small, G. J.; Hayes, J. M.; Silbey, R. J. *J. Phys. Chem.* **1992**, *96*, 7499.

36. Sauer, K.; Lindsay Smith, J. R.; Schultz, A. J. *J. Am. Chem. Soc.* **1966**, *88*, 2681.

37. (a) Wu, H.-M.; Reddy, N. R. S.; Small, G. J. *J. Phys. Chem. B*, **1997**, *101*, 651. (b) Wu, H.-M.; Small, G. J. *Chem. Phys.* **1997**, *218*, 225.

38. Reddy, N. R. S.; Picorel R.; Small, G. J. *J. Phys. Chem.* **1992**, *96*, 6458.

39. Hayes, J. M.; Gillie, J. K.; Tang, D.; Small, G. J. *Biochim. Biophys. Acta* **1988**, *932*, 287.

40. Hayes, J. M.; Lyle, P. A.; Small, G. J. *J. Phys. Chem.* **1994**, *98*, 7337.

Table 1. Optimized parameters from multiexponential fits to two-color absorption difference profiles for LH2 complexes from *Rps. acidophila* at ambient pressure.[a]

T, K	Pump, nm	Probe, nm	τ_1 (A_1)	τ_2 (A_2)
19	805	880	1.60 (0.95)	188 (–1.00)
19	812	880	1.47 (0.83)	316 (–1.00)
19	810	850	1.51 (0.81)	77 (–1.00)
19	810	859	1.61 (0.90)	320 (–1.00)
19	810	866	1.62 (0.73)	65 (–1.00)
51	810	866	1.50 (0.74)	42 (–1.00)
130	810	866	1.14 (0.78)	58 (–1.00)

[a] All lifetimes are in ps. Positive and negative amplitudes correspond to PB/SE rise and decay components, respectively. Uncertainties in amplitudes are ± 0.05.

Table 2. Hole burning data for *Rps. acidophila* chromatophores at ambient pressure.

Burn Wavenumber	12321	12362	12405	12454	12489	12499	12526	12549
cm^{-1} (label in Fig. 9)	(a)	(b)	(c)	(d)	(e)	(f)	(g)	(h)
Holewidth, cm^{-1}	4.9	4.8	4.4	4.8	5.4	5.2	>10[†]	>10[†]
%-holedepth	8	7	10	4	4	2	3*	2*
Burn fluence, J/cm^2	55	55	55	40	55	40	160	80

B800 band absorption maximum = 12445 cm^{-1}. FWHM of B800 band = 145 cm^{-1}.
Uncertainty in the %-holedepth values is ± 0.5 except for holes marked by an asterisk where it is ± 1.
[†]Due to poor signal to noise ratio, precise determination was not possible, see text.

Table 3. Hole burning data for *Rps. acidophila* chromatophores at 270 MPa.

Burn Wavenumber, cm^{-1} (label in Fig. 10)	12353 (a)	12386 (b)	12420 (c)	12453 (d)	12501 (e)	12547 (f)
Holewidth, cm^{-1}	4.8	5.4	7.7	9.0	>10†	>10†
%-holedepth	8*	6	9	6	4*	3*
Burn fluence, J/cm^2	55	135	270	270	270	270

B800 band absorption maximum = 12420 cm^{-1}. FWHM of B800 band = 160 cm^{-1}.
For uncertainty in the %-holedepth values see Table 2.
†Due to poor signal to noise ratio, precise determination was not possible, see text.

Table 4. Hole burning data for *Rps. acidophila* chromatophores at 375 MPa.

Burn Wavenumber, cm^{-1}	12306	12343	12373	12399	12439	12478
Holewidth, cm^{-1}	5.4	5.4	5.1	5.2	5.3	~8
%-holedepth	11*	12	11	8*	5*	4*
Burn fluence, J/cm^2				80		

B800 band absorption maximum = 12415 cm^{-1}. FWHM of B800 band = 200 cm^{-1}.
For uncertainty in the %-holedepth values see Table 2.

Table 5. Calculated B800→B850 energy transfer times.

B800-B850 Energy Gap (cm^{-1})	950					1000	1050
Temperature (K)	4.2	19	51	130	300[a]	4.2	4.2
Energy transfer time (ps)	2.9	2.4	1.4	0.89	0.76	3.2	3.5

[a] At 300 K, the experimentally observed energy gap is 850 cm^{-1}. For this energy gap we calculate the energy transfer time to be 0.73 ps which differs very little from the value calculated using an energy gap of 950 cm^{-1}.

Table 6. Calculated intra-B800 energy transfer times.

	Ω_0 (cm^{-1})					
T (K)	80	60	50	40	30	20
4.2	1170 ps	29 ps	7.1 ps	2.4 ps	1.1 ps	0.66 ps
77	3.3 ps	1.2 ps	0.82 ps	0.61 ps	0.49 ps	0.43 ps

FIGURE CAPTIONS

Figure 1. 4.2 K absorption spectra of chromatophores (solid curves) and B800-850 antenna complexes (broken curves) from (a) *Rb. sphaeroides* and (b) *Rps. acidophila* at 1 atm. The sample optical density at the B800 band maximum was 0.4. The separation of the B800 and B850 bands is 780 cm^{-1} for *Rb. sphaeroides* and 950 cm^{-1} for *Rps. acidophila*, respectively. The widths of the B800, B850 and B875 bands of *Rb. sphaeroides* are 150 cm^{-1}(130 cm^{-1}), 250 cm^{-1} (220 cm^{-1}) and 235 cm^{-1}, respectively. Values within parentheses refer to the B800-850 isolated complex. The corresponding values for *Rps. acidophila* are 145 cm^{-1} (126 cm^{-1}), 220 cm^{-1} (215 cm^{-1}) and 225 cm^{-1}.

Figure 2. Steady state absorption spectrum of LH2 complexes of *Rps. acidophila* at 19 K and ambient pressure, with superimposed spectra of laser pump and probe pulses used in some of the time-resolved experiments. The laser spectra (mutually normalized here for comparison) were measured during experiments using a Czerny-Turner monochromator (7.9 nm/mm dispersion) imaged onto the linear CCD array of a Unidata BP2048 beam profiler.

Figure 3. Two-color absorption difference profile for LH2 complexes from *Rps. acidophila* at 19 K and ambient pressure, excited and probed at 805 and 880 nm. Negative-going signal is dominated throughout by photobleaching and stimulated emission. Fitting parameters are given for this and other two-color profiles in Table 1.

Figure 4. Two-color absorption difference profiles for LH2 complexes form *Rps. acidophila* at 19 K and ambient pressure. Excitation wavelength is 810 nm; probe wavelengths are (from top) 866, 859, and 850 nm.

Figure 5. Temperature dependence of absorption difference profiles for LH2 complexes from *Rps. acidophila* at ambient pressure, excited and probed at 810 and 866 nm. Sample temperatures are (1) 19 K, (2) 51 K, (3) 130 K. Curves are congruent at earliest times, because prompt signals are dominated by SE from laser-excited B800 states. Remainder of rise feature is fitted with single-exponential kinetics in all three cases.

Figure 6. Absorption difference spectra of LH2 complexes from *Rps. acidophila* at fixed time delays, pumped at 783 nm and probed at ~5 nm intervals from 780 to 815 nm. Time delays are -100 fs through 400 fs (top) and 400 fs to 8 ps (bottom). These spectra were assembled from two-color profiles accumulated at 19 K and ambient pressure in 8 windows.

Figure 7. Two-color absorption difference profiles for LH2 complexes from *Rps. acidophila* at 19 K and ambient pressure, excited at several wavelengths from 778 to 810 nm and probed at 808 nm.

Figure 8. 4.2 K B800 absorption profile of *Rps. acidophila* B800-850 complex at 1 atm. Arrows locate burn wavelengths. Holes were burned with an intensity of 1 W/cm^2 for 5 minutes. Burn wavenumbers (holewidths) are (a) 12399 cm^{-1} (5.8 cm^{-1}), (b) 12431 cm^{-1} (5.6 cm^{-1}), (c) 12464 cm^{-1} (6.2 cm^{-1}), (d) 12472 cm^{-1} (5.5 cm^{-1}), (e) 12497 cm^{-1} (8.3 cm^{-1}) and (f) 12530 cm^{-1} (10.2 cm^{-1}). Inset shows a 50 cm^{-1} scan of two holes at (a) 12399 cm^{-1} (broken curve) and (e) 12497 cm^{-1}, respectively. (For comparison, the holes are offset along the wavenumber axis.)

Figure 9. 4.2 K B800 absorption profile of *Rps. acidophila* chromatophores at ambient pressure. Arrows locate the burn wavelengths. Burn wavenumbers are (a) 12321 cm^{-1}, (b) 12362 cm^{-1}, (c) 12405 cm^{-1}, (d) 12454 cm^{-1}, (e) 12489 cm^{-1}, (f) 12499 cm^{-1}, (g) 12526 cm^{-1} and (h) 12549 cm^{-1}. The burn conditions were: burn laser intensity = 900 mW/cm^2 and burn time = 1 min except (g) 3 minutes. (h) 90 seconds, (d) and (f) 45 seconds. Inset shows (50 cm^{-1} scan) two holes at (b) 12362 cm^{-1} (broken curve) and (g) 12526 cm^{-1}, respectively. (For comparison, the holes are offset along the wavenumber axis.)

Figure 10. 4.2 K B800 absorption profile of *Rps. acidophila* chromatophore at 270 MPa. Arrows locate the burn wavelengths. Burn wavenumbers and times are (a) 12353 cm^{-1}, 1 min, (b) 12386 cm^{-1}, 2.5 min, (c) 12420 cm^{-1}, 5 min, (d) 12453 cm^{-1}, 5 min, (e) 12501 cm^{-1}, 5 min and (f) 12547 cm^{-1}, 5 min. A burn laser intensity of 900 mW/cm^2 was used. Inset shows (50 cm^{-1} scan) two holes burned at (b) 12386 cm^{-1} (broken curve) and (d) 12453 cm^{-1}, respectively. For comparison, the holes are offset along the wavenumber axis.

Figure 11. Simulation of B800 absorption profile (broken curve) and 11 non-saturated holes (solid curve) burned in the B800 band using Eqs. (1) and (2) from ref. 34. The input parameters are: $\Gamma_I = 130$ cm^{-1}; $S = 0.3$; $\gamma = 2.5$ cm^{-1}; and $T = 4$ K. The values of ω_m and the full width at half maximum of the one phonon profile were equal to 30 cm^{-1}. Right inset shows the corresponding %-hole depths (ratio of the ZPH depth to the absorption at the same frequency). Left inset shows a 140 cm^{-1} scan (experimental) of saturated hole burned at 12444 cm^{-1} of NF57 mutant at 4.2 K.

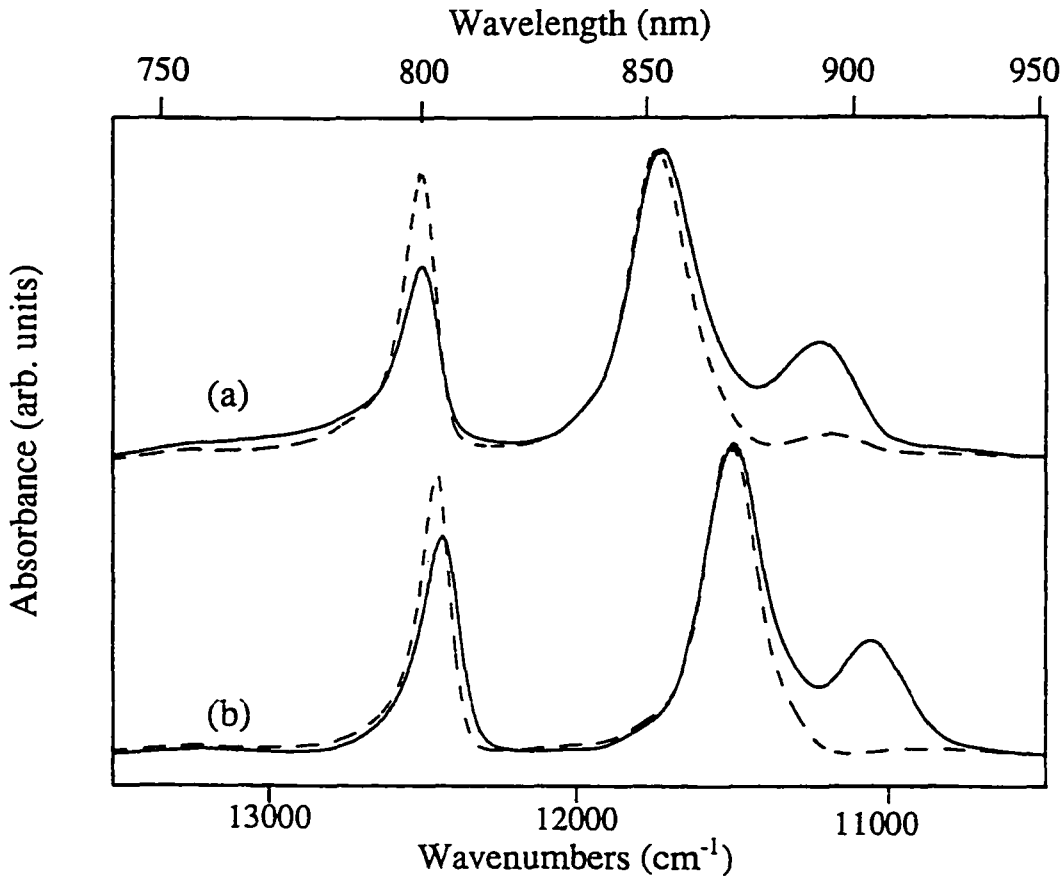
Wavelength (nm)
750
800
850
900
950
Absorbance (arb. units)
(a)
(b)
13000
12000
11000
Wavenumbers (cm-1)

Figure 1

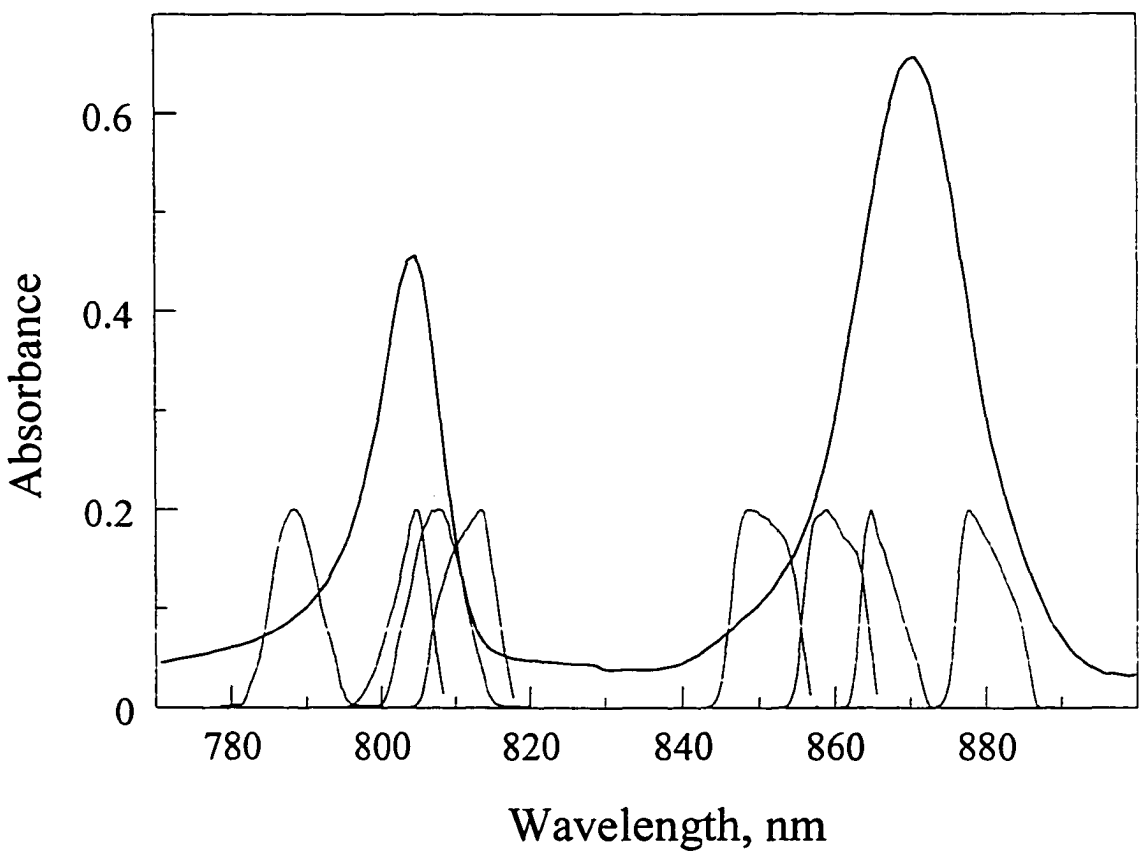

Figure 2

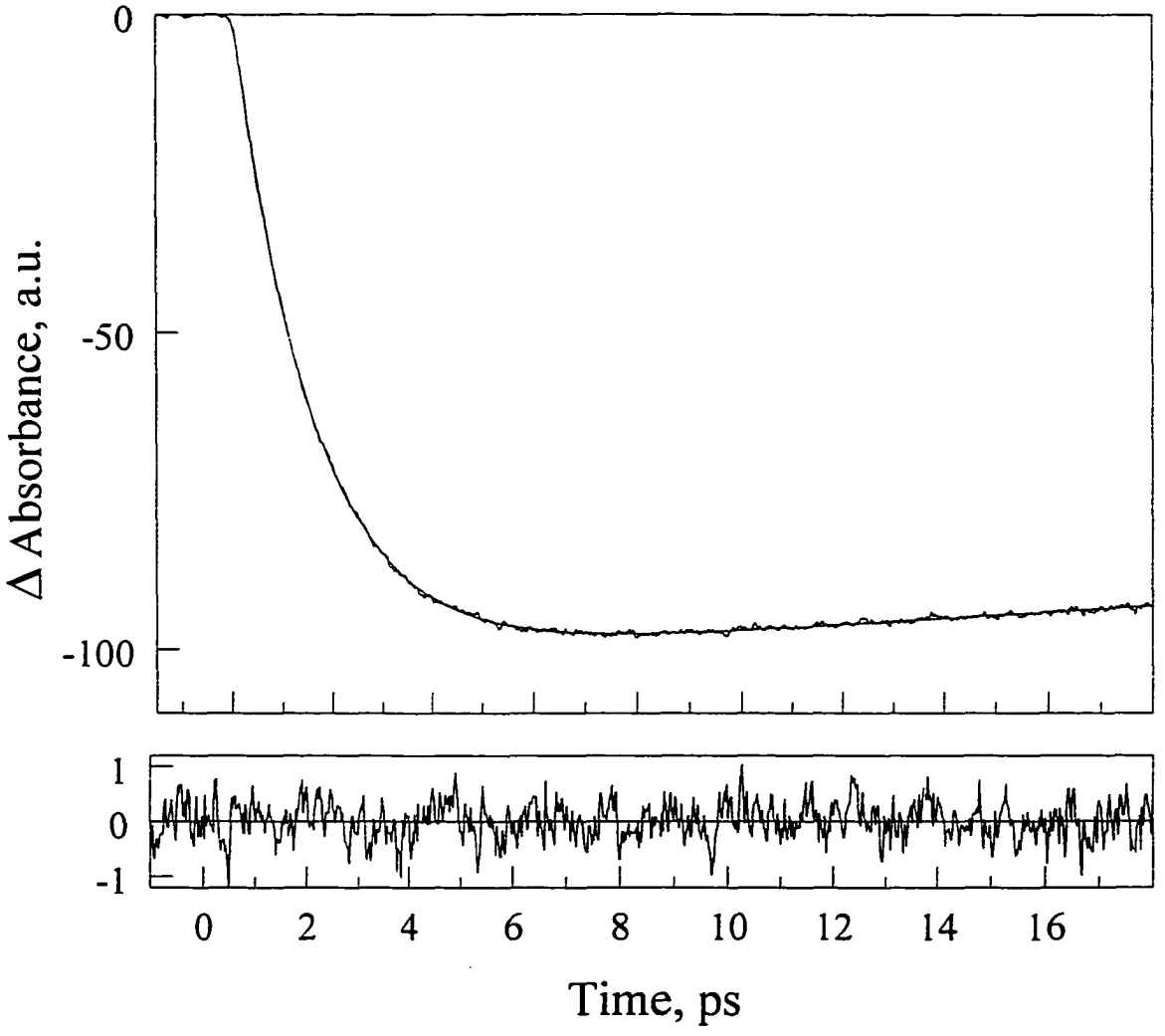

Figure 3

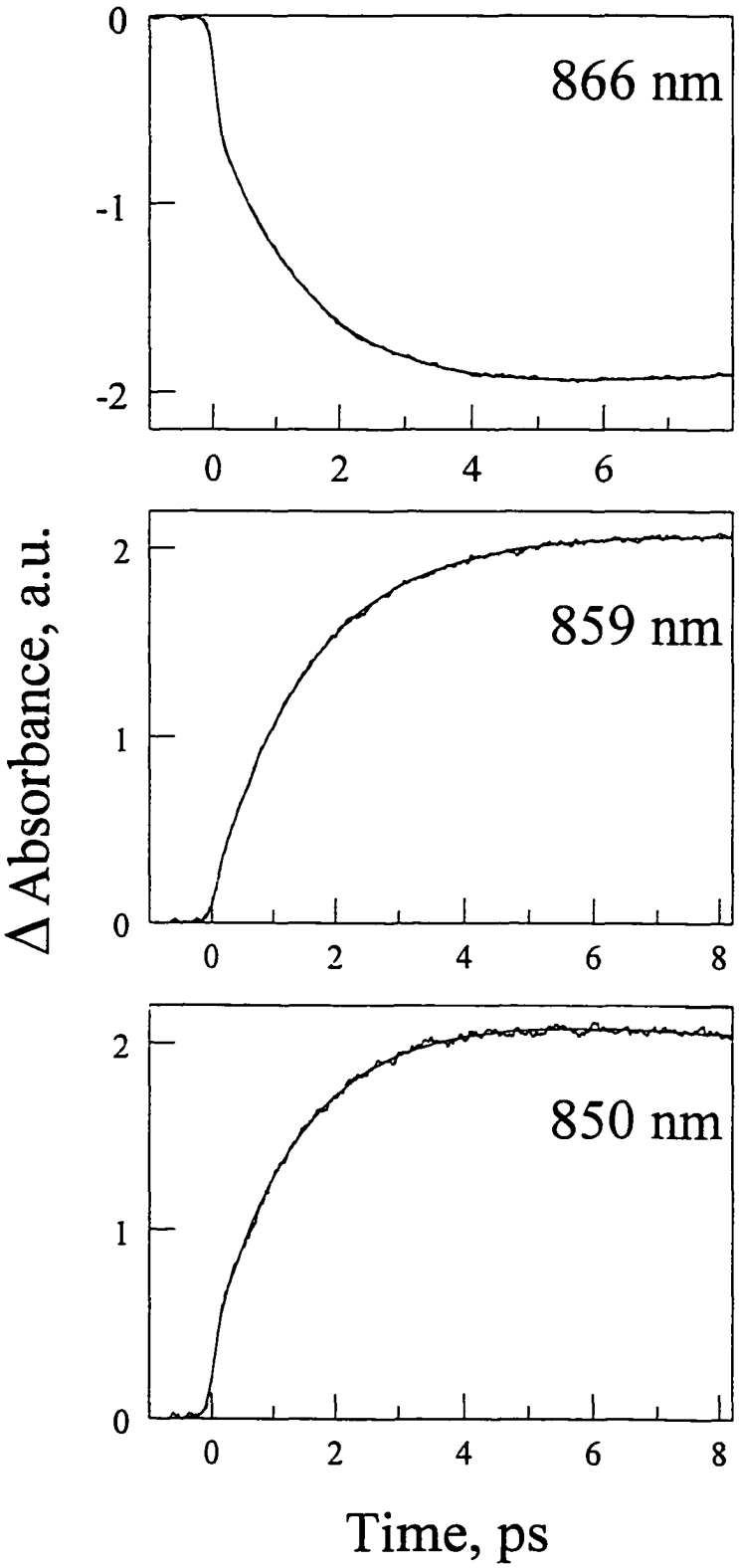

Figure 4

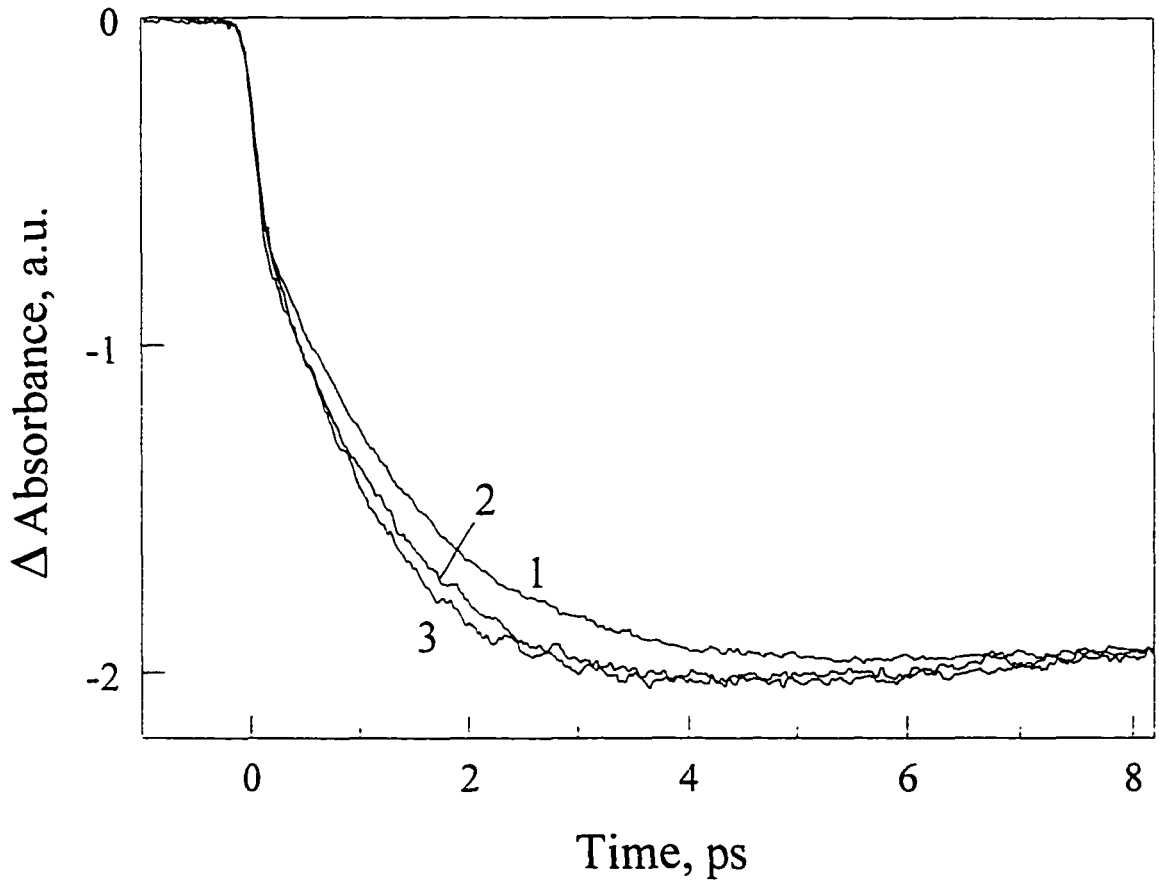

Figure 5

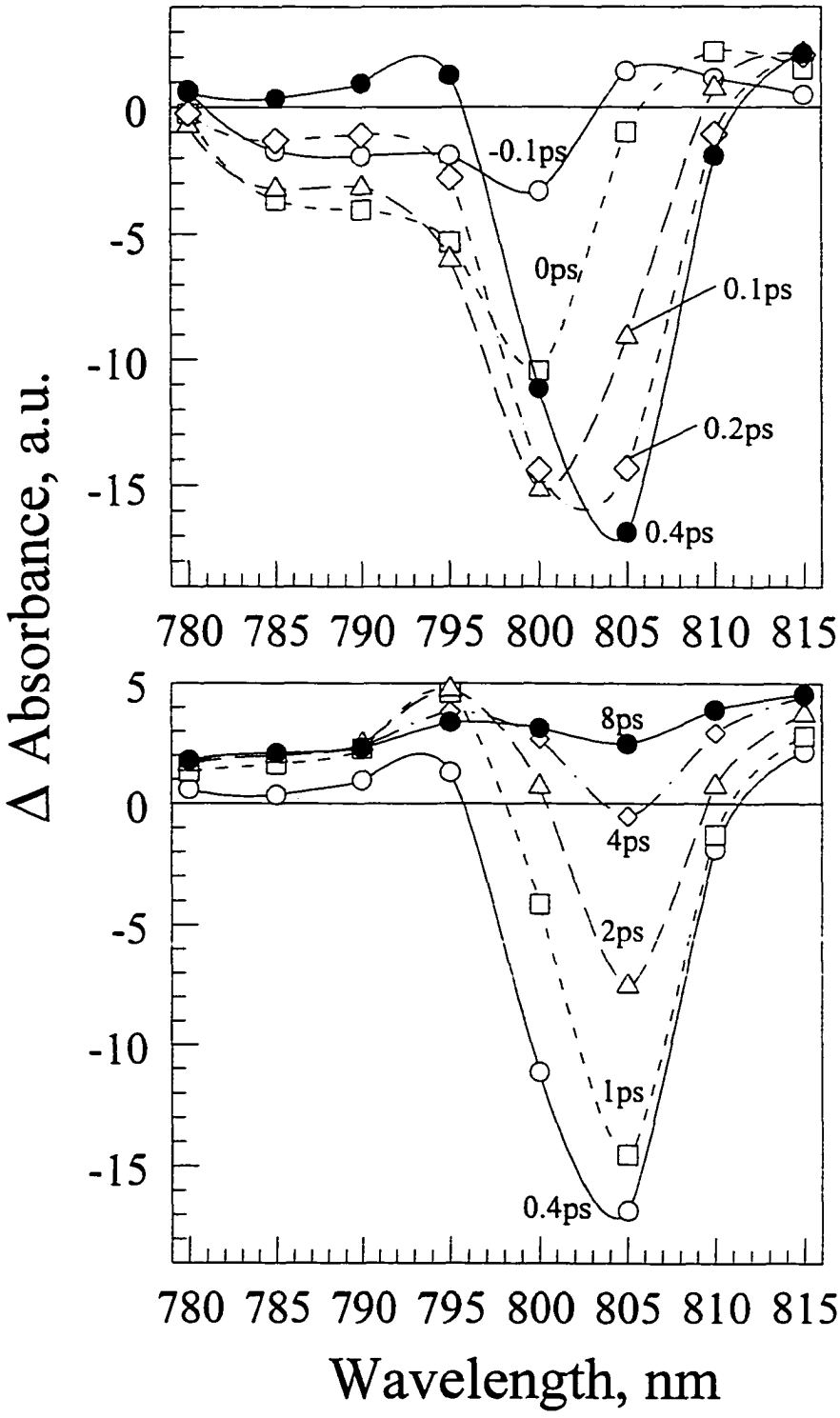
Δ Absorbance, a.u.
0
-5
-10
-15
-0.1ps
0ps
0.1ps
0.2ps
0.4ps
780 785 790 795 800 805 810 815
5
0
-5
-10
-15
8ps
4ps
2ps
1ps
0.4ps
780 785 790 795 800 805 810 815
Wavelength, nm

Figure 6

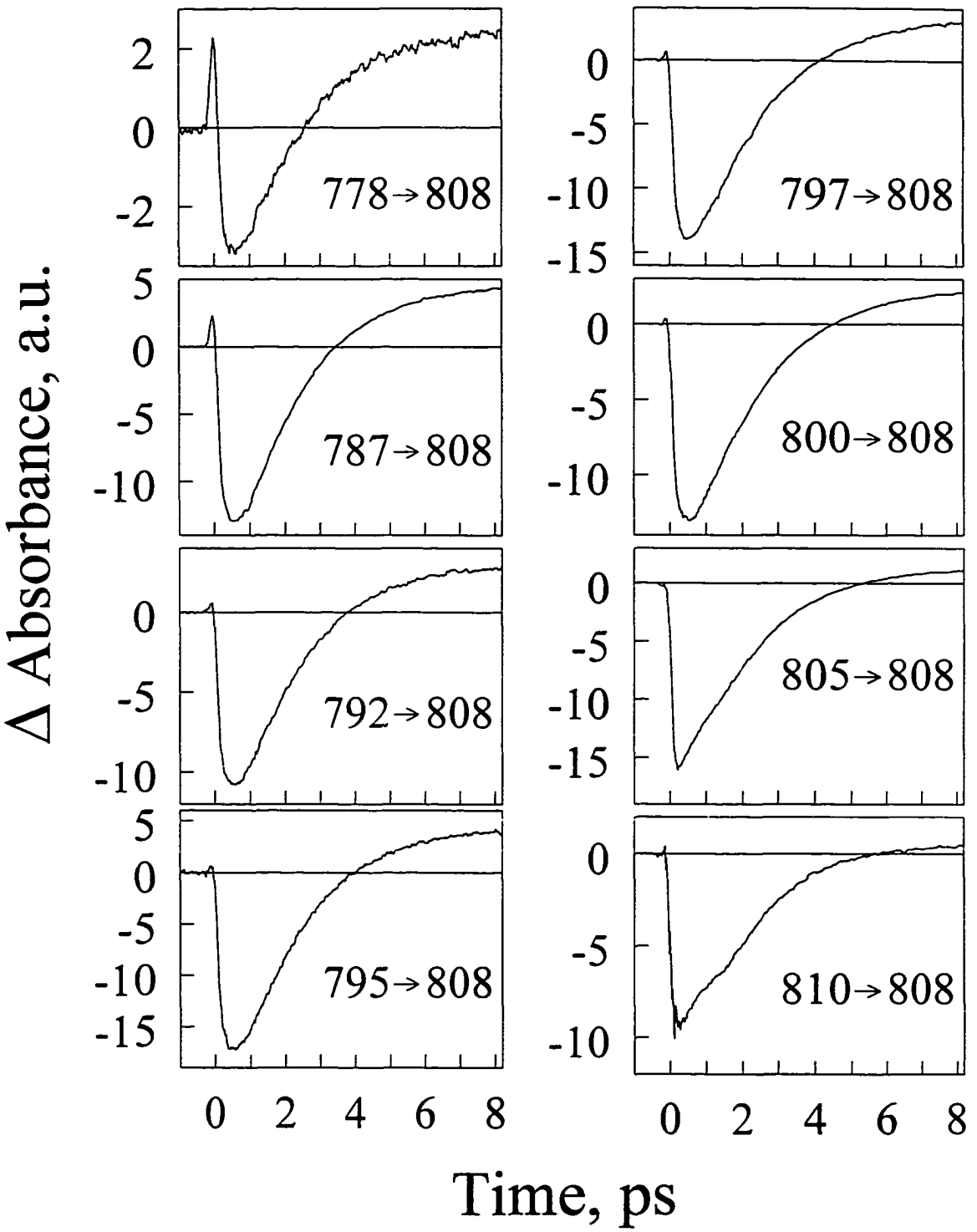
Δ Absorbance, a.u.
778→808
797→808
787→808
800→808
792→808
805→808
795→808
810→808
Time, ps

Figure 7

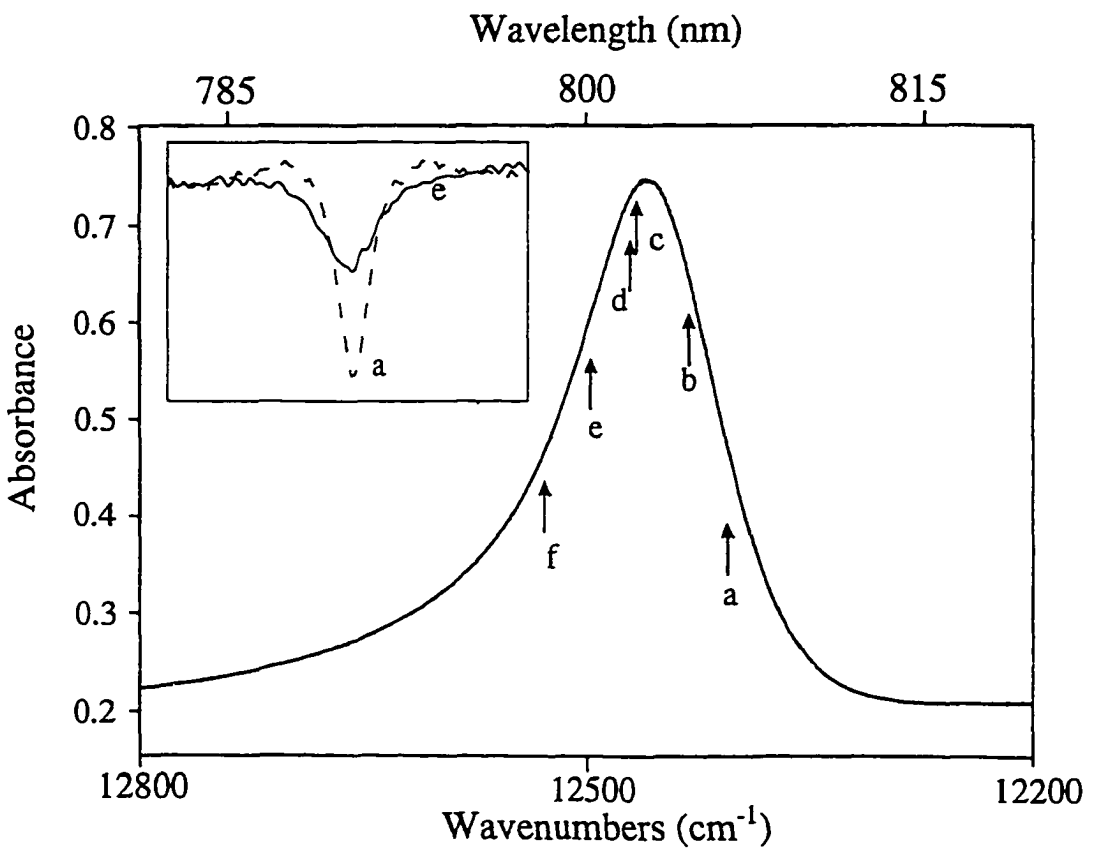
Wavelength (nm)
785
800
815
0.8
0.7
0.6
0.5
0.4
0.3
0.2
Absorbance
e
a
c
d
b
e
f
a
12800
12500
12200
Wavenumbers (cm-1)

Figure 8

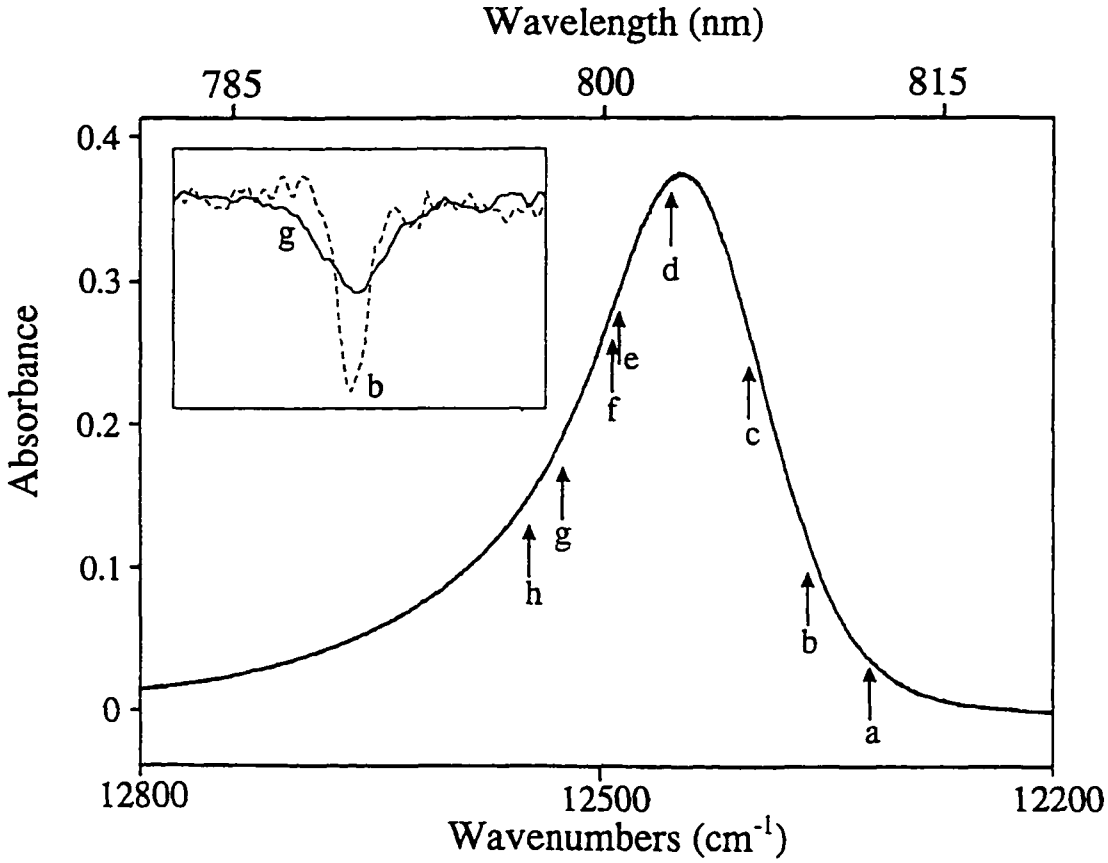
Wavelength (nm)
785
800
815
0.4
0.3
0.2
0.1
0
Absorbance
g
b
d
e
f
c
g
h
b
a
12800
12500
12200
Wavenumbers (cm-1)

Figure 9

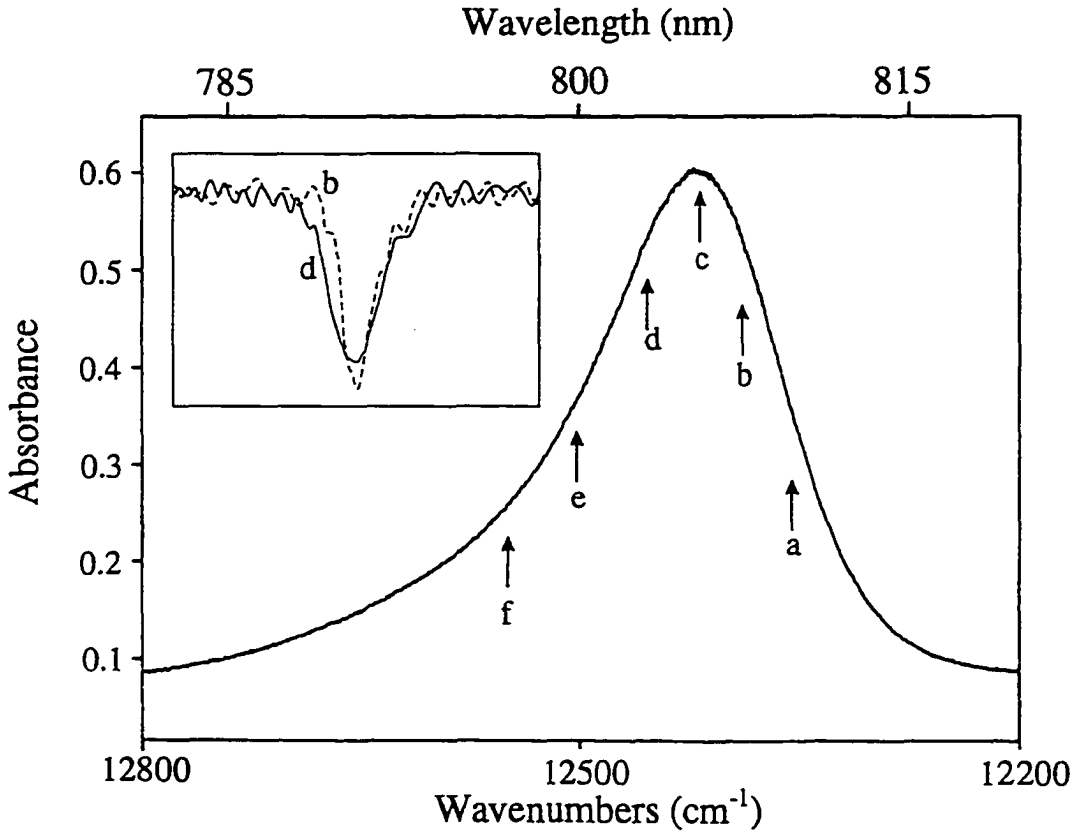
Wavelength (nm)
785
800
815
0.6
0.5
0.4
0.3
0.2
0.1
Absorbance
b
d
c
d
b
e
a
f
12800
12500
12200
Wavenumbers (cm-1)

Figure 10

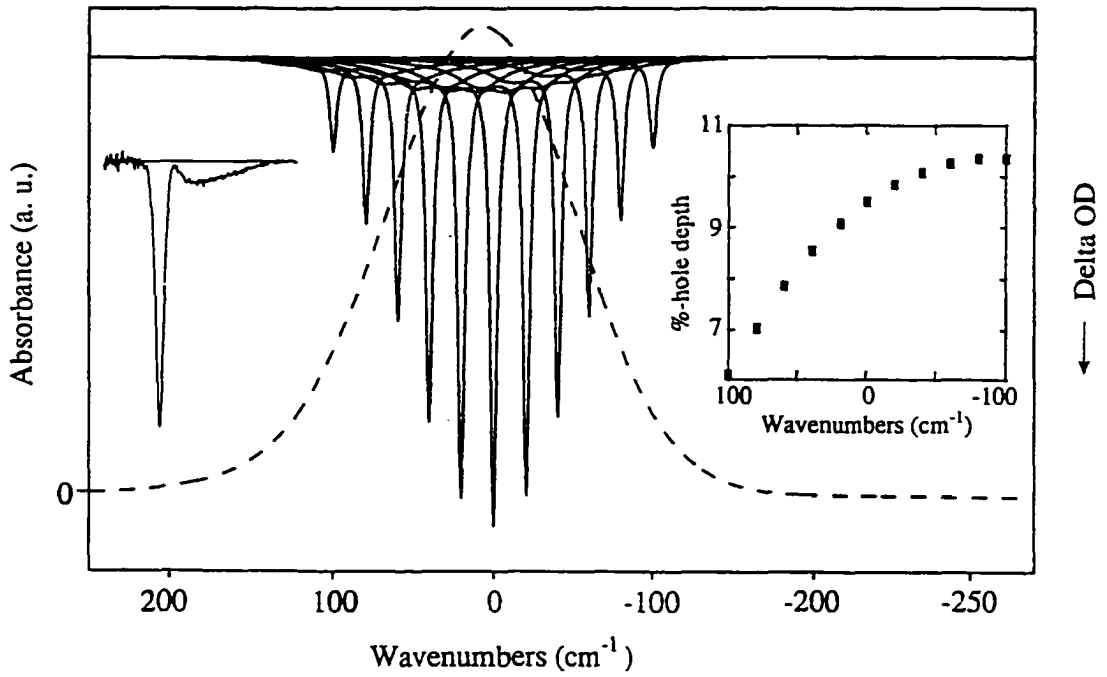
Absorbance (a. u.)
0
200
100
0
-100
-200
-250
Wavenumbers (cm-1)
11
9
7
%-hole depth
100
0
-100
Wavenumbers (cm-1)
Delta OD

Figure 11

CHAPTER 4. COMPARISON OF THE LH2 ANTENNA COMPLEXES OF *RHODOPSEUDOMONAS ACIDOPHILA* (STRAIN 10050) AND *RHODOBACTER SPHAEROIDES* BY HIGH PRESSURE-ABSORPTION, -HOLE BURNING AND TEMPERATURE-DEPENDENT ABSORPTION SPECTROSCOPIES

A paper published in the *J. Phys. Chem. B* **1997**, *101*, 7641.

H.-M. Wu, M. Ratsep, R. Jankowiak, R. J. Cogdell and G. J. Small

ABSTRACT

The cyclic (C_n) light harvesting 2 (LH2 or B800-850) complexes of *Rps. acidophila* (strain 10050) and *Rb. sphaeroides*, isolated under identical conditions, are compared using the title spectroscopies. Thermal broadening and shifting data for the B850 absorption band reveal a structural change near 150 K for both species in the glycerol:water solvent used. The linear regions of thermal broadening above and below this temperature are shown to be consistent with dephasing via phonon-assisted relaxation between the B850 ring's exciton levels which contribute to the B850 absorption band. The theoretical model used predicts, for both species, that the nearest neighbor coupling(s) between bacteriochlorophyll *a* (BChl *a*) molecules of the B850 ring are significantly stronger, ca. 35%, for the low temperature structures. Moreover, the linear thermal broadening rates of *Rb. sphaeroides* are significantly lower than those of *Rps. acidophila* for both the low and high temperature regions. Analysis of the difference in rates with the above model indicates that the nearest neighbor BChl *a*-BChl *a* coupling(s) is ca. 20% weaker for *Rb. sphaeroides* at all temperatures. The observation that the thermal shift rate for the B850 band of *Rb. sphaeroides* is 2.2 times smaller than that of *Rps. acidophila* is consistent with this weaker

coupling. Pressure shift data for the B800 band indicate that the compressibility (κ) for *Rb. sphaeroides* is significantly larger than for *Rps. acidophila*, suggesting that the weaker excitonic coupling between B850 molecules of *Rb. sphaeroides* stems, at least in part, from looser packing of its α,β polypeptide pairs. A higher κ-value for *Rb. sphaeroides* provides an explanation for the observation that the linear rates for pressure broadening and shifting of the B850 band for the two species are similar. While the pressure- and temperature-dependent data for the B800 band of both species are consistent with weak excitonic coupling between nearest neighbor B800 molecules, the data for the B850 band (including pressure shifting of zero-phonon holes burned into the lowest exciton level of the B850 ring (B870)) require interpretation in terms of strong coupling. Although large, the pressure-shift rate for B870 holes burned on the high energy side of the B870 band (– 0.46 cm^{-1}/MPa) is a factor of 1.3 lower than on the low energy side. An interpretation for this variation in terms of energy disorder is given. Zero-phonon hole action spectra (4.2 K) for the B870 exciton level are presented which yield similar inhomogeneous widths for the B870 band of both species, ~ 120 cm^{-1}. For both species the apparent displacement of this band below the maximum of the B850 band is close to 200 cm^{-1}. A theoretical discussion on the relationship between the apparent displacement and excitonic level structure in the absence of energy disorder is given in the accompanying paper.

1. INTRODUCTION

The antenna of photosynthetic units are most often comprised of two or more structurally and electronically distinct light harvesting (LH) protein-chlorophyll (Chl) complexes which act in concert to channel solar excitation energy to the reaction center.[1,2] These complexes usually contain two or more strongly coupled Chl molecules which means that the $Q_y(S_1)$ states are extended with the nature of the delocalization, or occupation numbers of the contributing Chl molecules, determined by the structure of the complex. An

early example of where delocalized or nanoexcitonic states are important for understanding the absorption, circular dichroism and hole burned spectra is the FMO BChl *a* complex of *Prosthecochloris aestuarii*.[3,4] This complex is a C_3-trimer of subunits, with each subunit containing seven symmetry-inequivalent BChl *a* molecules.[5,6] Within a subunit nearest neighbor distances (Mg...Mg) approach 11 Å which results in pairwise excitonic couplings of about 150 cm^{-1}. Although the strongest coupling between molecules in different subunits is only ~ 20 cm^{-1},[4] the excitonic level splitting from it was resolved by hole burning[3] and fluorescence polarization[7,8] at low temperatures. Thus, consideration of the full trimer is essential for an improved understanding of the electronic states.

Unfortunately, the presence of seven symmetry/energy inequivalent BChl *a* molecules has precluded a completely satisfactory understanding of the exciton levels of the FMO complex since there is no accurate approach to calculating Q_y-excitation energies of individual BChl *a* molecules in different protein and ligand environments.[9] Given additional complications, *vide infra*, it is highly desirable to study complexes which carry symmetry that is sufficiently high to eliminate or greatly reduce the problem of symmetry-inequivalence. The LH1 and LH2 complexes of purple bacteria are ideal because of their high cyclic symmetry. Furthermore, their electronic structures and energy transfer dynamics has long been subjects of much interest (for a recent review see Sundström and van Grondelle[10]). In *Rhodobacter sphaeroides*, *Rhodopseudomonas acidophila* (strain 10050) and, as another example, *Rhodospirillum molischianum*, LH1 and LH2 are often referred to as B875 and B800-850, respectively, because of the approximate location, in nm, of their BChl *a* band maxima at room temperature. Structural models for LH1 and LH2 put forth during the middle to late 1980s have in common an α,β polypeptide pair (heterodimer) that binds two BChl *a* molecules at the periplasmic side of the membrane and, in the case of LH2, one BChl *a* at the cytoplasmic side (see Zuber and Cogdell[2] for a recent review). It was generally believed that some type of cyclic arrangement of α,β pairs constituted the "unit

cell" of the two complexes with the BChl *a* molecules at the periplasmic side responsible for the B850 and B875 absorption bands of LH2 and LH1, respectively; the BChl *a* molecules bound at the cytoplasmic side being responsible for B800 of LH2.

Recently, the X-ray structure of the LH2 complex of *Rps. acidophila* (strain 10050) was reported at a resolution of 2.5 Å.[11] The structure revealed that this complex is a cyclic 9-mer of α,β pairs. The arrangement of the BChl *a* molecules is shown in Figure 1 where the arrows, which lie nearly in the membrane plane, indicate the direction of Q_y-transition dipoles. Several Mg...Mg separation distances are indicated. The relatively large separation of 21 Å between adjacent B800 molecules results in weak coupling, $V \sim -20$ cm^{-1},[12] consistent with hole burning data which indicated that excitonic effects are unimportant for the B800 ring.[13-16] However, the B850 nearest neighbor distances of 8.9 and 9.6 Å lead to large coupling energies, $V \sim +300$ cm^{-1}.[12,17] Thus, and as first deduced on the basis of hole burning data,[18] exciton level structure is expected to be important for understanding the nature of the B850 absorption band and, for example, the B800→B850 energy transfer process. Figure 1 reveals that the B850 ring of 18 BChl *a* molecules should be viewed as a 9-mer of dimers. There are, however, two choices for the dimer, one associated with the 8.9 Å separation distance and the other with the distance of 9.6 Å. From an excitonic level structure point of view, however, the choice of dimer is inconsequential. The monomers of either dimer are symmetry-inequivalent and so, strictly speaking, the dimers should be referred to as heterodimers. More recently, the X-ray structure of the isolated LH2 or B800-850 complex of *Rhodospirillium molischianum* was reported.[19] Interestingly, LH2 was shown to be an 8-mer of α,β polypeptide pairs. A detailed discussion of the differences in the two structures is given by Koepke et al.[19] Suffice it to say that the picture which has the B800 molecules weakly coupled and the B850 molecules strongly coupled remains intact for LH2 of *Rs. molischianum* with the distances indicated in Figure 1 for *Rps. acidophila* and orientations of the B850 molecules relative to each other very similar to those of *Rs.*

molischianum. However, the orientations of the B800 molecular transition dipoles relative to those of the B850 molecules in the two species are quite different although the B800→B850 transfer rates are similar, ~ 2 ps, as measured at liquid helium temperatures.[20] Concerning the LH1 complex, it appears to be a cyclic 16-mer of BChl *a* dimers with an inner diameter large enough to house the reaction center complex.[21]

An X-ray structure of the LH2 complex from *Rb. sphaeroides* has yet to be determined. One purpose of this paper is to provide a comparison of the Q_y-electronic structures of the LH2 complexes of *Rps. acidophila* and *Rb. sphaeroides* based on the temperature and pressure dependencies of optical absorption and hole spectra. For clarity and ease of later discussion, Figure 2 shows the absorption spectra of both species at 4.2 K and at 250 K (ambient pressure). At the bottom is the exciton level structure from ref. (22) calculated in the nearest dimer-dimer coupling approximation for the B850 molecules of *Rps. acidophila*, see accompanying paper.[23] (The calculations of refs. (12,17) establish that the B800 molecules have little effect on the electronic structure of the B850 molecules and vice-versa.) The level structure of Figure 2 is positioned so as to place the lower and strongly allowed E_1 level at the maximum of the B850 absorption band of *Rps. acidophila* at 4.2 K. The C_9-symmetry and structure of the complex leads to this E_1 level carrying almost all of the absorption intensity of the B850 molecules,[12] at least in the absence of energy disorder due to the glass-like structural heterogeneity of the complex.[24] (This state of affairs also applies to the level structure of the B850 molecules of *Rs. molischianum*.[16,24]) The presence of B850 levels in the near vicinity of B800 as well as the significantly different B800-B850 energy gap for the two species should be noted.

Before reviewing some recent work on the excitation energy transfer and relaxation dynamics of the LH2 complex, it is appropriate first to provide a definition of strong excitonic coupling. Categorization as strong means that the splittings between the exciton levels, as determined by the static lattice Hamiltonian, are large relative to the dephasing-

induced widths of the levels produced by nuclear motions of the bath (protein), the energy disorder of symmetry-equivalent Chl molecules resulting from the glass-like structural heterogeneity of proteins, and the exciton-phonon coupling. Prior to the introduction of spectral hole burning into the field of photosynthesis, very little was known about the last three of these energy terms (for reviews see refs. (25-27)). Fortunately, the exciton-phonon coupling for antenna protein complexes is weak, ~ 10-20 cm^{-1}, which means that it can be treated perturbatively. As for structural heterogeneity and energy disorder, spectral hole burning experiments revealed that it leads to inhomogeneous broadenings of Q_y-absorption bands of 100-200 cm^{-1}. Recent femtosecond[28-30] and nonlinear polarization measurements[31] have revealed that this magnitude of inhomogeneous broadening persists at room temperature. Furthermore, spectral hole burning established that there is little correlation between the Q_y-state energies of different individual complexes in the ensemble of complexes being studied. This was an important finding since structural heterogeneity then leads to a distribution of values for a donor-acceptor electronic energy gap associated with energy or electron transfer. If sufficiently wide relative to the homogeneous width of the nuclear factor in the nonadiabatic rate expression, this distribution can lead to non-single exponential (dispersive) kinetics for the transfer process of the ensemble as discussed in refs. (32-37). Having defined strong coupling, we note that energy disorder in a nanostructure such as the LH2 complex can destroy its cyclic symmetry and lead, for example, to localization effects for the electronic excitations of the nanostructure. Such localization, however, does not represent dynamics since it is determined by Schrödinger's time-independent equation. Recently, the question of localization effects in the LH1 and LH2 complexes has received increasing attention.[38-42] The above considerations relate to the applicability of conventional Förster theory to energy transfer dynamics. It is a weak coupling theory in which the static intermolecular potential energy is the trigger in the rate expression for transfer and the absence of inhomogeneous broadening is assumed. If the

donor-acceptor state coupling is weak, however, it can be readily modified for a distribution of energy gap values.[36] When excitonic couplings dominate the electronic dephasing from bath interactions, Förster theory is inapplicable. In this case inter-exciton level relaxation requires modulation of intermolecular interactions by librational or translational motions of the chromophores as discussed in the book Davydov[43] (for reviews see refs. (44,45)). This mechanism has been invoked to explain the ~ 200 fs excitation energy relaxation dynamics of the aforementioned FMO complex.[3,46]

By way of review we turn next to the excitation energy / relaxation dynamics of the LH2 complex. We consider first the B800→B850 energy transfer process, the most detailed experimental and theoretical study of which can be found in ref. (47) for *Rps. acidophila.* This work, which reviews earlier time domain and hole burning studies, strongly indicates that the primary mechanism of the transfer is of the Förster type for all organisms, one that involves spectral overlap between the fluorescence origin band of the weakly coupled B800 molecules and vibronic levels which build on the origin absorption band of the B850 molecules as originally proposed by Reddy et al.[18] The model and calculations of ref. (47) take into account the inhomogeneous broadening of both bands and the homogeneous broadening of the B850 band and utilizes previously determined Franck-Condon factors for BChl *a* intramolecular modes and protein phonons. They account well for the weak dependence of the B800→B850 transfer rate on temperature (~ $(0.7\ ps)^{-1}$ at room temperature and ~ $(2\ ps)^{-1}$ at liquid helium temperatures), on pressure,[15,47] on mutation[48] and on species which, in combination, lead to a variation in the B800-B850 energy gap from ~ 450 to ~ 1050 cm^{-1}.

Concerning the excitation energy relaxations involving the B850 molecules, spectral hole burning studies of LH2 of *Rb. sphaeroides* and *Rps. acidophila* established that the B850 absorption band is characterized by significant homogeneous broadening at 4.2 K.[14,49] (This is in sharp contrast with the B800 band which is mainly inhomogeneously

broadened.[13,18]) For example, a homogeneous broadening of ~ 200 cm^{-1} was determined for *Rb. sphaeroides* which represented 70% of the full width of the B850 band. The model put forth by Reddy et al.[14,18] for the homogeneous broadening is that it is due to ultra-fast relaxation between exciton levels that contribute to the B850 band. They estimated that relaxations occur as fast as ~ 100-200 fs. Subsequent femtosecond experiments established that relaxations do occur on this time scale. In particular, Savikhin and Struve determined that relaxation occurs in ~ 80 fs at room temperature and ~ 200 fs at 19 K.[47] Thus, the temperature dependence is weak. The model of Reddy et al. preceded the structure determinations of LH2. With reference to the exciton level diagram of Figure 2, the lowest level (A symmetry) lies 100 cm^{-1} below the allowed doubly degenerate E_1 level, in close agreement with the calculations of Sauer et al.[12] and Alden et al.[17] The A level (commonly referred to as B870) has been resolved and characterized by zero-phonon hole (ZPH) action spectroscopy at 4.2 K in *Rb. sphaeroides*,[49] *Rps. acidophila*[14] and *Rs. molischianum*.[20] The ZPH action spectrum for *Rb. sphaeroides*, for example, indicated that B870 lies 250 cm^{-1} below the maximum of the B850 absorption band which, for the sample studied, carried a width of 270 cm^{-1}. Comparison of this 250 cm^{-1} value (gap) with those for the other two species suggests that the gap increases with increasing width of the B850 band. The results of very recent hole burning experiments on the isolated LH2 complex from *Rps. acidophila* are consistent with this.[22] An apparent energy gap of 200 cm^{-1} was obtained for a sample that exhibited a B850 bandwidth of 200 cm^{-1}, a gap which is still 100 cm^{-1} larger than the calculated values.[12,17] As discussed in refs. (22,24), structural heterogeneity, which leads to energy disorder (diagonal and/or off-diagonal) associated with the ring of B850 dimers, is very likely important for understanding the above gap, the absorption intensity of B870 and splitting of the degeneracies of levels indicated in Fig. 2. We return to this in sections 3. and 4. as well as in the accompanying paper.[23]

In this paper experimental results are presented which we believe are important for the development of a firm understanding of the exciton level structure and inter-exciton level relaxation dynamics of the B850 ring of BChl *a* molecules. They also allow for a quite detailed comparison of the LH2 complexes of *Rps. acidophila* and *Rb. sphaeroides*. This is important since an X-ray structure for LH2 of the latter species is unavailable. The results also pertain to the temperature dependence of nearest neighbor BChl *a*-BChl *a* couplings in the B850 ring. This is important since calculations of the exciton level structure are based on the room temperature X-ray structure, the results of which are often compared with low temperature spectroscopic data. The results presented include the temperature and pressure dependences of LH2's Q_y-absorption spectrum and the pressure dependences of the ZPH of B870, the lowest energy exciton level. Theoretical analyses of some of the results are given, the details of which are presented in the accompanying paper.[23] That paper also presents hole burning data on the temperature dependence of the spectral dynamics of the B870 exciton level which are important for understanding the exciton level structure of the B850 molecules. We also present in that paper an analysis of energy disorder on the level structure and absorption properties of the B850 ring.

2. EXPERIMENTAL

The LH2 complexes of *Rps. acidophila* (strain 10050) and *Rb. sphaeroides* were isolated according to the procedure described in ref. (50). (The same preparation led to the X-ray diffraction structure of the B800-850 complex of *Rps. acidophila*.) After dilution in glycerol:water solution (2:1 by volume) containing 0.1% LDAO in water, samples were contained in a polypropylene cryogenic tube and cooled in a Janis 8-DT liquid helium cryostat. Typical values for the optical density at the B850 band maximum were close to 0.5. A Bruker IFS 120HR Fourier transform spectrometer was used to record the preburn and postburn spectra. The burn laser was a Coherent CR 899-21 Ti:sapphire laser (linewidth of

0.07 cm^{-1}) pumped by a 15 W Coherent Innova 200 Ar-ion laser. Burn fluences, burn wavelengths and read resolutions are given in the figure captions. A more detailed description of the hole-burning apparatus can be found in ref. (51). For temperature dependence studies, a Lake Shore temperature controller (Model 330) was used to stabilize the temperature. After the diode reading reached the pre-set temperature, the sample was allowed to equilibrate for 15 minutes prior to initiating absorption or hole burning measurements.

The high pressure apparatus has been described in detail,[52] including the procedure used to measure pressure. To ensure good optical quality, the sample was contained in a gelatin capsule (5 mm outside diameter) and then housed in a specially designed high pressure cell (maximum pressure rating of 800 MPa) with four sapphire windows (thickness of 4 mm) providing optical access. The cell was connected to a three-stage hydraulic compressor (Model U11, Unipress Equipment Division, Polish Academy of Sciences) through a flexible thick-walled capillary (o.d./i.d. = 3.0 mm/0.3 mm). Helium gas was used as the pressure transmitting medium. With compression ratios of about 1, 5 and 79 for the three stages of the compressor, the highest pressure achievable is 1.5 GPa. A Janis 11-DT cryostat was used for cooling of the high pressure cell. High pressure - hole burning was performed at 12 K. At this temperature helium solidifies at ~ 75 MPa. Thus, in Figures 7 and 8 the indicated pressures are lower than this value.

3. RESULTS

As noted in the preceding section, samples of the isolated LH2 complex of *Rb. sphaeroides* and *Rps. acidophila* were isolated and purified using the same procedure. Frame a of Figure 2 shows the 4.2 and 245 K absorption spectra of the LH2 complex of *Rb. sphaeroides*. Frame b shows the same for *Rps. acidophila* at 4.2 and 250 K. The 4.2 K widths of the B800 band for *Rb. sphaeroides* and *Rps. acidophila* are equal, 125 cm^{-1}, while

for the B850 band they are 230 and 200 cm^{-1}, respectively. These widths are close to those reported in refs. (20,22). The narrowness is indicative of high sample quality, meaning that sample heterogeneity and inhomogeneous broadening due to the isolation and purification procedures and the glass forming solvent have been reduced to a low level. That the widths of the bands for the two species are so similar is important for comparison of the two species. In frame a of Figure 3 the B800 profiles of the two species are superimposed (solid curve, *Rb. sphaeroides*; dashed curve, *Rps. acidophila*). The similarity of the two profiles, including the high energy tailing is striking. Frame b compares the B850 absorption profiles. The energy scale for *Rb. sphaeroides* has been adjusted slightly so that its width for B850 is the same as that for B850 of *Rps. acidophila*, see figure caption. The solid arrow in frame b indicates the location of the lowest exciton level (B870)[20,22,49], *vide infra*. The low energy tailing due to this weakly absorbing level is very similar for both species. In addition, both B850 bands exhibit tailing on the high energy side (dashed arrow).

As mentioned, ZPH action spectroscopy has been previously used to characterize the weak B870 absorption band. Here, one burns a series of ZPH holes across the inhomogeneously broadened absorption profile with a constant burn fluence. The ZPH action spectra for *Rps. acidophila* and *Rb. sphaeroides* are compared in Figure 4 for the samples whose absorption profiles are shown in Figure 3. The dashed arrows in a (*Rb. sphaeroides*) and in b indicate the location of the center frequency of the action spectrum in the low energy tail of B850. For *Rps. acidophila* the center frequency lies 200 cm^{-1} below the B850 band maximum (the location of the allowed E_1 exciton level) with the action spectrum carrying an inhomogeneous width of 120 cm^{-1}. The quality of the action spectrum for *Rb. sphaeroides* is not as high due to the smaller number of ZPH. Its center frequency displacement (185 cm^{-1}) is slightly smaller than the value of 200 cm^{-1} for *Rps. acidophila*. As discussed in refs. (49), equating the center frequency displacement with the energy gap (ΔE) between the B870 level and the E_1 level involves some assumptions. For

example, the nonphotochemical hole burning quantum yield is independent of the burn frequency. In addition, our recent studies on the effects of diagonal and off-diagonal energy disorder on the exciton level structure of the B850 molecules and level absorption strengths[17,24] suggest that the assumption of constant absorption cross-section across the inhomogeneously broadened B870 profile needs examination. We consider this in the accompanying paper.[23] In earlier studies[14,22,49] it was reported that hole burning of B870 produces a broad satellite hole near the B850 absorption maximum. The same behavior was observed in this work (results not shown). The satellite structure is consistent with B870 and the states absorbing near the maximum being correlated by virtue of the wavefunctions being significantly delocalized.[3,49] It was also observed, as in refs. (14,18,49), that burning near and to the blue of the B850 absorption maximum results in a very broad hole, consistent with the B850 band being subject to large homogeneous broadening, cf. Introduction.

Temperature dependence studies

The results presented above establish that the 4.2 K B800 and B850 absorption profiles and B870 ZPH spectra of the isolated LH2 complexes of *Rps. acidophila* and *Rb. sphaeroides* are very similar, despite their B800-B850 energy gaps being very different; 955 and 775 cm^{-1}, respectively. These observations are important for comparison of the structures and electronic states of the two species. The similarity of the absorption profiles is maintained at higher temperatures. This is shown for B800 in Figure 5 where its width (fwhm) is plotted as a function of temperature for the two species. The thermal broadenings are nearly identical. The high energy tail of the B800 band contributes to the widths. The temperature dependence of the B800 band position is not shown because, for both species, it is independent of temperature between 4.2 K and room temperature (± 5 cm^{-1} uncertainty).

The temperature dependencies of the width (diamonds) and B800-B850 energy gap (solid circles) of the B850 band for the two species are shown in Figure 6 (note the differences between the vertical energy scales for the two species). Since the B800 band

maximum is independent of temperature, *vide supra*, the energy gap data points represent the temperature dependence of the B850 band's position or maximum. For both species this position is constant below about 150 K. This, together with the results for B800, means, in part, that the LH2 structure of both species undergoes little change below ~ 150 K or, put another way, that the temperature dependence of the complex's anharmonicity is weak below 150 K. Above ~ 150 K the B850 bands begin to shift to the blue with near linear rates (above ~ 170 K) of 0.87 ± 0.03 and 0.39 ±0.01 cm^{-1} K^{-1} for *Rps. acidophila* and *Rb. sphaeroides*, respectively. That this rate for *Rb. sphaeroides* is significantly lower must be a manifestation of structural differences between the two LH2 complexes. Furthermore, the observation that the B800 band position is independent of temperature between 4.2 K and room temperature means that the shifting of the B850 band above 150 K may well be a consequence of the temperature dependencies of nearest neighbor B850-B850 BChl *a* couplings. (That the B800 band position is independent of temperature indicates that the structural changes of the LH2 complex below ~ 150 K are not severe, i.e. are quite subtle.) Turning next to the thermal broadening of the two B850 bands, Figure 6 shows that there is a distinct break near 150 K. The straight lines through the data points are visual guides meant to indicate that there are regions of linear broadening. The linear broadening rates above and below ~ 150 K for *Rps. acidophila* are 0.47 and 0.64 cm^{-1} K^{-1} while for *Rb. sphaeroides* they are 0.36 and 0.52 cm^{-1} K^{-1}. That the break in thermal broadening occurs near 150 K (above which B850 shifts to the blue) should be noted. This temperature is close to the glass temperature (Tg) of the glycerol/water glass forming solvent.[20] The dramatic reduction in viscosity above Tg allows for structural changes of the protein complex as discussed in refs. (53,54). The faster rates of broadening below ~ 150 K together with the blue shifting of the B850 band strongly suggests that structural changes of the LH2 complex at this temperature result in a strengthening of nearest neighbor B850-B850 coupling for the low temperature structure, cf. section 4. It is important to compare the thermal broadening data for the B850 bands against those for the

B800 bands, Figure 5. Note that there is considerably more curvature to the thermal broadening of the B800 band. Thus, one may conclude that the primary mechanism for broadening of the B850 band is different from that for the B800 band, cf. section 4.

Pressure dependence studies

In previous studies of a number of photosynthetic complexes we have shown that the pressure dependencies of the Q_y-absorption spectrum and the ZPH of selected Q_y-states provide considerable insight into the strengths of nearest neighbor BChl-BChl couplings.[15,52,55] Earlier results on pressure dependent - hole burning studies of isolated chromophores in glasses, polymers and proteins[56,57] were important to the interpretations of the results for photosynthetic complexes. In these latter references the dependencies of the position and width of Q_y-absorption bands and ZPH were shown to be linear in pressure as observed for the isolated chromophores studied in refs. (56,57). However, the linear pressure shifts of Q_y-bands for complexes with strong BChl-BChl coupling, e.g. the special pair band of bacterial reaction centers and LH1 of purple bacteria, were observed to be about a factor of 5 larger than for isolated chromophores, ~ -0.5 vs. ~ -0.1 cm^{-1}/MPa.

In the present study one of our objectives was to determine the dependence of the B870's pressure shift on position within its inhomogeneously broadened profile. To this end, ZPH were burned at the positions indicated by the solid arrows in Figure 4, burn temperature of 12 K. The results are shown in Figures 7 and 8 for *Rps. acidophila* and *Rb. sphaeroides*, respectively. The linear pressure shifts in cm^{-1}/MPa are given in the figures. They range from – 0.45 to – 0.56 for *Rps. acidophila* in going from the high to low energy side of B870. The corresponding range for *Rb. sphaeroides* is from – 0.47 to – 0.60, essentially identical to that for *Rps. acidophila*. The increase in the pressure shift rate in going from the high to low energy sides of B870 is substantial, ~ 25% for the highest and lowest burn frequencies. Pressure broadening of the ZPH was observed to be strong, ~ 0.1 cm^{-1}/MPa for both species. This broadening prevented measurements to higher pressures than those indicated in the

figures. Since the hole spectra were recorded with a Fourier transform spectrometer we are able to report the linear pressure shifts and broadenings of the B800 and B850 absorption bands at 12 K for both species, Table I, where they are compared against the 4.2 K values previously determined for LH2 of *Rb. sphaeroides* (NF57 strain chromatophores devoid of LH1) for a sample which exhibited B800 and B850 absorption bandwidths of 170 and 280 cm^{-1}, respectively. These widths are significantly broader than those of the samples used in this study. The −0.39 and −0.38 cm^{-1}/MPa linear pressure shifts for the B850 band of *Rps. acidophila* and *Rb. sphaeroides* are identical within experimental uncertainty and about 25% greater in magnitude than that for the NF57 mutant. Because the results for this mutant were obtained using much higher pressures than those indicated in Figures 7 and 8, additional experiments were performed. Results for the pressure shifting and broadening for *Rps. acidophila* (85 K) and *Rb. sphaeroides* (100 K) are given in Figures 9 and 10. The linear shift and broadening rates are given in Table I along with those for the B800 band. The B850 linear shift rates at these higher temperatures are only slightly higher in magnitude than at 12 K as one might have anticipated on the basis of earlier works[15,52] which point out that the temperature dependence of compressibility of polymers and proteins is weak. Thus, the smaller linear pressure shift of B850 for the NF57 mutant is a real effect. However, its B850 pressure broadening rate is larger. This, together with the B870 linear pressure shifts given in Figures 7 and 8 and the similar linear pressure shift and broadening rates for B800 of *Rps. acidophila*, *Rb. sphaeroides* and the NF57 mutant suggest that structural heterogeneity and strong excitonic coupling are important for understanding the responses of the B850 band to pressure, cf. section 4. To conclude this subsection, we note that the much smaller pressure shifting and broadening rates of the B800 band relative to the B850 band, Table I, is consistent with the B800 molecules being weakly coupled as pointed out in ref. (15).

4. DISCUSSION

We begin with the results which allow for a comparison of the LH2 complexes of *Rps. acidophila* and *Rb. sphaeroides* and, when possible, the LH2 complex of *Rs. molischianum*. Following this, discussion of results which pertain to the exciton level structure of the B850 ring is presented. This discussion sets the stage for the accompanying paper.[23] In addition, we discuss the importance of structural heterogeneity (energy disorder) and strong excitonic interactions for understanding the responses of excitonic absorption bands to pressure.

Our results show that the isolated LH2 complexes of *Rps. acidophila* and *Rb. sphaeroides* are strikingly similar in several respects: (a) essentially identical 4.2 K B800 absorption profiles, including the high energy tailing, Figure 3; (b) identical thermal broadening of the B800 band, Figure 5, as well as an absence of thermal shifting; (c) similar 4.2 K B850 absorption profiles, both of which show nearly identical low energy tailing due to B870 and a distinct, weak tailing feature on the high energy side, Figure 3; (d) similar 4.2 K B870 ZPH action profiles, Figure 4, including the displacement of the profile maximum below the B850 absorption maximum ($\sim 200\ cm^{-1}$) and inhomogeneous broadening ($\sim 120\ cm^{-1}$); (e) nearly the same linear dependence on pressure of the position and width of the B850 band, Table I; and (f) nearly identical linear pressure shifting of B870 ZPH including the dependence of the shift rate on location of the burn frequency with the B870 absorption profile, Figures 7 and 8. To this list can be added the results of recent Stark experiments from Beekman, van Grondelle and coworkers[58] on the B850 band at 77 K which show that the dipole moment changes for *Rps. acidophila* and *Rb. sphaeroides* are similar.

Faced only with the above findings it would be reasonable to assert that the structures of the LH2 complexes of *Rps. acidophila* and *Rb. sphaeroides* are very similar, at least from the point of view of BChl *a* couplings within the B800 and B850 rings. (Although, on the basis of sequence homology of the LH2 complexes of the two species one can expect them to

have a similar fold of the α,β-polypeptide pair,[59] this does not exclude the possibility of significant differences at the level of detailed interactions between BChl *a* molecules and their interactions with the protein.) However, the thermal broadening and shifting data of Figure 6 for the B850 bands establish that there must be significant differences between the two B850 rings. Although these data for the two complexes are qualitatively similar, showing a distinct break at ~ 150 K, the near linear shift rate of 0.87 cm^{-1} K^{-1} above about 150 K for *Rps. acidophila* is 2.2 times higher than for *Rb. sphaeroides*. Recalling that the B800 band maximum is independent of temperature, it follows that the B800-B850 energy gap for *Rps. acidophila* is significantly larger at all temperatures, Figure 2. For example, the gaps for *Rps. acidophila* and *Rb. sphaeroides* in the low temperature limit are 955 and 775 cm^{-1}, respectively, while at ambient temperature they are 830 and 720 cm^{-1}. The thermal broadening rates for the two near linear regions shown in Figure 6 are about 30% higher for *Rps. acidophila*. The just mentioned differences are also observed for chromatophores.[20] They might be attributed to the LH2 complex of *Rb. sphaeroides* not being a 9-mer of α,β polypeptide pairs as is the case for *Rps. acidophila*. However, this view is questionable since the magnitude of the B800-B850 energy gap for *Rs. molischianum*, which based on the X-ray structure is an 8-mer, is nearly identical to that of *Rps. acidophila* at all temperatures.[20] Alternative explanations are considered next.

A. Temperature dependencies of the LH2 absorption spectrum

In consideration of why the energetic location of the B850 band and its temperature dependence are so different for *Rps. acidophila* and *Rb. sphaeroides*, it should be kept in mind that the differences between the two for the B800 band are small. This suggests that BChl *a*-protein residue interactions are not primarily responsible for the differences in the energetic location and temperature dependence of the B850 band. Such van der Waals and H-bonding interactions contribute significantly to the gas phase to protein dispersion (non-

excitonic) shifts of the Q_y-state energies of the BChl *a* molecules. Another possibility associated with the location of the Q_y-states prior to switching on the BChl *a*-BChl *a* couplings, is that the non-planarities[11,19] of the two B850 BChl *a* molecules of the α,β-polypeptide pair are different for *Rps. acidophila* (*Rs. molischianum*) and *Rb. sphaeroides*. Deviations from planarity are known to have a significant effect on Q_y-state energies.[9] This possibility or the preceding one, together with the assumption of invariance for nearest neighbor BChl *a*-BChl *a* couplings in the different species, do provide a possible solution to the problem being addressed. That is, and in reference to Fig. 2, the B850 band of *Rb. sphaeroides* is blue-shifted relative to *Rps. acidophila* (*Rs. molischianum*[20]) due to intermolecular interactions not associated with the excitonic couplings of the B850 ring. However, we favor the view that rests mainly on one or both of the nearest neighbor couplings of the B850 ring of *Rb. sphaeroides* being weaker than in *Rps. acidophila* or *Rs. molischianum*. In this picture, differences in van der Waals and H-bonding on interactions would be relatively unimportant. The results which most strongly suggest this possibility are the temperature dependencies of the B850 band, Figure 6. The linear broadening regions seen in Figure 6 are absent in the broadening curves of the B800 band (Figure 5) and, as will be shown, the broadening of the B850 band can be understood in terms of inter-exciton level relaxation involving phonon emission as suggested in ref. (20). For theoretical analysis of the data for B800 in Figure 5 it is necessary to subtract the low temperature residual width of ~ 125 cm^{-1}, due mainly to inhomogeneous broadening, from the data points. In so doing one finds that the broadening at temperatures higher than about 150 K follows close to a T^2-dependence.[60] This dependence is consistent with dephasing due to off-diagonal quadratic electron-phonon coupling which is commonly observed for electronic transitions of isolated chromophores in solids.[62-64] We take this as additional evidence for the B800 molecules behaving essentially like isolated chromophores, cf. Introduction. It is apparent that this quadratic dephasing mechanism for B800 is relatively

unimportant for B850. We suggest that this is a consequence of the levels of the B850 ring being far more delocalized.

Returning to Figure 6 we present a simple theoretical argument to explain the linear broadening regions. It is based on the inter-exciton level relaxation theory given in chapter four of ref. (43) and the theory of ref. (36). By necessity, we simplify by assuming that there are only two B850 exciton levels involved, the most reasonable choices being the allowed E_1 level centered near the maximum of the B850 band and the lower energy A (B870) level. This model is used first to estimate the extent to which nearest neighbor couplings strengthen for both *Rps. acidophila* and *Rb. sphaeroides* at temperatures below ~ 150 K. Following that we estimate how much weaker these couplings are for *Rb. sphaeroides* relative to *Rps. acidophila*. Let Ω be the frequency of the gap between the two levels and ω_{pr} the frequency of the promoting librational mode that couples the two levels. For our purposes it suffices to write the rate for relaxation from the upper to lower level as

$$k(T) = C\left(\frac{V^2}{\omega_{pr}\,\omega_{ph}}\right)(\bar{n}(\omega_{pr})+1)\,g_{ph}(\Omega-\omega_{pr})\,. \tag{1}$$

Here, V can be taken to be the nearest dimer-dimer coupling. The constant C includes geometrical factors which define how the variation of V via the promoting mode is proportional to V.[43] For what follows one can view C as a proportionality factor. Since it is unrealistic to assume that $\Omega = \omega_{pr}$, we invoke Franck-Condon active protein phonons with frequency ω_{ph} to satisfy energy conservation, i.e. $\Omega - \omega_{pr} - \omega_{ph} = 0$. In Eq. (1), $\bar{n}(\omega_{pr})$ is the thermal occupation number $[\exp(\hbar\omega_{pr}/kT) - 1]^{-1}$. The function g_{ph} multiplied by ω_{ph}^{-1} in the first bracketed term is the effective density of states provided by the phonons. We take g_{ph} to be smooth and slowly varying, meaning that we neglect its temperature dependence. In the high temperature limit, $\bar{n}(\omega_{pr}) = kT/\hbar\omega_{pr}$, i.e. one is in the linear broadening regime,

consistent with our data. (In ref. (20) it was estimated that $\omega_{pr} \sim 70\ cm^{-1}$ for *Rps. acidophila*). To proceed further, we assume that ω_{pr} is weakly dependent on temperature. As a result, Eq. (1) is simplified to

$$k(T) = C'\left(\frac{V^2}{\omega_{ph}}\right) T, \tag{2}$$

in the high temperature limit appropriate for the linear regions of broadening shown in Figure 6. Thus, $C'(V^2/\omega_{ph})$ governs the slopes of the linear broadening above and below ~ 150 K. Since our model has C′ independent of temperature, the difference in slopes for T > and < ~ 150 K is due to V^2/ω_{ph}. The difference in slopes (s) is given by

$$Ds = s(T > 150\ K) - s(T < 150\ K)$$

$$= C'\left[2V(DV)w_{ph}^{-1} - V^2 w_{ph}^{-2}(Dw_{ph})\right], \tag{3}$$

where ΔV and $\Delta\omega_{ph}$ are the changes in V and ω_{ph} due to the structural change near 150 K. It is reasonable to set $\Delta V = \beta V$ with V the value of V above ~ 150 K and β a constant dependent on species. Because the exciton level gap $\Omega = \omega_{pr} + \omega_{ph}$ and ω_{pr} is taken to be weakly dependent on temperature, $\Delta\omega_{ph}$ can be set equal to $\beta\omega_{ph}$ since Ω depends linearly on V. Thus,

$$\Delta s = \beta\left(C'V^2\,\omega_{ph}^{-1}\right). \tag{4}$$

We adopt the convention that $C'V^2\omega_{ph}^{-1}$ is the slope for T > ~ 150 K, i.e. $\Delta s < 0$. For *Rps. acidophila* this slope equals 0.47, Figure 6, and $\Delta s = -0.17$. Thus, $\beta = -0.36$, meaning that the low temperature (< ~ 150 K) value of V is 36% greater in magnitude than the high temperature value. The same procedure for *Rb. sphaeroides* leads to a value of 44%. Such increases are large and have a significant affect on the exciton level structure of the B850 ring as discussed in the accompanying paper.[23] For example, the exciton level structure

shown in Figure 2 was calculated with a nearest neighbor dimer-dimer coupling for the lower exciton manifold of – 200 cm^{-1} based on the room temperature X-ray structure.[12] If the above 36% increase is ascribed to this coupling, one has an interaction of – 270 cm^{-1}. Of course, one has in the B850 ring two dimers and two nearest neighbor monomer-monomer couplings, both of which may be affected by the structural change near 150 K.

Comparison of the linear broadenings of B850 for *Rps. acidophila* and *Rb. sphaeroides* in Figure 6 reveals that the linear rates for the latter are about 20% smaller for both the low and high temperature regions. According to the above model, the nearest neighbor monomer-monomer coupling(s) for *Rb. sphaeroides* is then about 20% smaller.

Although the above theoretical model is oversimplified, we believe it captures the essential physics behind the thermal broadening characteristics of the B850 band. Thus, we conclude that the nearest neighbor monomer-monomer coupling(s) of the B850 ring is weaker in *Rb. sphaeroides* than in *Rps. acidophila* (or *Rs. molischianum* since the temperature dependencies of its B850 band are nearly identical to those of *Rps. acidophila*[20]). Van der Waals and H-bonding interactions between protein residues and the BChl *a* may contribute to the thermal broadening and shifting of the B850 band but we believe such contributions are relatively unimportant.

To conclude this subsection we consider briefly the thermal shifting data shown in Figure 6 for the B850 band. For both *Rb. sphaeroides* and *Rps. acidophila* (also *Rs. molischianum*[20]) there is no shifting between liquid helium temperatures and ~ 150 K, the temperature at which there is a quite subtle (non-denaturing) structural change. Above ~ 150 K the B850 band shifts to the blue in a linear fashion with the rate for *Rps. acidophila* 2.2 times higher than *Rb. sphaeroides*. In contrast, the position of the B800 band is invariant to temperature up to 300 K (± 5 cm^{-1}). The contrasting behaviors for the B800 and B850 bands above ~ 150 K are consistent with excitonic interactions within the B850 ring being much stronger than within the B800 ring. That the shift rate for *Rps. acidophila* (*Rs.*

molischianum) is greater than the rate for *Rb. sphaeroides* is consistent with the assertion that excitonic interactions for the latter species are weaker than for *Rps. acidophila*. The linear blue-shifting of the B850 band which onsets above ~ 150 K is discussed further in the following subsection.

B. Pressure dependencies of the LH2 absorption spectrum

It was emphasized in section 3 that the linear pressure shifts of the B800 band for *Rps. acidophila* and *Rb. sphaeroides*, Table I, are comparable to the linear shifts observed for $\pi\pi^*$ states of isolated chromophores in polymers, glasses and proteins. By isolated we mean the absence of significant excitonic interactions between chromophores. It was noted that this is consistent with the X-ray structures of the LH2 complex and other data which indicate that excitation of the B800 molecules creates states which are highly localized, i.e. monomer-like, because of the weak excitonic couplings between B800 molecules. Based on earlier high pressure studies of photosynthetic complexes, it was pointed out that the higher linear pressure shifts of about – 0.4 cm^{-1}/MPa for the B850 bands are a signature for strong excitonic coupling. Based on all available high pressure data it appears that nearest neighbor Mg...Mg distances of $\lesssim$ 10 Å are required for shift rates significantly higher than – 0.15 cm^{-1}/MPa. For example, the shift rates for the three resolvable BChl *a* bands of the FMO complex at 805, 814 and 824 nm, *vide supra*, are in the range of – 0.08 to – 0.11 cm^{-1}/MPa.[52] The shortest Mg...Mg distance in this complex is 11 Å. For the special pair's P960 absorption band of the reaction center of *Rps. viridis*, the linear shift rate at 4.2 K is –0.42 cm^{-1}/MPa.[55] The Mg...Mg distance for the special pair is 7.2 Å. Noting that this distance is about 2 Å shorter than the nearest neighbor distances of the B850 ring and that P960's shift rate is identical to that of the B850 absorption band reported here for *Rb. sphaeroides* and *Rps. acidophila*, it is clear that factors other than the Mg...Mg distance are also important for understanding how pressure affects the level energies of excitonically

coupled systems. For example, one needs to understand the anisotropy of the compressibility and how this compressibility is related to the structure and interactions of Chl molecules within the complex. Such an understanding can be anticipated given, for example, the success of molecular dynamics and energy minimization computations in leading to a structure for the LH2 complex of *Rs. molischianum.*[19,65]

We turn next to the question of why the linear pressure shifts of the ZPH associated with the lowest exciton level (B870) of the B850 ring (Figures 7 and 8) are, on average, about 25% greater than that of the B850 absorption band for which the shift is ~ -0.40 cm^{-1}/MPa, Table I. Following that we consider the question of why the pressure shift of the B870 ZPH increases by ~ 25% in going from the high to low energy side of the inhomogeneously broadened B870 absorption profile.

It is proposed that the answer to the first question has its origin in energy disorder (diagonal and/or off-diagonal) stemming from the glass-like structural heterogeneity of proteins. The most detailed study of how energy disorder leads to splitting of degeneracies in a C_n-ring system and redistribution of oscillator strength between exciton levels is that of Wu and Small.[24] They employ symmetry adapted energy defect patterns for systematic analysis of the problem. (The focus of their work was the mixing of the allowed E_1 and forbidden A (B870) levels due to energy disorder and the relationship between the energy gap of these two levels and the absorption intensity of B870; see also the accompanying paper.[23]) What emerges, in part, from their calculations is that disorder-induced splitting of the allowed E_1 level, which is the dominant contributor to the B850 band, results in the lower and higher energy E_1 components shifting to the red and blue, respectively. Given that both components carry comparable absorption intensity,[24] it follows that the shifting of the B850 absorption band should be smaller than that of the B870 exciton level (which is selectively interrogated by hole burning) if the extent of energy disorder increases with increasing pressure. We note that this reasoning provides an explanation for why the pressure broadening of the B850

band, ~ 0.15 cm^{-1}/MPa, is a factor of seven times larger than that of the special pair band (P960) of the bacterial reaction center[15] since only a single exciton (dimer) level contributes to P960. The absence of pressure broadening of the B800 bands, Table I, also supports the notion that the underlying exciton level structure of the B850 band figures importantly in its pressure broadening and shifting.

The second question, which is why the linear pressure shift of the B870 complex increases as its absorption frequency shifts to the red, is a difficult one. Although a theory of linear pressure shifts exists for isolated chromophores in isotropic, homogeneous amorphous solids,[66] one does not exist for anisotropic excitonically coupled arrays. The theory of ref. (66) yields

$$\frac{\Delta\tilde{\nu}}{\Delta P} = n\,\kappa\,3^{-1}(\tilde{\nu}_{max} - \tilde{\nu}_{vac}) \tag{5}$$

for the shift rate with κ the compressibility, $\tilde{\nu}_{max}$ the frequency of the absorption maximum or hole at ambient pressure and $\tilde{\nu}_{vac}(> \tilde{\nu}_{max})$ is the gas-phase absorption frequency. The factor n is the power of the attractive chromophore-solvent interaction ($\propto R^{-n}$). When applied to the linear shifts of ZPH of isolated chromophores in polymers with n = 6, this equation yielded values for κ in reasonable agreement with bulk values.[67] For polymers and proteins κ is in the 0.05-0.15 GPa^{-1} range. In earlier works we applied Eq. 5 to relatively weakly coupled BChl complexes such as the FMO complex[52] and for this complex determined a value of $\kappa = 0.1$ GPa^{-1}. Since the B800 molecules are weakly coupled, we venture to use Eq. (5) to arrive at estimates for κ. From Table I, the 12 K linear pressure shifts of the B800 band for the isolated complexes of *Rps. acidophila* and *Rb. sphaeroides* are – 0.09 and – 0.15 cm^{-1}/MPa. Their $\tilde{\nu}_{max}$ (B800) values are 12445 and 12505 cm^{-1}. With $\tilde{\nu}_{vac}$ = 13,340 cm^{-1} [68] and n = 6 for the BChl *a*-protein interactions, Eq. (1) yields κ = 0.05 and 0.09 GPa^{-1} for *Rps. acidophila* and *Rb. sphaeroides*, respectively. This simple calculation opens up the possibility that *Rb. sphaeroides* possesses a higher κ-value than *Rps.*

acidophila. We return to this below. Returning to the problem of the dependence of B870's pressure shift on excitation frequency, one might suggest that the dependence is due to an increase in κ as the excitation frequency is tuned from high to low energy. Here, one would have to argue that the tightness of packing of the α,β-polypeptide pairs of the ring[11,19] is negatively correlated with decreasing B870 excitation frequency. The calculations of Wu and Small[24] provide support for such correlation. Their results indicate that the location of the inhomogeneously broadened B870 absorption profile (as well as its intensity) is determined, in part, by energy disorder (diagonal and/or off-diagonal) of the B850 ring and that the red-most absorbing B870 levels are associated with greater energy disorder and, as a consequence, stronger coupling with the allowed E_1-level. If increasing energy disorder is associated with greater structural disorder, which seems physically reasonable, it follows that the compressibility κ should increase with decreasing B870 excitation frequency. It should be pointed out that increasing energy disorder leads to greater electronic localization effects for the Q_y-states of the B850 ring. Currently, these disorder-induced localization effects are not well understood. They need to be since, otherwise, it will not be possible to firmly understand the ultra-fast inter-exciton level relaxations of the B850 ring (or those of the LH1 (B875) ring) and the effects of external electric field and pressure which are used to probe its structure and Q_y-electronic states.

To conclude this subsection we address the problem of why the pressure dependencies of the B850 bands of *Rps. acidophila* and *Rb. sphaeroides*, Figure 7, 8 and Table I, are so similar while the temperature dependencies are not, Figure 6. We interpreted the difference in temperature dependencies as being due to nearest neighbor BChl *a*-BChl *a* couplings of *Rb. sphaeroides* being about 20% weaker than those of *Rps. acidophila* (*Rs. Molischianum*[20]). In consideration of the above problem it is important to understand that the effects (physics) of increasing pressure at constant temperature are very different from those of decreasing temperature at constant pressure as recently discussed by Sesselman et al.

in their study of molecular chromophores imbedded in polymers.[56] For example, they show that the shift of the absorption frequency ($\bar{\nu}$) of a chromophore as the temperature is increased from T_1 to T_2 at constant pressure can be expressed as

$$\bar{\nu}(T_2) - \bar{\nu}(T_1) = \int_{T_1}^{T_2} \left(\frac{\partial \bar{\nu}}{\partial T}\right)_V dT - 3\left(\frac{\partial \bar{\nu}}{\partial P}\right)_T \int_{T_1}^{T_2} \frac{\alpha_\ell}{\kappa} dT, \tag{6}$$

where α_ℓ is the linear expansivity, the temperature dependence of which has been determined for polymers.[69] The first term on the R.H.S. is generally negative, a consequence of a reduction in phonon frequencies upon electronic excitation of the chromophore.[62,70] Since α_ℓ and κ are positive while $\left(\frac{\partial \bar{\nu}}{\partial P}\right)_T$ is negative , the second term is positive. Therefore, application of Eq. (6) to the B850 band's near linear blue-shifting at temperatures above ~ 150 K, Figure 6, requires that the second term dominates the first. A simple calculation shows that its application is justified. From our data we set $\left(\frac{\partial \bar{\nu}}{\partial P}\right)_T = -0.5$ cm^{-1}/MPa. For polymers and proteins the temperature dependence of κ is very weak.[67] Since linear shift data at high temperatures are being considered, we set $\kappa = 0.15$ GPa^{-1}. For polymers the temperature dependence of the expansivity is weak for $T \gtrsim 150$ K. We use an average value of $\alpha_\ell = 6 \times 10^{-5}$ K^{-1} for the temperature range 150-300 K based on the data of Lyon et al.[69] for poly(methylmethacrylate), PMMA. With these values the second term of Eq. (6) yields a B850 bandshift of 90 cm^{-1} for a temperature increase from 150 to 300 K. The experimental shifts for *Rb. sphaeroides* and *Rps. acidophila* are 55 and 125 cm^{-1}, respectively. The agreement is satisfactory. Thus, one can be confident that the second term of Eq. (6) is largely responsible for the linear blue-shifting of the B850 band at temperatures above about 150 K.

The absence of shifting at temperatures below 150 K can be understood, in part, by the strong nonlinear decrease in α_ℓ at lower temperatures. For example, α_ℓ (4 K) =

2.7×10^{-7} K^{-1} and α_ℓ (50 K) = 2.1×10^{-5} K^{-1} for PMMA. Furthermore, α_ℓ of the LH2 complex most likely undergoes an abrupt increase near 150 K due to the structural change. In addition, the first term in Eq. (6) is more likely to counter-balance the second term at lower temperatures.

In view of the above discussion it is apparent that the second term in Eq. (6) provides an explanation for the smaller linear temperature shift for B850 of *Rb. sphaeroides* when its κ -value is larger than that for *Rps. acidophila* and the difference in their thermal expansivities is small. Whether the latter assumption is correct is unclear. However, a larger κ-value for *Rb. sphaeroides* also provides a basis for understanding why the linear pressure shifts of B850 for the two species are identical given our conclusion that the monomer-monomer coupling(s) of the *Rb. sphaeroides* ring is the weaker of the two. To see this, consider that the coupling (V) is of the transition dipole-dipole type. (The electronic structure calculations referred to earlier indicate that electrostatic interactions dominate the coupling.) It follows, for an isotropic homogeneous system, that[57] the fractional change in V at pressure P is $\Delta V(P)/V = \kappa P$. Thus, one sees that if the lower value of V for *Rb. sphaeroides* is compensated for by a higher value of κ, both species could have identical linear pressure shifts for the B850 band. Of course, the B850 ring is hardly isotropic and some contribution to the coupling from electron-exchange cannot be excluded. Nevertheless, we see no reason why our basic idea would not withstand more realistic theoretical modeling.

C. Exciton and vibrational structure in the absorption spectrum of the LH2 complex

In reference to the calculated exciton level structure of *Rps. acidophila*'s B850 molecules in Figure 2, it was noted that the lowest energy level of E_1 symmetry carries essentially all of the absorption intensity. (The x and y axes of the membrane plane form a basis for the E_1 rep while the z-axis transforms like the A rep.) The asterisks in Figure 2 indicate two closely spaced doubly degenerate levels (E_3 and E_4 in the lower manifold; E_2

and E_4 in the upper one). As is evident from the results of electronic structure calculations, the lowest energy asterisk level(s) and the levels to lower energy can be viewed, to a good approximation, as a manifold spawned by the lowest energy and strongly allowed level of the basic dimer, see accompanying paper.[23] The remaining levels shown in Figure 2 are spawned by the nearly forbidden upper level of the basic dimer. Under strict C_9-symmetry, the E_2, E_3 and E_4 levels are symmetry forbidden in absorption. Although, for example, the lowest A level is symmetry allowed, the nearly in-plane (x,y) orientation of the Q_y-transition dipoles renders it close to forbidden, carrying considerably less than 1% of the intensity of the B850 band according to the calculations of Sauer et al.[12] A more detailed group theoretical discussion can be found in ref. (24) where the effects of diagonal and off-diagonal energy disorder on the exciton level structure and absorption strengths are treated.

The above discussion, together with a comparison of the calculated exciton level structure with the 4.2 K absorption spectrum of *Rps. acidophila*, suggests that the relatively weak high energy tail absorption of the B800 and B850 bands might be due to exciton levels made weakly allowed by energy disorder,[24] see also Figure 3. This possibility has been recently raised.[20,22] (On the basis of the results of Figure 4 and those of earlier hole burning studies[14,18,49] as well as electronic structure calculations,[12,17] the assignment of the weak low energy feature (B870) of the B850 band, solid arrow in Figure 3, as the lowest exciton level (A) of the B850 ring must be considered to be definitive.) The other possibility is that the weak high energy features of the B800 and B850 bands are vibrational bands. This was the interpretation given in ref. (18) which reported on the satellite hole structure of the LH2 absorption spectrum of *Rb. sphaeroides* (NF 57 species) produced by burning near to and on the high energy of the B850 absorption maximum. On the basis of the known Franck-Condon factors of BChl *a* vibrations, it was argued that the high energy tail absorption of B800 was about 2 orders of magnitude too intense for an assignment to low frequency modes which build on the B800 absorption (origin) band, see also ref. (22). The intensities of the

satellite holes relative to the B850 hole and a Franck-Condon analysis led to the tail absorption being assigned as three closely spaced modes near 920 cm^{-1} (combined Franck-Condon factor of 0.05) which build on the B850 origin band. Satellite hole features at 750, 560, 340 and ~ 200 cm^{-1} were also assigned to vibrational modes building on B850. With these assignments, the high energy tail absorption of B850 would be due mainly to the 200 and 340 cm^{-1} modes. (We note that the strongest Chl mode associated with the $S_1(Q_y) \leftarrow S_0$ electronic transition has a frequency near 750 cm^{-1} and a Franck-Condon factor of only 0.05.[18,71]) Although the model of ref. (18) led to experimental Franck-Condon factors for the above 200-920 cm^{-1} features in reasonable agreement with previously determined values, a number of developments have occurred since then that call their assignment to vibrations into question. These include the X-ray structure determination of the LH2 complex, electronic structure calculations, and access to samples of the isolated LH2 complex from *Rb. sphaeroides* and *Rps. acidophila* exhibiting very narrow B800 and B850 bands, such as reported here and in refs. (20,22). One argument against vibrational assignment is based on the 4.2 K absorption spectra of *Rps. acidophila* and *Rb. sphaeroides* which exhibit a B800-B850 energy gap of 955 and 775 cm^{-1}, respectively. With reference to the B800 band of *Rb. sphaeroides* at 4.2 K in frame a of Figure 2, the 750 cm^{-1} satellite hole reported in ref. (18) appears ~ 25 cm^{-1} to the red of the B800 maximum. The corresponding absorption is too weak to be discernible in the B800 absorption profile. If this hole feature is a vibrational mode which builds on the B850 origin band, it should be observable in the 4.2 K absorption spectrum of *Rps. acidophila*, frame b, since the B800-B850 gap of 955 cm^{-1} is 180 cm^{-1} larger than that of *Rb. sphaeroides*. It should appear at the position of the solid arrow with a peak intensity one-twentieth that of the B850 band, sufficient for direct observation (see ref. (18) where the 750 cm^{-1} mode building on the B800 absorption origin band is observed). It is absent. Furthermore, if the tail absorption on the high energy side of B850 was due to modes in the ~ 200-340 cm^{-1} region, the 750 cm^{-1} band should be more

intense than the tail absorption given its larger Franck-Condon factor.[71] A second argument is based on the tail absorption on the high energy side of the B800 band being nearly identical for both species. If this absorption for *Rb. sphaeroides* was due to modes near 920 cm^{-1} which build on the B850 origin band, the corresponding frequency for *Rps. acidophila* would be 1100 cm^{-1}. The difficulty here is that 1100 cm^{-1} is in a region of quite weak Franck-Condon activity.[72] The above discussion indicates that the high energy tail absorption of B800 and B850 as well as, for example, the 750 cm^{-1} satellite hole feature reported for *Rb. sphaeroides* are not vibrational features. A more convincing argument against vibrational assignment is provided in the accompanying paper[23] based on new satellite hole spectra. We propose that the high energy tail absorption of the B800 and B850 bands observed is due mainly to exciton levels of the B850 ring. It was pointed out in ref. (47) that those B850 exciton levels which are resonant with the B800 band may lead to mixed B800-B850 states relevant to the understanding of the additional sub-ps relaxation dynamics observed within the B800 band when the excitation is to the blue of the B800 absorption maximum. The sub-ps dynamics is observed for both *Rb. sphaeroides*[73,74] and *Rps. acidophila*.[47]

5. CONCLUDING REMARKS

In this paper the LH2 complexes of *Rps. acidophila* and *Rb. sphaeroides* were compared on the basis of the temperature and pressure dependencies of the B800 and B850 absorption bands, the pressure dependence of zero-phonon holes burned into the inhomogeneously broadened absorption band of the lowest energy exciton level (B870) and the zero-phonon hole action spectrum of B870. Interestingly, the simplest experiment, measurement of the temperature dependence of the absorption spectrum, revealed the greatest difference between the two species; specifically, for the B850 band. (The temperature dependencies of the shift and broadening of the B800 bands are identical for the two species,

consistent with weak excitonic interactions of the B800 ring of BChl *a* molecules.) A model was presented that has the weaker thermal broadening of the B850 band for *Rb. sphaeroides* being due to its nearest neighbor BChl *a*-BChl *a* coupling(s) being weaker than in the B850 ring of *Rps. acidophila*, ca. 20%. Unfortunately, it is not possible to determine the extents to which the two nearest neighbor couplings contribute to the weakening. Theoretical analysis showed that the significant thermal broadening of the B850 bands is consistent with phonon-induced relaxation between the exciton levels (E_1, A (B870)) that contribute to the B850 band with the strongly allowed E_1 level split because of energy disorder, see ref. (24) and accompanying paper.[23] Weaker BChl *a*-BChl *a* coupling for the B850 ring of *Rb. sphaeroides* suggested looser packing of its α,β-polypeptide pairs than in *Rps. acidophila* (or *Rs. molischianum* since the temperature dependencies of its B850 band and B800-B850 gap are very similar to those of *Rps. acidophila*[20]). Association of looser packing with a higher value of the compressibility κ provided a basis for understanding the weaker thermal shifting of the B850 band of *Rb. sphaeroides* relative to that of *Rps. acidophila* and the essentially identical linear pressure shifting and broadening of their B850 bands. We note that the larger linear pressure shifting for B800 of the isolated LH2 complex for *Rb. sphaeroides*, Table I, is consistent with its LH2 complex having a higher compressibility value than that of *Rps. acidophila*. It had been reported that[20] the temperature dependencies of the LH2 absorption bands for all three of the above species do not depend significantly on whether the LH2 complex is isolated or membrane bound. Thus, we are confident that the new results presented for isolated complexes pertain to chromatophores.

The overall model summarized above is the only one we could conceive of that provides a basis for understanding both the temperature and pressure dependencies of the LH2 absorption spectrum for *Rb. sphaeroides* and *Rps. acidophila*. From the point of view of pressure, we were strongly guided by earlier works on photosynthetic complexes. For example, while the pressure dependencies of the B800 band can be understood in terms of the

B800 molecules behaving like isolated chromophores interacting mainly with the protein bath, this is impossible for the B850 molecules or those of the LH1 (B875) complex.[15] For example, the linear pressure shifts of the B870 exciton level of the B850 ring given in Figures 7 and 8 are the largest yet observed for a photosynthetic complex, a factor of 4-5 times larger than for isolated chromophores in glasses, polymers or proteins. To use the pressure shifts of Figures 7 and 8 with Eq. (5) to arrive at isotropic compressibility values would lead to gross errors since this equation was derived for an isolated chromophore in an isotropic and homogeneous medium. Although the calculations presented in support of our model are necessarily oversimplified, e.g. the assumption of isotropy for compressibilities and thermal expansivities, we believe that the model will survive rigorous examination.

That the temperature dependencies for the absorption spectrum of LH2 complexes of *Rps. acidophila* and *Rs. molischianum* are so similar (including the B800-B850 energy gap) is interesting since the structures determined by X-ray crystallography reveal that they are, respectively, 9-mers and 8-mers of α,β-polypeptide pairs. Despite the fact that the sequence homology between the polypeptides of the two species is marginal,[19] the structures reveal that the orientations and Mg...Mg distances of BChl *a* molecules of the B850 rings are very similar. That the temperature dependencies of the B850 band for *Rb. sphaeroides* are distinctly different from those of the other two species provides additional support for the conclusion that the structure of the LH2 complex of *Rb. sphaeroides* is significantly different ("looser"), at least at the level of BChl *a*-BChl *a* interactions within the B850 ring. Although there is considerable homology between the polypeptides of *Rps. acidophila* and *Rb. sphaeroides* they are far from identical.[59] Thus, an X-ray structure of LH2 of the latter is probably required for elucidation of the differences in electronic couplings of their B850 BChl *a* rings as well as their BChl *a*-protein interactions.

The pressure dependent data presented here should be amenable to detailed analysis by molecular dynamics and energy minimization calculations given that such calculations

played an important role in the determination of the structure of *Rs. molischianum*'s LH2 complex.[19,65] Of particular interest would be the determination of the anisotropy of the compressibility of this complex for the three species considered in this paper.

Finally, the hole burning results for the lowest energy exciton level, B870, of the B850 ring should prove helpful for refinement of electronic structure calculations since they provide the apparent gap between this level and the strongly allowed E_1 level. The apparent low temperature gap for *Rps. acidophila* is 200 cm^{-1} while it is slightly smaller (~ 10%) for *Rb. sphaeroides*. (It was pointed out that this gap depends on the homogeneity or quality of the sample as gauged by the low temperature widths of the B800 and B850 absorption bands.) Although the B870 level is predicted to be essentially totally forbidden in absorption, the B870 absorption band carries 3% of the intensity of the entire B850 band. In the accompanying paper[23] we extend the work of Wu and Small[24] on the effects of energy disorder on the above energy gap and absorption intensity of B870 as well as other forbidden levels of the B850 ring. In doing so, the strengthening of nearest neighbor couplings below ~ 150 K is taken into account. Of particular interest is the correction to the above "apparent" energy gap due to a variation of the B870 transition dipole strength across B870's inhomogeneous absorption profile, a variation which results from a distribution of values for the energy disorder parameters. Experimental results which pertain to the exciton level structure of the B850 ring and the temperature dependence of the dephasing of the B870 level are also presented.

Acknowledgments

Research at the Ames Laboratory was supported by the Division of Chemical Sciences, Office of Basic Energy Sciences, U.S. Department of Energy. Ames Laboratory is operated for USDOE by Iowa State University under Contract W-7405-Eng-82. Research at

the University of Glasgow was supported by BBSRC and EU. We thank Dr. Klaus Schulten for providing us with preprints of his work prior to publication and for helpful discussions.

References and Notes

(1) Zuber, H.; Brunisholz, R. A. In *Cholrophylls,* Scheer, H., Ed.; CRC Press: Boca Raton, Florida, 1991; p 627.

(2) Zuber, H.; Cogdell, R. In *Anoxygenic Photosynthetic Bacteria*; Blankenship, R. E., Madigan, M. T., Bauer, C. E., Eds.; Kluwer Academic Publishers: Dordrecht, 1995; p 315.

(3) Johnson, S. G.; Small, G. J. *J. Phys. Chem.* **1991,** *95*, 471.

(4) Pearlstein, R. M. *Photosyn. Res.* **1991,** *31*, 213.

(5) Matthews, B. W.; Fenna, R. E. *Acc. Chem. Res.* **1980,** *13*, 309.

(6) Tronrud, D. E.; Schmid, M. F.; Matthews, B. W. *J. Mol. Biol.* **1986,** *188*, 443.

(7) van Mourik, F.; Verwijst, R. R.; Mulder, J. M.; van Grondelle, R. *J. Phys. Chem.* **1994,** *98*, 10307.

(8) van Mourik, F.; Verwijst, R. R.; Mulder, J. M.; van Grondelle, R. *J. Lumin.* **1994,** *53*, 499.

(9) Gudowska-Nowak, E.; Newton, M. D.; Fajer, J. *J. Phys. Chem.* **1990,** *94*, 5795.

(10) Sundström, V.; van Grondelle, R. In *Anoxygenic Photosynthetic Bacteria*; Blankenship, R. E., Madigan, M. T., Baller, C. E., Eds.; Kluwer Academic Publishers: Dordrecht, 1995; p 349.

(11) Freer, A.; Prince, S.; Sauer, K.; Papiz, M.; Hawthornthwaite-Lawless, A.; McDermott, G.; Cogdell, R.; Isaacs, N. W. *Structure* **1996,** *4*, 449.

(12) Sauer, K.; Cogdell, R. J.; Prince, S. M.; Freer, A. A.; Isaacs, N. W.; Scheer, H. *Photochem. Photobiol.*, **1996,** *64*, 564.

(13) van der Laan, H.; Schmidt, Th.; Visschers, R. W.; Visscher, K. J; van Grondelle, R.; Völker, S. *Chem. Phys. Letts.* **1990,** *170*, 231.

(14) Reddy, N. R. S.; Cogdell, R. J.; Zhao, L. Small, G. J. *Photochem. Photobiol.* **1993,** *57*, 35.

(15) Reddy, N. R. S.; Wu, H.-M.; Jankowiak, R.; Picorel, R.; Cogdell, R. J.; Small, G. J. *Photosyn. Res.* **1996**, *48*, 277.

(16) Hu, X.; Ritz, T.; Damjanovic, A.; Schulten. K. *J. Phys. Chem. B* **1997**, *101*, 3854.

(17) Alden, R. G.; Johnson, E.; Nagarajan, V.; Parson, W. W.; Law, C. J.; Cogdell, R. G. *J. Phys. Chem. B* **1997**, *101*, 4667.

(18) Reddy, N. R. S.; Small, G. J.; Seibert, M.: Picorel, R. *Chem. Phys. Letts.* **1991**, *181*, 391.

(19) Koepke, J.; Hu, X.; Muenke, C.; Schulten, K.; Michel, H. *Structure*, **1996**, *4*, 581.

(20) Wu, H.-M.; Reddy, N. R. S.; Cogdell, R. J.; Muenke, C.; Michel, H. and Small, G. J. *Mol. Cryst. Liq. Cryst.* **1996**, *291*, 163.

(21) Karrasch, S.; Bullough, P. A. and Ghosh, R. *EMBO J.* **1995**, *14*, 631.

(22) Wu, H.-M.; Reddy, N. R. S.; Small. G. J. *J. Phys. Chem. B* **1997**, *101*, 651.

(23) Chapter 5; Wu, H.-M.; Ratsep, M.; Lee, I.-J.; Cogdell, R. J.; Small, J. J. *J. Phys. Chem. B* **1997**, *101*, 7654.

(24) Wu, H.-M.; Small. G. J. *Chem. Phys.* **1997**, *218*, 225.

(25) Reddy, N. R. S.; Lyle, P. A.; Small, G. J. *Photosyn. Res.* **1992**, *31*, 167.

(26) Jankowiak, R.; Small, G. J. In *Photosynthetic reaction centers*, Deisenhofer, J.; Norris, J., Eds.; Academic Press: London, 1993; p. 133.

(27) Jankowiak, R.; Hayes, J. M.; Small, G. J. *Chem. Rev.* **1993**, *93*, 1471.

(28) Peloquin, J. M.; Lin, S.; Taguchi, A. K. W.; Woodbury, N. W. *J. Phys. Chem.* **1995**, *99*, 1349.

(29) Bradforth, S. E.; Jimenez, R.; van Mourik, F.; van Grondelle R.; G. R. Fleming, *J. Phys. Chem.* **1995**, *99*, 16179.

(30) Visser, H. M.; Somsen, O. J. G.; van Mourik, F.; van Grondelle, R. *J. Phys. Chem.* **1996**, *100*, 18859.

(31) Leupold, D.; Voigt, B.; Pfeiffer, M.; Bandilla, M.; Scheer, H. *Photochem. Photobio.* **1993**, *57*, 24.

(32) Du, M.; Rosenthal, S. J.;Xie, X.; DiMagno,T. J.; Schmidt, M.; Hanson, D. K.; Schiffer, M.; Norris, J. R.; Fleming, G. R. *Proc. Natl. Acad. Sci. USA* **1990,** *87*, 3552.

(33) Small, G. J.; Hayes, J. M.; Silbey, R. J. *J. Phys. Chem.* **1992**, *96*, 7499.

(34) Müller, M. G.; Griebenow, K.; Holtzwarth, A. R. *Chem. Phys. Lett.* **1992,** *199*, 465.

(35) Jia, Y.; DiMagno, T. D.;. Chan, C.-K.; Wang, Z.; Du, M.; Hanson, D. K.; Schiffer, M.; Norris, J. R.; Fleming G. R.; Popov, M. S. *J. Phys. Chem.* **1993,** *97*, 13180.

(36) Kolaczkowski, S. V.; Hayes, J. M.; Small, G. J. *J. Phys. Chem.* **1994**, *98*, 13418.

(37) Bixon, M.; Jortner, J.; Michel-Beyerle, M. E. *Chem. Phys.* **1995,** *197*, 389.

(38) Jimenez, R.; Dikshit, S. N.; Bradforth, S. E.; Fleming, G. R. *J. Phys. Chem.* **1996**, *100*, 6825.

(39) Pullerits, T.; Chachvisvilis, M.; Sundström, V. *J. Phys. Chem.* **1996**, *100*, 10787.

(40) Nagarajan, V.; Alden, R. G.; Williams, J. C.; Parson, W. W. *Proc. Natl. Acad. Sci. USA* **1996,** *93*, 13774.

(41) Chachvisvilis, M., thesis, Lund University (1996); Chachvisvilis, M.; Kühn, O; Pullerits, T.; Sundström, V. *J. Phys. Chem. B*, **1997**, *101*, 7275.

(42) Meier, T; Zhao, Y.; Chernyak, V.; Mukamel, S. *J. Chem. Phys.*, **1997**, *107*, 3876.

(43) Davydov, A. S. *Theory of Molecular Excitons*; Plenum Press: New York, 1971.

(44) Hochstrasser, R. M.; Prasad, P. N. In *Excited States*, Vol. 1; Lim, E. C., Ed.; Academic Press: New York, 1974. p 79.

(45) Johnson, C. K.; Small, G. J. In *Excited States*, Vol. 6; Lim, E. C., Ed.; Academic Press: New York, 1982; p 97.

(46) Gillbro, T. ESF Workshop on Electron and Energy Transfer Dynamics in Photosynthesis, and Model Systems; University of Tyvaskyla, Finland, Dec. 1994; p 10.

(47) Chapter 3; Wu, H.-M.; Savikhin, S.; Reddy, N. R. S.; Jankowiak, R.; Cogdell, R. J.; Struve, W. S.; Small, G. J. *J. Phys. Chem.* **1996**, *100*, 12022.

(48) van der Laan, H.; De Caro, C.; Schmidt, Th.; Visschers, R. W.; van Grondelle, R.; Fowler, G. J. S.; Hunter, C. N.; Volker, S. *Chem. Phys. Letts.* **1993**, *212*, 569.

(49) Reddy, N. R. S.; Picorel R.; Small, G. J. *J. Phys. Chem.* **1992**, *96*, 6458.

(50) Cogdell, R. J.; Hawthornthwaite, A. M. In *The Photosynthetic Reaction Center*, Vol. 1; Deisenhofer, J.; Norris, J. R., Eds.; Academic Press: San Diego, 1993; p. 23.

(51) Lyle, P. A.; Kolaczkowski, S. V.; Small, G. J. *J. Phys. Chem.* **1993,** *97*, 6924.

(52) Reddy, N. R. S.; Jankowiak, R.; Small, G. J. *J. Phys. Chem.* **1995**, *99*, 16168.

(53) Ansari, A.; Berendzen, J.; Braunstein, D.; Cowen, B. R.; Frauenfelder, H.; Hong, M. K.; Iben, I. E. T.; Johnson, J. B.; Ormos, P.; Sauke, T. B.; Scholl, R.; Schulte, A.; Steinbach, P. J.; Vittitow, J.; Young, R. D. *Biophys. Chem.* **1987**, 26, 337.

(54) Iben, I. E. T.; Braunstein, D.; Doster, W.; Fraunfelder, H.; Hong, M. K.; Johnson, J. B.; Luck, S.; Ormos, P.; Schulte, A.; Steinbach, P. J.; Xie, A. H.; Young, R. D. *Phys. Rev. Lett.* **1989**, *62*, 1916.

(55) Small, G. J. *Chem. Phys.* **1995**, *197*, 239.

(56) Sesselmann, Th.; Richter, W.; Haarer, D.; Morawitz, H. *Phys. Rev. B* **1987**, *36*, 7601.

(57) Zollfrank, J.; Friedrich, J. *J. Phys. Chem.* **1992,** *96*, 7889.

(58) Beekman, L. M. P.; Frese, R. N.; Fowler, G. J. S.; Picorel, R.; Cogdell, R. J.; van Stokkum, I. H. M.; Hunter, C. N.; van Grondelle, R. *J. Phys. Chem. B* **1997**, *101*, 7293.

(59) Olson, J.; Hunter, N. *Photochem. Photobio.* **1994**, *60*, 521.

(60) Using the theory of Hayes *et al.*[61] and the previously determined parameter values: S = 0.3; $\omega_m = 20$ cm^{-1}; $\gamma = 2.5$ cm^{-1}; $\Gamma_{inh} = 105$ cm^{-1} and a one-phonon bandwidth of 20 cm^{-1}, it was determined that the contribution to the broadening from linear electron-phonon coupling is relatively weak.

(61) Hayes, J. M.; Lyle, P. A.; Small, G. J. *J. Phys. Chem.* **1994**, *98*, 7337.

(62) Skinner, J. L. *Ann. Rev. Phys. Chem.* **1988**, *39*, 463.

(63) Osako I. S. In *Advances in Polymer Science,* Vol. 114; Dušek, K. Ed.; Springer-Verlag: Berlin, 1994; p 123.

(64) Di Bartolo, B *Optical Interactions in Solids*; John Wiley and Sons: New York, 1968; Chapter 15.

(65) Hu, X.; Xu, D.; Hamer, K.; Schulten, K; Koepke, J.; Michel, H. *Protein sciences*, **1995**, *4*, 1670.

(66) Laird, B. B.; Skinner, J. L. *J. Chem. Phys.* **1989,** *90*, 3274.

(67) Perepechko, I. Ed. *Low Temperature Properties of Polymers*, Pergamon, Oxford, 1980.

(68) Renge, I. *Chem. Phys.* **1992**, *167*, 173.

(69) Lyon, K. G.; Salinger, G. L.; Swenson, C. A. *Phys. Rev., B* **1979,** *19*, 4231.

(70) Burke, F. P.; Small, G. J. *Chem. Phys.* **1974,** *5*, 198.

(71) Gillie, J. K.; Small, G. J.; Golbeck, J. H. *J. Phys. Chem.* **1989**, *93*, 1620.

(72) Renge, I.; Mauring, K.; Avarmaa, R. *J. Lumin.* **1987**, *37*, 207.

(73) De Caro, C.; Visschers, R. W.; van Grondelle, R.; Völker, S. *J. Phys. Chem.* **1994**, *98*, 10584.

(74) Monshouwer, R.; de Zarate, I. O.; van Mourik, F.; van Grondelle, R. *Chem. Phys. Lett.* **1995**, *246*, 341.

Table 1. Pressure shift and broadening rates (cm^{-1}/MPa) for B800 and B850.

		Pressure shift		Pressure broadening	
Temperature		12 K	85 K	12 K	85 K
Rps. acidophila	B800	-0.09	-0.11	~ 0	~ 0
	B850	-0.39	-0.40	0.13	0.14
Temperature		12 K	100 K	12 K	100 K
Rb. sphaeroides	B800	-0.15	-0.14	~ 0	~ 0
	B850	-0.38	-0.41	0.15	0.23
Temperature		4.2 K	85 K	4.2 K	85 K
NF 57	B800	-0.08	-0.10	~ 0	~ 0
	B850	-0.28	-0.33	0.2	0.20

Figure Captions

Figure 1. A schematic (based on Fig. 1 in ref. 12) showing the arrangement of the 18 B850 (upper ring) and 9 B800 (lower ring) molecules in the LH2 antenna complex from *Rps. acidophila*. Within the circular array, nearest neighbor distances (Mg...Mg) between B850 molecules are either 8.9 Å or 9.6 Å. The 9.6 Å distance is that of the two BChl *a* molecules associated with the α,β polypeptide pair. The two B850 BChl *a* molecules nearest to a B800 molecule are separated by distances of 17.6 Å and 18.3 Å. The horizontal arrows indicate the directions of the Q_y-transition dipoles.

Figure 2. 4.2 K (dashed line) and ~ 250 K (solid line) absorption spectra of the isolated LH2 complex from *Rb. sphaeroides* (a) and *Rps. acidophila* (b). The numbers indicate the B800-B850 energy gaps in cm^{-1}. Also shown together is the calculated exciton manifold of the B850 ring (c) from ref. (22), see text. The lowest energy level of the l-manifold is j = 0 (A) followed next by the strongly absorbing j={1,8} (E_1) level which has been placed at the B850 absorption maximum of *Rps. acidophila* at 4.2 K. The asterisks indicate two closely spaced doubly degenerate levels.

Figure 3. Comparison of B800 (a) and B850 (b) absorption profiles of LH2 from *Rb. sphaeroides* (solid line) and *Rps. acidophila* (dashed line). All spectra span a range of 1000 cm^{-1} except the solid curve in b which spans a range of 1120 cm^{-1}. See text for the explanation of arrows.

Figure 4. 4.2 K B850 absorption and B870's zero-phonon-hole (ZPH) action spectrum (read resolution = 0.5 cm^{-1}) for LH2 of *Rb. sphaeroides* (a) and *Rps. acidophila* (b). The ZPH action spectra of B870 in a and b were generated with a constant burn fluence of 135 and 100 J/cm^2, respectively. The dashed arrows locate the center of the action spectra (185 and 200 cm^{-1} below the B850 band maximum for *Rb.*

sphaeroides and *Rps. acidophila*, respectively). The fractional OD changes for ZPH at the dashed arrows are 0.025 and 0.15 for *Rb. sphaeroides* and *Rps. acidophila*, respectively. The solid arrows indicate the burn wavelengths used in the study of the pressure dependence of B870 zero-phonon holes (see Figures 7 and 8). The action spectrum carries an inhomogeneous width of 135 ± 10 cm^{-1} in a and 120 ± 10 cm^{-1} in b.

Figure 5. Thermal broadening of the B800 absorption band for LH2 of *Rb. sphaeroides* (diamonds) and *Rps. acidophila* (circles). Bandwidth values are full width at half-maximum.

Figure 6. Temperature dependencies of the B800-B850 energy gap (circles) and B850 bandwidth (diamonds) for *Rb. sphaeroides* (a) and *Rps. acidophila* (b). For both species, the energy gaps remain constant (± 5 cm^{-1}) below about 150 K. For both species the position of the B800 band is independnet of temperature, see text. Linear regression lines for the bandwidths, together with their slopes (in units of cm^{-1} K^{-1}, uncertainty = ± 0.01 cm^{-1} K^{-1}), are shown to indicate the faster broadening rates in the temperature region (below ~ 150 K for both species).

Figure 7. Linear pressure shifting of B870 ZPH (read resolution = 1 cm^{-1}) for *Rps. acidophila*. Four holes were burned at 11352.4, 11319.3, 11262.1 and 11223.1 cm^{-1}, respectively, at 15 MPa and 12 K. A relatively high burn fluence of 500 J/cm^2 was used, since holewidths were not the focus of this study. With increasing pressure, all holes shifted linearly (see the solid lines) to the red with rates (in cm^{-1} MPa^{-1}, uncertainty = ± 0.01 cm^{-1} MPa^{-1} for the bottom three lines and ± 0.03 cm^{-1} MPa^{-1} for the uppermost one) indicated in the figure. For the pressure range used, no irreversible pressure shifting of B870 ZPH was observed (elastic behavior).

Figure 8. Linear pressure shifting of B870 ZPH (read resolution = 1 cm^{-1}) for *Rb. sphaeroides*. Four holes were burned at 11585.3, 11543.4, 11501.4 and 11458.9 cm^{-1}, respectively, at 11 MPa and 12 K. A relatively high burn fluence of 400 J/cm^2 was used, since holewidths were not the focus of this study. As pressure increased, all holes shifted linearly (see the solid lines) to the red with rates (in cm^{-1} MPa^{-1}, uncertainty = ± 0.03, ± 0.01, ± 0.01 and ± 0.02 cm^{-1} MPa^{-1} from top to bottom lines) indicated in the figure. For the pressure range used, no irreversible pressure shifting of B870 ZPH was observed.

Figure 9. B850 band pressure shifting (diamonds) and broadening (circles) data for *Rps. acidophila* at 85 K. Linear shift (solid line) and linear broadening (dashed line) rates are – 0.398 ± 0.003 cm^{-1} MPa^{-1} and 0.141 ± 0.001 cm^{-1} MPa^{-1}, respectively.

Figure 10. B850 band pressure shifting (diamonds) and broadening (circles) data for *Rps. acidophila* at 100 K. Linear shift (solid line) and linear broadening (dashed line) rates are – 0.410 ± 0.003 cm^{-1} MPa^{-1} and 0.234 ± 0.004 cm^{-1} MPa^{-1}, respectively.

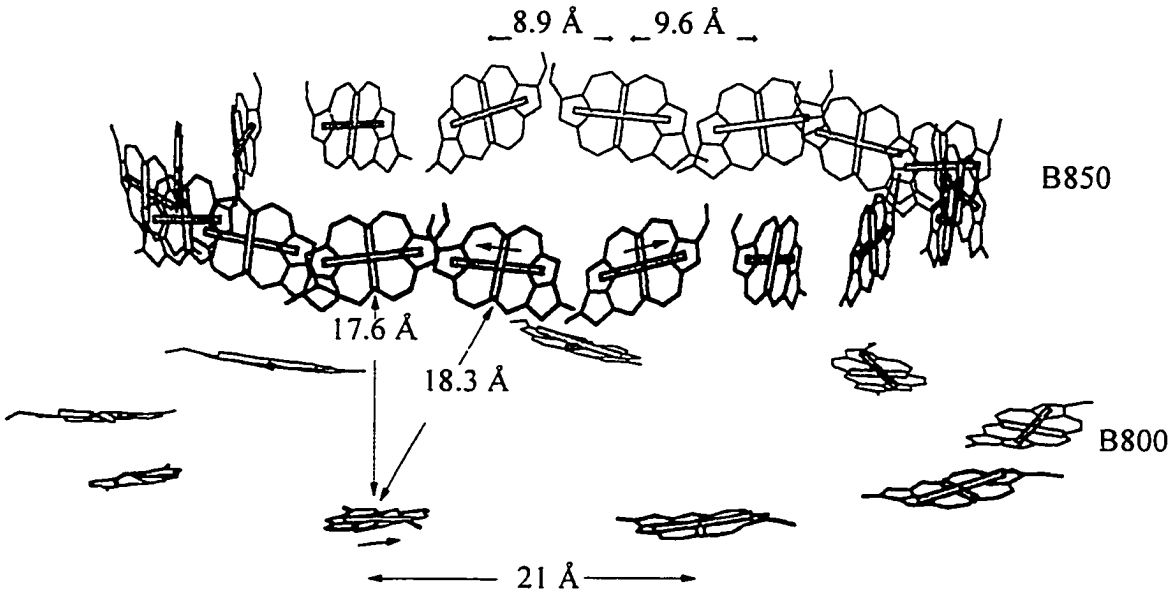

Figure 1

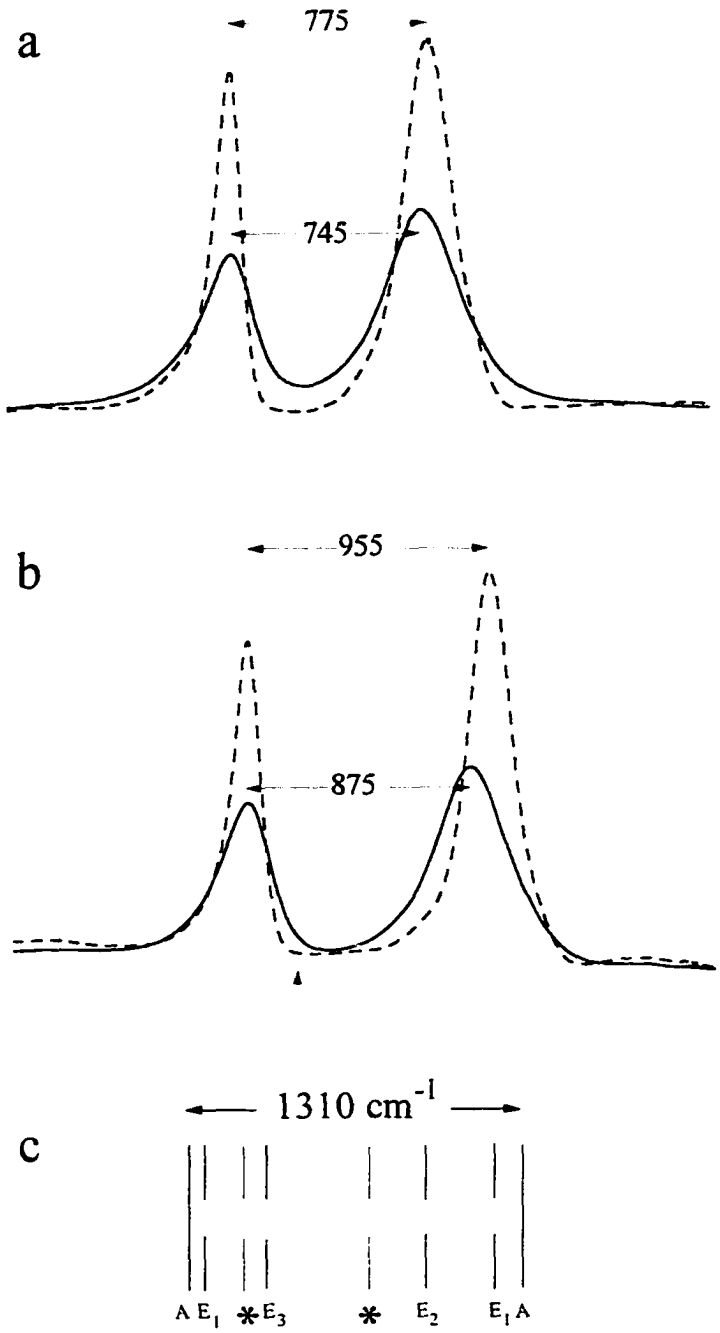

Figure 2

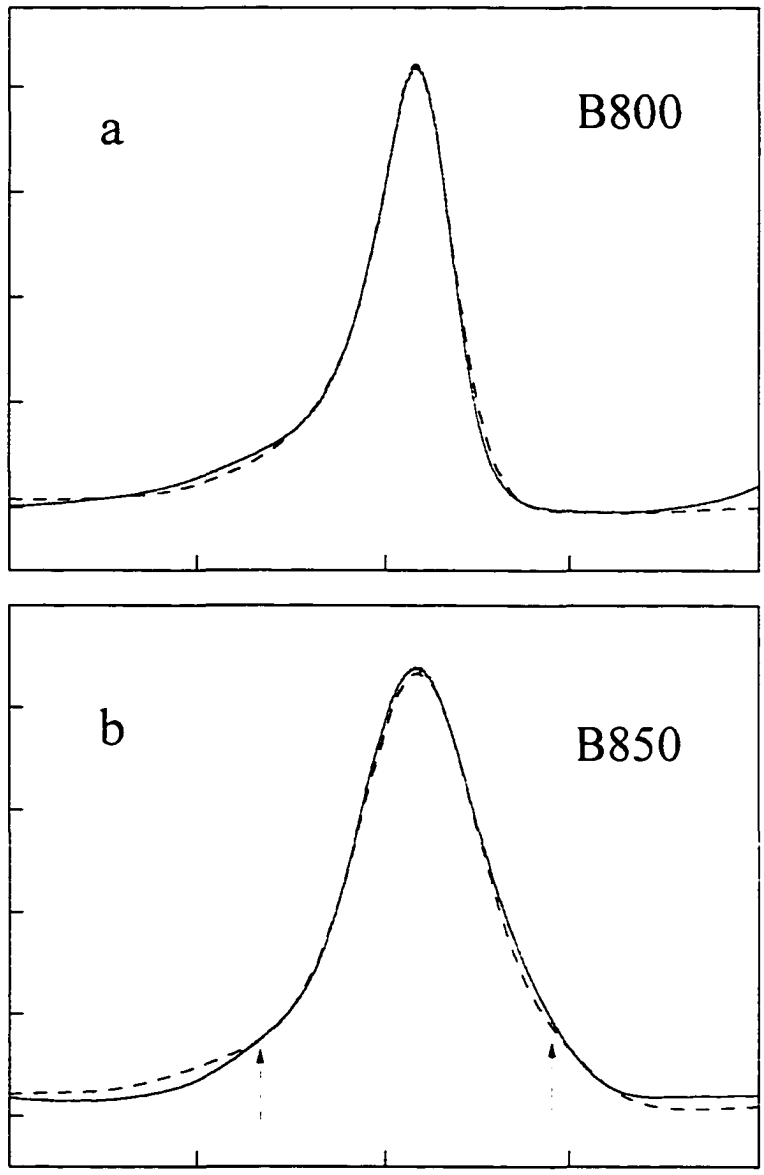

Figure 3

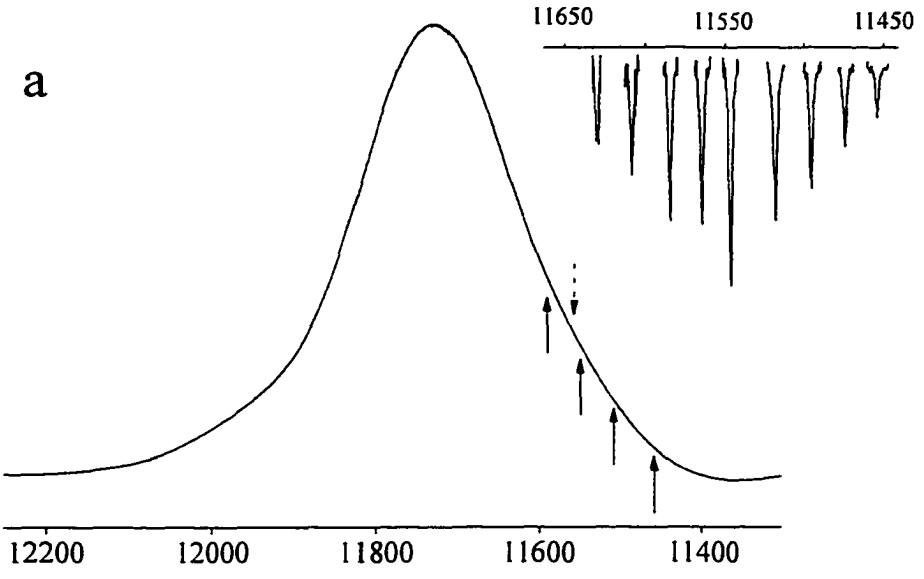
a
11650
11550
11450
12200
12000
11800
11600
11400
Wavenumber (cm-1)

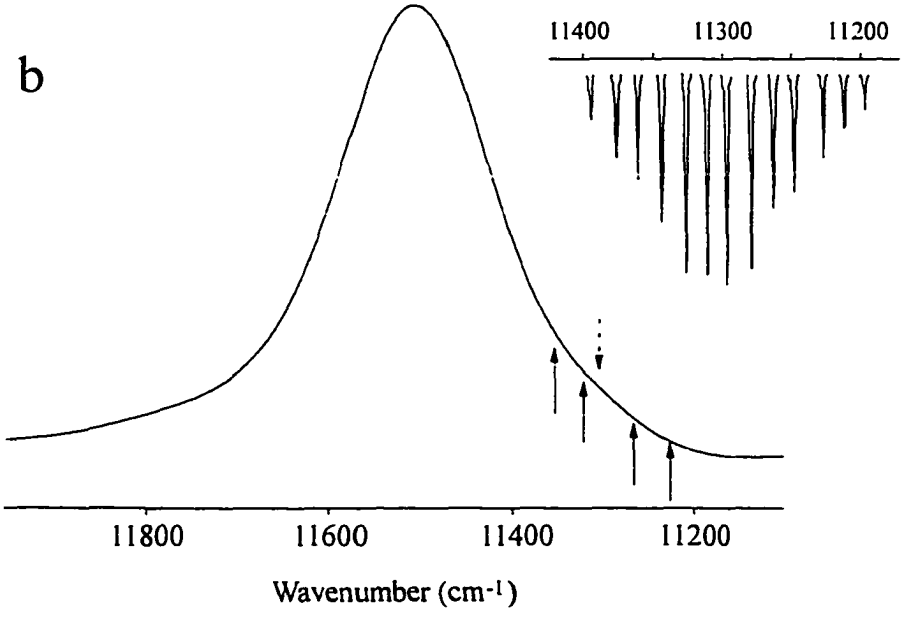
b
11400
11300
11200
11800
11600
11400
11200
Wavenumber (cm-1)

Figure 4

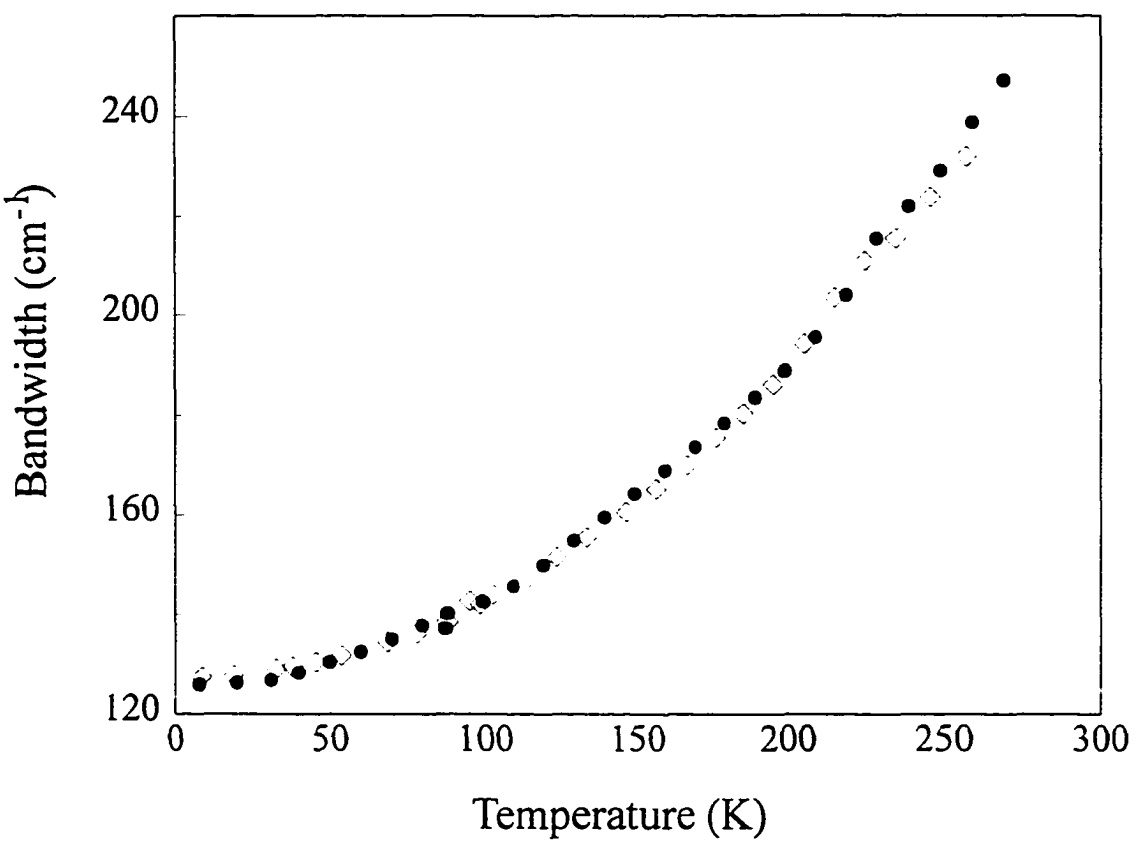
Bandwidth (cm-1)
240
200
160
120
0
50
100
150
200
250
300
Temperature (K)

Figure 5

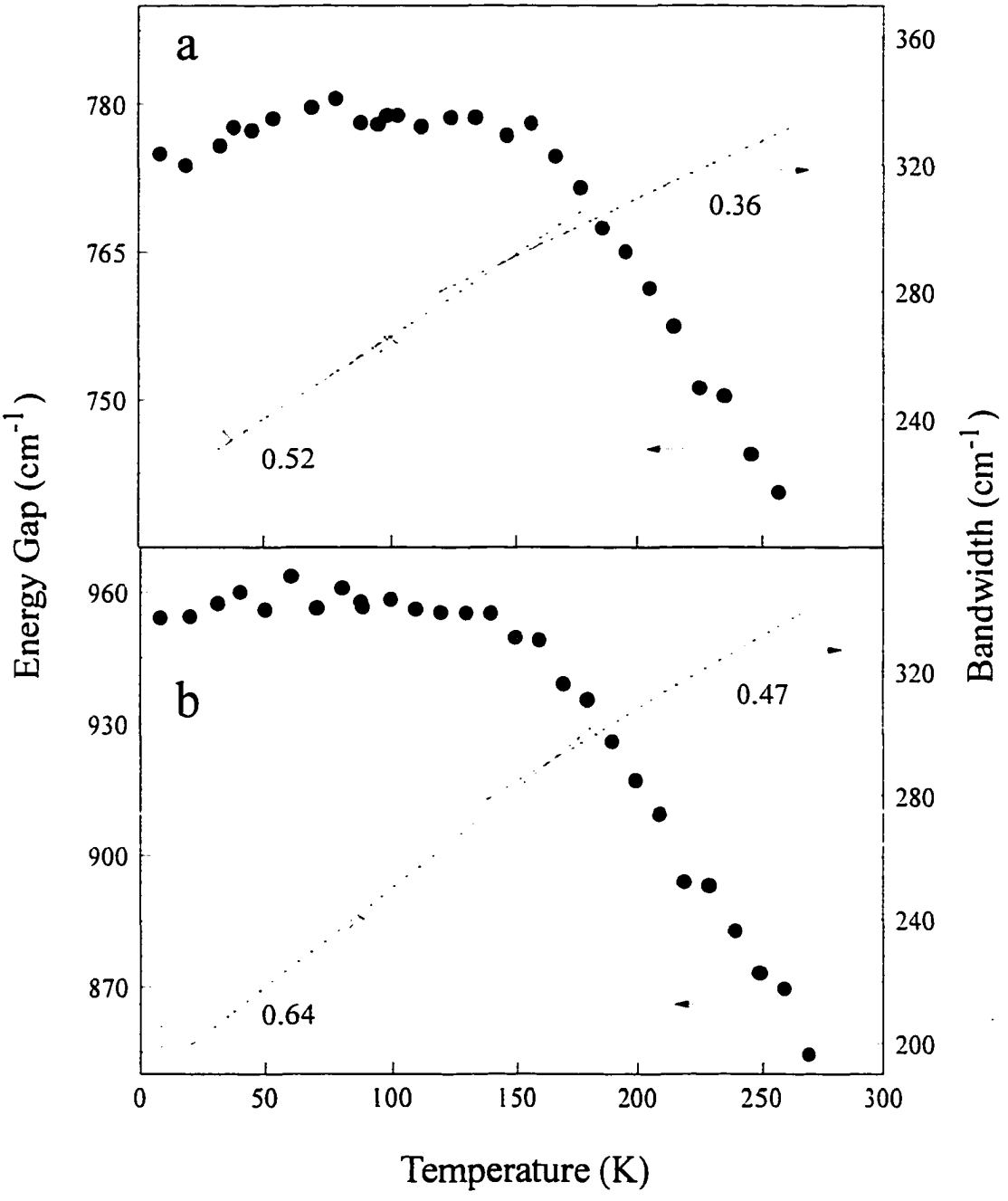
a
b
0.36
0.52
0.47
0.64
780
765
750
960
930
900
870
360
320
280
240
320
280
240
200
0
50
100
150
200
250
300
Energy Gap (cm-1)
Bandwidth (cm-1)
Temperature (K)

Figure 6

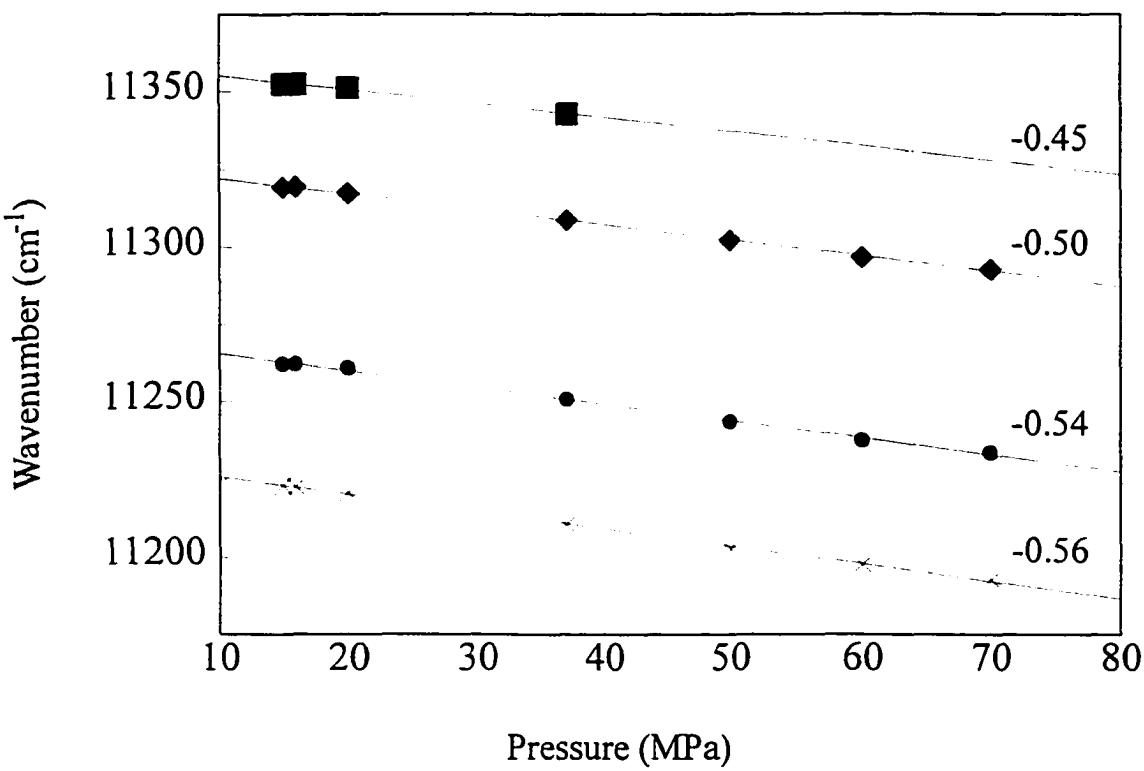
11350
11300
11250
11200
Wavenumber (cm-1)
10
20
30
40
50
60
70
80
Pressure (MPa)
-0.45
-0.50
-0.54
-0.56

Figure 7

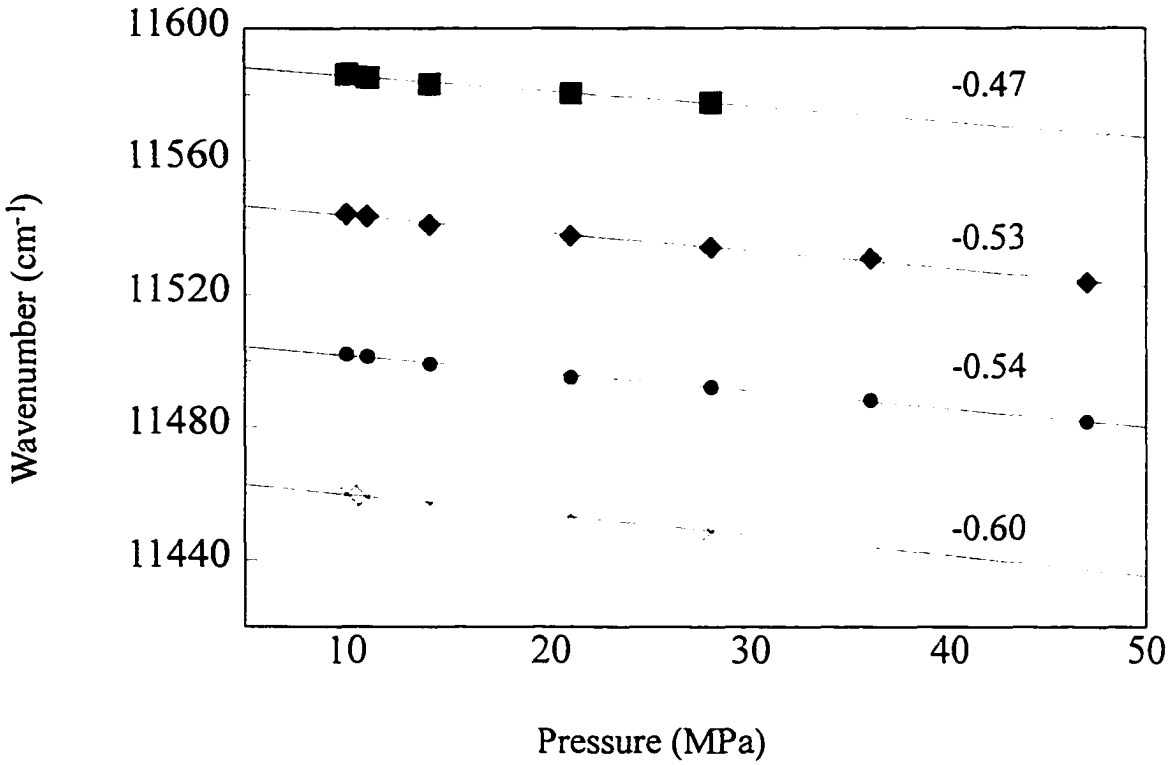
11600
11560
11520
11480
11440
Wavenumber (cm-1)
10
20
30
40
50
Pressure (MPa)
-0.47
-0.53
-0.54
-0.60

Figure 8

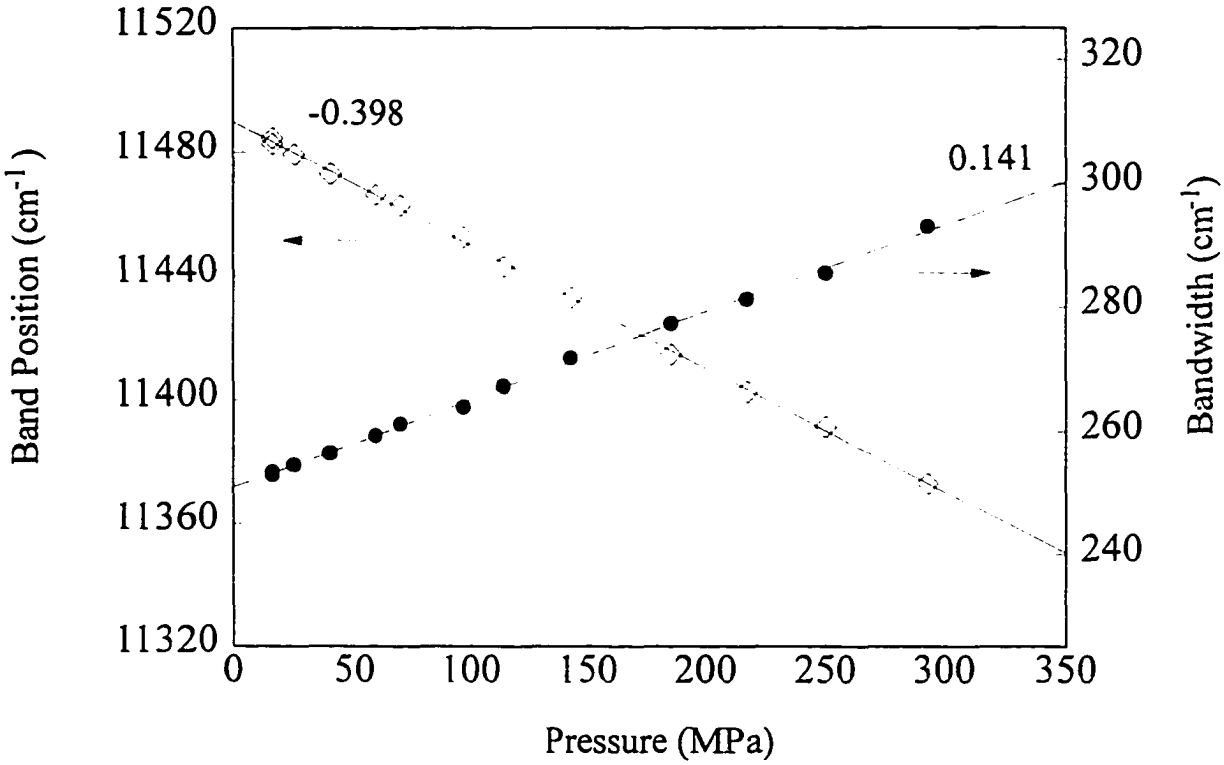
11520
11480
11440
11400
11360
11320
Band Position (cm-1)
-0.398
0.141
320
300
280
260
240
Bandwidth (cm-1)
0
50
100
150
200
250
300
350
Pressure (MPa)

Figure 9

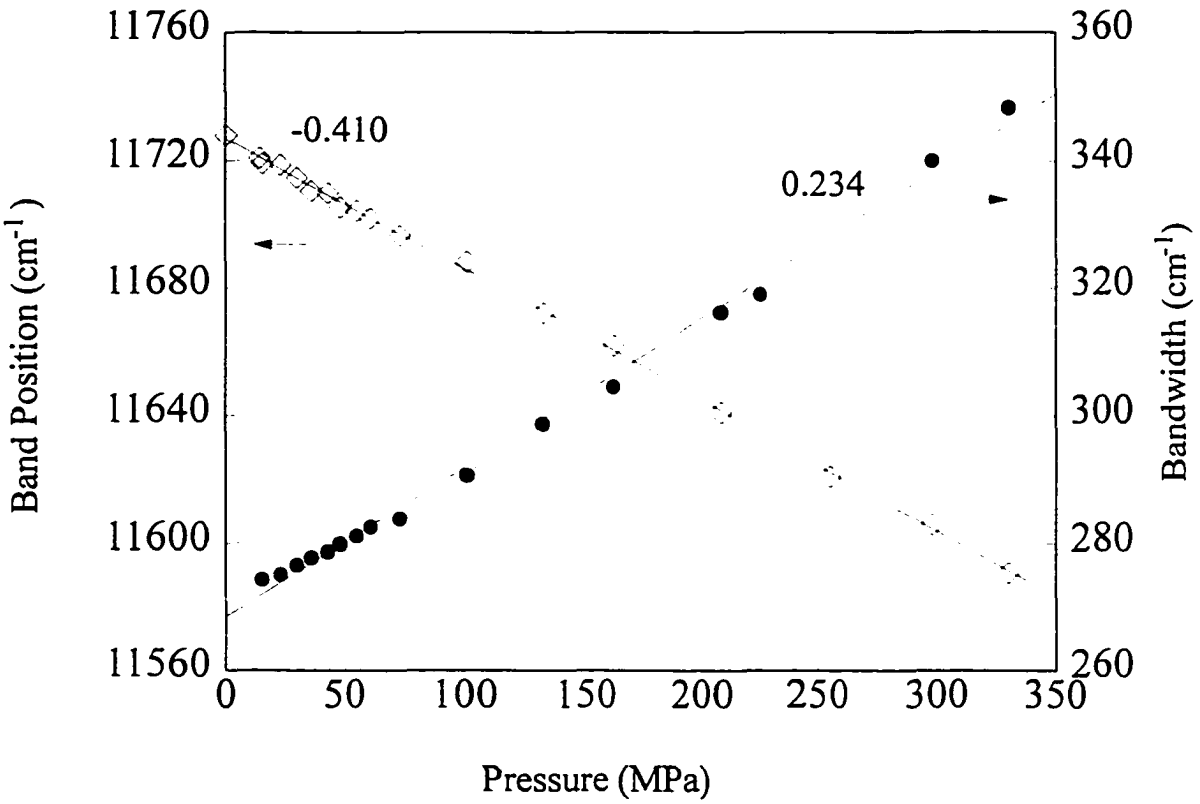
11760
11720
11680
11640
11600
11560
360
340
320
300
280
260
-0.410
0.234
0
50
100
150
200
250
300
350
Band Position (cm-1)
Bandwidth (cm-1)
Pressure (MPa)

Figure 10

CHAPTER 5. EXCITON LEVEL STRUCTURE AND ENERGY DISORDER OF THE B850 RING OF THE LH2 ANTENNA COMPLEX

A paper published in the *J. Phys. Chem. B*, **1997**, *101*, 7654.

H.-M. Wu, M. Ratsep, I.-J. Lee, R. J. Cogdell and G. J. Small

ABSTRACT

Experimental and theoretical results are presented on the exciton level structure of the B850 ring of bacteriochlorophyll *a* molecules for the light harvesting 2 (LH2) complex of *Rhodopseudomonas acidophila* (strain 10050) and the effects of energy disorder (due to structural heterogeneity) on the level structure. The work is an out-growth of the accompanying paper (Wu et al., *J. Phys. Chem. B* **1997**, *101*, 7641.) which reports on the temperature and pressure dependencies of the LH2 absorption spectrum and the zero-phonon hole action spectrum of the lowest energy exciton level of the complex, B870, as well a structural (non-denaturing) change of the complex near 150 K. The effects of energy disorder are analyzed using the theory of Wu and Small (*Chem. Phys.* 1997, in press) which employs symmetry adapted energy defect patterns. The analysis leads to a room temperature value of ~ 100 cm^{-1} for the splitting between B870 and the adjacent, strongly allowed E_1 level in the absence of disorder. Using the temperature dependent data of Wu et al., we arrive at a theoretical estimate for this splitting at temperatures below ~ 150 K of ~ 150 cm^{-1}, which is 50 cm^{-1} smaller than the "apparent" value of 200 cm^{-1} based on the 4.2 K B870 action spectrum. The 50 cm^{-1} difference is explained in terms of a distribution of values for the energy disorder parameter(s) which leads to a distribution of values for the oscillator strength of B870. Hole burning data on the temperature dependence of B870's optical dynamics are presented and analyzed. Below ~ 15 K the dynamics are dominated by two-

level systems of the protein with an effective dephasing frequency which carries a T^{α} –dependence with $\alpha \sim 1.3$. At temperatures above ~ 20 K the dephasing is strongly exponentially driven with an activation energy of ~ 100-140 cm^{-1}. A mechanism suggested for this dephasing is that it is due to upward scattering of the B870 level to the adjacent E_1 level by one-phonon absorption. New satellite hole spectra for the LH2 complex (isolated and chromatophores) are presented which lead to the assignment of the weak high energy tail absorption of the B800 and B850 absorption bands to B850 exciton levels of the B850 ring which are either symmetry forbidden or predicted to be very weakly absorbing in the absence of energy disorder.

1. Introduction

In the accompanying paper[1] (hereafter referred to as I) high pressure and temperature dependent absorption and hole-burned spectra for the light harvesting complex 2 (LH2 or B800-850) of *Rhodopseudomonas acidophila* (strain 10050) and *Rhodobacter sphaeroides* were presented. (The reader is referred to the Introduction of I for discussion of recent works on the structures, $Q_y(S_1)$-electronic states, and excitation energy transfer and relaxation dynamics of LH2 complexes.) The primary focus of I was to compare the LH2 complex of *Rps. acidophila*, for which a structure is known,[2] with that of *Rb. sphaeroides* for which a structure is unavailable. The LH2 complex of the former species is a cyclic C_9-array of α,β polypeptide pairs which bind nine bacteriochlorophyll *a* (BChl *a*) molecules responsible for absorption near 800 nm and nine BChl *a* dimers which absorb near 850 nm (room temperature values). The arrangement of the eighteen BChl *a* molecules of the B850 ring is shown in Figure 1 of I. It was concluded that the packing of the α,β-pairs for *Rb. sphaeroides* is looser than for *Rps. acidophila*, consistent with weaker excitonic coupling in the B850 ring and a higher value of the compressibility for the LH2 complex of the former species.

Of particular relevance to this paper are the following findings reported in I: the LH2 complex of both species in the glycerol/water solvent used undergoes a structural change near 150 K; the nearest neighbor BChl *a*-BChl *a* coupling(s) within the B850 ring is a factor of about 1.4 times stronger for the low temperature structure; this coupling for *Rb. sphaeroides* is a factor of about 1.2 times weaker than for *Rps. acidophila* at all temperatures; and the thermal broadening of the B850 band for both the low and high temperature structures is consistent with phonon-assisted relaxation between exciton levels that contribute to the B850 band. The most important contributing levels carry A and E_1 symmetry with the E_1 level responsible for almost all of the absorption intensity of the B850 absorption band.[3,4] The former level is often referred to as B870 and, based on the room-temperature X-ray structure for the LH2 complex of *Rps. acidophila*, is predicted to be essentially forbidden in absorption with an intensity substantially less than 1% of the E_1 level.[3] These electronic structure calculations predict that B870 should lie close to 100 cm^{-1} below the E_1 level. In what follows we denote this energy gap by ΔE. An experimental determination of ΔE is an important benchmark for electronic structure calculations.

The only values of ΔE currently available were determined by zero-phonon hole (ZPH) action spectroscopy.[5-7] As discussed in I, the value of ΔE has decreased as the quality of the samples studied has improved. (A perfectly reasonable definition of increasing quality or decreasing structural heterogeneity is a decrease of the B800 and B850 absorption bandwidths at all temperatures.) For example, for samples of *Rb. sphaeroides*, which yielded 4.2 K B850 absorption widths of 280 and 230 cm^{-1}, ΔE = 250 and 185 cm^{-1} at 4.2 K, respectively, while for samples of *Rps. acidophila*, which yielded 4.2 K widths of 430 and 200 cm^{-1}, values for ΔE of 270 and 200 cm^{-1} were reported. In ref. (7) it was found that B870 of *Rps. acidophila* carries ~ 3% of the intensity of the B850 band, a value which is significantly greater than the predicted value. (For samples exhibiting a 4.2 K B850 bandwidth as narrow as 200 cm^{-1}, B870 is observable as a weak but distinct low energy

feature of the B850 absorption band.[7]) In view of the above results for ΔE it is apparent that the average value of ΔE depends on the extent of structural heterogeneity or. equivalently, the extent of diagonal and off-diagonal energy disorder within and between B850 rings of the ensemble. Recently, Wu and Small[8] introduced symmetry adapted basis energy defect patterns (BDP) for analysis of energy disorder in cyclic arrays of coupled chromophores. Since any energy defect pattern can be written as a superposition of the orthogonal BDP, determination of the effects of each BDP allows for a systematic approach to the question of whether or not energy disorder can account for spectroscopic data given a zero-order C_n-Hamiltonian. The effects include splitting of degenerate exciton levels, modification of inter-exciton level spacings and redistribution of oscillator strength. Utilizing the zero-order Hamiltonian of Sauer et al.[3] for *Rps. acidophila*, which yields a ΔE-value of ~ 100 cm^{-1} in the absence of disorder, Wu and Small found that diagonal and/or off-diagonal energy disorder cannot increase ΔE to the apparent experimental value of 200 cm^{-1} without endowing B870 with far too much absorption intensity, ca. 15% of the intensity of the B850 absorption band.

In this paper we extend the work of Wu and Small by taking into account (i) the result from I that nearest neighbor BChl *a*-BChl *a* coupling(s) of the B850 ring increases by ~ 35% below 150 K, at which temperature the structural change occurs and (ii) a distribution of energy disorder parameter values associated with LH2 complexes of the ensemble. It is shown, for example, that an important consequence of the latter is a strong increase in the transition dipole strength for B870 of an individual LH2 complex as its energy displacement below the E_1 level increases due to energy disorder. As a result, the aforementioned experimental values for ΔE are only apparent and need to be corrected for the just-mentioned dependence in order to arrive at a ΔE-value for the complex in the absence of energy disorder. Such a value is estimated for both the low and high temperature LH2 structures of *Rps. acidophila*. It is the value for the high temperature structure that is most relevant to

electronic structure calculations since only a room temperature X-ray structure is available. Spectral hole burning data on the temperature dependence of the spectral dynamics of B870 are reported which provide a reasonable estimate for the value of ΔE at 4.2 K. Satellite hole spectra are presented which we believe speak to the location of other exciton levels of the B850 ring which are either strictly forbidden in absorption or very weakly allowed in the absence of energy disorder (see I for relevant discussion of weak features in the absorption spectrum of the LH2 complex). The reader is referred to I for a description of the hole burning apparatus and discussion of other aspects of the experiments.

2. Background on Electronic Structure of LH2 Complexes

Given that the X-ray structures for the LH2 complex of *Rps. acidophila* and *Rs. molischianum* are known, one can calculate its Q_y-electronic structure by simply diagonalizing the m×m Hamiltonian matrix associated with the m BChl *a* molecules of the complex as was done in refs. (3,4). For LH2 of *Rps. acidophila*, with its C_9-symmetry, m = 27 (9 B800 and 18 B850 molecules) while for *Rs. molischianum*, with its C_8 symmetry, m = 24 (8 B800 and 16 B850 molecules). The results of refs. (3,4) show that the effects of the B800 molecules on the excitonic structure of the B850 ring are small. Thus, we ignore the B800-B850 interactions in what follows. That the exciton levels obtained transform like the irreducible representations of the C_n-group is more apparent for the B850 ring when one frames the problem in terms of a dimer of the B850 ring.[8,9] As discussed in I, there are two choices for the dimer (see Figure 1 of I). For either dimer the upper (u) level is essentially forbidden in absorption while the lower (l) is strongly allowed. Irrespective of the choice of dimer, the u- and l-levels spawn exciton manifolds for the C_n-ring. (Since this paper is mainly concerned with the LH2 complex of *Rps. acidophila* n is taken equal to 9 in our calculations.) The projection operator technique of group theory[10,11] allows for generation of the exact eigenfunctions for both manifolds.[8] In the nearest dimer-dimer coupling

approximation which is, of course, less restrictive than the nearest monomer-monomer coupling approximation, the energies of the two exciton manifolds are given by

$$E_l^j = e_l + 2\,V_l \cos(2\pi j / n) \tag{1}$$

and

$$E_u^j = e_u + 2\,V_u \cos(2\pi j / n)\,, \tag{2}$$

where e_l and e_u are the energies of the two levels of the dimer, V_l and V_u are, respectively, the nearest neighbor dimer-dimer coupling energies for the lower and upper manifolds and j=0,1,...,n−1 with n the number of dimers in the ring. For n=9, the correspondence between j-values and irreducible representations is: j=0(A); j={1,8}(E_1); j={2,7}(E_2); j={3,6}(E_3) and j={4,5}(E_4). Following the generation of the u- and l-manifolds, one needs to consider the interactions between their respective exciton levels. The couplings are given by

$$H_{ul}^j = 2\,V_{ul} \cos(2\pi j / n)\,. \tag{3}$$

Because the Hamiltonian is totally symmetric, the coupling is restricted by symmetry to levels of the same j-value. The dimer-dimer couplings V_l, V_u and V_{ul} can be determined using the monomer-monomer coupling energies.[8] The B850 exciton level structure shown in Figure 2 of I was calculated with $e_u - e_l = 600$ cm^{-1}, $V_u = 100$ cm^{-1}, $V_l = -200$ cm^{-1} and $V_{ul} = 130$ cm^{-1}, slightly rounded off values determined using the monomer-monomer coupling energies of ref. (3) which were calculated using the room temperature X-ray structure for LH2 of *Rps. acidophila*. For convenience, the level structure is shown in Figure 1 along with the 4.2 K absorption spectrum of LH2 for *Rps. acidophila*. The lowest energy and strongly absorbing E_1 level is situated so as to be coincident with the B850 absorption maximum. As mentioned in the Introduction, the nearest neighbor monomer-monomer coupling(s) of the B850 ring appears to be a factor of 1.4 larger for the low temperature structure. A difficulty is that the relative contributions to this increase from the

two monomers of the dimer associated with the basic α,β-polypeptide unit and nearest neighbor monomers belonging to adjacent α,β-polypeptide units are not known. However, our calculations revealed that the lowest energy A(B870) and E_l levels and, to a lesser extent, the E_2 level are not very sensitive to how the increase in coupling is distributed (results not shown). The just-mentioned insensitivity is a consequence of V_l and V_u of Eqs. 1 and 2 carrying opposite sign, *vide supra*, and the coupling between the l- and u-manifolds being restricted to levels of the same j-value. While the energy ordering for the l-manifold is $A(B870)<E_l<E_2<E_3<E_4$, the ordering for the u-manifold is reversed. As a result, it is the coupling between the E_3 and E_4 levels of the two manifolds that are most affected by V_{ul}, Eq. 3, since they are most closely spaced.

The top and middle exciton level diagrams for the B850 ring shown in Figure 2 were calculated with $V_l = -270$ and -320 cm^{-1}, respectively, and values of $e_u - e_l$, V_u and V_{ul} the same as given above. The value of -270 cm^{-1} for V_l represents a ~ 35% increase over the -200 cm^{-1} value used to obtain the level structure shown in Figure 1. Thus, the larger nearest neighbor BChl *a*-BChl *a* couplings for the low temperature structure, *vide supra*, has been attributed entirely to V_l. The exciton level structure for $V_l = -320$ cm^{-1} is shown, in part, because of the possibility that the calculations of Sauer et al.,[3] which lead to $V_l \sim -200$ cm^{-1} for the high temperature structure, may underestimate the strengths of nearest neighbor BChl *a*-BChl *a* couplings of the B850 ring.[12] Finally, the exciton level diagram shown at the bottom of Figure 2 was calculated using only Eq. 1 with $V_l = -320$ cm^{-1}, i.e. the u-manifold of the basic dimer and interactions of its exciton levels with those of the l-manifold are neglected. Note that the right-most E_l levels of the three energy diagrams in Figure 2 are placed at the same energy and should be referred to the E_l level of Figure 1 which is coincident with the B850 absorption maximum.

Comparison of the lowest energy A(B870), E_l and E_2 levels for the three manifolds in Figure 2 shows that ΔE and E_l-E_2 gaps are quite similar. Analysis of the eigenvectors for

these levels associated with the upper two manifolds revealed that they are similar to those for the lowest manifold in the figure. This is not the case for the E_3 and E_4 levels as would be expected from earlier discussion. However, our main interest is in the B870, and lowest energy E_1 and E_2 levels. In particular, we are interested in the mixing of the B870 and E_1 levels due to energy disorder which destroys the cyclic symmetry; thereby, bringing absorption intensity to B870 as well as increasing ΔE.[4,8] To this end, it suffices to use the zero-order Hamiltonian for the B850 ring associated with only the l-level of the basic dimer, i.e. the Hamiltonian used to calculate the manifold at the bottom of Figure 2. The essential physics that emerges from our analysis of energy disorder would be unaffected by utilization of the complete Hamiltonian. Also, an exact treatment at this time is unwarranted because it is not clear which of the existing electronic structure calculations for the B850 ring is most reliable.

3. Results and Discussion

In the first part of this section we consider the problem of how energy disorder affects the lower exciton levels of the B850 ring of BChl *a* molecules associated with the B850 absorption band. Although the results of calculations presented are for *Rps. acidophila*, they are relevant to the LH2 complexes of *Rb. sphaeroides* and *Rs. molischianum*. Included also are temperature dependent hole burning data for the lowest energy level of the B850 ring, B870, for *Rps. acidophila* which lead to an estimate for the displacement of this level below the strongly absorbing E_1 level, i.e. ΔE. As mentioned, experimental determination of ΔE is an important benchmark for electronic structure calculations on the exciton level structure of the B850 ring. In the second part, new satellite hole spectra for the LH2 complex of *Rps. acidophila* and *Rb. sphaeroides* are presented which suggest assignment of certain weak features in the Q_y-absorption spectrum to other exciton levels of the B850 ring (see I).

A. Energy disorder and the B850 ring

In the preceding section it was emphasized that our primary interest is in how energy disorder affects the lowest A(B870), E_1 and E_2 levels of the B850 ring and that the basic physics can be uncovered using a zero-order Hamiltonian, H_0, for the lower, strongly allowed level of the basic dimer of the B850 ring. This Hamiltonian yields Eq. 1. In what follows, the subscript ℓ is dropped. We begin with a review of the results of ref. (8) where orthogonal basis defect patterns (BDP) were introduced. For C_9, the BDP transform like the $E_{j,\pm}$ irreducible representations with j=1-4. The single non-degenerate BDP is totally symmetric (A). For example, $E_{1,+}$ and $E_{1,-}$ are orthogonal partners for the separably degenerate j=1 and 8 representations of the C_9 group. The Hamiltonian for a C_n-array of chromophores (dimers for the case at hand) in the absence of disorder is

$$H_o = e\sum_{\alpha=0}^{n-1} |\alpha\rangle\langle\alpha| + \sum_{\alpha,\beta=0}^{n-1}{}' V_{\alpha,\beta}\,|\alpha\rangle\langle\beta|, \tag{4}$$

where Greek letters label the dimers or sites and e is the excitation energy of the dimer. The eigenfunctions of H_0 are delocalized and determined by symmetry to be[11]

$$|j> = n^{-1/2}\sum_{\alpha} B^{j\alpha^*}|\alpha>, \tag{5}$$

where $B = \exp(i2\pi/n)$. The normalization constant $n^{-1/2}$ holds when overlap between chromophores of the ring is neglected. Since we take the basic unit of the ring to be a dimer, it suffices to make the nearest dimer-dimer coupling approximation which, with Eqs. 4 and 5, leads to

$$E_j = e + 2V\cos(2\pi j/n) \tag{6}$$

for the exciton energies with V the nearest neighbor dimer-dimer coupling (V_ℓ of Eq. 1).

In the presence of disorder the Hamiltonian is

$$H = H_o + H_\lambda + H_v \,, \tag{7}$$

where H_λ governs the diagonal energy disorder of the ring:

$$H_\lambda = \sum_\alpha \lambda_\alpha |\alpha><\alpha| \,. \tag{8}$$

H_v, which defines the off-diagonal disorder, is given by

$$H_v = \sum_\alpha v_\alpha \left(|\alpha><\alpha+1| + |\alpha+1><\alpha|\right) . \tag{9}$$

For investigation of how these two defect Hamiltonians couple the zero-order delocalized levels it is most convenient[8] to express both in terms of the delocalized wavefunctions using

$$|\alpha> = n^{-1/2} \sum_j B^{j\alpha} |j> \,. \tag{10}$$

Given here are the main results for diagonal energy disorder (H_λ). (The physics revealed by our calculations with H_λ is essentially the same as the physics obtained from H_v.) For H_λ the coupling between delocalized levels r and s is

$$<r|H_\lambda|s> = \frac{1}{n} \sum_\alpha \lambda_\alpha \, B^{(r-s)\alpha} \,. \tag{11}$$

Any chosen energy defect pattern for the ring can be expressed as a superposition of BDP patterns since they form a complete set.[8] Thus, one can examine the effects of each and every BDP on the ring exciton structure so as to determine which, if any, are of primary importance. The projection operator technique of group theory[10,11] can be used to generate the BDP. Incorporation of the BDP in Eq. 11 leads to[8]

$$<r|H_\lambda^{E_{j,\pm}}|s> = \frac{\lambda_{j,\pm} \, N_{j,\pm}}{n} \sum_\alpha \left[\cos\left(\frac{2\pi j\alpha}{n}\right) \pm \cos\left(\frac{2\pi j(\alpha-1)}{n}\right) \right] e^{i2\pi\alpha(r-s)/n} \tag{12}$$

for E-type patterns. The + and – signs denote the orthogonal partners of each degenerate pattern. The set of square-bracketed terms obtained with $\alpha = 0,1,\ldots,n-1$ define the defect pattern. One can define normalized basis defect vectors

$$\underset{\sim}{D}_{j,\pm} = N_{j,\pm}\left(d^{\pm}_{j,0}, d^{\pm}_{j,1}, \ldots, d^{\pm}_{j,n-1}\right) \tag{13}$$

where the d-elements are given by the square bracketed terms in Eq. 12 and the normalization constant $N_{j,\pm}$ is defined by

$$N^{-2}_{j,\pm} = \sum_{\alpha}\left[\cos\left(\frac{2\pi j\alpha}{n}\right) \pm \cos\left(\frac{2\pi j(\alpha-1)}{n}\right)\right]^2 . \tag{14}$$

The relationship between $\lambda_{j,\pm}$ in Eq. 12 and the λ of the generator site defect used with the projection operator technique to obtain Eq. 12 from Eq. 11 is $\lambda_{j,\pm}\, N^{-1}_{j,\pm} = \lambda$. Put another way, once the value of the energy defect λ at a particular site (dimer) is defined, the projection operator generates the values of the energy defect at all other dimers. The resulting defect pattern depends on the symmetry of the BDP. The value of $\lambda_{j,\pm}$ is determined by the value of λ and $N_{j,\pm}$. The selection rule associated with Eq. 12 is

$$r - s = \pm j\,, \tag{15}$$

so that, for example, the $j = \pm 1$ (E_1) diagonal energy disorder pattern couples the $j = 0$ (A) level with the separably degenerate $j = 1$ and $j = n-1$ (E_1) levels. For n odd, which is the case considered here, the above selection rule also applies to the one and only non-degenerate BDP, $j = 0$ (A) with

$$< r|H^{A}_{\lambda}|r > = \frac{\lambda_o}{n^{1/2}} = \lambda\,, \tag{16}$$

which is independent of r.

Figure 3 shows the diagonal energy disorder patterns for $E_{1,\pm}$ and $E_{2,\pm}$ with the numbers located at the dimer sites defined by the components of $\underset{\sim}{D}_{j,\pm}$, Eq. 13. The results for all BDP are given in Table I. We note that the BDP from off-diagonal disorder are precisely the same but that in Figure 3 the coefficients of the BDP would be rotated by $\pi/9$ so as to be centered between neighboring dimers.[8]

Concerning the removal of exciton level degeneracies, it is important to note that the degeneracy of level E_j is removed, in first order, by a BDP with symmetry contained in the symmetric direct product $(E_j \times E_j)_+$. For C_9 and j=1-4, the BDP symmetries are, respectively, E_2, E_4, E_3 and E_1. However, a second order mechanism for removal of degeneracy exists because of the off-diagonal coupling defined by Eq. 11 and the associated selection rule, Eq. 16. These group theoretical predictions are in accordance with the results of calculations presented in ref. (8) and below.

The results of ref. (8) prove that it is the E_1 components of an energy defect pattern which dominate the mixing of the lowest energy level, B870 (A), of the B850 ring with the adjacent E_1 level, Fig. 1. This is expected given the selection rule of Eq. 15 and that the E_1 level lies closest in energy to B870. Thus, one can use BDP of E_1 symmetry to determine the basic consequences of coupling between B870 and the E_1 level, including the relationship between the energy gap ΔE and absorption intensity of B870. Before presenting the results of our calculations, it is important to point out the connection between the BDP shown in Figure 3 and the Hamiltonian H_λ, Eq. 8. The values of λ_α are determined by assigning a value of λ_0 to the generator site (dimer), dimer "0", and then calculating the magnitudes and signs of λ_α (α = 1-8) using the values of the site coefficients associated with the BDP being considered. As an example, for the $E_{1,+}$ BDP $\lambda_1 = \lambda_0$ and $\lambda_3 = -0.186\,\lambda_0$, Figure 3. Note that the symmetry of each $E_{j,\pm}$ defect pattern dictates that the sign of λ_0 is of no consequence. (However, when considering a superposition of BDP, rather than a single BDP, the relative signs of the λ_0-values for different BDP is important;[8] superpositions are not considered in this paper.) It is also the case that the effects of energy disorder on the exciton level structure from $E_{j,+}$ and $E_{j,-}$ patterns are identical for the same value of λ_0. In what follows we refer to the BDP pattern being used as E_1. Next it is necessary to consider glass-like fluctuations in the value of λ_0 from complex to complex in the ensemble. Gaussian randomness is assumed and, since the sign of λ_0 is irrelevant, a normalized half-Gaussian distribution for λ_0 centered

at zero is employed. We show here the results for V = – 320 cm^{-1}, Eq. 6, and a width for the half-Gaussian of 35 cm^{-1}. This value for V is appropriate for the low temperature structure, *vide supra*. The value for the width is viewed as reasonable given typical values of ~ 100-200 cm^{-1} for the inhomogeneous broadening of Q_y-transitions in photosynthetic complexes (see I and ref. (13) for discussion of works related to inhomogeneous broadening).

With V = – 320 cm^{-1}, the gap (ΔE) between B870 and the E_1 level is 150 cm^{-1} in the absence of energy disorder and B870 is forbidden in absorption. E_1 energy disorder couples the two levels, causing an increase in ΔE and non-zero absorption strength for B870. (B870 can be viewed as stealing oscillator strength from the strongly allowed E_1 level.) The solid rectangles in Figure 4 show how the %-absorption of B870 increases as ΔE increases due to increasing disorder (λ_0-value). The crosses define the half-Gaussian distribution for λ_0. Multiplying the two curves yields the B870 absorption profile of B870, open circles. The width of 115 cm^{-1} for this profile and its ΔE-value of ~ 200 cm^{-1} are in good agreement with the low temperature values determined by ZPH action spectroscopy. Thus, it is clear that the value of ΔE determined experimentally is too large relative to its value in the absence of energy disorder and needs to be corrected for the dependence of B870's oscillator strength on the value of λ_0. Using the B870 profile shown in Figure 4 it was determined that B870 carries 7% of the total absorption intensity of the B850 ring, a factor of 2 greater than the experimental value for *Rps. acidophila* reported in ref. (7). It was noted in this reference that the stated experimental value of 3% could be too low by ~ 2% (due to some uncertainty in the deconvolution analysis). Thus, at this time, we consider the factor of 2 disagreement acceptable.

The results shown in Figure 4 were obtained using a half-Gaussian distribution for λ_0 with a width of 35 cm^{-1}. It is instructive to examine the exciton level energy diagrams for various values of λ_0. Results are shown in Figure 5 for λ_0 = 0, 18, 35 and 53 cm^{-1}. The ΔE-values are, respectively 150, 165, 190 and 225 cm^{-1}. (Keep in mind that the probabilities for

these λ_0-values are governed by the half-Gaussian distribution.) We note first that the splitting of the highest energy level (E_4) with increasing λ_0 is 3.2 λ_0. This is expected since the removal of E_4-degeneracy is, in first order, produced by a BDP of E_1-symmetry, *vide supra*. As mentioned, a weaker mechanism for removal of degeneracy also occurs because of the energy disorder-induced coupling between different exciton levels, as governed by the selection rule of Eq. 15. For λ_0 = 18, 35 and 53 cm^{-1} the splittings from this higher order mechanism for the E_1-level (due to E_1 energy disorder) are 17, 57 and 103 cm^{-1}, respectively. We give these splittings because the absorption profile of B850 shown in Figure 1 imposes a limit on the extent of energy disorder. This profile is symmetrical in the central region although a slight bulging appears just to the right (low energy side) of the B850 maximum. Following the fitting procedure used in ref. (7), which takes into account inhomogeneous broadening as defined by the 120 cm^{-1} value for B870 and homogeneous broadening due to inter-exciton level relaxation, we performed simulations which showed that the splitting of the two comparably intense components of the E_1 levels[8] cannot be much larger than 60 cm^{-1}. (For example, a splitting of 100 cm^{-1} would be apparent in the B850 absorption profile.) It can be seen that the splittings (from the E_1 BDP) given above, when weighted by the λ_0-distribution, lead to a value less than 60 cm^{-1}. Of course, BDP of other symmetries would contribute to the E_1 splitting for an arbitrarily chosen defect pattern.[8] In particular, E_2 BDP (Figure 3) split the E_1 degeneracy in first order by 3.4 λ_0 (results not shown). Using the λ_0-distribution defined above with the E_2 BDP yielded an average splitting for the E_1 level of 80 cm^{-1}, somewhat larger than 60 cm^{-1}. Therefore, this λ_0-distribution is reasonably consistent with the low temperature absorption profile of B850. We hasten to point out, however, that we are considering one BDP at a time and that in the conventional approach of placing Gaussian randomness on the excitation energy at each site of the ring, one would be dealing with superpositions of BDP. Nevertheless, we believe that

the λ_0-distribution used provides a useful benchmark for future studies of energy disorder. Furthermore, the level of insight gained by using BDP is unprecedented.

To conclude this subsection we present the first results on the temperature dependence of the optical dynamics of B870, the lowest exciton level of the B850 ring, Figure 6. The vertical axis corresponds to the zero-phonon holewidth of B870 divided by 2, the homogeneous width of the zero-phonon line (ZPL) of B870.[14-16] The data points (circles) for each temperature were obtained by burning and reading at that temperature (shallow holes of fractional depth $\lesssim 0.05$ were used so as to minimize fluence broadening). The thermal broadening behavior is entirely reminiscent of that observed for the ZPL of isolated molecular chromophores in amorphous hosts such as glasses and polymers[15] with tunneling of the glass two-level systems (TLS) dominating the optical dynamics at lower temperatures and a thermally activated process becoming dominant at higher temperatures. In such systems, however, the latter process usually onsets near 10 K and has been ascribed to exchange coupling involving a pseudo-localized phonon of the chromophore, typical frequencies being in the 20-30 cm^{-1} range. (For this mechanism the temperature dependence is governed by the thermal occupation number $\bar{n}(\omega) = [\exp(\hbar\omega / kT) - 1]^{-1}$, where ω is the phonon frequency.) Familiarity with this function indicates that the activation energy for the rapid increase in holewidth that onsets near 20 K in Figure 5 is much higher, ~ 100 cm^{-1}. To the best of our knowledge, there is no evidence from hole burning and photon echo studies for pseudo-localized modes of such high frequency existing for large chromophores in glasses, polymers and proteins. It is important to mention the work of Völker and coworkers[17] in which it was reported that the width of ZPH (4.6 cm^{-1}) burned into the B800 band of LH2 is independent of temperature between 1.2 and 30 K. The 4.6 cm^{-1} width is determined by the B800→B850 energy transfer process.[17,18] The difference between the temperature dependencies of the B800 and B870 ZPH widths is dramatic, e.g. the B870 holewidth at 30 K is 25 cm^{-1}. The rapid increase in B870 dephasing above ~ 20 K precluded

measurement of its ZPH above ~ 35 K due to the accompanying strong decrease in hole burning efficiency. In view of the contrasting behaviors of B800 and B870 and that it is very unlikely that a pseudo-localized phonon involving librational type motion of a BChl molecule with a frequency as high as ~ 100 cm^{-1} exists, we believe that a different mechanism for the homogeneous broadening which onsets for B870 near 20 K is operative. We propose that a significant contribution to this broadening is due to scattering of the B870 exciton level to the adjacent, higher energy E_1 levels due to absorption of bath (protein) phonons with energies equal to the B870-E_1 energy gap ΔE (energy disorder splits the E_1 degeneracy, *vide supra*). Such scattering has been thoroughly studied in organic crystals; see, for example, refs. (19-21). By necessity, we simplify by using an average value for the energy gaps, ΔE, and express $\Gamma_h/2$, Figure 5, as

$$\Gamma_h / 2 = AT^{\alpha} + B\,\bar{n}(\Delta E)\,, \tag{17}$$

where $\bar{n}$ is the previously defined phonon thermal occupation number with phonon energy equal to ΔE. In other words, scattering from the B870 to E_1 level(s) occurs by one-phonon absorption. The first term in this equation is due to the aforementioned TLS of the protein and, possibly, the glass-forming solvent. A multitude of studies on isolated chromophores in amorphous and protein hosts have revealed the universal behavior of $\alpha = 1.3 \pm 0.1$ (see aforementioned references related to TLS). Figure 6 shows two of the fits to the data obtained with Eq. 17. For the solid and dashed curve fits, (ΔE, α) = (140 cm^{-1}, 1.35) and (97 cm^{-1}, 1.31), respectively (the A and B coefficients are given in the figure caption). All reasonable fits yielded an α-value between 1.3 and 1.4. Thus, we are confident that the optical dynamics of B870 at the lowest temperatures is dictated by TLS although we are unable to determine the contributions to the homogeneous broadening from pure dephasing and spectral diffusion.[15] Particularly interesting is that the magnitude of the TLS-induced homogeneous broadening of B870 is one to two orders of magnitude greater than observed

for isolated chromophores in amorphous hosts.[14,15,22] Since such a broadening mechanism is relatively unimportant for B800,[17] we plan to investigate, theoretically, whether the strength of this broadening for B870 is a consequence of excitonic delocalization. Our fits to the data of Figure 6 indicate that ΔE lies between ~ 100 and 140 cm^{-1}. To reduce this uncertainty would require data for temperatures higher than 35 K as a comparison of the two fits in Figure 5 would indicate. A value of $\Delta E \sim 140$ cm^{-1} based on the optical dynamics of B870 is consistent with our analysis of the ΔE-value and the absorption intensity of B870 given above.

To conclude this subsection we summarize the results which are important for calculations on the electronic structure of the B850 ring of *Rps. acidophila*. For the low temperature ($T < \sim 150$ K) structure the energy gap (ΔE) between B870 and the allowed E_1 level is close to 150 cm^{-1} in the absence of energy disorder. Inclusion of a physically reasonable amount of energy disorder leads to an apparent value for ΔE of 200 cm^{-1} and B870 carrying ~ 7% of the B850 ring's absorption intensity. Based on the results of I, ΔE at room temperature should be close to 100 cm^{-1} in the absence of disorder. This is close to the values calculated by Sauer et al.[3] and Alden et al.[4] The methods employed in these two works differ in that Alden et al. take into account electron exchange as well as electrostatic interactions and employ a different approach to dielectric screening. We believe the above findings are relevant to the B850 ring of *Rs. molischianum* since the nearest neighbor distances and orientations of its BChl molecules are nearly identical to those of *Rps. acidophila* and their B800-B850 energy gaps are nearly the same at all temperatures (the gap for both species being significantly larger than that of *Rb. sphaeroides*[9]). The ZPH action spectrum for B870 of *Rs. molischianum* (isolated LH2 complex) reported in ref. (9) led to an apparent ΔE-value of 290 cm^{-1}, nearly 100 cm^{-1} larger than the value reported here for *Rps. acidophila*. However, the *Rs. molischianum* samples used in ref. (9) yielded a large B850 absorption bandwidth of 355 cm^{-1} at 4.2 K, indicative of significant structural heterogeneity.

Given the discussion in the Introduction on the relationship between the apparent ΔE and inhomogeneous spectral broadening, we are confident that the above 290 cm^{-1} value for *Rs. molischianum* would be significantly reduced in LH2 samples exhibiting a B850 absorption bandwidth equal to the 200 cm^{-1} value reported here for *Rps. acidophila*. In future papers on inter-exciton level relaxation dynamics of the B850 ring (also the LH1 ring) the room temperature and low temperature (at least 77 K) absorption spectra of the samples studied should be reported so that the extent of structural heterogeneity and energy disorder can be assessed.

B. Satellite hole structure associated with burning of the B850 band

The structure being referred to is that of satellite holes which are produced as a result of nonphotochemical hole burning (NPHB) of the B850 absorption band. Under non-line narrowing conditions, the persistent hole produced in the B850 band is broad, as are the satellite holes which lie to higher energy of it, including those which lie within the B800 absorption band. Such satellite hole structure was first reported for the NF 57 mutant of *Rb. sphaeroides* chromatophores[18] (this mutant is devoid of LH1) and, somewhat later, the isolated LH2 complex of *Rps. acidophila*.[6] Because of the weakness of the satellite holes relative to the B850 hole and other factors (see section 4.C of I), they were assigned as intramolecular BChl *a* vibronic features which build, in a Franck-Condon sense, on the B850 "origin" hole. Based on new results it was argued in section 4.C of I that the vibronic interpretation is most likely incorrect, with proof of this, in the way of new satellite hole spectra, to be presented here. For consideration of the results presented below, we note that a vibronic interpretation of the satellite hole structure requires that the intensities of the satellite holes relative to the B850 hole be essentially invariant to sample preparation, species or whether the LH2 complex studied is isolated or membrane bound. It will be seen that this is not the case. We emphasize also that all persistent hole-burned spectra of antenna protein

complexes reported to date are of the non-photochemical type and that NPHB is generally observed only for chromophores imbedded in structurally disordered solids such as glasses and polymers or, for example, proteins with their glass-like structural disorder. As a result, the kinetics of NPHB are highly dispersive with a distribution of rates spanning several decades.[23,24] In the current mechanism of NPHB[25] the excess free volume of the glass, which is associated with the TLS,[26] plays a pivotal role.

Figure 7 shows two hole burned spectra for the isolated LH2 complex of *Rb. sphaeroides* obtained with a burn frequency located on the high energy side of the B850 band at $\omega_B \sim 11840$ cm^{-1}. The burn fluence used to obtain the lower spectrum was a factor of 2 higher than that of the upper spectrum. Features b and b′ correspond to the broad B850 hole mentioned above and their location relative to the B850 absorption maximum is similar to that reported in ref. (18) as is the case for features d, e and f. These last three features were assigned in that reference to vibronic holes due to ~ 340, 750 and 920 cm^{-1} BChl *a* vibrations,[27,28] respectively, which build on the B850 origin band. The problem with the vibronic interpretation is that the intensities of the d, e and f holes relative to the B850 hole in Figure 6 are significantly higher than those reported in ref. (18). For example, the integrated intensity of hole e relative to the B850 hole in the upper spectrum of Figure 7 is 0.5 while in the spectra of ref. (18) it is 0.05. (Results presented below for *Rps. acidophila* also negate the vibronic interpretation.) Holes a and a′ in Figure 7 are assigned to B870 as in ref. (6). The differences between the hole and anti-hole (asterisk) structures of the two spectra in the vicinity of B850 are intriguing. For example, the a-b gap in the upper spectrum of Figure 6 is ~ 200 cm^{-1} while in the lower spectrum it is 120 cm^{-1} (a′-b′). The only interpretation we can offer for the differences is based on the mechanism and dispersive kinetics of NPHB and the results presented earlier in this paper. In the earlier stages of burning, upper spectrum, one tends to burn complexes with B870 levels that are most red-shifted; i.e., complexes with greater energy disorder/structural heterogeneity. That is, there is positive correlation between

structural heterogeneity and NPHB efficiency. As one irradiates longer, B870 levels of individual complexes with less structural heterogeneity are burned out. However, understanding the differences between the hole and anti-hole structures of the two spectra is complicated by the phenomenon of light-induced hole filling (LIHF).[29] LIHF is most efficient when irradiation is in the region of the anti-hole which for $\pi\pi^*$ states lies to the blue of the hole, e.g. see the anti-hole (asterisk) in the lower spectrum of Figure 7 and Figures 8 and 9. Since ω_B lies on the blue side of B850, it is likely that some filling of the B850 hole and B870 hole occurs continuously during the burning process and that complexes can undergo multiple burning events. Given this, that NPHB involves a hierarchy of configurational events of the host medium[25] and the hole-anti-hole interferences, it would be difficult to achieve a detailed understanding of the evolution of the upper spectrum into the lower spectrum of Figure 7. The inflection feature c was not resolved in the spectra of ref. (18) and might correspond to the hole from the higher energy component of the allowed E_1 level split by energy disorder with hole b(b′) being the lower energy component. The anti-hole of the latter hole interferes with hole c in the same way that the anti-hole marked by the asterisk interferes with hole d and that of hole e interferes with hole f (see ref. (30) for a discussion of such interference). Note that holes d and f coincide with the high energy tail absorptions of B850 and B800. The question arises as to which exciton level NPHB occurs predominantly in following direct or indirect (B800→B850 energy transfer) excitation of the B850 band. It is probably the lowest level, B870, since it has a lifetime of several hundred picoseconds while the E_1-levels possess sub-picosecond lifetimes, see I for discussion. NPHB in the B870 exciton level leads to burning of higher energy levels of the B850 ring because they are correlated by excitonic delocalization. This effect was first demonstrated for the BChl *a* antenna complex of *P. aestuarii*.[31]

To further establish that the vibronic assignment for the aforementioned satellite holes is untenable we present Figures 8 and 9 for the isolated LH2 complex of *Rps. acidophila* and

chromatophores used to isolate LH2, respectively, see section 2 of I. In comparing these figures with Figure 7 for *Rb. sphaeroides* it is important to note that in Figure 7 the B800-B850 energy gap is 775 cm^{-1} while in Figures 8 and 9 for *Rps. acidophila* the gap is 965 and 950 cm^{-1}, respectively. Although the burn frequencies used to obtain the hole spectra in Figures 8 and 9 are located to the blue of the B800, coincident with the ZPH marked by ω_B, we found, as in refs. (6,18), that the broad hole and anti-hole (asterisk) features are similar to those obtained with excitation located within the B850 band (results not shown). In other words, the broad features are mainly due to NPHB following B800→ B850 energy transfer. We ignore, for the moment, holes 1 and 2 in Figure 8 due to the LH1 (B875) complex, and compare the LH2 hole spectra in Figures 7-9. First, holes a, b, d and e appear in all the spectra. Hole f, which is evident in Figures 7 and 9, is not obvious in Figure 8, probably because of its interference with the intense blue-shifted anti-hole of hole e. Given the ZPH action spectra for B870 reported in I and ref. (7) and discussions therein, a firm assignment of hole a to B870 can be made. Hole b is assigned to the components of the strongly allowed E_1 level. As mentioned, feature c in Figure 7 might be due to the hole of the higher energy E_1 component (the bending over of the anti-hole of hole b in Figure 8, which is indicated by the dashed arrow, could be due to this component). Hole d coincides with the weak tail absorption on the high energy side of the B850 band. It is unlikely that this absorption is vibronic (see section 4.C of I for the argument based on intramolecular BChl *a* Franck-Condon factors). Thus, we assign the absorption and hole d to the E_2 level which is made allowed by energy disorder. The disorder would be expected to split its 2-fold degeneracy and could cause a substantial red-shift of the lower energy E_2 component.[8] It was already argued, on the basis of the hole spectra in Figure 7, that the intensity of hole e is far too intense for it to be a vibronic hole building on hole b. The spectra in Figures 8 and 9 for *Rps. acidophila* confirm this. It was also argued, on the basis of Figure 7, that hole f is unlikely to be a vibronic feature building on either B800 or B850 (see also ref. (7)).

Comparison of the B800 absorption profile with the location of hole f indicates that it coincides with the weak absorption tail on the high energy side of B800.

With the e and f holes unlikely to be vibronic features, the question then is what are they due to. (In Figures 8 and 9, hole e cannot be interpreted as the result of downward energy transfer within the B800 band since it is produced by irradiation into the B850 band, Figure 7 and refs. (6,18), and unpublished results.) Two interpretations (models) are put forth. The first to be considered is suggested by electronic structure calculations[3,4] which place several of the exciton levels of the B850 ring in the near vicinity of the B800 band, see Figure 1. Coupling of these levels to Q_y-states of the B800 ring, if sufficiently strong, could then elicit a response of the B800 band to NPHB which occurs following excitation of levels within the B850 band. The second interpretation is that the protein/BChl *a* structural change produced by the just-mentioned NPHB is not confined to regions in only the near vicinity of B850 BChl *a* molecules, i.e. the structural change extends to the B800 ring, thereby producing satellite holes in B800. This model does not require the B800-B850 coupling of the first model. For both models, the extent and nature of the structural heterogeneity could to be important, influencing, for example the intensities of holes e and f relative to the B850 hole (b). The experimental results presented here do not allow for distinction between the two models for holes e and f. However, the high pressure hole burning and femtosecond pump-probe results for B800 reported in ref. (32) strongly indicate that the first model is the correct one for hole f and the high energy tail absorption of B800 it is associated with. More detailed high pressure - hole burning studies of the B800 band may lead to assignment of the mechanism responsible for hole e. Such experiments are planned.

Finally, we comment briefly on holes 1 and 2 of the LH1 absorption band (so-called B875) shown in Figure 8. The latter hole is very similar to that observed for B875 of chromatophores of *Rb. sphaeroides*.[5] In that work, however, the B875 band was broader than that of Figure 9 and hole 1 was not resolved. Nevertheless, the lowest energy exciton

level of the LH1 ring (see I) with which hole 1 is associated was resolved by ZPH-action spectroscopy and found to lie 85 cm^{-1} below the B875 absorption maximum, i.e. the gap analogous to the apparent $\Delta E = 200$ cm^{-1} of B850 is 85 cm^{-1} for B875. From Figure 9, we obtain $\Delta E = 120$ cm^{-1}. Recent theoretical modeling (including energy minimization and molecular dynamics) of the LH1 complex indicate that the orientations of the Q_y-transition dipoles of the 32 BChl *a* molecules in the C_{16}-ring are similar to those of the B850 ring.[33] Thus, the energy ordering of the B875 exciton levels is expected to be such that the A level (often referred to as B896) lies lowest in energy followed next by the E_1 and E_2 levels, etc. We point out, therefore, that the reduction in the value of the apparent ΔE from 200 cm^{-1} for B850 of *Rps. acidophila* (C_9) to 85 cm^{-1} for B875 is close to the value predicted by Equation 6 when it is assumed that the value of V and the energy disorder are similar for the two rings. Equation 6 predicts that ΔE for B875 should be 0.35 times the value for B850. We conclude that the assignment of Reddy et al.[5] of B896 to the lowest energy, weakly allowed exciton level of the LH1 ring is correct.

5. Concluding Remarks

Because of their high cyclic symmetries, the LH1 and LH2 antenna complexes are ideally suited for improving our understanding of excitonic level structure and inter-exciton level relaxation dynamics in photosynthetic complexes and other nanostructures where strong coupling is important. That the basic α,β-polypeptide pairs of the LH1 and LH2 "rings" are symmetry-equivalent simplifies the problem considerably since the dimers (BChl *a*) of both are energetically equivalent in the absence of glass-like structural heterogeneity of the protein. Such heterogeneity is now known to be important at biological temperatures. However, the effects of energy disorder produced by such heterogeneity on excitonic level structure and dynamics cannot be well understood before the excitonic level structure in the absence of disorder is. Understanding this structure well, even in the absence of disorder is a

non-trivial problem. We have in this work confirmed that B870 is the lowest energy level (A symmetry) of the B850 ring. We further determined values of ~ 100 and 150 cm^{-1} for the energy gap (ΔE) between B870 and the strongly allowed and adjacent E_1 level of the B850 ring for the low and high temperature structures of *Rps. acidophila*'s LH2 complex, respectively (see I). These values are important benchmarks for electronic structure calculations. The data presented on the temperature dependence of the optical dynamics of the B870 exciton level of *Rps. acidophila* were shown to be consistent with a low temperature ΔE-value in the range of ~ 100-140 cm^{-1}. We emphasize again that the structural change of the LH2 complex which occurs near 150 K is by no means anything close to denaturing. The structural change has no effect on the B800 absorption band (see I) but it suffices to alter nearest neighbor BChl *a*-BChl *a* couplings of the B850 ring. (The structural change occurs for both the isolated LH2 complex and the LH2 complex in chromatophores for *Rps. acidophila*, *Rb. sphaeroides* and *Rs. molischianum*[9] and unpublished results.) Reddy et al. concluded, on the basis of zero-phonon hole action spectra, that B896 is the lowest energy exciton level of the LH1 complex. The results presented here and the structure modeling calculations of ref. (8) establish that the assignment for B896 of Reddy et al. is correct.

Additional assignments for the B850 ring's excitonic level structure were made. The weak high energy tail of the B850 band was ascribed to the lowest energy E_2 level which borrows intensity from the allowed E_1 level by virtue of energy disorder. The corresponding tail of the B800 band was assigned to the highest energy exciton levels of the B850 ring which are quasi-resonant with B800. Coupling of these levels with the Q_y-states of the B800 ring is one mechanism by which they can attain oscillator strength. As pointed out in refs. (1,32), such mixing may play a role in the excitation energy relaxation dynamics within the B800 band.

The effects of energy disorder on the level structure of the B850 were examined using the recently introduced symmetry-adapted basis defect patterns (BDP). Only diagonal energy disorder was considered since the results obtained with off-diagonal disorder are similar. Attention was focused on the lowest energy A (B870), E_1 and E_2 levels and a BDP of E_1 symmetry since it couples the A and E_2 levels with the allowed E_1 level. It was shown that there is a strong increase in the transition dipole strength for B870 of an individual LH2 complex as its displacement (ΔE) below the E_1 level increases due to disorder. Thus, the value of ΔE determined by ZPH action spectroscopy (the apparent value) needs to be corrected for this effect. This was done and a value of $\Delta E \sim 150$ cm^{-1}, in the absence of disorder, was obtained for the low temperature structure. The above results lead to the following picture for the B850 absorption band at low temperatures. Energy disorder removes the degeneracy of the E_1 level with an average splitting of a few tens of cm^{-1}, but no greater than ~ 60 cm^{-1}. For such splittings both components of the E_1 level should carry comparable transition dipole strengths,[8] unpublished results. The disposition of B870 has been discussed. We only add that we were able to reconcile how B870 carries only a few percent of the absorption intensity of the B850 ring when the apparent ΔE-value of 200 cm^{-1} is a factor of 2 greater than the calculated values for the room temperature structure. The E_2 level, like B870, borrows intensity from the E_1 level with energy disorder removing its degeneracy. All told, one has 5 levels which contribute to the overall B850 absorption profile, a finding of relevance, for example, to ultra-short pulse experiments. The above picture should remain essentially intact for the high temperature structure with some minor differences due to weaker excitonic couplings for the high temperature structure and, possibly, the structural heterogeneity being temperature dependent. With regard to the latter, it was shown that the effects of energy disorder on the B850 ring's excitonic structure become more important as the inhomogeneous contribution from heterogeneity to the width of the B850 band increases.

Acknowledgments

Research at the Ames Laboratory was supported by the Division of Chemical Sciences, Office of Basic Energy Sciences, U.S. Department of Energy. Ames Laboratory is operated for USDOE by Iowa State University under Contract W-7405-Eng-82. Research at the University of Glasgow was supported by BBSRC and EU. We thank Dr. Klaus Schulten for providing us with preprints of his work prior to publication and for helpful discussions.

References and Notes

(1) Chapter 4; Wu, H.-M., Ratsep, M.; Jankowiak, R.; Cogdell, R. J.; Small, G. J. *J. Phys. Chem. B* **1997**, *101*, 7641.

(2) Freer, A.; Prince, S.; Sauer, K.; Papiz, M.; Hawthornthwaite-Lawless, A.; McDermott, G.; Cogdell, R.; Isaacs, N. W. *Structure* **1996**, *4*, 449.

(3) Sauer, K.; Cogdell, R. J.; Prince, S. M.; Freer, A. A.; Isaacs, N. W.; Scheer, H. *Photochem. Photobiol.*, **1996**, *64*, 564.

(4) Alden, R. G.; Johnson, E.; Nagarajan, V.; Parson, W. W.; Law, C. J.; Cogdell, R. G. *J. Phys. Chem. B* **1997**, *101*, 4667.

(5) Reddy, N. R. S.; Picorel R.; Small, G. J. *J. Phys. Chem.* **1992**, *96*, 6458.

(6) Reddy, N. R. S.; Cogdell, R. J.; Zhao, L. Small, G. J. *Photochem. Photobiol.* **1993**, *57*, 35.

(7) Wu, H.-M.; Reddy, N. R. S.; Small. G. J. *J. Phys. Chem., B* **1997**, *101*, 651.

(8) Wu, H.-M.; Small. G. J. *Chem. Phys.* **1997**, *218*, 225.

(9) Wu, H.-M.; Reddy, N. R. S.; Cogdell, R. J.; Muenke, C.; Michel, H. and Small, G. J. *Mol. Cryst. Liq. Cryst.* **1996**, *291*, 163.

(10). Tinkham, M. *Group Theory and Quantum Mechanics*, McGraw-Hill: New York, 1964.

(11) Hochstrasser, R. M. *Molecular Aspects of Symmetry*, W. A. Benjamin Inc.: New York, 1966.

(12) Hu, X.; Ritz, T.; Damjanovic, A.; Schulten, K. *J. Phys. Chem. B*, **1997**, *101*, 3854.

(13) Jankowiak, R.; Small, G. J. In *Photosynthetic reaction centers*, Deisenhofer, J.; Norris, J., Eds.; Academic Press: London, 1993; p. 133.

(14) Völker, S. In *Relaxation Processes in Molecular Excited States*, Fünfschilling, J., Ed. ; Kluwer Academic Publisher: Dordrecht, 1989, p. 113.

(15) Narasimhan, L. R.; Littau, K. A.; Pack, D. W.; Bai, Y. S.; Elschner, A.; Fayer, M. D. *Chem. Rev.* **1990**, *90*, 439.

(16) Jankowiak, R; Hayes, J. M.; Small, G. J. *Chem. Rev.* **1993**, *93*, 1471.

(17) van der Laan, H.; Schmidt, Th.; Visschers, R. W.; Visscher, K. J; van Grondelle, R.; Volker, S. *Chem. Phys. Letts.* **1990**, *170*, 231.

(18) Reddy, N. R. S.; Small, G. J.; Seibert, M.; Picorel, R. *Chem. Phys. Letts.* **1991**, *181*, 391.

(19) Robinette, S. L.; Stevenson, S. H.; Small, G. J. *J. Chem. Phys.* **1978**, *69*, 5231.

(20) Port, H.; Rund, D.; Small, G. J.; Yakhot, V. *Chem. Phys.* **1979**, *39*, 175.

(21) Robinette, S. L.; Stevenson, S. H.; Small, G. J. *J. Luminesc.* **1979**, *18/19*, 219.

(22) Reinot, T.; Kim, W.-H.; Hayes, J. M.; Small, G. J. *J. Chem. Phys.* **1996**, *104*, 793.

(23) Kenny, M.; Jankowiak, R.; Small, G. J. *Chem. Phys.* **1990**, *146*, 47.

(24) Kim, W.-H.; Reinot, T.; Hayes, J. M.; Small, G. J. *J. Phys. Chem.* **1995**, *99*, 7300.

(25) Shu, L.; Small, G. J. *J. Opt. Soc. Am.* **1992**, B *9*, 724.

(26) Cohen, M. H.; Grest, G. S. *Phys. Rev. Lett.* **1980**, *45*, 1271.

(27) Renge, I.; Mauring, K.; Avarmaa, R. *J. Lumn.* **1987**, *37*, 207.

(28) Gillie, J. K.; Small, G. J.; Golbeck, J. H. *J. Phys. Chem.* **1989**, *93*, 1620.

(29) Shu, L.; Small, G. J. *J. Opt. Soc. Am.* **1992**, B *9*, 738.

(30) Lee, I.-J.; Hayes, J. M.; Small, G. J. *J Chem. Phys.* **1989**, *91*, 3463.

(31) Johnson, S. G.; Small, G. J. *J. Phys. Chem.* **1991**, *95*, 471.

(32) Chapter 3; Wu, H.-M.; Savikhin, S.; Reddy, N. R. S.; Jankowiak, R.; Cogdell, R. J.; Struve, W. S.; Small, G. J. *J. Phys. Chem.* **1996**, *100*, 12022.

(33) Hu, X.; Schulten, K. 1997, technical report UIUC-TB-97-02, University of Illinois at Urbana-Champaign.

Table 1. Normalized coefficients of basis defect patterns for C_9

	site number								
	0	1	2	3	4	5	6	7	8
A	0.333	0.333	0.333	0.333	0.333	0.333	0.333	0.333	0.333
$E_{1,+}$	0.443	0.443	0.236	-0.082	-0.361	-0.471	-0.361	-0.082	0.236
$E_{1,-}$	0.161	-0.161	-0.408	-0.464	-0.303	0	0.303	0.464	0.408
$E_{2,+}$	0.361	0.361	-0.236	-0.443	0.082	0.471	0.082	-0.443	-0.236
$E_{2,-}$	0.303	-0.303	-0.408	0.161	0.464	0	-0.464	-0.161	0.408
$E_{3,+}$	0.236	0.236	-0.471	0.236	0.236	-0.471	0.236	0.236	-0.471
$E_{3,-}$	0.408	-0.408	0	0.408	-0.408	0	0.408	-0.408	0
$E_{4,+}$	0.082	0.082	-0.236	0.361	-0.443	0.471	-0.443	0.361	-0.236
$E_{4,-}$	0.464	-0.464	0.408	-0.303	0.161	0	-0.161	0.303	-0.408

Figure Captions

Figure 1. The 4.2 K absorption spectrum of LH2 complex from *Rps. acidophila* (strain 10050) and exciton manifold of the B850 ring. The manifold was calculated using Eqs. 1-3 with $e_u - e_l$, V_l, V_u and V_{ul} equal to 600, –200, 100 and 130 cm^{-1}, respectively. The labels A and E_1-E_4 correspond to the irreducible representations of the C_9 group. The vertical arrow locates B870, the lowest level of the B850 ring, see ref. 7. The asterisks indicate two closely spaced doubly degenerate levels.

Figure 2. Exciton level manifolds of the B850 ring calculated with different parameter values (the energy scales for the three manifolds are the same). The top and middle manifolds were calculated with $V_l = -270$ and -320 cm^{-1}, respectively, and values of the other parameters the same as those given in the caption to Figure 1. The bottom diagram shows the l-manifold generated using only Eq. 1 with $V_l = -320$ cm^{-1}, see text. From top to bottom, the energy gap between B870 and the adjacent strongly allowed E_1 level (ΔE) equals 122, 160 and 150 cm^{-1}, respectively. The asterisk indicates two closely spaced doubly degenerate levels.

Figure 3. Normalized basis energy defect patterns (BDP) for $E_{1,\pm}$ and $E_{2,\pm}$ of the C_9 group. The numbers inside the circles designate the sites, while those outside the circles are the components of the normalized basis defect vectors, Eq. 13, see text. The patterns for off-diagonal energy disorder are obtained by rotating the coefficients in the figure by $\pi/9$ so as to be centered between neighboring dimers.

Figure 4. Effect of $E_{1,+}$ diagonal energy disorder on the energy and absorption strength of B870. The solid squares show how the fraction of the B850 ring's total oscillator strength

carried by B870 increases with ΔE (the B870-E_1 level energy gap) which increases with increasing disorder (value of the disorder parameter λ_0, see text). The simulated B870 absorption profile is shown by open circles. The crosses define the half-Gaussian distribution for the disorder parameter λ_0. See text for discussion.

Figure 5. Exciton energy level diagrams for $E_{1,+}$ diagonal energy disorder. From a to d, λ_0 = 0, 18, 35 and 53 cm^{-1}, respectively. The energy division of ordinate is 200 cm^{-1}. Dashed lines indicate the correlations of the levels in the presence of disorder with those of the defectless C_9-ring. The asterisk indicates two closely spaced levels. As λ_0 increases, ΔE and the total span of the levels increases. Note the lifting of degeneracies due to disorder. See text for further discussion.

Figure 6. Thermal broadening of B870 ZPH burned in the isolated LH2 complex of *Rps. acidophila* (circles) and two fits calculated using Eq. 17. ZPH were read with resolutions ranging from 0.5 to 6 cm^{-1}, depending on the temperature region. A resolution of 0.3 cm^{-1} was used periodically to check ZPH burned at about 5 K and the results were consistent with those shown in the figure. The solid line was obtained with A = 0.055 cm^{-1}; α = 1.35; B = 8000 cm^{-1}; ΔE = 140 cm^{-1}, while the dashed line was generated with A = 0.058 cm^{-1}; α = 1.31; B = 800 cm^{-1}; ΔE = 97 cm^{-1}.

Figure 7. The 4.2 K absorption and hole-burned spectra of LH2 from *Rb. sphaeroides*. The B800 and B850 band maxima(widths) are 12510(135) cm^{-1} and 11735(245) cm^{-1}. The burn frequency is ~ 11840 cm^{-1}. The burn fluence employed was 1250 J/cm^2 and 2300 J/cm^2 for the upper and lower hole burned spectrum, respectively. The two hole burned spectra are offset along the ordinate for clarity.

Figure 8. The 4.2 K absorption and hole-burned spectra of LH2 from *Rps. acidophila*. The B800 and B850 band maxima(widths) are 12440(160) cm^{-1} and 11475(220) cm^{-1}. The burn frequency (ω_B) of 12522 cm^{-1} produced a 4% deep ZPH. The burn fluence employed was 450J/cm^2. See text for the explanation of the dashed arrow and other details.

Figure 9. The 4.2 K absorption and hole-burned spectra of *Rps. acidophila* chromatophores. The B800, B850 and B875 band maxima(widths) are 12445(150) cm^{-1}, 11495(220) cm^{-1} and 11060(255) cm^{-1}. The burn frequency (ω_B) of 12473 cm^{-1} produced a 7% deep ZPH. The burn fluence employed was 225J/cm^2. See text for other details.

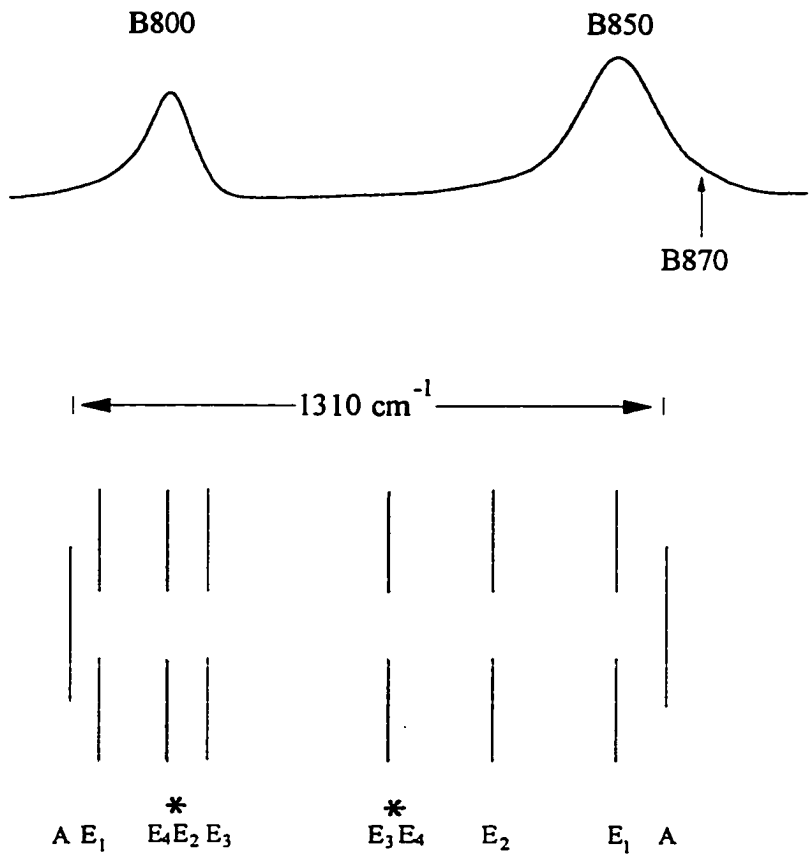

Figure 1

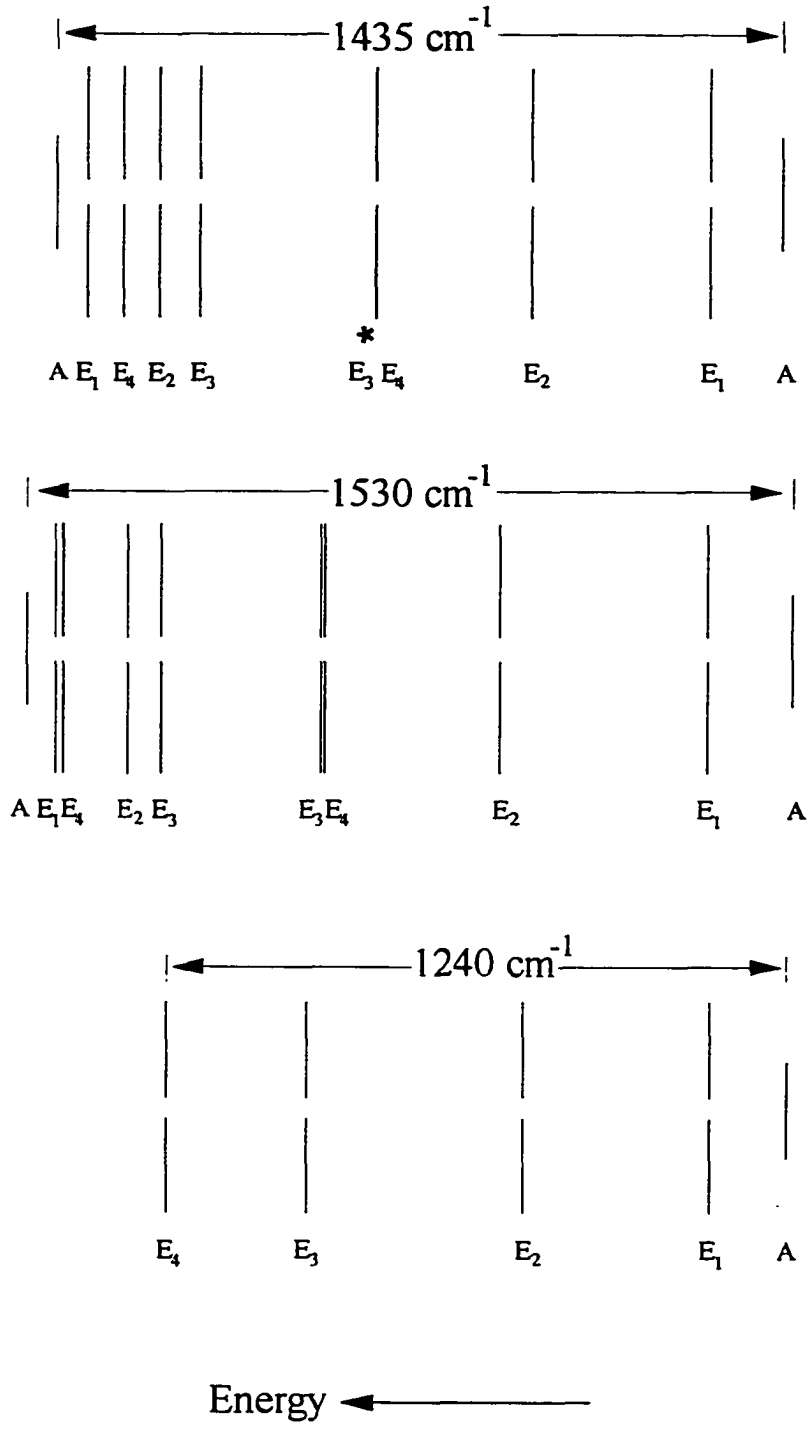
1435 cm-1
A E1 E4 E2 E3
E3 E4
E2
E1 A
1530 cm-1
A E1E4 E2 E3
E3E4
E2
E1 A
1240 cm-1
E4
E3
E2
E1 A
Energy

Figure 2

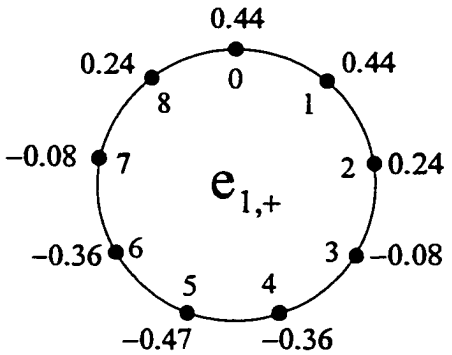
0.44
0.24
0.44
0
8
1
−0.08
7
2
0.24
$e_{1,+}$
−0.36
6
3
−0.08
5
4
−0.47
−0.36

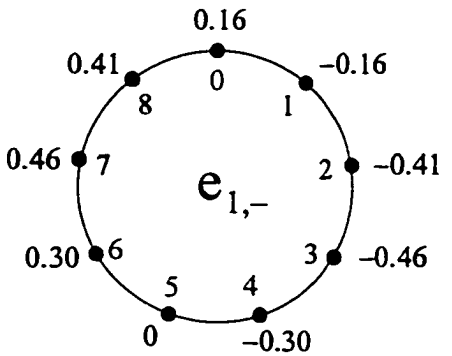
0.16
0.41
−0.16
0
8
1
0.46
7
2
−0.41
$e_{1,-}$
0.30
6
3
−0.46
5
4
0
−0.30

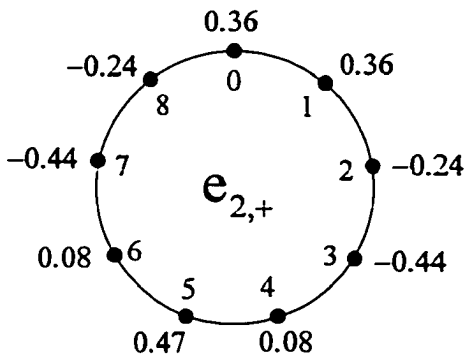
0.36
−0.24
0.36
0
8
1
−0.44
7
2
−0.24
$e_{2,+}$
0.08
6
3
−0.44
5
4
0.47
0.08

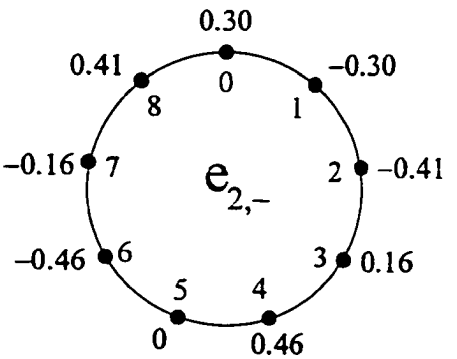
0.30
0.41
−0.30
0
8
1
−0.16
7
2
−0.41
$e_{2,-}$
−0.46
6
3
0.16
5
4
0
0.46

Figure 3

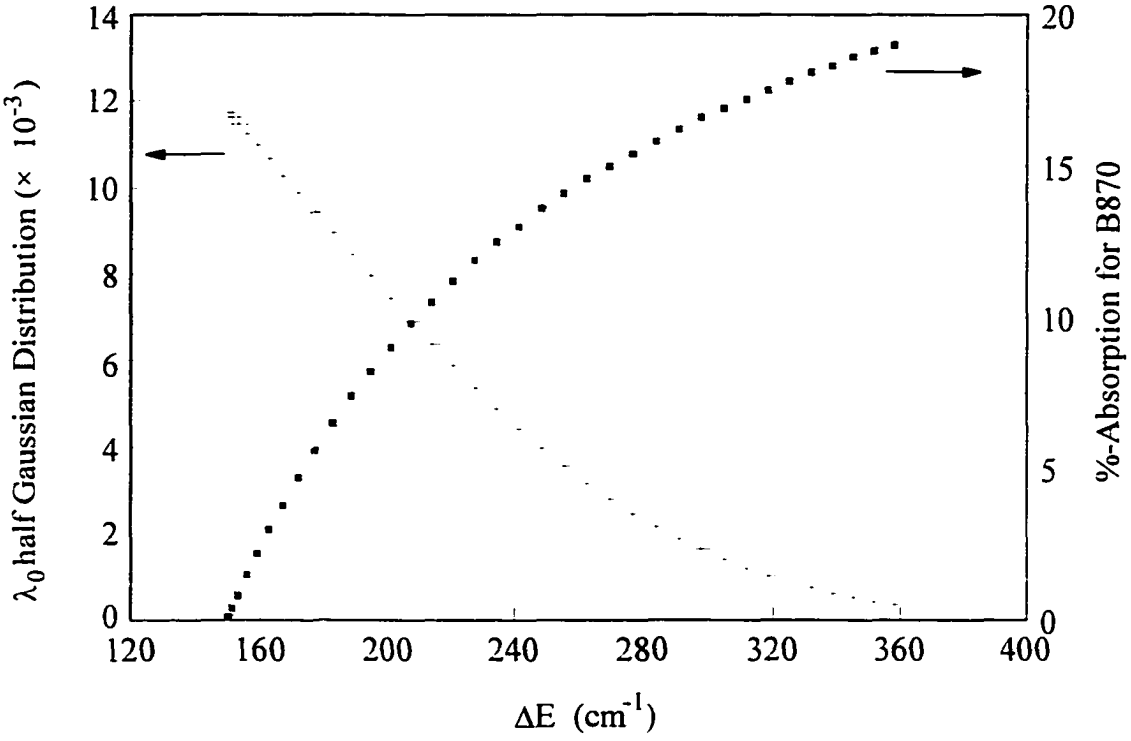
14
12
10
8
6
4
2
0
120
160
200
240
280
320
360
400
20
15
10
5
0
λ_0 half Gaussian Distribution (× 10^{-3})
%-Absorption for B870
ΔE (cm^{-1})

Figure 4

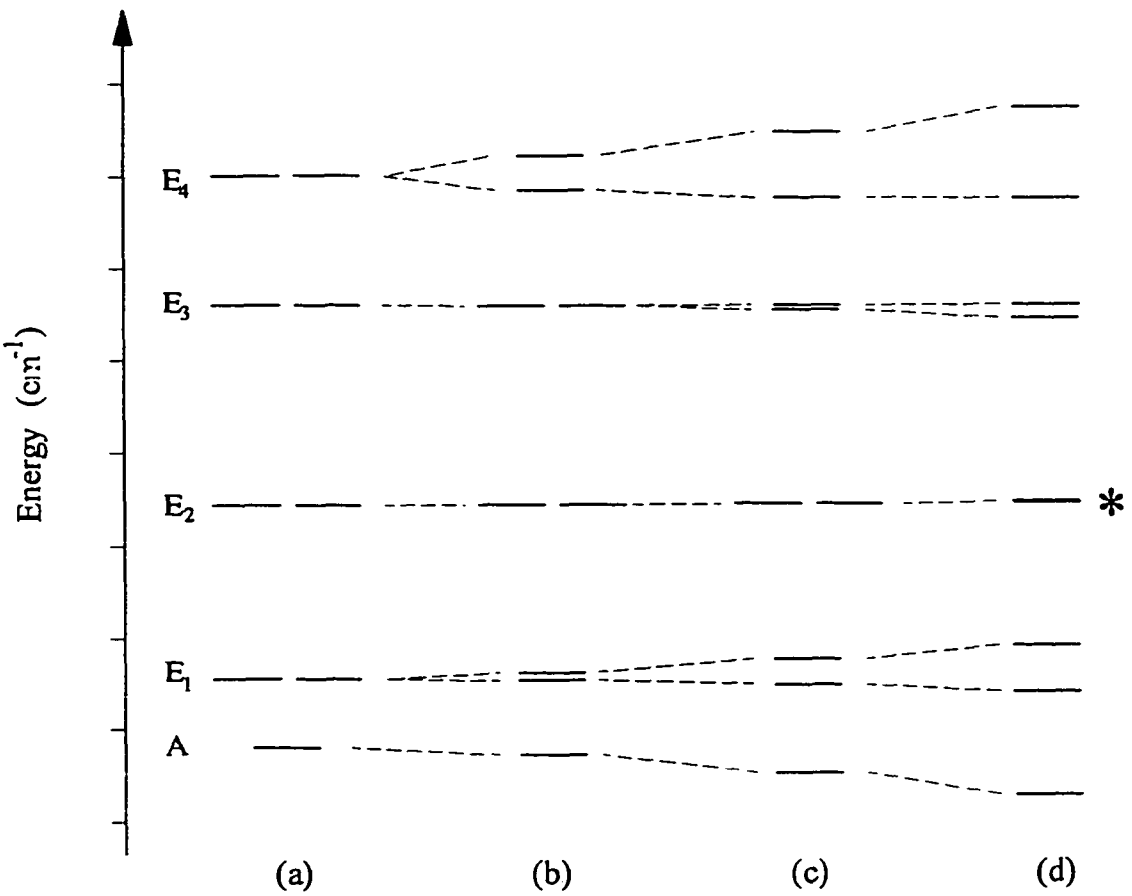

Figure 5

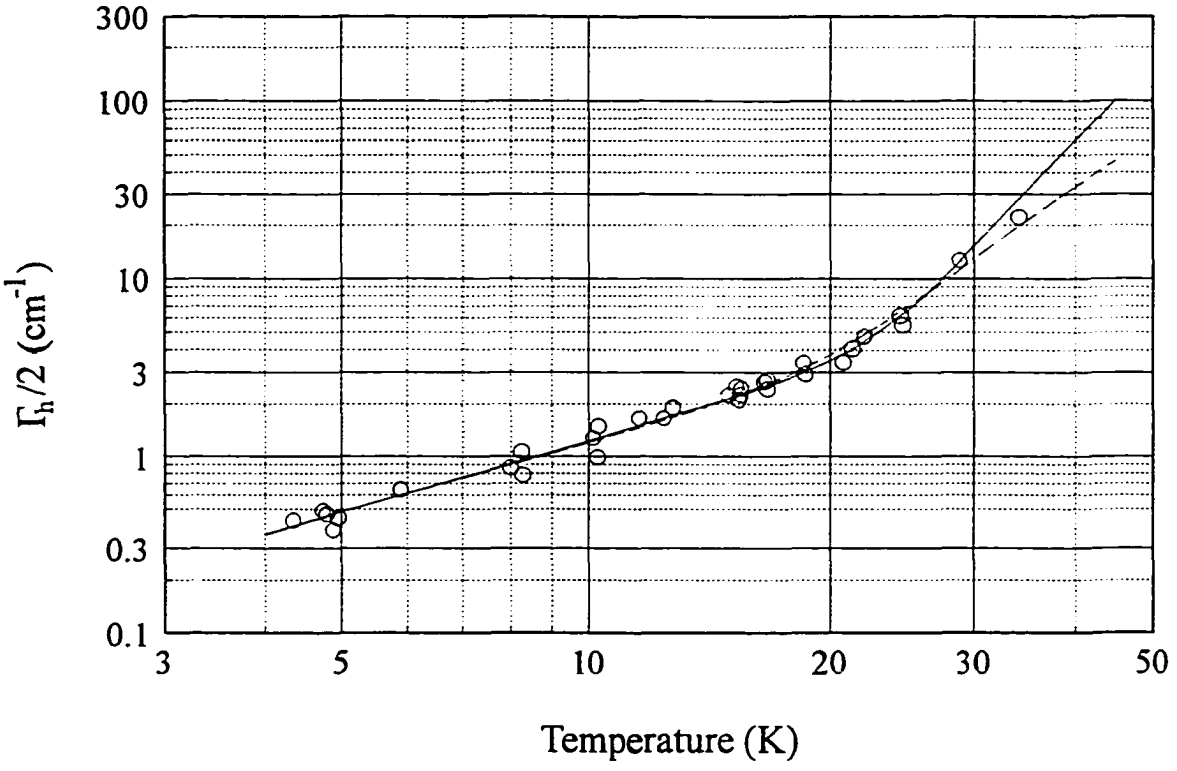

Figure 6

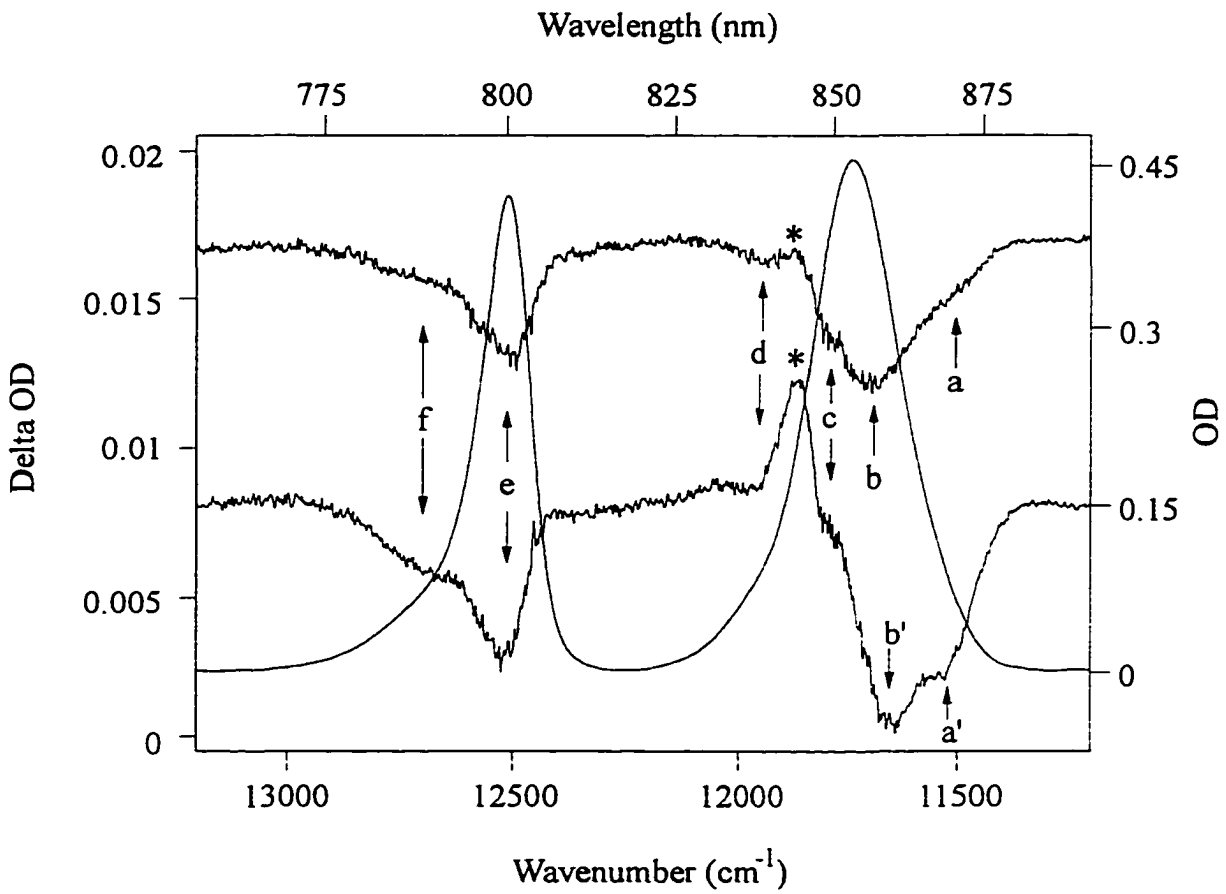
Wavelength (nm)
775
800
825
850
875
0.02
0.015
0.01
0.005
0
Delta OD
0.45
0.3
0.15
0
OD
f
e
d
c
b
a
b'
a'
*
*
13000
12500
12000
11500
Wavenumber (cm-1)

Figure 7

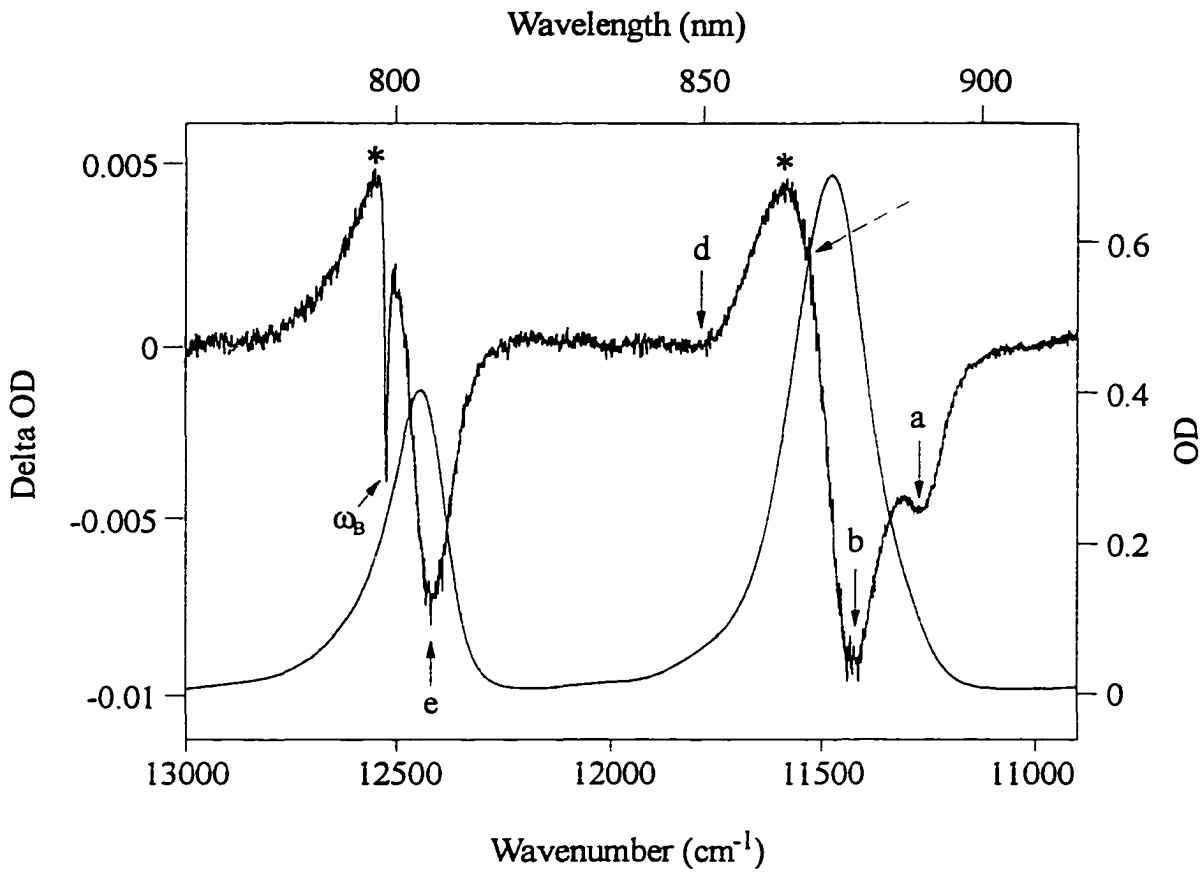
Wavelength (nm)
800
850
900
0.005
0
-0.005
-0.01
Delta OD
0.6
0.4
0.2
0
OD
*
*
d
a
b
e
ω_B
13000
12500
12000
11500
11000
Wavenumber (cm^{-1})

Figure 8

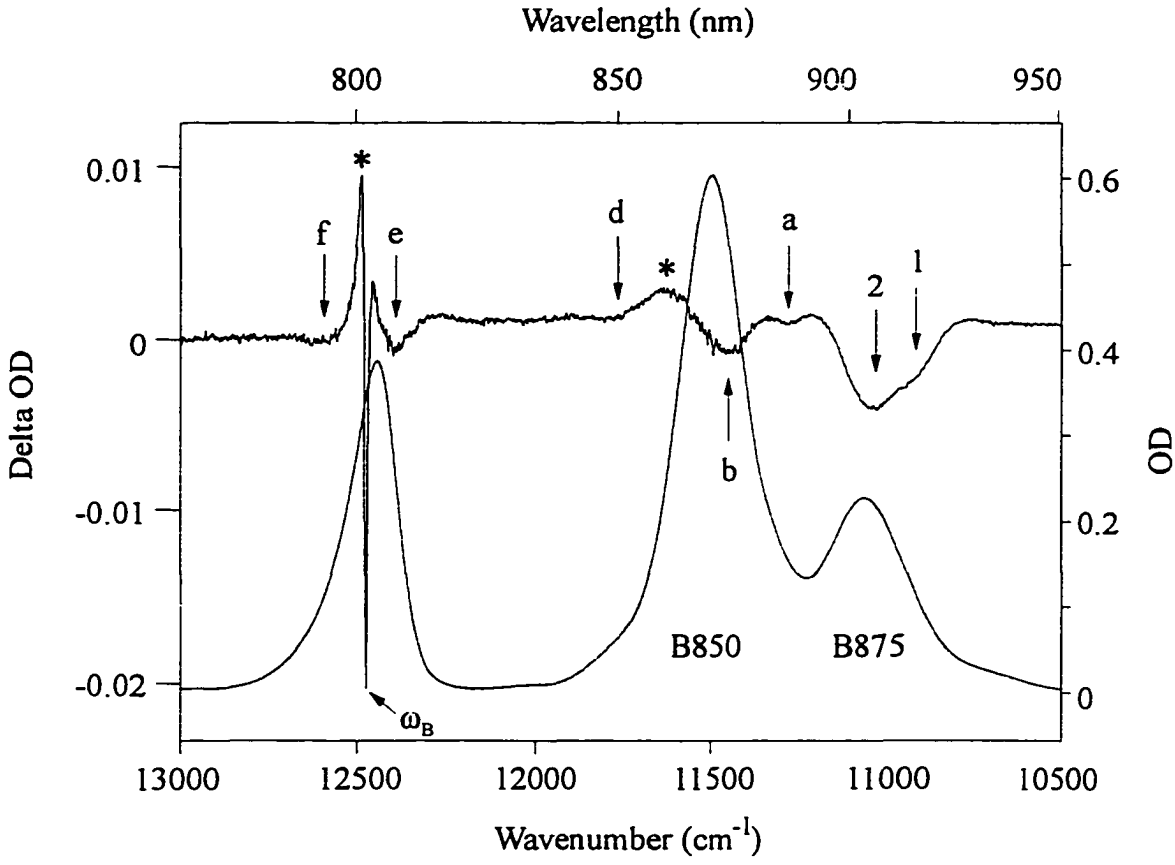
Wavelength (nm)
800
850
900
950
0.01
0
-0.01
-0.02
Delta OD
0.6
0.4
0.2
0
OD
f
e
d
a
2
1
b
B850
B875
ω_B
13000
12500
12000
11500
11000
10500
Wavenumber (cm^{-1})

Figure 9

CHAPTER 6. SYMMETRY-BASED ANALYSIS OF THE EFFECTS OF RANDOM ENERGY DISORDER ON THE EXCITONIC LEVEL STRUCTURE OF CYCLIC ARRAYS: APPLICATION TO PHOTOSYNTHETIC ANTENNA COMPLEXES

A paper published in the *J. Phys. Chem. B* **1998**, *102*, 888.

H.-M. Wu and G. J. Small

Abstract

We extend the work of Wu and Small (*Chem. Phys.* **1997**, 218, 225) who introduced symmetry-adapted basis defect patterns (BDP) for systematic analysis of the effects of random static energy disorder (diagonal or off-diagonal) on the excitonic level structure of cyclic C_n arrays of chromophores. Examples include the B850 and B875 rings of bacteriochlorophyll (BChl) molecules associated with the LH2 and LH1 antenna complexes of purple bacteria for which, so far, n = 8, 9 and 16. Calculation of the localization/extendedness (chromophore occupation number) patterns and participation numbers of the exciton levels reveals that the effects of random disorder on the exciton levels which contribute to the critically important B850 or B875 absorption band can be understood in terms of a single BDP of e_1 symmetry ("hidden correlation" effect). This is a consequence of the structures of the complexes, the complexes falling in the weak disorder regime and the strict symmetry selection rules which govern the couplings between zero-order exciton levels by BDP. The above finding greatly simplifies computational studies on the effects of random disorder on the spectroscopic properties of the above bands. Our results show that interpretation of electric field (Stark) effects on the B850 and B875 absorption bands must include the effects of energy disorder. Similarities

and differences between the effects of diagonal and off-diagonal energy disorder are discussed as is the relevance of our findings to the superradiant properties of the LH complexes.

1. Introduction

We recently introduced symmetry-adapted basis defect patterns (BDP) for analysis of the effects of static diagonal and off-diagonal energy disorder on the excitonic structure and spectroscopic properties of cyclic (C_n) arrays of coupled chromophores.[1,2] Motivation for doing so was that light harvesting (LH) antenna complexes of purple photosynthetic bacteria exhibit C_n-symmetry with n = 8,[3] 9[4] and 16,[5] the chromophore being a bacteriochlorophyll (BChl) molecule. The LH2 complex of *Rhodopseudomonas acidophila* is an example of C_9 with nine α,β polypeptide pairs, each of which bind a pair of BChl molecules at the periplasmic side of the membrane. The eighteen strongly coupled BChl molecules with nearest neighbor couplings of ~ 300 cm^{-1} [6] give rise to the B850 absorption band shown in Figure 1 for the isolated complex at 4.2 K.[7] The structure of the BChl pair is such that essentially only its lowest energy excitonic component carries absorption intensity.[8] It turns out that[2] the exciton levels which contribute to the B850 band are well described by the Hamiltonian indicated by the circular array of nine transition dipoles shown in Figure 1. Each dipole corresponds to that of the lowest energy component of the BChl pair. To a high degree of accuracy, these dipoles can be taken to be perpendicular to the C_9 rotation axis. Recent experimental data have led to a value of ~ – 300 cm^{-1} for the nearest neighbor dimer-dimer dipole coupling (V) at cryogenic temperatures.[9] The excitonic level structure from ref. (9) calculated with V = – 320 cm^{-1} and Eq. (3) of this paper is shown below the absorption spectrum in Figure 1. The relative energies of the levels are in the unit of cm^{-1}. Each level is labeled by its C_9 irreducible representation (rep) A or E_j with j = 1-4 (see section 2 for further discussion). Only the

A level and separably degenerate E_1 level are symmetry allowed in absorption but the near in plane (perpendicular to the C_9 axis) orientation of the BChl transition dipoles renders the A level essentially forbidden (carrying less than 1% of the absorption intensity of the B850 band according to the calculations of Sauer et al.[6]). For this reason, the E_1 level in Figure 1 is placed at the B850 band maximum. As discussed in refs. (1,2), energy disorder splits the degeneracies of the E-type levels, couples energetically different levels and provides forbidden levels with absorption strength by virtue of their mixing with the allowed E_1 level. The tail absorption on the low energy side of B850 is due to the A level (often referred to as B870). The high energy tail absorption has recently been assigned to the E_2 level.[2] Hole burning data show that at 4.2 K the inhomogeneous broadening of B870 (Γ_{inh}) is 120 cm^{-1} for high quality samples, that the B870 absorption maximum lies 200 cm^{-1} to the red of the B850 maximum and that B870 carries 3-5% of the total absorption intensity of the B850 band.[10] These results were explained in terms of energy disorder.[1,2,10] The situation where only the A, E_1 and E_2 levels contribute to the B850 band also holds for *Rs. molischianum* for which the symmetry is C_8 (16 BChl molecules). Based on the results of Hu et al.,[11] the same would appear to be true for the B875 band of LH1 with its C_{16} symmetry (32 BChl molecules).

The high cyclic symmetry of the above nano-rings invites a group theoretical approach to the study of the effects of energy disorder since an arbitrary defect pattern can be written as a linear combination of the BDP. By examining the effects from each BDP, one has a systematic approach to the question of whether energy disorder can account for spectroscopic data given a zero-order C_n-Hamiltonian.[1,2] There are also strict selection rules governing the coupling of the zero-order exciton levels by the BDP, see section 2. As shown here, however, the BDP approach is most useful for weak disorder. By weak disorder is meant that the disorder-induced coupling matrix elements between energetically different levels is comparable to or smaller than the zero-order level spacings. We show

that the aforementioned complexes satisfy weak disorder. In order to do so one requires data that define the maximum (average) experimentally allowed disorder (MEAD). At this point we mention only that Wu et al.,[2] using the B850 profile shown in Figure 1 and $\Gamma_{inh} = 120\ cm^{-1}$, showed that the maximum average splitting of the degeneracy of the E_1 level is ~ 60 cm^{-1} and that absorption due to the E_3 and E_4 levels is not observed.[2]

The paper is organized as follows. Section 2 provides a review of the theory of ref. (1) and definition of the exciton level participation number N which is a rough gauge of localization or extendedness (L-E). Section 3 presents the results of diagonal energy disorder calculations on the L-E (occupation number) patterns and N-values for the C_9 system of Figure 1. (Similarities and differences between diagonal and off-diagonal disorder for weak and strong disorder as well as between C_9 and C_8 are discussed.) The results provide strong support for the suggestion by Wu et al.[2] that one need only consider a single BDP of $e_1{}^{12}$ symmetry to understand the effects of random disorder on the exciton levels that contribute to the B850 band. The section ends with results which show that consideration of energy disorder is important for interpretation of electric field (Stark) effects on this band. Conclusions are given in the last section along with additional remarks on utility of our symmetry based approach.

2. Theoretical Background

We begin with a review of the main results from refs. (1,2). In the presence of disorder the Hamiltonian for a C_n system is

$$H = H_o + H_\lambda + H_v\ , \tag{1}$$

where H_0 is the Hamiltonian in the absence of disorder with delocalized eigenfunctions

$$|j\rangle = n^{-1/2} \sum_{\alpha=0}^{n-1} B^{j\alpha *} |\alpha\rangle\ , \tag{2}$$

and energies

$$E_j = e + 2V\cos(2\pi j / n)\,, \tag{3}$$

with j = 0,1,...,n−1 labeling the delocalized exciton levels or irreducible representations (reps) of the C_n group. In Eq. (2), B = exp(i2π/n). The correspondence between j-values and reps for n = 9 is: j = 0 (A); j = {1,8} (E_1); j = {2,7} (E_2); j = {3,6} (E_3) and j = {4,5} (E_4). The two reps in each curly bracketed term are separably degenerate. An alternative and equivalent way of expressing the degenerate pairs is {1,−1}, {2,−2}, {3,−3} and {4,−4}. For n = 8, another case of importance in photosynthesis, one has: j = 0 (A); j = {1,7} (E_1); j = {2,6} (E_2); j = {3,5} and j = 4 (B). In Eq. (3), e is the site excitation energy, V is the nearest neighbor coupling and α labels the ring site ($|\alpha\rangle$ is the localized site wavefunction). Returning to Eq. (1), H_λ and H_v govern the diagonal and off-diagonal energy disorder, respectively. Starting with the usual expressions for H_λ and H_v in the site representation, and writing the site wavefunction as

$$|\alpha\rangle = n^{-1/2}\sum_j B^{j\alpha}|j\rangle\,, \tag{4}$$

it follows that the couplings between delocalized levels r and s are given by[1,2]

$$\langle r|H_\lambda|s\rangle = \frac{1}{n}\sum_\alpha \lambda_\alpha B^{(r-s)\alpha}\,, \tag{5}$$

and

$$\langle r|H_v|s\rangle = \frac{1}{n}\sum_\alpha v_\alpha B^{(r-s)\alpha}(B^{-s}+B^{r})\,. \tag{6}$$

Here, λ_α is the diagonal energy defect at site α and v_α is the defect associated with coupling between sites α and α + 1. It is at this point where one introduces the BDP which transform like the reps of the C_n group. The BDP are obtained using the projection

operator technique.[13,14] This technique would be familiar to those who, for example, have used it to generate the π-molecular orbitals of benzene. The normalized C_9-coefficients of the BDP for diagonal energy disorder are given in Table 1. To avoid confusion we use lower case Roman letters to label the reps for BDP and upper case for the exciton levels. Inspection of Table 1 reveals that only the e_3 BDP (with the obvious exception of the BDP carrying a symmetry) does not reduce the symmetry to C_1. The e_3 BDP reduce the symmetry to C_3. Normalized C_8 coefficients are given in Table 2, from which one observes that the BDP of b symmetry reduces the C_8 symmetry to C_4 while BDP of e_2 symmetry reduce C_8 to C_2. The BDP for off-diagonal disorder are precisely the same as given in Tables 1 and 2 when the coefficients of the BDP are rotated by π/9 and π/8, respectively, so as to be centered between neighboring sites. As mentioned earlier, any chosen energy defect pattern for the ring can be expressed as a superposition of BDP patterns since they form a complete set. Thus, one can examine the effects of each and every BDP on the ring exciton structure so as to determine which are of primary importance. Incorporation of the BDP in Eq. (5) leads to[1,2]

$$\langle r|H_{\lambda}^{e_{j,\pm}}|s\rangle = \frac{\lambda_{j,\pm}\, N_{j,\pm}}{n} \sum_{\alpha} \left[\cos\left(\frac{2\pi j\alpha}{n}\right) \pm \cos\left(\frac{2\pi j(\alpha-1)}{n}\right)\right] e^{i2\pi\alpha(r-s)/n} \tag{7}$$

for e-type BDP. The (±) subscripts denote the partner BDP for a given value of j. The set of square-bracketed terms with $\alpha = 0,1,\ldots,n-1$ define the defect pattern with $N_{j,\pm 1}$ being the normalization constant for the BDP (as defined in ref. (1)). The relationship between $\lambda_{j,\pm}$ and the λ-value for the generator defect site (λ_g) used with the projection operator technique is $\lambda_{j,\pm}N_{j,\pm} = \lambda_g$. In simpler terms, once the value of λ_g is set (without loss of generality one can associate λ_g with λ_0 for site "zero" of the ring), the values of the defect at all other sites are determined by symmetry as prescribed by Tables 1 and 2. For the totally symmetric (a) BDP, the square bracketed term in Eq. (7) is replaced

by unity for every site α. For n even, where one has a BDP of b symmetry, the square bracketed term in Eq. (7) is replaced by $(-1)^{\alpha}$.

The matrix elements for off-diagonal disorder are given by[1]

$$\langle r|H_{v}^{ej,\pm}|s\rangle = \frac{v_{j,\pm}\, N_{j,\pm}}{n}\sum_{\alpha}\left[\cos\left(\frac{2\pi j\alpha}{n}\right)\pm\cos\left(\frac{2\pi j(\alpha-1)}{n}\right)\right]B^{(r-s)\alpha}[B^{-s}+B^{r}]. \tag{8}$$

Coupling selection rules. The selection rule associated with the matrix elements of Eqs. (7) and (8) is[1,2]

$$r-s=\pm j, \tag{9}$$

with j defining the BDP which couple exciton levels r and s. The degeneracy of level E_r is removed, in first order, by a BDP with symmetry contained in the symmetric direct product $(E_r \times E_r)_+$. For C_9 with r = 1–4, the symmetries of the BDP are, respectively, e_2, e_4, e_3 and e_1. For C_8 with r = 1–3, they are e_2, b and e_2. These results also follow from Eq. (9).

The participation number N. The problem of localization of electrons or electronic excitations by energy disorder in infinite one- and higher dimensional structurally disordered solids is an old one[15] but one of current interest (for reviews see refs. (16-18)). As it turns out, it is generally more difficult to determine and characterize extended (not perfectly localized at some site) states than a completely localized state.[16] The brute force approach to the problem, where one imposes Gaussian randomness on site energies (H_λ) or nearest neighbor site-site couplings (H_v), poses an enormous computational problem, especially for macroscopic systems (thus, and as discussed in refs. (16-18), scaling theories have been applied to the problem). In the course of studying the above problem the participation number N was introduced as a rough gauge for localization or extendedness. An eigenstate, $|\psi\rangle$, of the Hamiltonian for the disordered system can be expressed as

$$|\psi\rangle = \sum_{\alpha} c_{\alpha\psi} |\alpha\rangle , \tag{10}$$

where $|\alpha\rangle$ is the site wavefunction. The participation number N, which was recently used in the study of LH complexes of purple bacteria,[19-21] is defined by

$$\frac{1}{N_{\psi}} = \sum_{\alpha} \left| c_{\alpha\psi} \right|^4 . \tag{11}$$

In an aside to his review article,[22] Thouless noted that $N_{\psi} = n$ for all states $|\psi\rangle$ of a perfect (no disorder) cyclic system, i.e., all states are completely delocalized. This result follows immediately from Eqs. (2), (10) and (11). He also concluded that, in the limit of very small random energy disorder, $N_{\psi} = 2n/3$ for all doubly degenerate levels (for non-degenerate levels like A of C_9 or A and B of C_8, $N_{\psi} = n$). Monshouwer et al.[21] concluded that $N_{\psi} = 2n/3$ for degenerate levels even in the absence of disorder. This conclusion is incorrect since, in the absence of disorder, the Hamiltonian carries C_n-symmetry, meaning that the wavefunctions must be of the Bloch type, as in Eq. (2). It is worthwhile to comment briefly on the derivation of the $N_{\psi} = 2n/3$ result which was not given by Thouless. The derivation follows once one notes that random disorder, no matter how small, destroys the C_n-symmetry, meaning that one needs to abandon the Bloch wavefunctions of Eq. (2) and consider the *sin-* and *cos-* type functions:

$$|j_{\sin}\rangle = 2^{1/2} n^{-1/2} \sum_{\alpha} \sin(2\pi j\alpha / n) |\alpha\rangle \tag{12a}$$

and

$$|j_{\cos}\rangle = 2^{1/2} n^{-1/2} \sum_{\alpha} \cos(2\pi j\alpha / n) |\alpha\rangle \tag{12b}$$

in the limit where disorder approaches zero. Equations (12) and (11) would appear, with a first glance proof, to be consistent with the $N_{\psi} = 2n/3$ result. However, closer inspection

reveals that the proof breaks down whenever j/n = 1/4 (or an odd multiple of 1/4), where j labels the exciton level and n is the order of the cyclic group. Thus, the $N_\psi = 2n/3$ result is valid for n odd. For n even, one needs to be careful. For example, for n = 6 or 10, the $N_\psi = 2n/3$ result holds. It does not hold for n = 8 and the E_2 degenerate pair. It is not difficult to show that $N_\psi = n/2 = 4$ for both components of E_2 of C_8. For the case of C_{16}, $N_\psi = n/2 = 8$ for the components of the E_4-exciton level.

3. Results and Discussion

As discussed in the Introduction, the C_9-arrangement of in-plane (perpendicular to the C_9 axis) transition dipoles shown in Figure 1 provides a good model for interpretation of spectroscopic data on the B850 absorption band of *Rps. acidophila*. The same is true for the corresponding band of *Rs. molischianum* and the B875 band of the LH1 complex for which C_9 is replaced by C_8 and C_{16}, respectively. For all three of these bands, only the A, E_1 and E_2 exciton levels contribute, as indicated in Fig. 1 for the B850 band of *Rps. acidophila*. Again, in the absence of energy disorder the E_2-level (also E_3 and E_4) are symmetry forbidden in absorption while the A level is rendered essentially forbidden because of the structure of the LH2 complex. In view of the calculations of Sauer et al.[6] and Alden et al.,[23] we take the A level to be totally forbidden in the absence of disorder (their calculations indicate that the A level carries significantly less than 1% of the absorption cross-section of the symmetry allowed E_1 level. To understand what we mean by hidden correlation, we recall that when Gaussian randomness is imposed on the excitation energies or nearest neighbor couplings of the sites of infinite systems, one has a total absence of correlation. The same would be true for the nano-ring systems considered here, where the imposition of Gaussian randomness accounts for fluctuations in excitation energies or couplings as one moves from one ring to the next in the ensemble. On the other hand, the basis defect patterns defined in section 2 are perfectly correlated. That is,

given a BDP and the value of the defect at one site, one automatically knows the values of the defects at all other sites. At first glance, one might think, therefore, that BDP are of little use for understanding the effects of random energy disorder on nano-ring systems. This turns out not to be true for weak disorder as defined in Section 1. That BDP are potentially useful follows in this case when it is noted that any arbitrary defect pattern can be written as a linear combination of BDP, that the matrix elements defined by Eqs. (7) and (8) are comparable to or small relative to the spacings between adjacent delocalized exciton levels and that disorder-induced coupling is governed by the selection rule $r-s = \pm j$ of Eq. (9). (Recall also that the first order splitting of a degenerate exciton level r is determined by BDP of symmetry contained in $(E_r \times E_r)_+$.) Thus, one observes that e_1 BDP could be of particular importance since they couple adjacent (most closely spaced) levels. The importance of e_1 BDP for understanding the nature of the B850 absorption band has been pointed out by Wu et al.,[2] who emphasized that they couple both the forbidden A and E_2 levels with the strongly allowed E_1 level and that, for example, the absorption intensity of the A level and its displacement below the E_1 level are strongly influenced by BDP of e_1 symmetry. The dominance of the e_1 BDP components of random disorder patterns in determining the nature of the excitonic level structure underlying the B850 band is an example of what we mean by hidden correlation.

We proceed now to present the results of calculations which support the conclusions of Wu et al. and address the problem of the localization patterns for the A, E_1 and E_2 levels associated with the B850 band of *Rps. acidophila*. Localization or extendedness for these levels was not considered by Wu et al. For the sake of brevity, we present results only for diagonal energy disorder although we comment on similarities and differences between diagonal and off-diagonal disorder.

We begin with results obtained with randomly generated diagonal defect patterns for the C_9-ring. For each random pattern the values of the site defects were uniformly

scaled so as to yield results consistent with experimental results;[10] namely, that the A level should carry ~ 5-10% of the total absorption intensity of the B850 band (denoted by I(%) in Table 3), that the energy spacing between the A and E_1 levels (ΔE in Table 3) should be ~ 200 cm^{-1} and that the splitting of the degeneracy of the strongly allowed E_1 level (ΔE_1 in Table 3) should be no greater than ~ 60 cm^{-1}.[2] For the sake of brevity, any defect pattern that yields results consistent with these experimental results will be referred to as a MEAD (maximum experimentally allowed disorder) pattern. Each random pattern was then decomposed into its BDP components[1] and their contributions to I, ΔE and ΔE_1 analyzed. The conclusions to be drawn from the results given in Table 3 for a particular pattern are consistent with the results from other random defect patterns. They are also consistent with results obtained with diagonal disorder localized at a single site on the ring. We remind the reader that we are concerned with the weak disorder regime, one that is appropriate for the systems being considered. Line 19 of Table 3 gives the results for the random defect pattern with I = 10.4%, ΔE = 208 cm^{-1} and ΔE_1 = 34 cm^{-1} (ΔE_2, which is the splitting of the E_2-level degeneracy, is considered below). Lines 1 and 2 give the results for the $e_{1,+}$ and $e_{1,-}$ BDPs, respectively, while line 3 corresponds to the combination of $e_{1,+}$ and $e_{1,-}$. Comparison of the I- and ΔE-values of lines 1-3 with those of line 19 and the observation that I = 0% and ΔE ~ 150 cm^{-1} (defect-free value) for every line in which the $e_{1,+}$ and $e_{1,-}$ contributions are excluded, firmly establishes the importance of e_1 BDP to the underlying level structure of the B850 band. Turning next to the ΔE_2 column, one can see that the degeneracy splitting of the E_2 level (77 cm^{-1}, line 19) is due almost entirely to e_4 BDP, as expected from the selection rules given in section 2. With that in mind, the question arises as to why in lines 1-3 the ΔE_1 values are not close to zero since the e_2 BDP which split the E_1 level in first order are excluded. The reason is that because the E levels are separably degenerate, a second order mechanism for removal of degeneracy exists, one that involves coupling between levels subject to the selection rule

of Eq. (9). That is, the e_1 BDP in lines 1-3 couple the E_1 components with the nearby A and E_2 levels. This higher order effect is not important for the E_4 level since it is relatively far removed from the other levels. Not included in Table 3 are results for the %-intensity of the E_2 level. It is zero when the contributions from e_1 BDP to the random pattern are excluded. This is expected since e_1 BDP couple E_2 with the allowed E_1 level. Because the spacing between the E_2 and E_1 levels is larger than that between the A and E_1 levels, Fig. 1, intensity borrowing by the E_2 level is less than that of the A level.

Localization or extendedness. The above results indicate that e_1 BDP, and to a lesser extent, e_2 BDP are very important for understanding the underlying exciton level structure of the B850 band of *Rps. acidophila*. This is also the case for the B850 band of *Rs. molischianum* where the symmetry of the LH2 complex is C_8 and, most likely, also the B875 absorption band of the LH1 complex which carries C_{16} symmetry. We have performed a large number of calculations on the participation numbers (N) and localization-extendedness (L-E) patterns for C_9 and C_8 symmetry. By L-E pattern we mean the set $\{|c_{\alpha\psi}|^2\}_{\alpha=0}^{n-1}$ for the level $|\psi\rangle$, see Eq. (10). Thus, $|c_{\alpha\psi}|^2$ is the probability that the excitation resides on dimer α. The calculations included diagonal and off-diagonal random disorder and disorder associated with $e_{j,+}$ and $e_{j,-}$ BDP (also the BDP of b symmetry for C_8).

Figure 2 shows the $e_{1,+}$ diagonal disorder L-E patterns for all exciton levels (A-E_4) of our C_9 system obtained for very weak disorder, $\lambda_0 = 1.8$ cm^{-1}. λ_0 is the value of the energy defect at site "0". Values of the defect at the other eight sites are readily obtained using Table 1. Each of the nine patterns shown are labeled by A or $E_{j,l}$ or $E_{j,h}$, where l and h denote lower and higher energy components of the E_j levels whose two-fold degeneracy is removed by disorder and j = 1-4. At the top of each pattern are 5-digit numbers which are the energies of the levels in the unit of cm^{-1}. (With reference to Eq. (3), e has been set equal to zero and V = –320 cm^{-1}, *vide supra*.) To the immediate

right of each energy value is the value of the participation number N. As predicted in section 2, N = 6 for all levels except the A level for which N = 9. These limiting N-values are also obtained for the $e_{1,-}$, e_2 and e_4 BDP (e_3 BDP yield different results since they leave the system with C_3 symmetry, although, for example, N = 9 for the A level). Furthermore, for very weak disorder, the L-E patterns from off-diagonal and diagonal disorder are the same. As can be seen from Figure 2, the patterns for levels E_j vary significantly with j and $E_{j,l}$ and $E_{j,h}$ patterns complement each other.

Figure 3 shows the L-E patterns obtained with $\lambda_0 = 140$ cm^{-1}. This value of λ_0 for the $e_{1,+}$ BDP satisfies the MEAD condition. Note, for example, that $\Delta E = 220$ cm^{-1} and $\Delta E_1 = 56$ cm^{-1}. The L-E patterns were found to change smoothly as λ_0 was increased from 1.8 cm^{-1} to higher values.[24] Comparison of Figures 2 and 3 reveals how the A level has undergone a single "clump" localization for $\lambda_0 = 140$ cm^{-1} with N = 4.9. Since the B850 sites are dimers, the number of BChl molecules which contribute significantly is ~ 10.[25] One observes also that the $E_{4,l}$ level is more extended at $\lambda_0 = 140$ cm^{-1} than at $\lambda_0 = 1.8$ cm^{-1}, in contrast with the $E_{4,h}$ level. Thus, the well-known adage that increasing diagonal energy disorder leads to greater localization for all levels does <u>not</u> generally pertain to the systems considered here. The increase in N for $E_{4,l}$ from 6.0 to 7.5 is compensated by the decrease in N for $E_{4,h}$ to 4.4 We note that L-E patterns of the $e_{1,-}$ BDP are similar to those of the $e_{1,+}$ BPP for C_9 and weak disorder. Significant differences occur for strong disorder.[24] (For C_8, $e_{j,+}$ and $e_{j,-}$ BDP yield identical results since their BDP are related by a $\pi/4$ or $\pi/2$ rotation, see Table 2.)

We investigated the effects of adding e_2 BDP to e_1 BDP since e_2 BDP split the degeneracy of the E_1 level in first order. The L-E patterns have been obtained with $\lambda_0(e_{1,+}) = 140$ cm^{-1} (the value used in Figure 3) and a very small value for $\lambda_0(e_{2,-})$ of -4.1 cm^{-1} (results not shown). Comparison with Figure 3 reveals that this $e_{2,-}$ disorder has essentially no effect on the L-E patterns (as expected, the energies of the $E_{1,h}$ and $E_{1,l}$

levels are slightly perturbed). This is also the case when $e_{2,+}$ is added rather than $e_{2,-}$ and when $e_{1,+}$ is replaced by $e_{1,-}$. Figure 4 gives the results for $\lambda_0(e_{1,+}) = 140$ cm^{-1} and $\lambda_0(e_{2,-}) = -50$ cm^{-1}, a MEAD value. Comparison of this figure with Figure 3 ($\lambda_0(e_{1,+}) = 140$ cm^{-1}) shows that the A level is hardly affected by the $e_{2,-}$ defect pattern, as expected. Interestingly, its effect on $E_{1,l}$ and $E_{1,h}$, although greater than its effect on the A level, are not profound even though the $e_{2,-}$ BDP splits the E_1 degeneracy in first order; the $E_{1,l}$ and $E_{1,h}$ energies are shifted by only about -10 cm^{-1} and their participation numbers change by -0.4 and $+0.5$, respectively. The weak effect on the E_1 levels is, to a considerable extent, a consequence of their second order couplings with the A and E_2 levels via the $e_{1,+}$ BDP. Such couplings are likely mainly responsible for the significant increase in the extendedness of the $E_{2,l}$ and $E_{2,h}$ levels with the addition of the $e_{2,-}$ defect pattern.

Before presenting L-E patterns for random diagonal energy disorder, it is instructive to examine the patterns for e_4 BDP. Results are given in Figure 5 for $\lambda_0(e_{4,+}) = 12$ cm^{-1}, a MEAD value which splits the degeneracy of the E_2 level by 69 cm^{-1} in first order. The major point is that the L-E patterns and participation numbers are very similar to those shown in Figure 2 for very weak disorder ($e_{1,+}$) which splits the degeneracy of the E_4 level by only 2 cm^{-1}. That much stronger e_4 disorder has only a weak effect is a consequence of it coupling only the A and E_4 levels which are far removed each other, Figure 1. The L-E patterns for $E_{2,l}$ and $E_{2,h}$ of Figure 5 are essentially set by the sin- and cos-type wavefunctions of Eq. (12).

L-E patterns for <u>random</u> diagonal disorder (MEAD) are shown in Figure 6. Uniform reduction of the site defects by a factor of 10 yielded L-E patterns similar to those of Figure 2 (results not shown). Comparison of Figures 7 and 3 ($\lambda_0(e_{1,+}) = 140$ cm^{-1}) is of particular interest since both correspond to MEAD. Importantly, the patterns for the A

and E_1 levels, which are of primary interest, are similar (confirmed for other random disorder patterns). This is also the case for the E_2 and E_4 levels.

To summarize, we have demonstrated that the effects of random diagonal energy disorder on level structure underlying the B850 band of *Rps. acidophila* can be investigated using a single e_1-type BDP (hidden correlation effect). This affords a substantial simplification for computational studies along with a deeper understanding of the physics involved. Now one need only place a Gaussian distribution on $\lambda_0(e_{1,+})$ or $\lambda_0(e_{1,-})^2$ to explore localization/extendedness, exciton level absorption intensities, and other spectroscopic properties of individual complexes in an ensemble. In ref. (2), Wu et al. used a half-Gaussian distribution for $\lambda_0(e_{1,+})$ with a width of 140 cm^{-1} to simulate B870 absorption spectrum. The width of 115 cm^{-1} for the profile and its ΔE value of ~ 200 cm^{-1} were in good agreement with the low-temperature values determined by zero-phonon hole action spectroscopy.[10] The hidden correlation effect proposed in this paper justifies their use of $e_{1,+}$ BDP alone in the simulation.

C_8 and C_{16} ring systems. Diagonal energy disorder calculations were also performed on the C_8 B850 ring of BChl molecules of *Rs. molischianum*. Briefly, it was also found that the effects of random disorder on the exciton levels contributing to its B850 band are well-modeled using an e_1 type BDP, cf. Table 2. Extensive calculations have not yet been performed on the C_{16} ring of LH1 although preliminary results indicate that e_1 type BDP can also be used for its B875 band.

Diagonal versus off-diagonal random energy disorder. One expects differences in the L-E patterns from these two types of random disorder since the equivalent of a single site diagonal defect for off-diagonal disorder involves two nearest neighbor sites. An interesting question is how strong the random disorder needs to be in order for the L-E patterns from the two types of disorder to be significant? We have performed some calculations which speak to this question. In the limit of very weak random disorder, the

diagonal and off-diagonal L-E patterns for the exciton levels of our C_9 system were found to be identical. In the limit of very strong diagonal disorder, N = 1 for all levels. In sharp contrast, the N-values from off-diagonal random disorder are in the range of ~ 2-3. In other words, no matter how strong the off-diagonal random disorder, no level becomes completely localized. Other calculations showed that significant differences between the L-E patterns from the two types of disorder onset in the weak disorder regime; weaker than the MEAD condition defined earlier. Calculations were also performed for "single site" disorder. We mention only that in the limit of very strong single site diagonal disorder, one level is totally localized (N = 1) while N = 2n/3 = 6 for all other levels. These findings are understandable when one recognizes that in this limit, one has essentially a linear J-aggregate with n = 9–1 = 8. Indeed, the L-E patterns for such a J-aggregate were found to be very similar to those of the C_9 ring.

Energy disorder and the Stark effect. Recently, we reported Stark hole-burning results on the A (B870) exciton level of the B850 ring for *Rps. acidophila*, *Rs. molischianum* and *Rb. sphaeroides*.[26] The quantity of interest which is determined in such experiments is $|\Delta\underline{\mu}| \equiv \Delta\mu$, the permanent dipole moment change between the ground electronic state and the A level. In that reference it was pointed out that $\Delta\mu$ for the A level is similar for all three species ($f\Delta\mu \sim 1.2$ D, where f is the local field correction) and that this value is a factor of 3 smaller than the values determined by classical Stark modulation spectroscopy (SMS) on the entire B850 absorption band.[27] The analysis of the data in ref. (27) assumed that all levels which contribute to the B850 band carry the same $\Delta\mu$ value and vector sense in the single complex (the effects of energy disorder were not considered). We present one line of argument for the just-mentioned assumptions of ref. (27) requiring scrutiny. As reviewed in ref. (28), earlier Stark optical experiments on the BChl molecule indicate that $\Delta\underline{\mu}$ is quite close to being parallel to the in-plane y-axis of the molecule. INDO quantum chemical calculations that, for all intent and purposes, $\Delta\underline{\mu}$ of

the BChl molecule is parallel to the y-axis.[29] Given the structure of the LH2 complex, one can view dipole vectors on the ring shown in Figure 1 as the in-the-membrane-plane (i.p.) molecular contributions to the dipole moment change of individual sites. Independent of the way the symmetry-related i.p. dipoles of sites are oriented on the circle, $\Delta\mu_{i.p.} = 0$ for all exciton levels of the entire ring in the absence of energy disorder. This state of affairs changes significantly when energy disorder is introduced as will be discussed in detail elsewhere.[30] Here we present only $\Delta\mu_{i.p.}$ results for $e_{1,+}$ disorder for $\lambda_0 = 1.8$ (very weak disorder), 70 and 140 cm^{-1} (MEAD), Figure 7.

A value of 1.0 (arbitrary unit) for $\Delta\mu_{i.p.}$ corresponds to the value of the dipole moment change for the single site (dimer). Except for the E_4 levels, $\Delta\mu_{i.p.}$ is close to zero for very weak disorder. That the E_4 levels carry a significant dipole moment change is consistent with their single clump L-E patterns shown in Figure 2. The $E_{4,l}$ and $E_{4,h}$ patterns become more and less extended, respectively, as λ_0 increases, see Figure 3. This explains the opposite dependence of their $\Delta\mu_{i.p.}$ value on λ_0 seen in Figure 7. Of particular relevance to the B850 band are the A-E_2 levels. Figure 7 reveals that even for MEAD, $\Delta\mu_{i.p.} < 1.0$ for all levels and that the largest $\Delta\mu_{i.p.}$ values occur at the bottom (A level) and top of the exciton band. As one proceeds towards the middle of the band, $\Delta\mu_{i.p.}$ decreases as a result of the E_2 and E_3 level L-E patterns being more equally distributed around the ring, see Figure 3. These general features were shown to hold for random diagonal disorder. The $E_{1,l}$ and $E_{1,h}$ levels, which are the main contributors to the B850 band, carry comparable absorption intensities. Figure 7 shows, however, that their $\Delta\mu_{i.p.}$ values differ by about a factor of 2. Just as important, is that their $\Delta\mu_{i.p.}$ vectors are not parallel, making instead an angle of 180°. The angles $\Delta\mu_{i.p.}(E_{1,l})$ and $\Delta\mu_{i.p.}(E_{1,h})$ make with $\Delta\mu_{i.p.}(A)$ are 0 and 180°, respectively. In future work we plan to determine whether energy disorder can explain the aforementioned discrepancy between the $\Delta\mu$

values determined by SMS and Stark hole-burning. In so doing, one needs to take into account the out-of-the-membrane plane component of $\Delta\mu$.

Finally, we point out that in using e_1 BDP to model the effects of energy disorder, one must take into account a distribution of $\lambda_0(e_1)$ values.[2] Concerning high resolution hole-burning experiments, single complexes are not probed. Rather, one interrogates a subset of complexes whose zero-phonon absorption lines are degenerate. Members of this subset can have protein conformations which, from the perspective of glass-like disorder, differ significantly. Thus in hole burning, a distribution of λ_0 values must still be reckoned with. This reasoning is consistent with the observation in ref. (26) that $\Delta\mu$ for the A level (B870) of the B850 manifold varied only slightly as the burn frequency was tuned across the inhomogeneously broadened absorption profile of B870.

4. Concluding Remarks

In this paper we have explored further the usefulness of basis energy defect patterns (BDP) for analysis of the effects of static energy disorder on the excitonic level structure of C_n LH complexes of purple bacteria. Based on a comparison of the localization-extendedness (L-E) or occupation number patterns as well as participation numbers (N) stemming from random disorder and from individual BDP, we conclude that the effects of diagonal or off-diagonal disorder at low temperatures on the A, E_1 and E_2 levels which contribute to the B850 absorption band can be understood using a single e_1 BDP, the hidden correlation effect. (This is also likely the case for the B875 band of LH1.) The hidden correlation effect is a consequence of the structural details of the complexes and the fact that the complexes fall in the weak disorder regime where the zero-order levels spacings are greater than or comparable to the disorder-induced couplings between energetically different levels. The above conclusion is likely to hold at room temperature since the temperature dependencies of the B800 and B850 bands of the LH2 complex and

the B875 band of LH1 indicate that their inhomogeneous broadenings are weakly dependent on temperature[21] (see Monshouwer et al.[21] for additional arguments).

The ability to use a single e_1 BDP greatly simplifies computational studies of the effects of random static disorder on the spectroscopic and photophysical properties of the B850 and B875 bands since one need only consider a single Gaussian distribution for say λ_0 ($e_{1,+}$), in the case of diagonal disorder. (λ_0 is the value of the defect at site zero, the generator site.) This is the procedure used in ref. (2) where the focus was on understanding the displacement of the A level (B870) below the B850 absorption maximum as well as the B870 absorption intensity. In addition to computational simplicity, one gains valuable insight on which disorder-induced couplings are most important. It should be noted that the usefulness of BDP becomes limited as one moves into the strong disorder regime or when n becomes too large. We see no reason why our symmetry based approach would not be useful for reasonably short linear arrays in the weak disorder regime.

The C_9 L-E patterns of Figures 2-6 appear to be the most detailed yet reported for a C_n system. An interesting observation for the weak disorder regime is that the patterns for the split components of degenerate exciton levels E_j are already essentially set in the limit of very weak disorder (compare Figures 2 and 3). An explanation for this based on Eqs. (12) was given. Certain confusions over the exciton level participation numbers N for C_n systems in the limit of infinitesimally small random disorder were clarified. For n odd, N(A) = n and N = 2n/3 for the two components of all degenerate levels. For n even, N(A) = N(B) = n but $N(E_{j,l},E_{j,h}) = n/2$ when j/n = 1/4 (or an odd multiple of 1/4). For all other degenerate levels the 2n/3 result still holds.

Although the results presented are for diagonal energy disorder and the C_9 B850 ring of *Rps. acidophila*, calculations were also performed for off-diagonal energy disorder for random and BDP defect patterns. For magnitudes of disorder which lie well within the

weak disorder regime (*vide supra*), the L-E patterns and participation numbers were found to be similar for diagonal and off-diagonal disorder. As the strong disorder limit is approached, some significant differences occur and as one moves well into the strong disorder regime, similarities between the two types of disorder essentially disappear, see section 3. The question of whether for the LH complexes one has to worry about off-diagonal disorder is a difficult one. We suggest, however, that it is relatively unimportant. Our reasoning is based on the fact that, at low temperatures, the inhomogeneous broadenings (slightly greater than 100 cm^{-1}) of the B850 and B875 bands are a factor of 2-3 times smaller than those of isolated "guest" molecules in glasses and polymers; this, despite the fact that in the LH complexes one has strong nearest neighbor BChl-BChl couplings. Perhaps more convincing is that the inhomogeneous broadening of the B800 absorption band of the LH2 complex is identical to that of the B850 band.[9] The 9 and 8 BChls of the B800 rings of *Rps. acidophila* and *Rs. molischianum* are weakly coupled with $V \sim -25$ cm^{-1},[6,31] compared to the nearest neighbor dimer-dimer couplings of ~ -300 cm^{-1} for the B850 ring. Thus, we think it most likely that the energy disorder which is of primary importance for the B850 and B875 rings is of the diagonal type caused by small glass-like fluctuations in the structure of the α,β polypeptide pair as one moves around the ring and between single rings of the ensemble of complexes which are studied.

It was shown that the L-E patterns and their associated permanent dipole moments are important for interpretation of electric field effects on the B850 absorption band. Such patterns as well as the corresponding wavefunctions are required for calculation of phonon-induced inter-exciton level relaxation rates,[32-34] a firm understanding of exciton delocalization or extendedness, and superradiance from single or ensembles of complexes.[21,35] The superradiance enhancement is defined as the radiative dipole strength of the exciton level divided by that of the isolated chromophore. Monshouwer et al.[21] measured an enhancement of 2.8 for the A (B870) level of an ensemble of LH2 complexes

at 4.2 K. Since this level is essentially forbidden for perfect C_n symmetry, the superradiance is the result of energy disorder which also leads to clump localization of the A level. One can calculate the enhancement from the percentage of the total absorption of the B850 ring carried by B870. Based on the results of calculations presented here and in ref. (2), we estimate an average percentage of ~ 10. For 18 BChl molecules one has, therefore, an average enhancement of ~ 2. The reader is referred to ref. (35) for a detailed discussion on the temperature dependence of superradiance.

Finally, we suggest that the clump L-E patterns of the B870 level might be important for understanding the LH2→LH1 energy transfer process, especially at low temperatures. This can be seen from Figure 8 which shows an arrangement of LH2 complexes around the LH1 complex. The broad dark lines of the former are meant to indicate the localization regions for the B870 level. The distribution of distances between these regions and the BChl molecules of the LH1 ring could lead to dispersive kinetics for the above transfer process. Such kinetics have recently been reported.[36]

Acknowledgments

Research at the Ames Laboratory was supported by the Division of Chemical Sciences, Office of Basic Energy Sciences, U.S. Department of Energy. Ames Laboratory is operated for USDOE by Iowa State University under Contract W-7405-Eng-82. We would like to thank R. Monshouwer and R. van Grondelle of the Vrije Universiteit of the Netherlands and S. Mukamel of the University of Rochester for preprints of their works prior to publication and J. Fajer and M. Newton of Brookhaven National Laboratory for providing us with their calculated permanent dipole moments for the BChl molecules of the FMO complex. The authors also thank S. Mukamel for useful discussions concerning various mechanisms, static disorder and dynamics which lead to localization effects in nano-systems and Costas Soukalis of Iowa State University for enlightening us on recent

advances in the understanding of disorder-induced localization effects in non-organic systems..

REFERENCES AND NOTES

1. Wu, H.-M.; Small. G. J. *Chem. Phys.* **1997**, *218*, 225.

2. Chapter 5; Wu, H.-M., Ratsep, M.; Lee, I.-J.; Cogdell, R. J.; Small, G. J. *J. Phys. Chem. B* **1997**, *101*, 7654.

3. Koepke, J.; Hu, X.; Muenke, C.; Schulten, K. Michel, H. *Structure*, **1996**, *4*, 581.

4. Freer, A.; Prince, S.; Sauer, K.; Papiz, M.; Hawthornthwaite-Lawless, A.; McDermott, G.; Cogdell, R.; Isaacs, N. W. *Structure* **1996**, *4*, 449.

5. Karrasch, S.; Bullough, P. A.; Ghosh, R. *EMBO J.* **1995**, *14*, 631.

6. Sauer, K.; Cogdell, R. J.; Prince, S. M.; Freer, A. A.; Isaacs, N. W.; Scheer, H. *Photochem. Photobiol.* **1996**, *64*, 564.

7. There are nine weakly coupled BChl molecules at the cytoplasmic side of the membrane which give rise to an absorption band at 800 nm, the B800 band. It is only the B850 band that is of interest here.

8. It is the $S_1(Q_y) \leftarrow S_0$ $\pi\pi^*$ transition of the BChl molecule that is involved.

9. Chapter 4; Wu, H.-M.; Ratsep, M.; Jankowiak, R.; Cogdell, R. J.; Small, G. J. *J. Phys. Chem. B* **1997**, *101*, 7641.

10. Wu, H.-M.; Reddy, N. R. S.; Small. G. J. *J. Phys. Chem. B* **1997**, *101*, 651.

11. Hu, X.; Ritz, T.; Damjanovic, A.; Schulten, K. *J. Phys. Chem. B* **1997**, *101*, 3854.

12. To avoid confusion with exciton levels we use lower case letters for BDP symmetries.

13. Tinkham, M. *Group Theory and Quantum Mechanics*, McGraw-Hill: New York, 1964.

14. Hochstrasser, R. M. *Molecular Aspects of Symmetry*, W. A. Benjamin Inc.: New York, 1966.

15. Anderson, P. W. *Phys. Rev.* **1958**, *109*, 1492.

16. Lee, P. A.; Ramakrishnan, T. V. *Rev. Mod. Phys.* **1985**, *57*, 287.

17. Kramer, B.; MacKinnon, A. *Rep. Prog. Phys.* **1993**, *56*, 1469.

18. Skinner, J. L. *J. Phys. Chem.* **1994**, *98*, 2503.

19. Jimenez, R.; Dikshit, S. N.; Bradforth, S. E.; Fleming, G. R. *J. Phys. Chem.* **1996**, *100*, 6825.

20. Kühn, O.; Sundström, V *J. Phys. Chem. B* **1997**, *101*, 3432.

21. Monshouwer, R.; Abrahamsson, M.; van Mourik, F.; van Grondelle, R. *J. Phys. Chem. B* **1997**, *101*, 7241.

22. Thouless, D. J. *Phys. Rep.* **1974**, *13*, 93.

23. Alden, R. G.; Johnson, E.; Nagarajan, V.; Parson, W. W.; Law, C. J.; Cogdell, R. G. *J. Phys. Chem. B* **1997**, *101*, 4667.

24. Interestingly, when λ_0 of $e_{1,+}$ becomes very large (infinite disorder limit), N = 1 for one level and N = 2 for all others. For the $e_{1,-}$ BDP, N = 1 for all levels. An explanation for this difference can be found in Table 1. It is that for $e_{1,+}$ there are pairs of sites which have the same defect value whereas for $e_{1,-}$, all sites have different defect values (the same behavior exists for the e_2 and e_4 BDP). For random disorder, the probability that two or more sites have the same defect value is vanishingly small. Thus, for diagonal energy disorder, N = 1 for all levels in the infinite disorder limit. For off-diagonal disorder this is not the case, see text.

25. We remind the reader that our calculations are tailored to low temperature data.

26. Ratsep, M.; Wu, H.-M.; Hayes, J. M.; Small, G. J. *Spectrochim Acta A*, in press.

27. Beekman, L. M. P.; Frese, R. N.; Fowler, G. J. S.; Picorel, R.; Cogdell, R. J.; van Stokkum, I. H. M.; Hunter, C. N.; van Grondelle, R. *J. Phys. Chem. B* **1997**, *101*, 7293.

28. Lockhart, D. J.; Boxer, S. G. *Proc. Natl. Acad. Sci. USA* **1988**, *85*, 107.

29. Gudowska-Nowak, E.; Newton, M. D.; Fajer, J. *J. Phys. Chem.* **1990**, *94*, 5795.

30. Ratsep, M.; Wu, H.-M.; Hayes, J. M.; Blankenship, R. E.; Cogdell, R. J.; Small, G. J., *J. Phys. Chem. B.* in press.

31. The B800 L-E patterns for V = – 25 cm^{-1} were calculated for the random defect pattern of Figure 8. The A, E_1 and E_4 levels were found to be essentially localized at a single site.

32. Davydov, A. S. *Theory of Molecular Excitons*; Plenum Press: New York, 1971.

33. Hochstrasser, R. M.; Prasad, P. N. In *Excited States*, Vol. 1; Lim, E. C., Ed.; Academic Press: New York, 1974. p 79.

34. Johnson, C. K.; Small, G. J. In *Excited States*, Vol. 6; Lim, E. C., Ed.; Academic Press: New York, 1982; p 97.

35. Meier, T.; Chernyak, V.; Mukamel, S. *J Phys. Chem. B* **1997**, *101*, 7332.

36. Nagarajan, V.; Alden, R. G.; Williams, J. C.; Parson, W. W. *Proc. Natl. Acad. Sci. USA* **1996**, *93*, 13774.

Table 1. Normalized coefficients of basis defect patterns for C_9.

	Site Number								
	0	**1**	**2**	**3**	**4**	**5**	**6**	**7**	**8**
a	0.333	0.333	0.333	0.333	0.333	0.333	0.333	0.333	0.333
$e_{1,+}$	0.443	0.443	0.236	-0.082	-0.361	-0.471	-0.361	-0.082	0.236
$e_{1,-}$	0.161	-0.161	-0.408	-0.464	-0.303	0	0.303	0.464	0.408
$e_{2,+}$	0.361	0.361	-0.236	-0.443	0.082	0.471	0.082	-0.443	-0.236
$e_{2,-}$	0.303	-0.303	-0.408	0.161	0.464	0	-0.464	-0.161	0.408
$e_{3,+}$	0.236	0.236	-0.471	0.236	0.236	-0.471	0.236	0.236	-0.471
$e_{3,-}$	0.408	-0.408	0	0.408	-0.408	0	0.408	-0.408	0
$e_{4,+}$	0.082	0.082	-0.236	0.361	-0.443	0.471	-0.443	0.361	-0.236
$e_{4,-}$	0.464	-0.464	0.408	-0.303	0.161	0	-0.161	0.303	-0.408

Table 2. Normalized coefficients of basis defect patterns for C_8.

	Site Number							
	0	**1**	**2**	**3**	**4**	**5**	**6**	**7**
a	0.354	0.354	0.354	0.354	0.354	0.354	0.354	0.354
$e_{1,+}$	0.462	0.462	0.191	-0.191	-0.462	-0.462	-0.191	0.191
$e_{1,-}$	0.191	-0.191	-0.462	-0.462	-0.191	0.191	0.462	0.462
$e_{2,+}$	0.354	0.354	-0.354	-0.354	0.354	0.354	-0.354	-0.354
$e_{2,-}$	0.354	-0.354	-0.354	0.354	0.354	-0.354	-0.354	0.354
$e_{3,+}$	0.191	0.191	-0.462	0.462	-0.191	-0.191	0.462	-0.462
$e_{3,-}$	0.462	-0.462	0.191	0.191	-0.462	0.462	-0.191	-0.191
b	0.354	-0.354	0.354	-0.354	0.354	-0.354	0.354	-0.354

Table 3. Calculated results for a random diagonal defect pattern.

Line	$e_{1,+}$	$e_{2,+}$	$e_{3,+}$	$e_{4,+}$	$e_{1,-}$	$e_{2,-}$	$e_{3,-}$	$e_{4,-}$	I	ΔE	ΔE_1	ΔE_2
1	X								6.8	184	27	0.1
2					X				4.7	172	17	0.1
3	X				X				9.1	201	40	0.3
4		X				X			0.0	151	34	1.1
5			X				X		0.0	149	0.0	0.0
6				X				X	0.0	149	0.0	75
7	X	X			X	X			10.4	210	15	1.2
8	X		X		X		X		8.8	200	50	9.7
9	X			X	X			X	9.2	201	46	89
10		X	X			X	X		0.0	150	34	2.8
11		X		X		X		X	0.0	150	31	76
12			X	X			X	X	0.0	149	2.0	74
13	X	X	X		X	X	X		10.1	207	25	9.9
14	X	X		X	X	X		X	10.4	209	24	86
15	X		X	X	X		X	X	9.3	202	56	79
16		X	X	X		X	X	X	0.0	149	33	77
17	X	X	X	X					8.2	191	4.4	74
18					X	X	X	X	4.9	173	30	30
19	X	X	X	X	X	X	X	X	10.4	208	34	77

The disorders are 121, 148, 129, 137, 101, −157, 10.4, −113 and 105 cm^{-1} at sites 0 to 8, respectively, generated randomly according to a Gaussian distribution centered at 0 with a standard deviation of 150 cm^{-1}. By using Eq. (16) of ref. (1), the random defect pattern can be expressed as a linear combination of C_9 BDP. The resulting λ_0 for a, $e_{1,+}$ through $e_{4,+}$ and $e_{1,-}$through $e_{4,-}$ BDP are 53.5, 91.2, −12.0, 13.9, −12.0, −25.5, 19.5, 22.3 and −29.5 cm^{-1}, respectively. X's in a line indicate the BDP components of the random defect pattern being considered.

FIGURE CAPTIONS

Figure 1. The 4.2 K absorption profile of B850 of the LH2 complex from *Rps. acidophila*. The dashed arrow indicates the low energy tail absorption due to the lowest A exciton level, B870. At the bottom is the exciton level structure in the absence of disorder calculated with Eq. (3) and a nearest dimer-dimer coupling of V = – 320 cm^{-1} for a cyclic 9-mer. Each level is labeled by its C_9 irreducible representation and its energy in cm^{-1} (e of Eq. (3) is set to zero). The strongly transition-allowed E_1 levels are placed at the B850 band maximum. At the upper left-hand corner is a simple diagram showing the arrangement of transition dipoles for a cyclic 9-mer.

Figure 2. Localization-Extendedness (L-E) patterns for the exciton levels of a C_9-ring in the presence of very weak $e_{1,+}$ diagonal energy disorder (λ_0 = 1.8 cm^{-1}; V = – 320 cm^{-1}). Since the 9 chromophores labeled by the integers 0 to 8 are arranged on the ring, sites 0 and 8 are nearest neighbors. Included at the top of each pattern are the energy of the level in cm^{-1} and the corresponding participation number N. See text for further explanation.

Figure 3. Localization-Extendedness (L-E) patterns obtained with $\lambda_0(e_{1,+})$ = 140 cm^{-1}. see Figure 2 caption.

Figure 4. Localization-Extendedness (L-E) patterns obtained with $\lambda_0(e_{1,+})$ = 140 cm^{-1} and $\lambda_0(e_{2,-})$ = – 50 cm^{-1}, see Figure 2 caption.

Figure 5. Localization-Extendedness (L-E) patterns obtained with $\lambda_0(e_{4,+})$ = 12 cm^{-1}, see Figure 2 caption.

Figure 6. Localization-Extendedness (L-E) patterns obtained with a random diagonal disorder for the C_9 ring. The disorders are 329, 83.5, – 18.1, 6.53, – 253, – 143, – 71.0, – 102, – 65.8 cm^{-1} at sites 0 to 8, respectively. These values were generated randomly for a Gaussian distribution centered at 0 and with a standard deviation of 150 cm^{-1}. By using Eq. 16 of ref. (1), the random defect pattern can be expressed as a linear combination of C_9 BDP. The resulting λ_0 values for a, $e_{1,+}$ through $e_{4,+}$ and $e_{1,-}$ through $e_{4,-}$ BDP are – 26.0, 157, 42.3, 24.8, 7.76, 4.01, – 3.67, 89.3 and 33.1 cm^{-1}, respectively.

Figure 7. The in-plane permanent dipole moment change ($\Delta\mu_{i.p.}$) for all exciton levels of C_9 in the presence of $e_{1,+}$ diagonal energy disorder. For each level, λ_0 is 1.8, 70 and 140 cm^{-1} from left to right, respectively. $\Delta\mu_{i.p.}$ = 1.0 (arbitrary units) is that of a single site. For $\lambda_0(e_{1,+})$ = 1.8 cm^{-1}, $\Delta\mu_{i.p.}$ for all levels is ~ 0 except for $E_{4,l}$ and $E_{4,h}$, see text.

Figure 8. LH2 complexes surrounding the LH1 complex which encircles the reaction center. The broad dark lines of the LH2 rings are meant to indicate the "clump" localization of the A (B870) exciton level of LH2. The actual arrangement of LH2 complexes is not known.

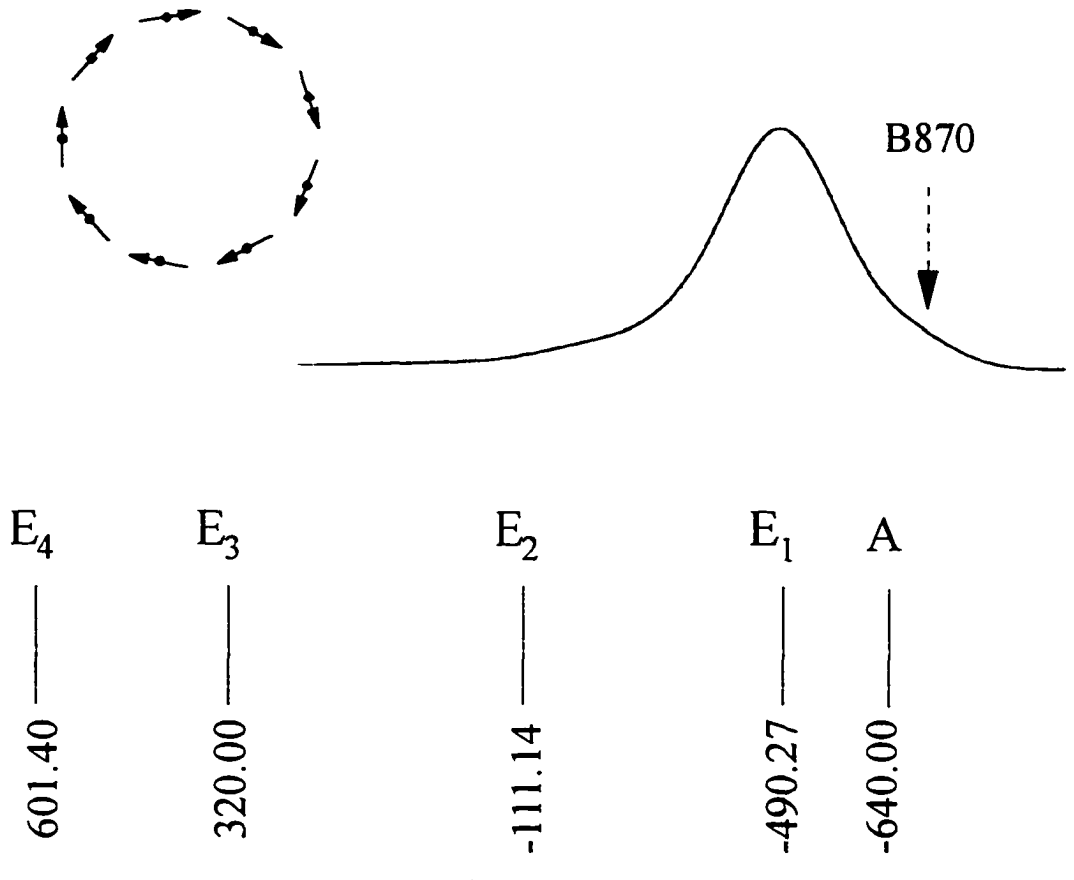

Figure 1

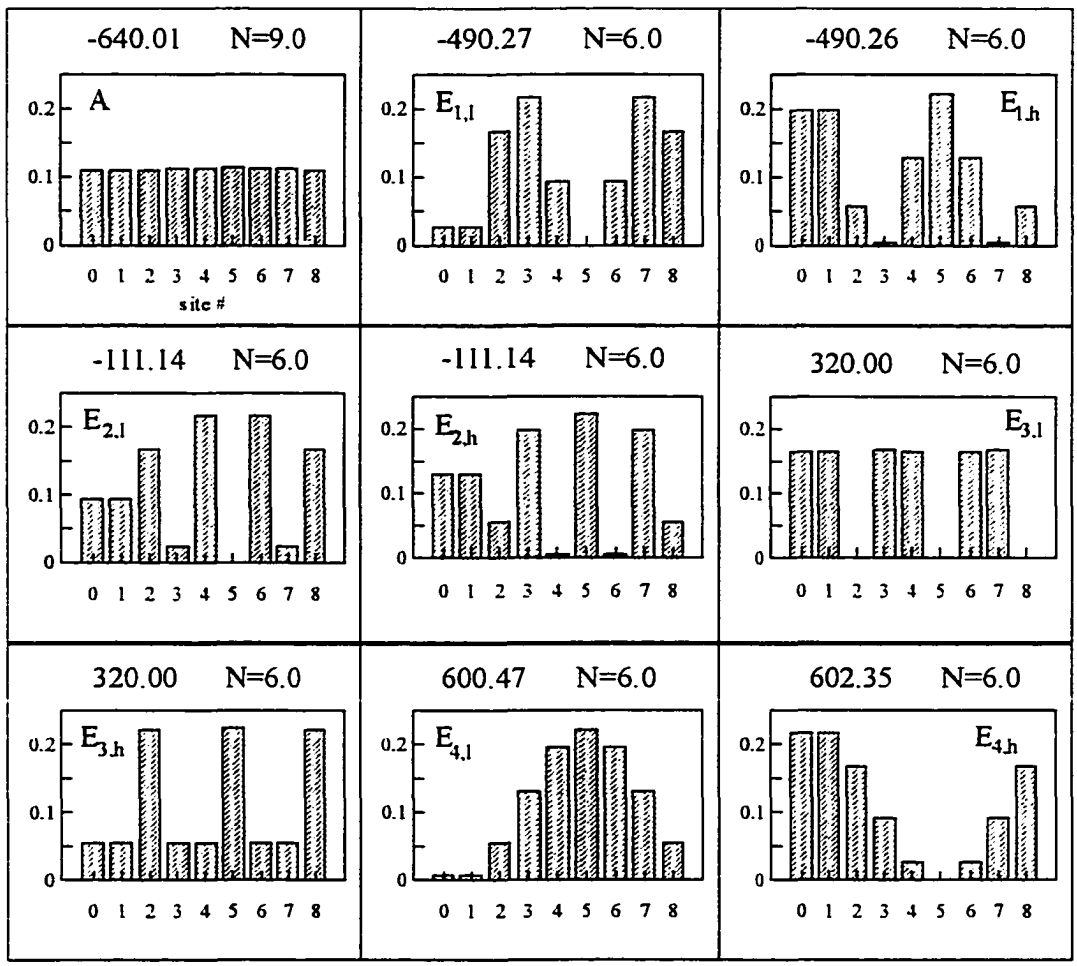
-640.01 N=9.0
A
-490.27 N=6.0
E1,l
-490.26 N=6.0
E1,h
-111.14 N=6.0
E2,l
-111.14 N=6.0
E2,h
320.00 N=6.0
E3,l
320.00 N=6.0
E3,h
600.47 N=6.0
E4,l
602.35 N=6.0
E4,h
0.2
0.1
0
0 1 2 3 4 5 6 7 8
site #

Figure 2

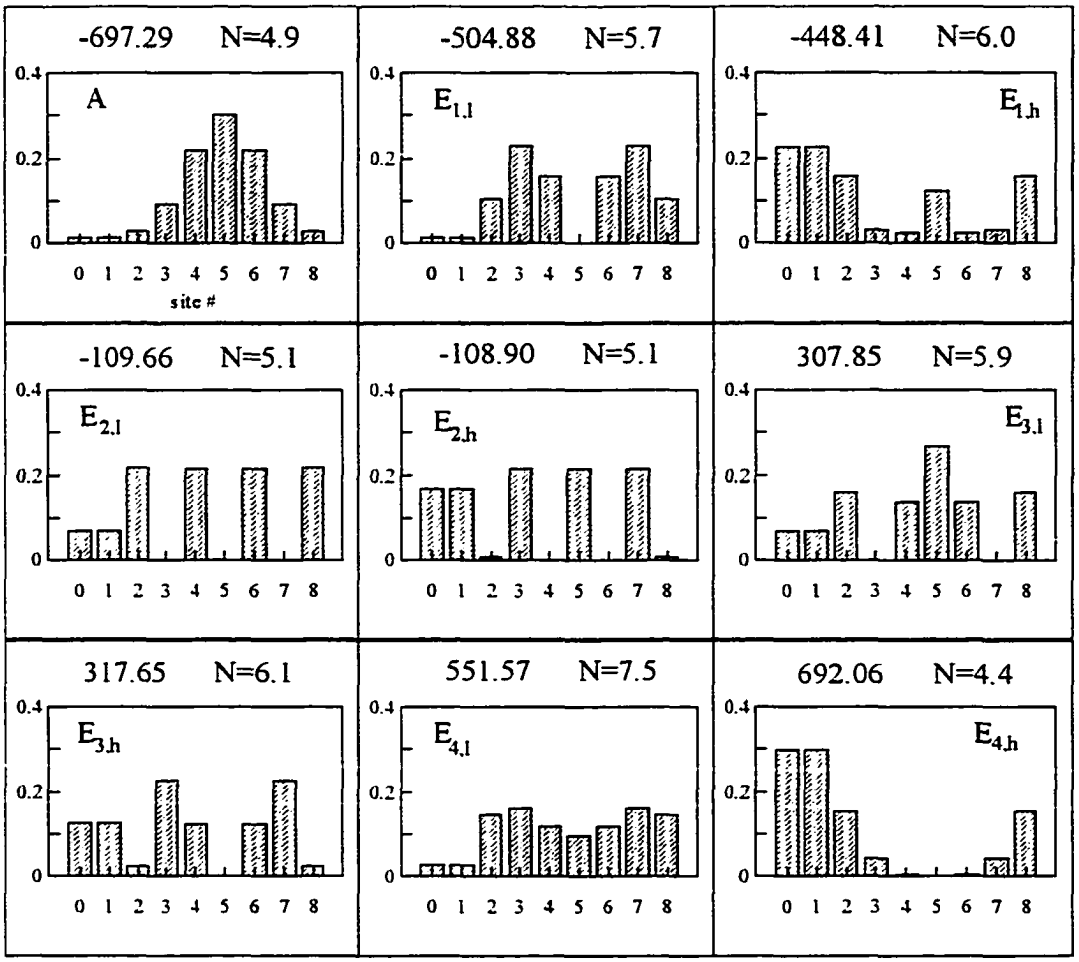
-697.29 N=4.9
A
-504.88 N=5.7
E1.l
-448.41 N=6.0
E1.h
-109.66 N=5.1
E2.l
-108.90 N=5.1
E2.h
307.85 N=5.9
E3.l
317.65 N=6.1
E3.h
551.57 N=7.5
E4.l
692.06 N=4.4
E4.h
0.4
0.2
0
0 1 2 3 4 5 6 7 8
site #

Figure 3

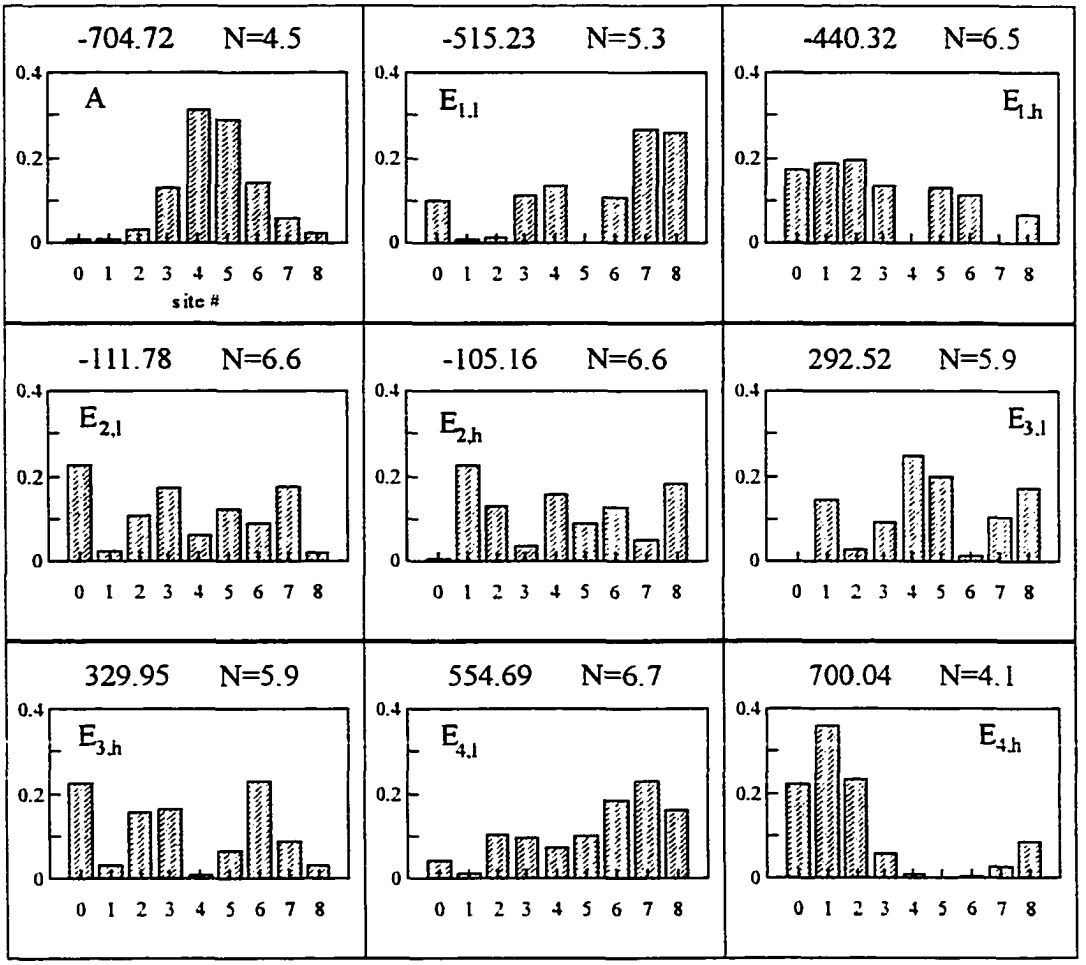
-704.72 N=4.5
A
-515.23 N=5.3
$E_{1,l}$
-440.32 N=6.5
$E_{1,h}$
-111.78 N=6.6
$E_{2,l}$
-105.16 N=6.6
$E_{2,h}$
292.52 N=5.9
$E_{3,l}$
329.95 N=5.9
$E_{3,h}$
554.69 N=6.7
$E_{4,l}$
700.04 N=4.1
$E_{4,h}$
0.4
0.2
0
0 1 2 3 4 5 6 7 8
site #

Figure 4

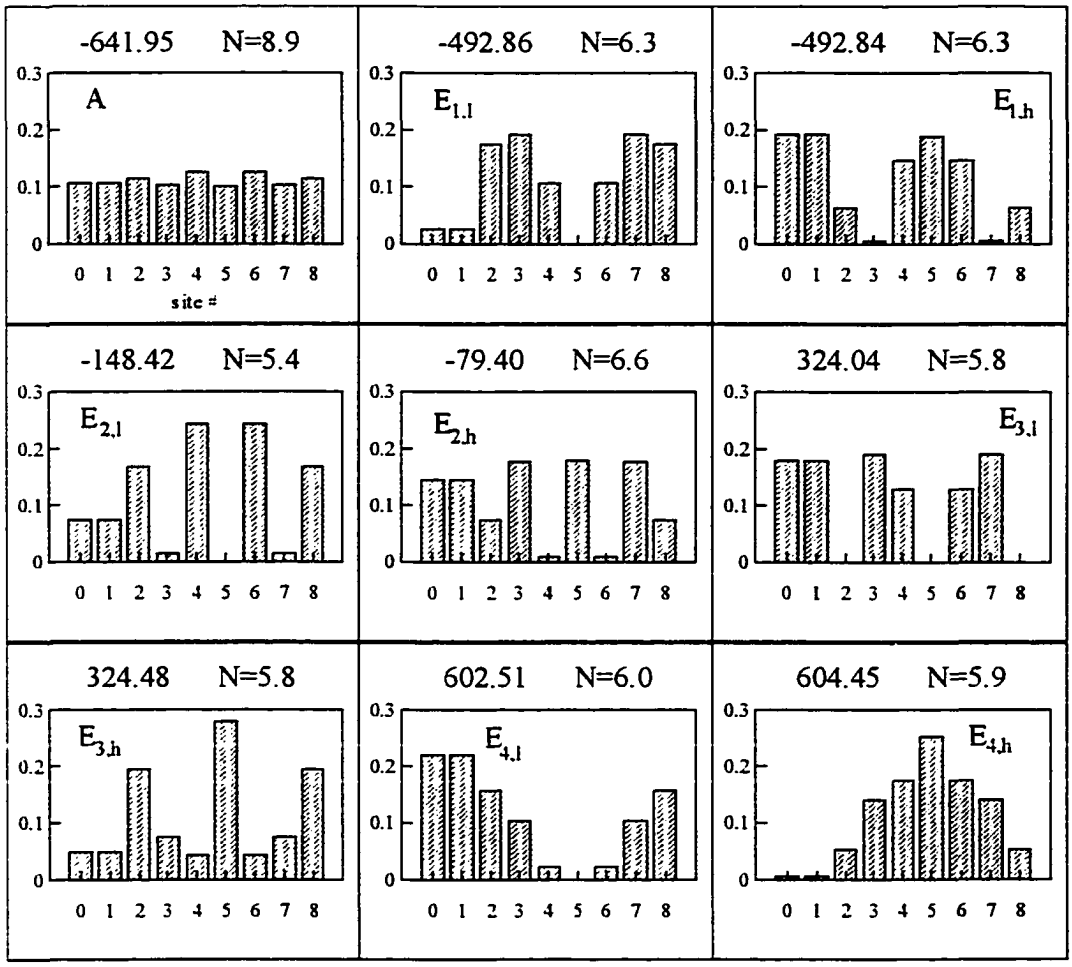
-641.95 N=8.9
A
-492.86 N=6.3
E1,l
-492.84 N=6.3
E1,h
-148.42 N=5.4
E2,l
-79.40 N=6.6
E2,h
324.04 N=5.8
E3,l
324.48 N=5.8
E3,h
602.51 N=6.0
E4,l
604.45 N=5.9
E4,h
0.3
0.2
0.1
0
0 1 2 3 4 5 6 7 8
site #

Figure 5

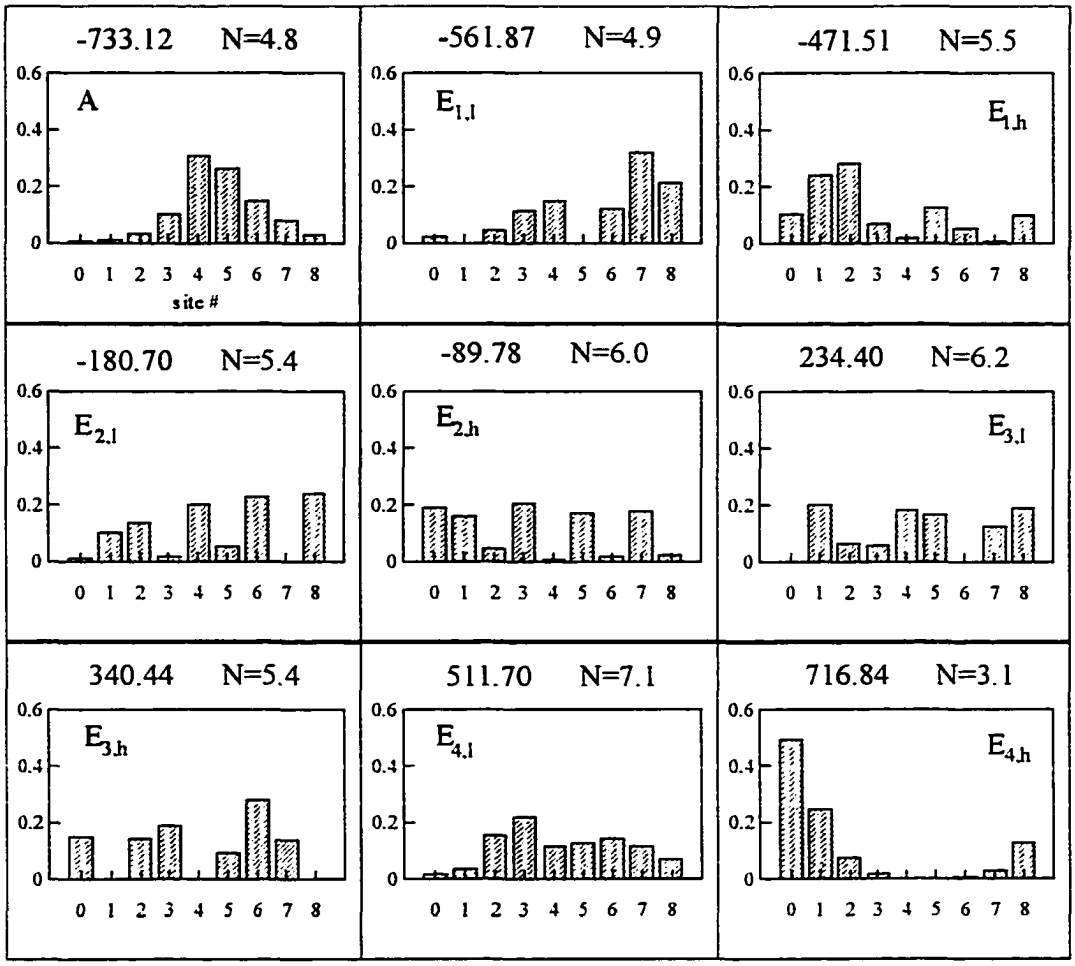
-733.12 N=4.8
A
-561.87 N=4.9
E1.l
-471.51 N=5.5
E1.h
-180.70 N=5.4
E2.l
-89.78 N=6.0
E2.h
234.40 N=6.2
E3.l
340.44 N=5.4
E3.h
511.70 N=7.1
E4.l
716.84 N=3.1
E4.h
0.6
0.4
0.2
0
0 1 2 3 4 5 6 7 8
site #

Figure 6

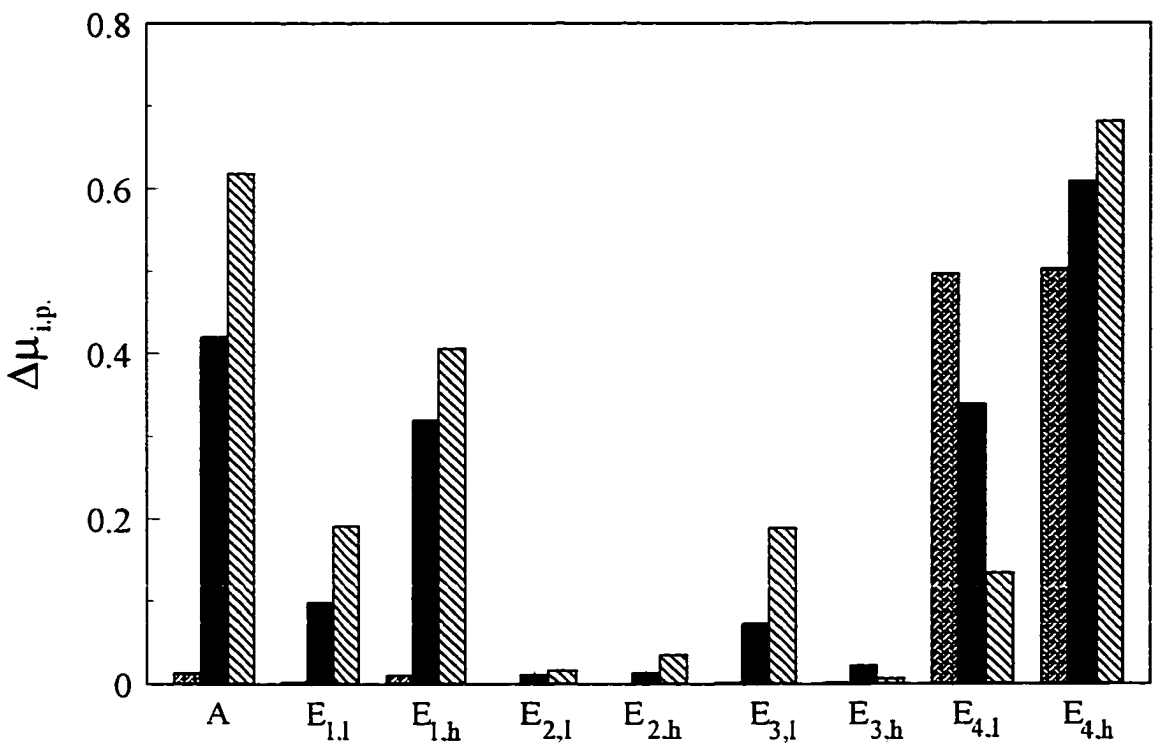

Figure 7

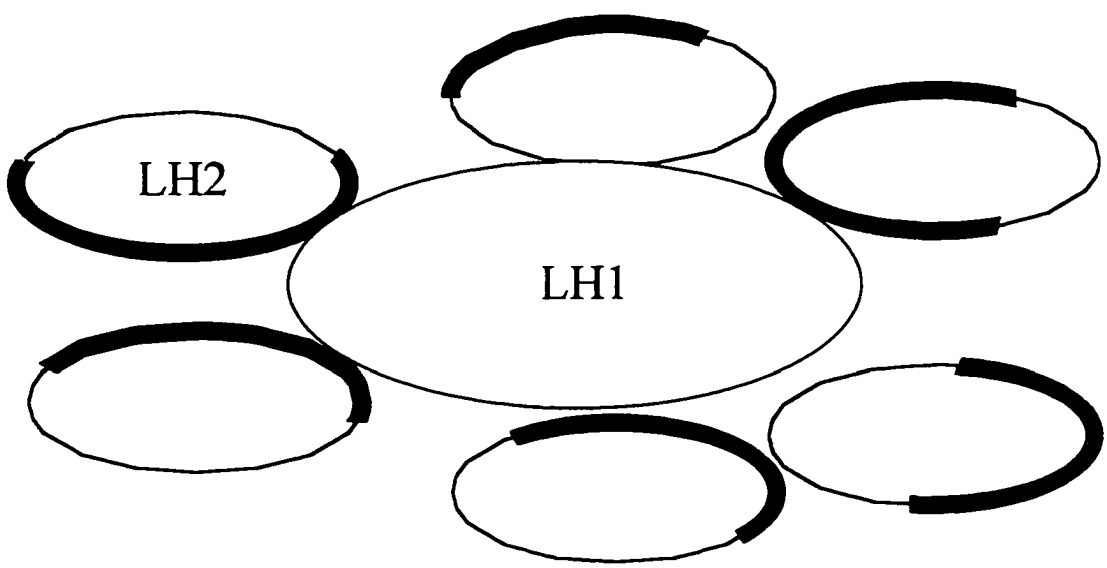

Figure 8

CHAPTER 7. STARK HOLE-BURNING STUDIES OF THREE PHOTOSYNTHETIC COMPLEXES

A paper accepted by the *J. Phys. Chem. B*, in press.

M. Rätsep, H.-M. Wu, J. M. Hayes, R. E. Blankenship, R. J. Cogdell and G. J. Small

Abstract

Stark hole-burning spectroscopy at 1.8 K was used to determine the dipole moment changes $f \cdot \Delta\mu$ (f, the local field correction factor) for the B800 absorption band of the light harvesting 2 (LH2) complex of *Rhodobacter sphaeroides, Rhodopseudomonas acidophila* (strain 10050) and *Rhodospirillum molischianum*. Hole-burning values of $f \cdot \Delta\mu$ for the lowest energy exciton level (B870) associated with LH2's B850 band have recently been reported (Rätsep et al., *Spectrochim. Acta*, in press). Values for the lowest energy exciton level (B896) associated with the B875 band of the LH1 complex of *Rb. sphaeroides* (wild-type chromatophores and a LH1 only mutant) and the 825 nm band of the bacteriochlorophyll *a* (FMO) antenna complex of *Chlorobium tepidum* are also reported. For each band, $f \cdot \Delta\mu$ was determined for burn laser polarization parallel and perpendicular to the Stark field E_S and several burn frequencies. The dependencies on laser polarization and burn frequency are typically quite weak. Importantly, $f \cdot \Delta\mu$ values for the above bands are small, falling in the range ~ 0.5-1.2 D, with the lowest and highest values associated with the 825 nm band of the FMO complex and B800 band of the LH2 complex, respectively. For the B896 band of the LH1 complex, $f \cdot \Delta\mu \approx 0.8$ D. Such small values are consistent with the very weak linear electron-phonon coupling of antenna protein complexes as determined by hole-burning spectroscopy. Overall, the values for

$f \cdot \Delta\mu$ from classical Stark modulation (CSM) studies (Gottfried et al., *Biochim. Biophys. Acta* **1991**, *1059*, 63; Beekman et al., *J. Phys. Chem. B*, **1997**, *101*, 7293) are larger, in the cases of B850 and B875, by a factor of 3-4. (In CSM spectroscopy, one analyzes the response of the entire absorption band to the external field.) Discussion of the discrepancies between the two Stark techniques is given. It appears that difficulties inherent to the analysis procedure of CSM spectroscopy can lead to unreliable values for dipole moment and polarizability changes associated with absorption bands of photosynthetic complexes, especially when several excitonic levels contribute to the band, e.g. B850 and B875. An explanation for the small hole-burning values of $f \cdot \Delta\mu$ for the B870 and B896 levels associated with C_n cyclic arrays of strongly coupled BChl *a* dimers is given based on structural, symmetry and energy disorder considerations. A key point is that, in the absence of energy disorder, the component of $\Delta\mu_j$ (j labeling the exciton level) perpendicular to the C_n axis is zero. Energy disorder, which destroys the C_n symmetry and leads to localization effects, results in non-zero values which may depend on j when the protein-induced contribution to $\Delta\mu_j$ is taken into account.

1. Introduction

In the preceding paper[1] we presented absorption and hole burning results on the effects of pressure and temperature on the B875 absorption band of the light harvesting complex 1 (LH1) of *Rhodobacter sphaeroides* (wild-type chromatophores and an LH1 only mutant). Of particular importance to this paper is that the linear pressure shifts of – 0.60 and – 0.67 cm^{-1}/MPa for the B875 band and the lowest exciton level (B896) of the B875 ring of BChl *a* molecules are very large, about 6-7 times larger than observed for weakly coupled BChl *a* molecules in protein complexes and $\pi\pi^*$ states of isolated chromophores in polymers and proteins. (A relevant example of weakly coupled BChl *a* molecules are those responsible for the B800 absorption band of the LH2 complex of purple bacteria.) In

that paper (referred to, hereafter, as I) it was argued that the above large pressure shifts cannot be explained in terms of electrostatic BChl *a*-BChl *a* interactions and BChl *a*-protein interactions. It was estimated that, in combination, these interactions provide a shift of only about – 0.2 cm^{-1}/MPa, a value which is supported by the pressure shift data for the B800 band of the LH2 complex and the Q_y-bands of the BChl *a* antenna complex of *Chlorobium tepidum*. It was concluded that electron-exchange interactions between nearest neighbor BChl *a* molecules of the B875 ring are mainly responsible for the largeness of the pressure shifts and that such interactions are also important for the B850 ring of the LH2 complex (see I for descriptions of the structural arrangement of the BChl *a* molecules in the cyclic (C_n) B850 and B875 rings; the lowest energy exciton level of the B850 BChl *a* ring is often referred to as B870. Like B896, it carries A symmetry in the absence of disorder.) Electron-exchange leads to charge-transfer (CT) states which mix with the neutral $Q_y(\pi\pi^*)$ states of the cyclic arrays as discussed by Alden et al.[2]

Accepting that CT states are important for understanding the exciton band structures of the B850 and B875 rings, a natural next step is to study the effect of external electric (Stark) fields on the B850 and B875 absorption bands and the exciton levels that contribute to them. That is, a significant CT contribution to the exciton wavefunctions can lead to large dipole moment changes ($\Delta\mu$) for $S_1(Q_y) \leftarrow S_0$ transitions.[3] $\Delta\mu$ can be viewed as the sum of $\Delta\mu_0$ and $\Delta\mu_{ind}$ where $\Delta\mu_0$ is the molecular component and $\Delta\mu_{ind}$ the matrix-induced component. Classical Stark modulation (CSM) spectroscopy, in which the response of an absorption band to the applied field is determined, has been extensively applied to the special pair band of the bacterial reaction center (see, for example, refs. (4-6)). A value of $f \cdot \Delta\mu_{CSM} = 5.2$ D at 77 K for the special pair (P) band of *Rb. sphaeroides*, P870, was determined[6] using the theory of Liptay[7] for analysis. f is the local field correction factor.[8] The analysis also led to a large polarizability change,

$f^2 \cdot Tr(\Delta\underline{\alpha}) \sim 1000$ Å^3, which is over one order of magnitude larger than the value for monomeric BChl *a*.[9] The large polarizability change, together with the observation that $f \cdot \Delta\mu_{CSM} = 5.2$ D is a factor of 2-3 times larger than the values for absorption bands of the reaction center associated with weakly coupled BChl *a* and BPheo *a* cofactors, led to the conclusion that the strong response of the special pair band is the result of P^* (asterisk denoting excited state) carrying significant CT character. CSM studies of isolated BChl *a* molecules in polymer films which yielded values for $f \cdot \Delta\mu_{CSM}$ in the range of ~ 2.0-2.5 D[4] also figured into this conclusion. That the CT character of P^* leads to a large dipole moment change is consistent with the results of hole burning experiments which showed that the P870 band is characterized by strong linear electron-phonon coupling with the Huang-Rhys factor S equal to 1.8 and 1.5 for modes centered near 30 and 120 cm^{-1}. These couplings lead to a large optical reorganization energy of 230 cm^{-1}.[10] The reader is referred to ref. (11) for details. In that work it was emphasized that the electron-phonon coupling for the B875 and B850 bands (also the B800 band of the LH2 complex) is a factor of 20-30 times weaker, meaning that the BChl *a* molecules and protein are essentially blind to the optical excitations associated with these bands.

Results from CSM studies at 77 K of the B800, B850 and B875 bands of *Rb. sphaeroides*, *Rps. acidophila* and *Rs. molischianum* have recently been reported.[12,13] Values of $f \cdot \Delta\mu_{CSM}$ and $f^2 \cdot Tr(\Delta\underline{\alpha})$ for B850 and B800 of the LH2 complexes are given on the right side of Table I. Although the $f \cdot \Delta\mu_{CSM}$ values for B850 are about 30% smaller than that of P870, they are considerably larger than those for B800 of *Rps. acidophila* and *Rb. sphaeroides*. Furthermore, the B850 polarizability changes are large and comparable to the value for P870. It was concluded that, like P870, CT states make a significant contribution to the neutral $\pi\pi^*$ exciton levels of the B850 ring.

The resolution of Stark spectroscopy is significantly improved by utilizing spectral hole burning. This combination has proven to be powerful for analysis of $\Delta\underline{\mu}$ associated

with the $S_1 \leftarrow S_0$ transitions of isolated molecular chromophores in amorphous polymer films at liquid helium temperatures.[14-27] Stark hole burning has also been reported for mesoporphyrin-IX in horseradish peroxidase.[28] Because the zero-phonon holes (ZPH) of the chromophores in these systems are very narrow ($\lesssim$ 1 GHz) at liquid helium temperatures, modest field strengths (few tens of kV/cm) could be used to determine the matrix-induced ($\Delta\mu_{ind}$) and molecular ($\Delta\mu_o$) contributions to the change in dipole moment between the ground and excited electronic states. In some of these studies the Stark cell configuration allowed for propagation of the laser burn and read beams perpendicular to the external field ($\underline{E}_S$) so that the Stark effect on the ZPH could be determined with burn laser polarization parallel and perpendicular to $\underline{E}_S$. Use of both polarizations is important for determination of $\Delta\mu_{ind}$ and $\Delta\mu_o$. We note that a dependence of $\Delta\mu_{ind}$ on the location of the burn wavelength within the inhomogeneously broadened absorption band yields additional information on the polarizability of the chromophore and the internal electric field ($\underline{E}_{int}$) it experiences.[17]

Stark hole-burning has recently been applied to the LH2 complex of purple bacteria.[29] The results for $f \cdot \Delta\mu_{||}$ and $f \cdot \Delta\mu_{\perp}$ are given on the left side of Table I. The subscripts on $\Delta\mu$ denote laser polarization parallel and perpendicular to the Stark field, $\underline{E}_S$. The significance of a difference between the values of $f \cdot \Delta\mu_{||}$ and $f \cdot \Delta\mu_{\perp}$ is discussed in section 4. Although the agreement between the Stark hole-burning and CSM values for $\Delta\mu$ of B800 (*Rb. sphaeroides*) is good, the values for B850 of all three species are very different. (We remind the reader that B870 is the lowest energy exciton level of the B850 BChl *a* ring.) Possible explanations for the large discrepancies are given in section 4. We note at this point, however, that the small value of $\Delta\mu \sim 1.1$ D for B870 determined by hole-burning is consistent with weak electron-phonon coupling.

CSM spectroscopic values of $f \cdot \Delta\mu$ and $f^2 \cdot \mathrm{Tr}(\Delta\underline{\alpha})$ for the B875 band of the LH1 complex have also been reported.[12] They are similar to the CSM values for the B850

band, see sections 3 and 4. In this paper we report $\Delta\mu$-values from hole-burning for the B896 exciton level of wild-type and LH1 only mutant chromatophores of *Rb. sphaeroides*. In addition, values for the B800 band of *Rps. acidophila* and *Rs. molischianum* and the lowest energy Q_y-band (825 nm) of the Fenna-Matthews-Olson (FMO) BChl *a* antenna complex of *Chlorobium tepidum* are reported for comparison against CSM values.[30]

2. Experimental

The reader is referred to I (section 2 and references therein) for the procedures used to obtain wild-type (WT) and LH1 only mutant chromatophores of *Rb. sphaeroides*, and details concerning the glycerol:water glass-forming solvent and detergents used. Samples of the FMO complex from *Cb. tepidum* were prepared as described in Savikhin et al.[31] Complexes were dissolved in a glycerol:water mixture (70:30 by volume).

Samples were contained in gelatin capsules (0.13 ml/o.d. = 4.5 mm) purchased from Torpac Inc. Prior to insertion into the Stark cell, the gelatin capsule *filled* with sample was allowed to soften for about 5 minutes at room temperature so that it could be mechanically squeezed by the two copper electrodes of the Stark cell. This procedure yielded an optical path length perpendicular to the applied field of ~ 6 mm with a distance of ~ 2 mm between the electrodes. Teflon spacers were used to set the distance between the electrodes ($\pm$ 0.05 mm). The Stark field could be applied parallel or perpendicular to the burn laser polarization by positioning a polarizer placed in front of the Stark cell. The probing light (unpolarized) was colinear with the burning beam. A Trek Inc. Model 610 C DC high voltage power supply (0 to $\pm$ 10 kV) was used. By changing the polarity of the power supply a maximum Stark field of ~ 100 kV/cm was achievable. Holes were initially burned at the highest field with a chosen polarity.

All measurements were made at 1.8 K in a Janis 10 DT liquid helium cryostat. With the sample immersed in pumped liquid helium, arcing never occurred at our

maximum voltage. With an optical path length of ~ 6 mm, the concentration of the chromatophores and complexes was sufficiently low to ensure formation of high quality glasses. In this regard, use of gelatin capsules was important. Optical densities of the samples were adjusted to ~ 0.5 in the spectral regions where hole burning was performed.

The burn laser was a Coherent CR899-21 Ti:Sapphire laser (linewidth of 0.07 cm^{-1}) pumped by a 15 W Coherent Innova 200 Ar-ion laser. The preburn and postburn absorption spectra were obtained by using a Bruker IFS120 HR Fourier transform spectrometer, the difference of such spectra being the persistent nonphotochemical hole burned spectrum. Spectral holes for B896 of the B850 ring were burned with linearly polarized light to fractional O.D. depths in the range of 0.06–0.14. Typical burn intensities were ~ 200 mW/cm^2 with burn times of ~ 120 s. Holes in the lowest energy band of the FMO complex at ~ 825 nm were burned to fractional depths of 0.2–0.3. Typical burn intensities and burn times were ~ 50 mW/cm^2 and ~ 10 s.

3. Results and Analysis

We present first the Stark hole-burning results for the BChl *a* antenna complex of *Cb. tepidum* and then the results for the LH1 and LH2 complexes. Before doing so we present a brief review of some basic physics for an isolated chromophore in a matrix. The Stark shift of the optical transition frequency of the absorber is given by[15]

$$\Delta\omega = -\hbar^{-1}\left[(\Delta\underline{\mu}_o + \Delta\underline{\alpha}\cdot\underline{E}_{int})f\underline{E}_S + \frac{1}{2}(f\underline{E}_S)\cdot\Delta\underline{\alpha}\cdot(f\underline{E}_S)\right], \tag{1}$$

where, for simplicity, we take the local field correction factor f to be a scalar. $\Delta\underline{\mu}_0$ is the molecular dipole moment change. E_{int} is the matrix field experienced by the absorber and $\Delta\underline{\mu}_{ind} = \Delta\underline{\alpha}\cdot E_{int}$ with $\Delta\underline{\mu}_{ind}$ the dipole moment change induced by the matrix field. $\Delta\underline{\alpha}$ is the molecular polarizability difference tensor. The first and second terms in square brackets depend linearly and quadratically on the Stark. As discussed in ref. (29), E_{int} in

molecular systems is large, $\gtrsim 10^6$ V/cm (see also refs. (6,17,18)), which is an order of magnitude larger than the maximum Stark fields used in Stark hole-burning experiments. As a result, only the linear Stark effect was observed for the B800 and B870 bands of the LH2 complex and all isolated chromophores in polymer, glass and protein matrices.[14-29,32,33] Thus, the second term in Eq. (1) is of no importance for Stark hole-burning with the field strengths we employ.

Considering further the case of isolated molecules in glassy matrices, let γ be the angle between the molecular dipole moment difference vector $\Delta\underline{\mu}_o$ and the transition dipole vector $\underline{d}$. Linearly polarized light preferentially burns out those molecules with $\underline{d}$ parallel to the polarization vector $\underline{e}$ of the light. The experimentally observed dipole moment change can be written as $\Delta\underline{\mu} = \Delta\underline{\mu}_o + \Delta\underline{\mu}_{ind}$, where $\Delta\underline{\mu}_{ind}$ is the matrix-induced contribution. When $\Delta\underline{\mu}_o$ is dominant, the photoselection phenomenon enables one to probe molecules for which the angle between $\Delta\underline{\mu}_o$ and $\underline{e}$ is well-defined (shallow hole limit). As discussed in refs. (15,28), Stark splitting of the hole can be observed for an angle between $\underline{e}$ and $\underline{E}_S$, which depends on the value of γ. For example, for $\gamma = 0$ or π Stark splitting occurs for parallel polarization while broadening occurs for perpendicular polarization. The situation is reversed for $\gamma = \pm \pi/2$. However, when $\Delta\underline{\mu}_{ind}$ is dominant, only Stark broadening is expected for both polarizations. This is because the orientation of $\Delta\underline{\mu}_{ind}$ relative to $\underline{d}$ or $\underline{e}$ is random for a glassy matrix, i.e. the matrix field varies significantly from site to site.

The assumption of random orientations for $\Delta\underline{\mu}_{ind}$ for Chl molecules in photosynthetic complexes is questionable since the structure of the protein around these chromophores is well-defined even though the Q_y-absorption bands do suffer from significant inhomogeneous broadening. For example, Gafert et al.[28] observed Stark hole splitting for two of the three sites of mesoporphyrin substituted in horseradish peroxidase. For the same molecule in a glass, only Stark broadening was observed for both laser

polarizations. However, for the B800 and B870 bands of the LH2 complex, Stark broadening of the ZPH was observed for both parallel and perpendicular laser polarizations.[29] Further discussion of differences between isolated chromophores in glasses and Chl molecules in photosynthetic complexes is given later.

BChl *a* antenna complex of *Cb. tepidum*. The 4.2 K Q_y-absorption spectrum of this BChl *a* (FMO) complex from *Prosthecochloris aestuarii* and *Cb. tepidum* exhibit prominent bands at 825, 814 and 805 nm.[34,35] Although the X-ray structure for the former species has been known for many years,[36] the structure for *Cb. tepidum* was only recently reported.[37] For both, the complex is a C_3 trimer of subunits which contain seven symmetry inequivalent BChl *a* molecules. Differences in the relative orientations of the BChl *a* molecules and distances between them for the two structures are minor.[37] Some potentially significant differences in H-bonding and BChl *a*-protein residue distances are observed. Spectral hole burning results led to the conclusion that the 825 nm band is contributed to by two closely spaced, ~ 40 cm^{-1}, exciton levels of the trimer associated with the lowest energy level of the subunit with the lowest level at 827 nm.[34] This finding led to excitonic structure calculations that yielded results which provide some support for this conclusion,[38,39] (there are, however, differences between the overall results of these two theoretical works, see section 4). It should be noted that it was assumed in refs. (38,39) that the three subunits of the trimer are identical, i.e. energy disorder due to structural heterogeneity was ignored. The implications of energy disorder for the above trimer interpretation for the 825 nm band are considered in section 4. In this subsection, Stark hole-burning data are presented for the 825 nm band of the FMO complex (*Cb. tepidum*). Stark hole-burning is not possible for exciton levels higher in energy than the 825 nm band due to hole-broadening from subpicosecond inter-exciton level relaxation processes.

Stark hole-burning was performed at several burn frequencies (ω_B) between 12161 and 12076 cm^{-1}, from the high to low energy sides of the 825 nm band. No dependence of the Stark results on ω_B was observed. Some hole profiles obtained with $\omega_B \approx 12115$ cm^{-1} are shown in figure 1 for laser polarization perpendicular and parallel to the Stark field E_S. These polarizations lead to hole broadening and splitting, respectively. To the best of our knowledge, this is the first time Stark hole-splitting for a photosynthetic complex has been observed. The data are plotted in figure 2 where it is seen that the Stark splitting is linear in E_S. For $E_S \gtrsim 40$ kV/cm, the broadening of the hole profile varies linearly with E_S. The observation of Stark splitting for $\underline{e} \parallel \underline{E}_S$ but not for $\underline{E} \perp \underline{E}_S$ means that the angle γ between $\Delta\underline{\mu}$ and the transition dipole $\underline{d}$ of B827 is smaller than 45°.[28] To arrive at an upper limit for γ, the Stark effect on the hole profile for angles (χ) of 0, 30, 60 and 90° between $\underline{e}$ and $\underline{E}_S$ were determined with $E_S = 100$ kV/cm, figure 3. Stark splitting is not observed for $\chi = 60°$ and the splitting for $\chi = 30°$ is considerably smaller than the splitting for $\chi = 0°$ (1.1 and 1.4 cm^{-1}, respectively). Comparison of the hole profiles in figure 3 with the results of theoretical simulations in ref. (40) led to $\gamma \lesssim 15°$. The smallness of γ and the observation that the Stark splitting ($\Delta\omega_{SS}$) is maximum for $\chi \approx 0°$ means that in the well-known expression (see, for example, ref. (41))

$$\Delta\omega_{SS} = (29.8)^{-1}\, f \cdot \Delta\mu\, \underline{E}_S \cos\theta\,, \tag{2}$$

the angle, θ, between $\Delta\underline{\mu}$ and $\underline{E}_S$ is $\lesssim 15°$ so that $\cos\theta \gtrsim 0.97$. In Eq. (2) the units of $\Delta\omega_{SS}$, $\Delta\mu$ and E_S are cm^{-1}, Debye and kV/cm. This equation with the data in figure 2 yields $f \cdot \Delta\mu_{\parallel} = 0.42 \pm 0.05$ D, where $\Delta\mu$ is the total dipole moment change. That the Stark effects do not depend on ω_B means that statistical fluctuations in structure from complex to complex are too small to be reflected in $\Delta\mu$. The Stark splittings plotted in figure 2 were measured directly from the hole profiles. Since the Stark split components overlap and broaden with increasing field strength, it is necessary to simulate the hole

profiles so as to arrive at a more accurate value for $f \cdot \Delta\mu_{||}$. The simulations with identical Gaussian lineshapes for the split components led to $f \cdot \Delta\mu_{||} = 0.51 \pm 0.06$ D (the 70, 80, 90 and 100 kV/cm profiles were used), which is slightly larger than the 0.42 D value.

The solid curve through the Stark broadening data in figure 2 is a theoretical fit obtained using the theory of Kador et al.[16] which is valid when the variance of $\Delta\mu$ is small.[42] They define the parameter

$$F = \frac{2\, f \cdot \Delta\mu\, E_S}{\hbar(\gamma' + \gamma_d')}, \tag{3}$$

where γ' is the homogeneous width of the zero-phonon line and γ_d' the additional width associated with artifacts such as saturation broadening. The sum $(\gamma' + \gamma_d')$ is the width at zero-field. When $F \lesssim 3.5$, their general expression for Stark broadening simplifies considerably to

$$\Gamma(F) = 2(\gamma' + \gamma_d')(1 + F^2)^{1/2}. \tag{4}$$

The above inequality is satisfied in our experiments. For sufficiently large F, $\Gamma(F) \propto F$ which depends linearly on E_S. It should be noted that the theory, as applied to isolated protein complexes in a glass, takes into account their random orientations. This randomness is responsible for the Stark broadening with $\underline{e} \perp \underline{E}_S$. The fit in figure 2 yielded $f \cdot \Delta\mu_{\perp} = 0.72 \pm 0.06$ D which is slightly larger than the value of 0.51 D for $f \cdot \Delta\mu_{||}$ (see section 4 for discussion of this difference).

LH1 only mutant chromatophores. Stark hole-burning was performed with ω_B-values between 11074 and 11169 cm^{-1}, a range that spans the B896 absorption band due to the lowest energy exciton level of the B875 ring of BChl *a* molecules, see I for details. No dependence on ω_B was observed. Furthermore, symmetric Stark broadening of the holes with no shifting was observed for $\underline{e}$ parallel as well as perpendicular to $\underline{E}_S$. No difference in the field dependence of the hole profile on laser polarization was

observed. Hole profiles ($\underline{e} \perp \underline{E}_S$) obtained with $\omega_B = 11169$ cm^{-1} are shown in figure 4. The broad holes displaced ~ 16 cm^{-1} to the right (red) of the ZPH are pseudo-phonon sideband holes. Holewidth as a function of field strength is given in figure 5. The solid curve is the fit obtained using Eq. (4) with $f \cdot \Delta\mu = 0.78 \pm 0.06$ D. The data clearly point to a linear Stark effect. The absence of Stark splitting and identical Stark broadening for both laser polarizations indicate that the angle γ between $\Delta\underline{\mu}$ and the transition dipole $\underline{d}$ varies from complex to complex in the ensemble studied. From Table I one observes that $\Delta\mu$ for B896 of the LH1 mutant is slightly smaller than the values for the B870 exciton level of the B850 ring of the LH2 complexes.

LH1 of wild-type chromatophores from *Rb. sphaeroides*. Stark hole-burning was performed with ω_B-values between 11056 and 11155 cm^{-1} located within the B896 band which lies ~ 40 cm^{-1} to the red of B896 in the LH1 mutant. As in the case of the mutant, symmetric Stark broadening with no shifting was observed for both $\underline{e}$ parallel and perpendicular to $\underline{E}_S$ with the broadening being independent of ω_B and laser polarization. Typical results are shown for $\omega_B = 11124$ cm^{-1} and $\underline{e}$ parallel to $\underline{E}_S$ in the bottom frame of figure 5. The solid curve through the data points is a theoretical fit, *vide supra*. Averaging over the fits to all data resulted in $f \cdot \Delta\mu = 0.84 \pm 0.06$ D which, within experimental uncertainty, is the same as the value for the LH1 mutant.

B800 band of *Rps. acidophila* and *Rs. molischianum*. Because of the large variation in the $\Delta\mu_{CSM}$ values for the B800 band of the LH2 complex of the above two species and *Rb. sphaeroides*, Table I, we performed Stark hole-burning experiments on isolated complexes of *Rps. acidophila* (strain 10050) and *Rs. molischianum*. The 4.2 K absorption spectra were identical to those shown in refs. (43-45). Hole burning was performed at several burn frequencies ranging in value from close to the maximum of the B800 band to about 100 cm^{-1} lower in energy. The values for $f \cdot \Delta\mu_{\perp}$ and $f \cdot \Delta\mu_{||}$ are given in Table II. Values for B800 of chromatophores and the isolated LH2 complex of

Rb. sphaeroides are also given. All values for $f \cdot \Delta\mu_{\perp}$ and $f \cdot \Delta\mu_{||}$ in Table II were obtained by averaging the values obtained with different burn frequencies.

The main results from this section are summarized in Table II. For comparison, results from CSM studies are also included.

4. Discussion

825 nm band of the FMO complex. The Stark splitting and broadening data of figure 2 for laser polarization parallel and perpendicular to E_S led, respectively, to $f \cdot \Delta\mu_{||} = 0.51$ D and $f \cdot \Delta\mu_{\perp}$[42] $= 0.72$ D. (Both values are considerably smaller than the CSM value for the B825 band, Table II.) Observation of Stark splitting means that the angle γ between $\Delta\mu$ and the transition dipole is quite well-defined. The results of figure 3 led to an upper limit for γ of 15°. That $f \cdot \Delta\mu_{\perp}$ is somewhat larger than $f \cdot \Delta\mu_{||}$ indicates that there may be a random contribution to the matrix field. Consistent with this is that the two components of the Stark split hole profile broaden with increasing field strength, *vide infra*.

Interpretation of the above results requires an understanding of the excitonic structure of the FMO trimer. The presence of 7 symmetry inequivalent BChl *a* molecules in the subunit complicates the problem since they have different site (excitation) energies. Pearlstein arrived at his site energies by fitting calculated absorption, circular dichroism (CD) and hole burned spectra to the experimental spectra.[38] (BChl *a*-BChl *a* electrostatic coupling energies were calculated using the point-monopole approximation with a static dielectric constant ε of 1.) BChl *a* 7 (numbering scheme of ref. (36)) was assigned the lowest site energy. The Q_y-transition dipole of BChl *a* 7 makes an angle of 11° with the C_3 axis. Calculations for the trimer led to the result that the 825 nm band is contributed to by two exciton levels at 826.4 and 824.1 nm. These levels are associated primarily with BChl *a* 7 (there is some contribution from BChl *a* 6) and the symmetry equivalent BChl *a*

molecule in each of the other two subunits. The two levels carry E and A symmetry, respectively, with the latter (polarized parallel to the C_3 axis) carrying almost all of the absorption intensity of the 825 nm band. Subsequently, linear dichroism (LD) spectra for *P. aestuarii* were published[46] which indicate that the 825 nm band is polarized close to perpendicular to the C_3 axis.[47] Using Pearlstein's coupling energies, Gülen performed calculations in which the site energies were assigned by fitting to the absorption, LD and triplet-singlet (T-S) spectra.[39] BChl *a* 6 was assigned the lowest site energy. Its Q_y-transition dipole makes an angle of 69° with the C_3-axis. Results for the trimer led to the 825 nm band being contributed to by E and A levels at 825.2 and 824.8 nm associated with BChl *a* 6 and to a, lesser extent BChl *a* 5 (transition dipole angle with C_3 of 94.3°). The E level at 825.2 nm carries almost all of the absorption intensity. Based on the absorption, LD and T-S spectra, the calculations of Gülen would appear to be the more reliable although she made no attempt to fit the CD spectrum. Again, both works were influenced by the hole burning results of ref. (34) which led to the assignment of the holes at 827.1 and 824.4 nm to "partner" A and E trimer levels. (In ref. (34) a symmetry assignment for these two levels was not possible.)

The calculations of Pearlstein and Gülen and the interpretation of the two-hole structure observed for the 825 nm band given in ref. (34) assumed that the subunits of a given trimer are energetically equivalent. Inhomogeneous broadening of the Q_y-absorption bands was viewed as being due to glass-like fluctuations in structure from trimer to trimer in the ensemble being studied. As mentioned in the Introduction to I, considerable progress has recently been made in understanding how energy disorder leads to localization effects for the states of coupled BChl molecules in photosynthetic complexes. For example, in ref. (48), which builds on refs. (49,50), we studied localization-extendedness for the exciton levels of the B800 and B850 BChl *a* rings of the LH2 complex of purple bacteria (see also ref. 2). Of relevance to the FMO complex is that the nearest neighbor

coupling energy of the B800 ring is weak, – 25 cm^{-1} (ε = 2.0).[51] Inclusion of an experimentally acceptable level of energy disorder led to the conclusion that the levels of the B800 ring are essentially completely localized on single BChl *a* molecules. The calculations of Pearlstein on the FMO complex identified only two pair-wise couplings between monomers belonging to different subunits of any significance. One involves BChl *a* 7 with its symmetry equivalent BChl *a* molecules in the other two subunits; coupling of 8 cm^{-1} for ε = 2. The other involves BChl *a* 2 with BChl *a* 5 of another subunit; coupling of 10 cm^{-1} for ε = 2. Given the smallness of these couplings and that the inhomogeneous broadenings of the 825 nm band of the FMO complex and the B800 band are comparable (~ 100 cm^{-1} in the low temperature limit), it seems most likely that the states of the FMO trimer are localized on single subunits.[52] The recent calculations of Buck et al. are consistent with this.[53] It follows from the structure of the complex and the results of Gülen that our measured $f \cdot \Delta\mu_{||}$ value for the 825 nm band can be viewed as being representative of a single BChl *a* molecule for either her model or that of Pearlstein. During this writing we became aware of very recent work by Louwe et al.[54,55] in which LD- absorption detected magnetic resonance and LD-T-S results are reported. Excitonic calculations[56] tailored to these new results and the absorption, LD and CD spectra led to significantly improved overall fittings. It was found that the seven states of the subunit are highly localized on individual BChl *a* molecules with the 825 nm band attributed to BChl *a* 3 whose Q_y-dipole makes an angle of 109° with the C_3 axis of the trimer. The results of Louwe et al. provide additional support for our $f \cdot \Delta\mu_{||}$ value of 0.51 D for the 825 nm band being mainly associated with a single BChl *a* molecule of the subunit.

In what follows we consider that $f \cdot \Delta\mu_{||}$ = 0.5 D is representative of the value for $f \cdot \Delta\mu$ of a BChl *a* molecule in the FMO subunit. One has that $f \cdot \Delta\mu = f(\Delta\mu_0 + \Delta\mu_{ind})$. The observation of Stark splitting proves that the angle γ between $\Delta\mu$ and the transition dipole is well-defined. The data indicate that $\gamma \lesssim 15°$. If $\Delta\mu_{ind}$ is random, as in glasses,

this means that $\Delta\mu_0 >> \Delta\mu_{ind}$ so that $\Delta\mu_0 \approx 0.5$ D. CSM data for monomer BChl *a* in a poly(methyl methacrylate) (PMMA) film led to $\gamma \approx 12°$.[4] For the monomer the optical transition is generally taken to be close to parallel with the in-plane y-axis, i.e. Q_y. INDO quantum chemical calculations of the type performed in ref. (57), model C, predict that $\Delta\mu_0$ and the Q_y-transition dipole for all seven BChl *a* molecules are parallel to within a couple of degrees.[58] However, a protein is not a glass and, thus, the assumption of randomness for $\Delta\mu_{ind}$ is questionable, *vide supra*. Of course, one would like to have a reliable value of $\Delta\mu_0$ for the BChl *a* monomer. A value for $f \cdot \Delta\mu$ of 2.4 ± 0.2 D at 77 K for BChl *a* monomer in a PMMA film has been determined by CSM spectroscopy.[4] (The value in PS films is the same within experimental uncertainty.[63]) This is a factor of 5 larger than our value for the FMO complex and over a factor of 2 larger than the value for B800 of the LH2 complex of *Rb. sphaeroides*, Table I. For Chl *a* monomer in a poly(vinylbutyral) (PVB) film, however, a value for $f \cdot \Delta\mu_{ind}$ from Stark hole-burning at 2 K has been reported. It is 0.33 ± 0.01 D.[20] It was also determined in the same work that $f \cdot \Delta\mu_0 \lesssim 0.15$ D, Table III. CSM studies of monomer Chl *a* in PMMA at 77 K resulted in $f \cdot \Delta\mu = 0.7$ D[59] and in isopropanol (118 K), 0.95 D.[60] Again, there is a discrepancy between the Stark hole-burning and CSM values. The discrepancy cannot be attributed to a significant difference between the static dielectric constants (ε) of PVB and PMMA. Very precise measurements of ε between 2.5 and 300 K for 23 polymers, including PVB and PMMA, have been reported.[19] For all polymers, the temperature dependence of ε below ~ 100 K is negligible. The ε-values for PVB and PMMA in the low temperature limit are 2.55 and 2.71, respectively. The local field corrections, as judged by $f = (\varepsilon+2)/3$, are too small to account for the above discrepancy. Temperature effects appear to be negligible. (As discussed in I, structural changes due to thermal expansivity are negligible below about 100 K.)

The value of 0.33 D for $f \cdot \Delta\mu_{ind}$ (Chl *a*) was determined from Stark hole-broadening data. It was shown that this value is consistent with

$$\Delta\mu_{ind}(D) = -0.04 + 8.8 \cdot 10^{-24}\ \Delta\alpha / MW;\ \ r = 0.975 \qquad (5)$$

which was arrived at on the basis of Stark hole-burning data for 11 isolated π-electron chromophores (see upper part of Table III for examples) in PVB and values of $\Delta\alpha$ from solvent shift measurements.[61] MW is the molecular weight of the chromophore (the phytyl tail of Chls is excluded). The unit of $\Delta\alpha$ is $Å^3$. r = 0.975 is the linear regression coefficient. For Chl *a*, $\Delta\alpha = 18 \pm 3\ Å^3$. With MW = 598, Eq. (5) yields $f \cdot \Delta\mu_{ind} = 0.34$ D which is quite close to the experimental value. We note that with $\Delta\alpha = 18\ Å^3$, $\varepsilon = 2.55$ and $f \cdot \Delta\mu_{ind} = 0.33$ D, the internal (matrix) field of PVB is $4 \cdot 10^6$ V/cm which can be compared with the value of $0.9\text{-}1.9 \cdot 10^6$ V/cm for polystyrene.[17]

Solvent shift data for BChl *a* led to $\Delta\alpha = 16 \pm 3\ Å^3$ [9] which, within experimental uncertainty, is the same as the value for Chl *a*. Thus, in PVB, the value of $f \cdot \Delta\mu_{ind}$ for BChl *a* from Eq. (5) is also ~ 0.3 D. The upper part of Table III lists the value of the Stark-hole burning values for $f \cdot \Delta\mu_{ind}$ for centrosymmetric molecules in PVB and in some cases also PMMA and polystyrene (PS). Note that the values are in the range ~ 0.1 to 0.3 D. The value for chlorin in PVB is 0.17 D ($f \cdot \Delta\mu_0 = 0.47$ D). For mesoporphyrin in horseradish peroxidase, $f \cdot \Delta\mu_{ind} \sim 0.05$ D ($f \cdot \Delta\mu_0 = 0.15$ D). In view of these results and the applicability of Eq. (5) to the class of similar molecules considered, we consider a value of 0.3 D for $f \cdot \Delta\mu_{ind}$ of BChl *a* in PVB or PMMA to be a reasonable estimate.

What are the implications of this value for the CSM value of $f \cdot \Delta\mu = 2.4$ D for BChl *a* in PMMA and PS? With $f \cdot \Delta\mu_{ind} \approx 0.3$ D, $f \cdot \Delta\mu_0 \approx 2$ D, the intrinsic or molecular dipole moment change. The problem is that if $f \cdot \Delta\mu_0$ is that large (more than a factor of 10 larger than the value for Chl *a*, *vide supra*), one would expect to observe a

Stark splitting of holes burned into the B800 band of the LH2 complex.[64] Stark splitting was not observed for either of the two laser polarizations, only broadening. The broadening data for the three species studied led to values of $f \cdot \Delta\mu$ in the range 0.6–1.2 D, Table II. The absence of Stark splitting indicates that $\Delta\mu_{ind}$ is at least a factor of 2 larger than $\Delta\mu_0$[28] which means that $f \cdot \Delta\mu_0 \lesssim 0.5$ D. Thus, it might appear that a value for $f \cdot \Delta\mu$ of 2.4 D for BChl *a* in PMMA and PS from CSM spectroscopy is unphysically large. However, such a conclusion would be incorrect were it to be the case that in polymer films the geometry of the BChl *a* molecule is distorted from that in protein complexes (rotation of the acetyl group of ring I and out-of-plane deformations are two possibilities). In a polymer there would presumably be a distribution of distortions which further complicates the situation. If this possibility is correct then it would be the case that $f \cdot \Delta\mu$ values for BChl *a* in polymer films are of little use in interpreting Stark data for photosynthetic complexes. It is important, therefore, to perform Stark hole-burning experiments on BChl *a* in polymer films Such experiments are planned.

To conclude this subsection we consider further the values of 0.51 D and 0.72 D for $f \cdot \Delta\mu_{||}$ and $f \cdot \Delta\mu_{\perp}$ of the 825 nm band of the FMO complex. It was noted that the two Stark split components for $\underline{e} \,||\, E_S$, which yielded a dipole moment change 0.51 D, broadened with increasing field strength. The broadening suggests that there is a random contribution to $\Delta\mu_{ind}$ in addition to a contribution to the induced dipole moment change vector that is relatively well-defined with respect to the molecular frame. (We consider it unphysical to assume that the 0.51 D dipole moment change is entirely molecular, i.e. equal to $f \cdot \Delta\mu_0$). The well-defined contribution might be associated with the "inner shell" of the protein matrix with the random contribution coming from the "outer shell" and, perhaps, even the glass forming solvent. Fitting of the Stark broadening data with Eq. (4) led to $f \cdot \Delta\mu_{ind}$ (random) ≈ 0.5 D. Whether or not the model in which $\Delta\mu_{ind} = \Delta\mu_{ind}$ (non-random) + $\Delta\mu_{ind}$ (random) can explain why $f \cdot \Delta\mu_{\perp}$ is slightly larger than $f \cdot \Delta\mu_{||}$ is

unclear. We note that one is dealing with vectorial quantities, i.e. $f \cdot \Delta\underline{\mu}_{||} = f \cdot \Delta\underline{\mu}_0 + f \cdot \Delta\underline{\mu}_{ind}$ (non-random). Although it is reasonable to assume that $\Delta\underline{\mu}_{ind}$ (non-random) lies mainly in the plane of the BChl *a* molecule, it is not obvious that it is parallel to $f \cdot \Delta\underline{\mu}_0$. Assuming that they are and that the prediction $f \cdot \Delta\mu_{ind} \approx 0.3$ D is correct, then $f \cdot \Delta\mu_0 \approx 0.2$ D which is close to the upper limit for Chl *a* determined by Stark hole-burning.

LH1 and LH2 antenna complexes. There are two findings from the Stark hole-burning experiments which were unanticipated. First, the values of $f \cdot \Delta\mu$ for the B800 band and the B875 and B896 bands of the B850 and B875 BChl *a* rings are not very different, Tables I and II. The values fall in the range of ~ 0.6-1.2 D. Such values are not much larger than those of the 825 nm band of the FMO complex. Second, the CSM values for $f \cdot \Delta\mu$ are significantly larger than the hole-burning values. This is also the case for the 825 nm band of the FMO complex, *vide supra*. Potential problems with the application of CMS spectroscopy to photosynthetic complexes are considered in the following subsection. In this subsection we consider only the results from Stark hole-burning.

As discussed, the optical excitation of the B800 rings are most likely mainly localized on single BChl *a* molecules. That $f \cdot \Delta\mu$ for B800 is somewhat larger than that of the 825 nm band of the FMO complex, Table II, might be due to the hydrophilic protein environment (charged residues) of the B800 molecules[65,66] which results in a higher internal field ($f \cdot \Delta\mu_{ind}$) than exists in the FMO complex. The question arises as to why for both laser polarizations, $\underline{e} \,||\, \underline{E}_S$ and $\underline{e} \perp \underline{E}_S$, only Stark broadening is observed when Stark splitting for the 825 nm band of the FMO complex is observed for $\underline{e} \,||\, \underline{E}_S$. The answer might simply be the result of the intrinsic 4-5 cm^{-1} ZPH widths of the B800 band being larger than the ~ 0.6 cm^{-1} ZPH widths of the 825 nm band. With reference to figure 1, one can see that if the Stark split components were broadened by a factor of about 3, the splitting would be unobservable. Thus, the model for the 825 nm band in which

$\Delta\mu_{ind} = \Delta\mu_{ind}$ (non-random) + $\Delta\mu_{ind}$ (random) may apply to B800. Of course, the possibility that the random component for B800 is relatively larger than for the 825 nm band cannot be excluded. In any event, we view the values of $f \cdot \Delta\mu$ obtained for both bands as representative for localized BChl *a* Q_y-transitions in proteins.

The smallness of $f \cdot \Delta\mu$ for the B870 and B896 bands[67] was unanticipated because the BChl *a* molecules of their associated rings are strongly coupled and because of the large CSM values of $f \cdot \Delta\mu$ and $f^2 \cdot Tr(\Delta\underline{\alpha})$ for the B850 and B875 bands. Furthermore, the high pressure results of I strongly indicate that electron-exchange (CT states) is an important ingredient of the coupling. (We note that with $f^2 \cdot Tr(\Delta\underline{\alpha}) \approx 1000$ Å^3, representative CSM value from Tables I and II, it follows that $f \cdot \Delta\mu_{ind} \approx 3$ D when $\Delta\underline{\alpha}$ is taken to be disc-like, a value much larger than our values for B870 and B896.) A key question is why the $f \cdot \Delta\mu$ values for B870 and B896 are so small. In an attempt to answer this question we further[48] examine the implications of symmetry (C_n) and symmetry breaking on the Stark spectroscopy of the B850 and B875 rings (bands). Following the notation of refs. (48-50), let $|\alpha>$ be the wavefunction of the BChl *a* dimer,[68] this wavefunction being associated with the absorption band of interest, B850 or B875. We may assume that $|\alpha>$ is corrected for CT character from electron exchange between the two monomers of the dimer. In the absence of energy disorder the states associated with the absorption band are delocalized,[69]

$$|j\rangle = n^{-1/2} \sum_{\alpha=0}^{n-1} B^{j\alpha^*} |\alpha\rangle, \; j = 0,\ldots,n-1 \tag{6}$$

where $B = \exp(i2\pi/n)$ with α labeling the dimer of the C_n ring. For the B850 and B875 bands, only $j = 0$ (A), $j = \{1,n-1\}$ (E_1) and $j = \{2,n-2\}$ (E_2) are relevant.[50] The above wavefunction is deficient in that it does not account for electron exchange between neighboring dimers. Let $|\alpha,\alpha+1>_{CT}$ denote the charge transfer wavefunction associated

with electron exchange between dimers α and $\alpha+1$. The corresponding delocalized wavefunctions are given by

$$|j\rangle_{CT} = n^{-1/2} \sum_{\alpha} B^{j\alpha^*} |\alpha,\alpha+1\rangle_{CT} . \tag{7}$$

Since the Hamiltonian is totally symmetric, mixing of $|j>$ and $|j>_{CT}$ is restricted to levels with the same j-value. Thus, when mixing is taken into account, the delocalized wavefunctions are given by

$$|\Psi_j\rangle = n^{-1/2} \sum_{\alpha} B^{j\alpha^*} [C_j|\alpha\rangle + D_j|\alpha,\alpha+1\rangle_{CT}] . \tag{8}$$

It follows easily that the dipole moment for state j is

$$\langle\Psi_j|\underline{d}|\Psi_j\rangle \equiv \underline{\mu}_j = n^{-1} \sum_{\alpha} [C_j^2 \underline{\mu}_{\alpha} + D_j^2 \underline{\mu}_{\alpha,\alpha+1}] \tag{9}$$

when optical transitions between neutral Q_y-states and CT states and between different CT states are neglected. (Given the structures of the B850 and B875 rings this neglect is reasonable. For example, in the optical spectra of the LH1 and LH2 there is no evidence for CT optical transitions originating from the ground electronic state.) In Eq. (9), $C_j^2 + D_j^2 = 1$. The key point we wish to make follows when one recognizes that $\underline{\mu}_{\alpha}$ and $\underline{\mu}_{\alpha+1}$ can be written as $\underline{\mu}_{\alpha}^{ip} + \underline{\mu}_{\alpha}^{op}$ and $\underline{\mu}_{\alpha,+1}^{ip} + \underline{\mu}_{\alpha,+1}^{op}$, where ip and op designate the components perpendicular and parallel to the C_n axis. For the cyclic C_n arrays it follows from Eq. (9) that $\mu_j^{ip} = 0$. This is also true for the ground electronic state. Actually, the vanishing of the ip component is dictated by symmetry. Based on Stark spectroscopic data, electronic structure calculations (*vide supra*) and the structures of the B850 and B875 rings (see figure 1 of I), one expects that both $\underline{\mu}_{\alpha}$ and $\underline{\mu}_{\alpha,\alpha+1}$ should be close to perpendicular to the C_n rotation axis, i.e. the op contribution should be small. That μ_j or $\Delta\mu_j$ should be close to zero in the absence of energy disorder is consistent with the results of recent quantum chemical calculations which take into account the CT states.[70] It was

shown by Wu and Small[48] how experimentally acceptable levels of energy disorder can lead to non-zero values for $\Delta\mu_j^{ip}$ due to localization effects. In that work only the first term in square brackets of Eq. (9) was considered but inclusion of the second term does not affect their conclusions. It was found that the j=0 (A or B870) level of the B850 ring undergoes single "clump" or arc-like localization whereas the split components of the strongly allowed E_1 level undergo double-clump localization with their localization patterns complementing each other.[71] It was found that the values of $\Delta\mu^{ip}$ for the two components can be significantly different and, just as important, that the vectorial senses of their dipole moment changes can differ by 180°. Thus, the assumptions made in interpretation of the CSM data for the B850 and B875 bands[12,13] deserve scrutiny. They are that the components which contribute to these bands carry the same value of $\Delta\mu$ and vectorial sense. As expected, the results of ref. (48) show that the energy disorder-induced value for $\Delta\mu^{ip}$ of B870 is larger than those of the E_1 components which, in turn, are larger than those of the adjacent and higher energy components of the E_2 level. The E_2 components may be responsible for the high energy tailing of the B850 and B875 bands.[50] One possible reason for why Stark broadening is observed for both laser polarizations is that the extent of energy disorder varies from complex to complex in the sample, which lead to distributions of values for $\Delta\mu^{ip}$ and vectorial sense.

The above symmetry-based conclusions concerning μ_j^{ip} or $\Delta\mu_j^{ip}$ apply when the matrix (protein)-induced contribution to the dipole moments are taken into account. However, the treatment given above, which leads to Eq. (9), does not take this contribution into account. Determination of the matrix-induced contribution would involve calculation of the polarizability changes $\Delta\underline{\alpha}_j$ of the exciton levels with respect to the ground electronic state. One could start with a delocalized excited state basis set based on the Q_y, Q_x and B $\pi\pi^*$ states of the BChl *a* molecule. (Lower energy CT states which couple most strongly with the Q_y $\pi\pi^*$ states would need to be included.) In calculating the

polarizabilities $\underline{\alpha}_j$ of the levels associated with the B850 and B875 bands it would be necessary to take into account the two-exciton transitions associated with the Q_y-manifold as well as transitions between the one-exciton states of that manifold.[72] The important question which could be addressed by such calculations is whether or not the dependence of $\Delta\alpha_j$ on j is strong, with j labeling the levels that contribute to the B850 or B875 band, *vide infra*.

Stark hole-burning and classical modulation spectroscopies. The results of Tables I-III show that the values of $f \cdot \Delta\mu$ determined by CSM are generally significantly larger than those determined by hole-burning. In attempting to understand the apparent discrepancies it is important to know that with CSM spectroscopy the theory of Liptay[7] is used, in approximate form, to analyze the response of an absorption band to the external field. This involves fitting the Δ-absorbance (ΔA) spectrum to the sum of the first and second derivatives of the absorption spectrum and, when necessary, also the zeroth derivative. These derivatives relate, respectively, to changes in the polarizability, dipole moment and oscillator strength. This requires an absorption spectrum with very high S/N ratio. In refs. (12,13) the low S/N ratios for the B800, B850 and B875 bands necessitated fitting each band with a sum of skewed gaussians. By necessity, the gaussians of each band are assumed to have identical $\Delta\underline{\alpha}$ and $\Delta\underline{\mu}$[73] We have argued that this assumption for the B850 and B875 bands is doubtful because of their underlying exciton level structures and energy disorder. With Stark hole-burning, as reported on here and in the references cited, one is concerned only with the linear Stark effect and the high resolution of the technique allows one to probe single excited states. Furthermore, the theory used to analyze the data was designed for the problem at hand, i.e. inhomogeneously broadened bands across which a variation in $\Delta\mu$ is taken into account. The ability to study this variation is an important attribute of Stark hole-burning. A disadvantage of the technique is that, with typical attainable field strengths, it cannot be applied to states with ultra-short

lifetimes (e.g. the E_1 and E_2 levels of the B850 and B875 bands) because of excessive hole-broadening.

If agreement between the Stark hole-burning and CSM values for $f \cdot \Delta\mu$ was to be reached, one might have expected it for the 825 nm band of the FMO complex and the B800 band of the LH2 complex. Table II reveals, however, that this is not the case. Given the disagreements between the B800 results for *Rps. acidophila* and *Rs. molischianum*, it may be that the quite close agreement for *Rb. sphaeroides* is fortuitous. Interestingly, the hole-burning value of 1.2 D for B800 of *Rs. molischianum* is larger than those for the other two species as is the case for CSM. Beekman et al.[13] have suggested that the large CSM value of 2.8 D for *Rs. molischianum* relative to the 1.5 D value for *Rps. acidophila* might be due to the central Mg of their B800 BChl *a* molecules being ligated, respectively, by a formyl-methionine and aspartate (charged). The reader is referred to that reference for discussion of other structural differences which may lead to different matrix fields. It should be noted, however, that the hole-burning value of $f \cdot \Delta\mu$ for B800 of *Rb. sphaeroides* is larger than that of *Rps. acidophila*, the opposite of what is observed by CSM. Furthermore, the hole-burning value of 1.2 D for *Rs. molischianum* cannot be viewed as large, especially if one accepts the CSM value of ~ 2.5 D for $f \cdot \Delta\mu$ of monomer BChl *a* in PMMA and PS films. For reasons given earlier, however, we think that the CSM values for monomer BChl *a* and Chl *a* are too high.

The discrepancies between the $f \cdot \Delta\mu$ values from the two techniques are even more striking for the B850 and B875 bands, Tables I and II. The CSM values are 3-4 times higher. As mentioned, the assumptions made in the analysis of the CSM spectra of these complex bands are questionable. However, the hole-burning values are for the lowest energy (j=0) exciton level, B870 and B896, respectively. With reference to the last sentence of the preceding section, it is possible that the polarizability of this level is smaller than those of the split (by energy disorder) components of the E_1 level which carry

most of the transition dipole strength for absorption from the ground state. However, the square of the transition dipole from the ground state to an exciton level j is only one of many terms, *vide supra*, that enter into the expression for the polarizability tensor. Electronic structure calculations, with and without energy disorder, followed by detailed simulations of the CSM profiles of the B850 and B875 bands appear to be required for a firm understanding of the hole-burning and CSM results. The reader is referred to Somsen et al.[72] for theoretical discussion of the problems associated with applying the conventional CSM analysis procedure to bands contributed to be closely spaced exciton levels.

Acknowledgments

Research at the Ames Laboratory was supported by the Division of Chemical Sciences, Office of Basic Energy Sciences, U.S. Department of Energy. Ames Laboratory is operated for USDOE by Iowa State University under Contract W-7405-Eng-82. Research at the University of Glasgow was supported by BBSRC and EU. Research at Arizona State University was supported by grant DE-FG03-97ER20267 from the Energy Biosciences program of USDOE. We are indebted to Dr. Hartmut Michel for providing samples of the isolated LH2 complex of *Rs. molischianum*, to Drs. Jack Fajer and Marshall Newton of the Brookhaven National Laboratory for providing calculated values for $\Delta\mu_0$ of the seven BChl *a* molecules of the FMO complex, to Professor Shaul Mukamel for providing the results of ref. (72) prior to submission to publication, to Professors Arnold Hoff and Thijs Aartsma for preprints of refs. (54,55), to Professor Bill Parson and Ethan Johnson for providing their calculated $\Delta\mu$-values for the excited states of the LH2 complex of *Rps. acidophila* and to Professor Steve Boxer for providing values of $f \cdot \Delta\mu$ for Chl *a* in PMMA films.

References and Notes

(1) Wu, H.-M.; Rätsep, M.; Jankowiak, R.; Gogdell, R. J.; Small, G. J. *J. Phys. Chem. B* **1998**, in press.

(2) Alden, R. G.; Johnson, E.; Nagarajan, V.; Parson, W. W.; Law, C. J.; Cogdell, R. G. *J. Phys. Chem. B* **1997**, *101*, 4667.

(3) We will refer to the S_1 states as Q_y even when they are an admixture of neutral $\pi\pi^*$ and CT states.

(4) Lockhart, D. J.; Boxer, S. G. *Proc. Natl. Acad. Sci. USA*, **1988**, *85*, 107.

(5) DiMagno, T. J.; Bylina, E. J.; Angerhofer, A.; Youvan, C. D.; Norris, J. R. *Biochemistry* **1990**, *29*, 899.

(6) Middendorf, T. R.; Mazzola, L. T.; Lao, K.; Steffen, M. A.; Boxer, S. G. *Biochim. Biophys. Acta* **1993**, *1143*, 223.

(7) Liptay, W. In *Excited States*, Lim, E. C., Ed. Academic Press: New York, 1974, pp. 129-229.

(8) The Lorentz isotropic local field correction, $f = (\varepsilon + 2)/3$, has been used for photosynthetic complexes with a static dielectric constant ε of about 2.

(9) Renge, I. *J. Phys. Chem.* **1993**, *97*, 6582.

(10) Lyle, P. A.; Kolaczkowski, S. V.; Small, G. J. *J. Phys. Chem.* **1993**, *97*, 6924.

(11) Small, G. J. *Chem. Phys.* **1995**, *197*, 239.

(12) Beekman, L. M. P.; Steffen, M.; van Stokkum, I. H. M.; Olsen, J. D.; Hunter, C. N.; Boxer, S. G.; van Grondelle, R. *J. Phys. Chem. B* **1997**, *101*, 7284.

(13) Beekman, L. M. P.; Frese, R. N.; Fowler, G. J. S.; Picorel, R.; Gogdell, R. J.; van Stokkum, I. H. M.; Hunter, C. N.; van Grondelle, R. *J. Phys. Chem. B* **1997**, *101*, 7293.

(14) Bogner, U.; Schätz, P.; Seel, R.; Maier, M. *Chem. Phys. Lett.* **1983**, *102*, 267.

(15) Meixner, A. J.; Renn, A.; Bucher, S. E; Wild, U. P. *J. Phys. Chem.* **1986**, *90*, 6777.

(16) Kador, L.; Haarer, D.; Personov, R. *J. Chem. Phys.* **1987**, *86*, 5300.

(17) Kador, L.; Jahn, S.; Haarer, D.; Silbey, R. *Phys. Rev. B* **1990**, *41*, 12215.

(18) Meixner, A. J.; Renn, A.; Wild, U. P. *Chem. Phys. Lett.* **1992**, *190*, 75.

(19) Altmann, R. B.; Renge, I.; Kador, L.; Haarer, D. *J. Chem. Phys.* **1992**, *97*, 5316.

(20) Altmann, R. B.; Haarer, D.; Renge, I. *Chem. Phys. Lett.*, **1993**, *216*, 281.

(21) Johnson, L. W.; Murphy, M. D.; Pope, C.; Foresti, M.; Lombardi, J. R. *J. Chem. Phys.* **1987**, *86*, 4335.

(22) Renn, A.; Bucher, S. E.; Meixner, A.J.; Meister, E. C.; Wild, U. P. *J. Luminescence* **1988**, *39*, 181.

(23) De Caro, C; Renn, A.; Wild, U. P.; Johnson L. W. *J. Luminescence* **1991**, *50*, 309.

(24) Orrit, M.; Bernard, J.; Zumbusch, A.; Personov, R. I. *Chem. Phys. Lett.* **1992**, *196*, 595.

(25) Vauthey, E.; Holliday, K.; Wei, C.; Renn, A.; Wild, U. P. *Chem. Phys.* **1993**, *171*, 253.

(26) Vauthey, E.; Voss, J.; de Caro, C.; Renn, A.; Wild, U. P. *Chem. Phys.* **1994**, *184*, 347.

(27) Altmann, R. B.; Kador, L.; Haarer, D. *Chem. Phys.* **1996**, *202*, 167.

(28) Gafert, J.; Friedrich, J.; Vanderkooi, J. M.; Fidy, J. *J. Phys. Chem.* **1995**, *99*, 5223.

(29) Rätsep, M.; Wu, H.-M.; Hayes, J. M.; Small, G. J. *Spectrochim. Acta,* in press.

(30) Gottfried, D. S.; Stocker, J. W.; Boxer, S. G. *Biochim. Biophys. Acta* **1991**, *1059*, 63.

(31) Savikhin, S.; Zhou, W.; Blankenship, R. E.; Struve, W. S. *Biophys. J.* **1994**, *66*, 110.

(32) Köhler, M.; Gafert, J.; Friedrich, J.; Falk, H.; Meyer, J. *J. Chem. Phys.* **1996**, *100*, 8567.

(33) Jackson, J. B.; Goodwin, M. G.; *Biochim. Biophys. Acta* **1993**, *1144*, 199.

(34) Johnson, S. G.; Small, G. J. *J. Phys. Chem.* **1991**, *95*, 471.

(35) Reddy, N. R. S.; Jankowiak, R.; Small, G. J. *J. Phys. Chem.* **1995**, *99*, 16168.

(36) Fenna, R. E.; Matthews, B. W. *Nature* **1975**, *258*, 573.

(37) Li, Y.-F.; Zhou, W.; Blankenship, R. E.; Allen, J. P. *J. Mol. Biol.* **1997**, *271*, 456.

(38) Pearlstein, R. M. *Photosyn. Res.* **1992**, *31*, 213.

(39) Gülen, D. *J. Phys. Chem.* **1996**, *100*, 17683.

(40) Schätz, P.; Maier, M. *J. Chem. Phys.* **1987**, *87*, 809.

(41) Hochstrasser, R. M. *Accounts. Chem. Res.* **1973**, *6*, 263.

(42) In arriving at a value for $f \cdot \Delta\mu_{\perp}$ that part of the theory of ref. (16) which assumes that the variance of $\Delta\mu$ is zero was used. However, in that reference it is shown that the introduction of a Gaussian distribution for $\Delta\mu$ makes only a small difference when F of Eq. (3) is $\lesssim 3.5$.

(43) Wu, H.-M.; Reddy, N. R. S.; Cogdell, R. J.; Muenke, C.; Michel, H. and Small, G. J. *Mol. Cryst. Liq. Cryst.* **1996**, *291*, 163.

(44) Wu, H.-M.; Reddy, N. R. S.; Small. G. J. *J. Phys. Chem. B* **1997**, *101*, 651.

(45) Chapter 4; Wu, H.-M.; Ratsep, M.; Jankowiak, R.; Cogdell, R. J.; Small. G. J. *J. Phys. Chem. B* **1997**, *101*, 7641.

(46) van Mourik, F.; Verwijst, R. R.; Mulder, J. M.; van Grondelle, R. *J. Chem. Phys.* **1994**, *98*, 10307.

(47) The same polarization is observed for *Cb. tepidum*; Melkozernov, A. N.; Olson, J. M.; Blankenship, R. E., to be published.

(48) Chapter 6; Wu, H.-M.; Small. G. J. *J. Phys. Chem. B* **1998**, *102*, 888.

(49) Wu, H.-M.; Small. G. J. *Chem. Phys.* **1997**, *218*, 225.

(50) Chapter 5; Wu, H.-M.; Ratsep, M.; Lee, I.-J.; Cogdell, R. J.; Small, G. J. *J. Phys. Chem. B* **1997**, *101*, 7654

(51) Sauer, K.; Cogdell, R. J.; Prince, S. M.; Freer, A. A.; Isaacs, N. W.; Scheer, H. *Photochem. Photobiol.*, **1996**, *64*, 564.

(52) The double hole structure of the 825 nm band can be understood in terms of energy transfer from two higher energy subunits to the lowest energy subunit.

(53) Buck, D. R.; Savikhin, S.; Struve, W. S. *Biophys. J.* **1997**, *72*, 24.

(54) Louwe, R. J. W.; Vrieze, J.; Aartsma T. J.; Hoff, A. J. *J. Phys. Chem. B*, **1997**, *101*, 11273.

(55) Louwe, R. J. W.; Vrieze, J.; Hoff, A. J.; Aartsma T. J. *J. Phys. Chem. B*, **1997**, *101*, 11280.

(56) Coupling energies of Pearlstein were uniformly reduced by about a factor of 2. It was argued that the energy disorder relative to the excitonic couplings between subunits of the trimer is sufficiently large to cause localization on a single subunit.

(57) Gudowska-Nowak, E.; Newton; M. D.; Fajer, J. *J. Phys. Chem.* **1990**, *94*, 5795.

(58) Fajer, J.; Newton, M., private communication.

(59) Boxer, S. G., private communication.

(60) Krawczyk, S. *Biochim. Biophys. Acta*, **1991**, *1056*, 64.

(61) Renge, I.; Mölder, U.; Koppel, I. *Spectrochim. Acta A* **1985**, *41*, 967.

(62) Altmann, R. B *Diploma Thesis*, Bayreuth University, 1988.

(63) Lockhart, D. J.; Boxer, S. G. *Biochemistry* **1987**, *26*, 664.

(64) The energy disorder calculations of ref. (48) indicate that the Q_y-excitations of the B800 ring are essentially localized on single B800 molecules. The situation for the B850 and B875 rings is different, *vide supra*.

(65) Freer, A.; Prince, S.; Sauer, K.; Papiz, M.; Hawthornthwaite-Lawless, A.; McDermott, G.; Cogdell, R.; Isaacs, N. W. *Structure* **1996**, *4*, 449.

(66) Koepke, J.; Hu, X.; Muenke, C.; Schulten, K.; Michel, H. *Structure*, **1996**, *4*, 581.

(67) That the values of $f \cdot \Delta\mu$ for B870 of *Rps. acidophila* and *Rs. molischianum* are essentially identical establishes that ring size (C_9 vs. C_8) is of little importance. That the values of $f \cdot \Delta\mu$ for B870 of the isolated LH2 complex and WT chromatophores of *Rb. sphaeroides* are so similar suggests that the isolation procedure has, at best, a weak effect on E_{int}.

(68) Here we are free to associate the dimer with the basic α,β polypeptide pair.

(69) Hochstrasser, R. M. *Molecular Aspects of Symmetry,* W. A. Benjamin: New York, 1966.

(70) Parson, W. W.; Johnson, E., private communication.

(71) These findings for localization are valid for weak energy disorder which means that the disorder-induced matrix elements between energetically different exciton levels are comparable to or smaller than the spacings between the levels. Low temperatuare absorption and hole burned spectra are consistent with weak energy disorder.[48]

(72) Somsen, O. J. G.; Chernyak, V.; van Grondelle, R.; Mukamel, S., *J. Phys. Chem. B*, submitted.

(73) This assumption is made even when the S/N ratio of the absorption band is high enough to yield acceptable first and second derivatives.

Table 1. Earlier Stark results for the LH2 complex.

Complex	Band	$f \cdot \Delta\mu_{\|\|}$ (D)[a]	$f \cdot \Delta\mu_{\perp}$ (D)[a]	Band	$f \cdot \Delta\mu_{CSM}$ (D)[b]	$f^2 \cdot Tr(\Delta\underline{\alpha})$ (Å^3)[b]
Rb. sph.	B870	1.10 ± 0.1	1.44 ± 0.1	B850	4.2 (3.3)[c]	619
Rps. acid.	B870	←1.0 ± 0.05→		B850	3.2	1250
Rs. moli.	B870	←1.2 ± 0.1→		B850	3.2	1420
Rb. sph.	B800	1.1 ± 0.2	0.8 ± 0.2	B800	1.1 (0.9)[c]	5

[a] Results from ref. (29).
[b] Results from ref. (13) except for c. which are from ref. (30). CSM ≡ Stark modulation spectroscopy at 77 K. Typical stated uncertainties for $\Delta\mu_{CSM}$ are ± 0.1 D.

Table 2.[a] New Stark-hole burning results and previously published classical Stark modulation results.

Complex	Band	$f\Delta\mu_{\parallel}$ (D)	$f\Delta\mu_{\perp}$ (D)	Band	$f\Delta\mu_{CSM}$ (D)	$f^2Tr(\Delta\alpha)(Å^3)$
Rb. sph., LH1 (mutant)	B896	0.78 ± 0.06		B873	3.5[b]	1800[b]
Rb. sph., chromat.	B896	0.84 ± 0.08		—	—	—
Rb. sph., chromat.	B800	0.8 ± 0.1	0.7 ± 0.1	—	—	—
Rb. sph., LH2	B800	0.9 ± 0.1	0.7 ± 0.1	B800	1.1[c] (0.9[d])	5[c]
Rsp. acid., LH2	B800	0.62 ± 0.06	0.55 ± 0.06	B800	1.5[c]	—
Rs. moli., LH2	B800	1.2 ± 0.2		B800	2.8[c]	290[c]
FMO, *Cb. tepidum*	B825	0.51 ± 0.06	0.72 ± 0.04	B825	1.4[d]	—
				B813	1.9[d]	—
				B805	1.9[d]	—

[a] chromat. ≡ chromatophore, all other complexes in the table are isolated. [b]Ref. (12). [c]Ref. (13). [d]Ref. (30).

Table 3. Summary of previously determined $f \cdot \Delta\mu_{ind}$ values for the $S_1(\pi\pi^*)$ states of relevant molecules isolated in amorphous hosts.

Molecule	Matrix[a]	ε	$f \cdot \Delta\mu_{ind}$ (D)		Ref.
Zn-tetrabenzoporphin	PVB	3.0	0.29		16
tetra-tert-butylphthalocyanine	PVB	2.55	0.27		62
tetraphenylporphin	PS	2.48	0.21		19
	PVB	2.55	0.10		19
	PMMA	2.71	0.15		19
tetrapropylporphycene	PS	2.48	0.18		19
	PVB	2.55	0.15		19
	PMMA	2.71	0.17		19
octaethylporphin	PS	2.5	0.11		17
	PS	2.56	0.10		18
	PVB	3.02	0.17		18
	PMMA	3.45	0.22		18
chlorophyll *a*	PVB	2.55	0.33		20
mesoporphyrin-IX	glass		0.06		28
	protein		0.05	$f \cdot \Delta\mu_0 = 0.15$	
chlorin	PVB	3.0	0.17	$f \cdot \Delta\mu_0 = 0.47$	15

[a] PVB, PS and PMMA denote poly(vinyl butyral), poly(styrene) and poly(methyl methacrylate).

Figure Captions

Figure 1. Stark effect on zero-phonon holes burned into B825 of the BChl *a* antenna complex from *Cb. tepidum*. Left and right frames for burn laser polarization perpendicular and parallel to the Stark field, E_S, respectively.

Figure 2. Dependence of the holewidth and Stark splitting on the zero-phonon holes of B825 of *Cb. tepidum* on electric field for perpendicular (circles) and parallel (diamonds) burn laser polarization. The burn frequencies were 12119 cm^{-1} and 12113 cm^{-1}, respectively. The solid curves are theoretical fits calculated using Eq. (4) with $f \cdot \Delta\mu_{\perp} = 0.72$ D (broadening) and Eq. (2) with $f \cdot \Delta\mu_{||} = 0.42$ D (splitting).

Figure 3. Stark effect on the hole profile of B825 of *Cb. tepidum* for angles (χ) of 0, 30, 60 and 90° between burn laser polarization and electric field of $E_S = 100$ kV/cm.

Figure 4. Stark effect on zero-phonon holes burned into B896 of *Rb. sphaeroides* LH1 only mutant. Burn laser polarization was perpendicular to the Stark field. The spectra were obtained in order from top to bottom, the field strengths $E_S = 0$-100 kV/cm are indicated on figure.

Figure 5. Dependence of the B896 holewidth of *Rb. sphaeroides* on electric field. Upper frame: LH1 only mutant, burn frequency 11169 cm^{-1}, laser polarization is perpendicular to electric field. Lower frame: wild-type chromatophore, burn frequency 11124 cm^{-1}, laser polarization is parallel to electric field. The solid curve is theoretical fit calculated using Eq. (4) with $f \cdot \Delta\mu = 0.78$ D (upper frame) and $f \cdot \Delta\mu = 0.84$ D (lower frame).

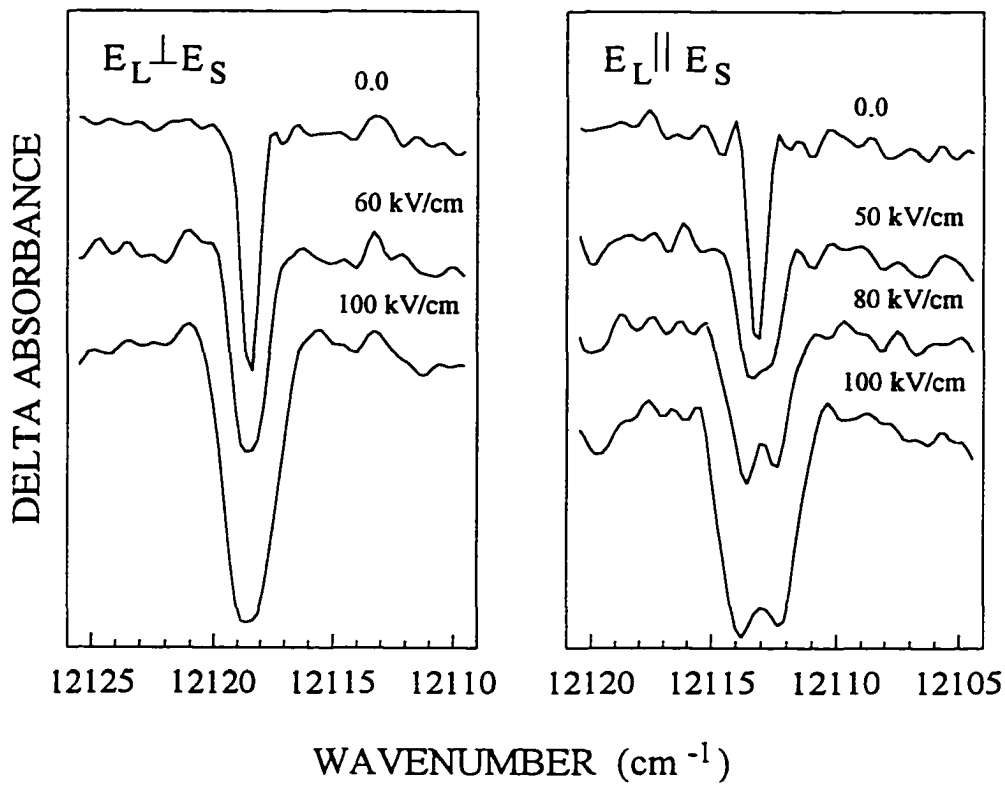
$E_L \perp E_S$
0.0
60 kV/cm
100 kV/cm
$E_L \| E_S$
0.0
50 kV/cm
80 kV/cm
100 kV/cm
DELTA ABSORBANCE
12125 12120 12115 12110
12120 12115 12110 12105
WAVENUMBER (cm^{-1})

Figure 1

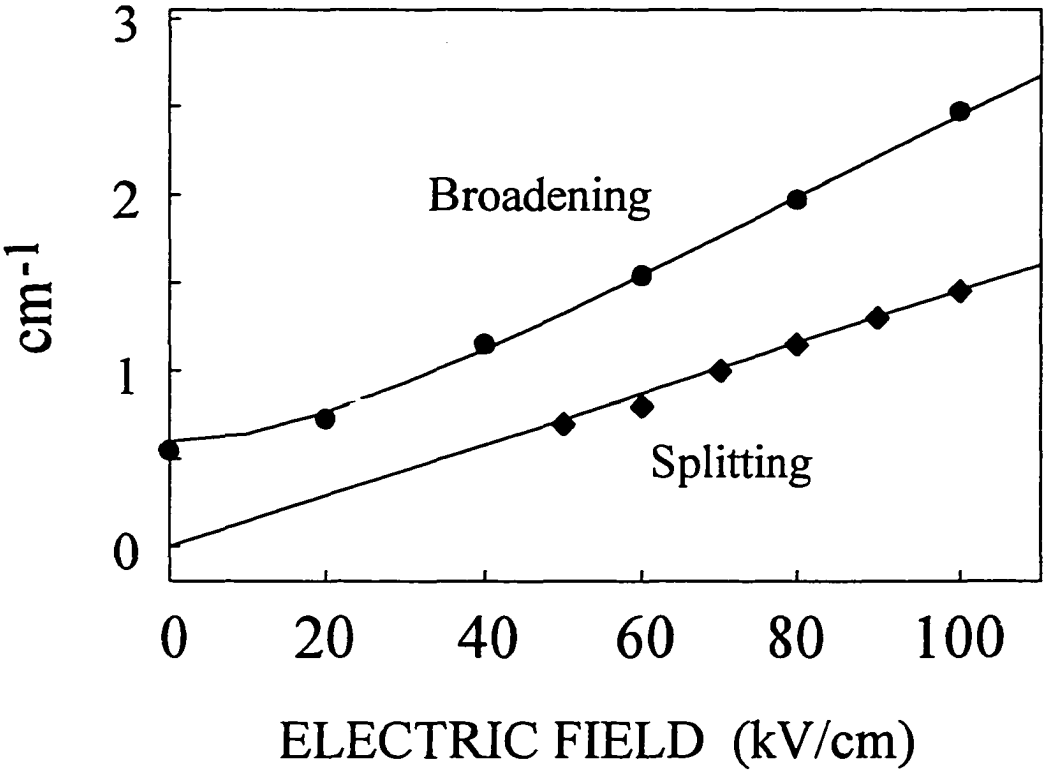
3
2
1
0
cm-1
Broadening
Splitting
0
20
40
60
80
100
ELECTRIC FIELD (kV/cm)

Figure 2

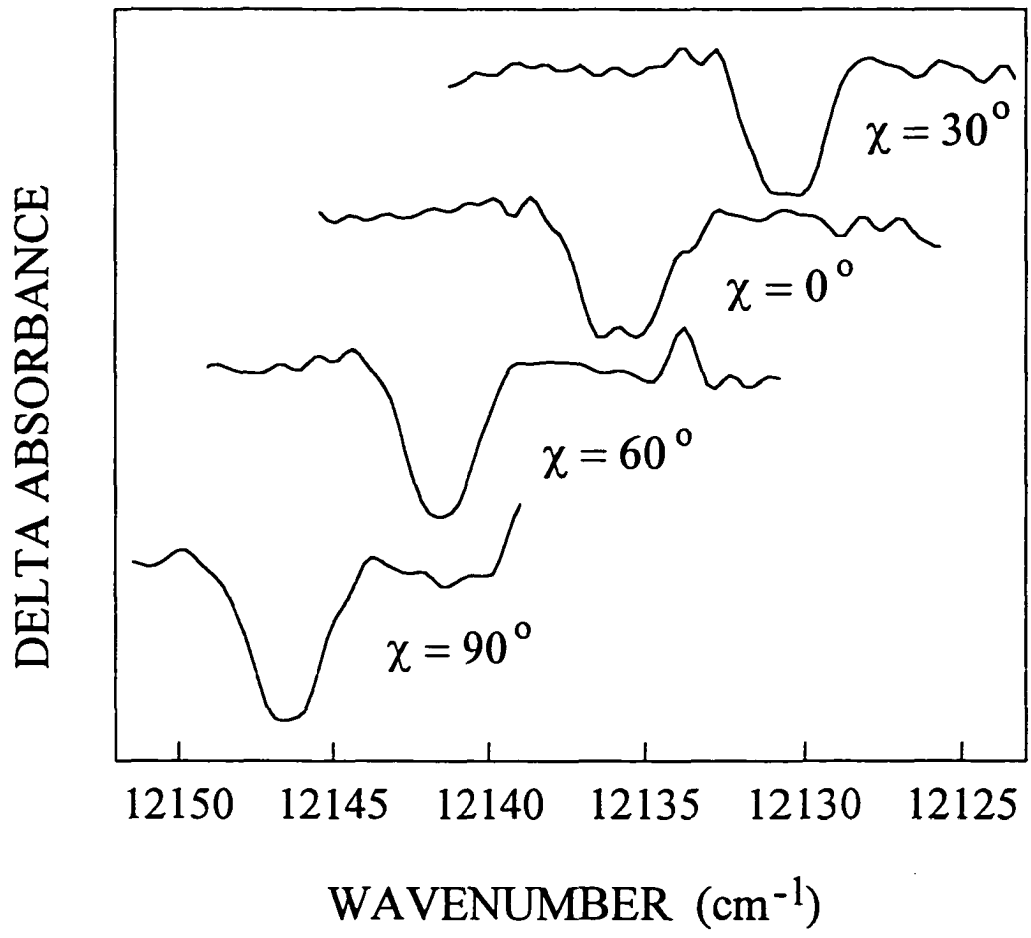
DELTA ABSORBANCE
χ = 30°
χ = 0°
χ = 60°
χ = 90°
12150
12145
12140
12135
12130
12125
WAVENUMBER (cm-1)

Figure 3

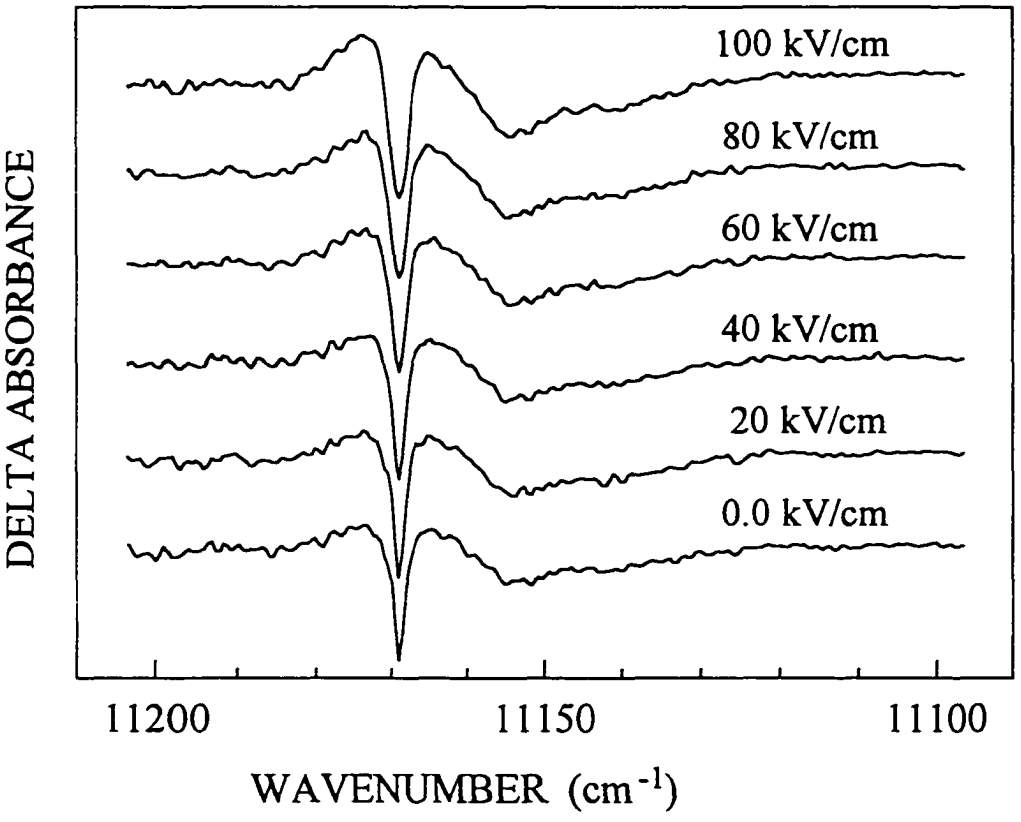
100 kV/cm
80 kV/cm
60 kV/cm
40 kV/cm
20 kV/cm
0.0 kV/cm
DELTA ABSORBANCE
11200
11150
11100
WAVENUMBER (cm-1)

Figure 4

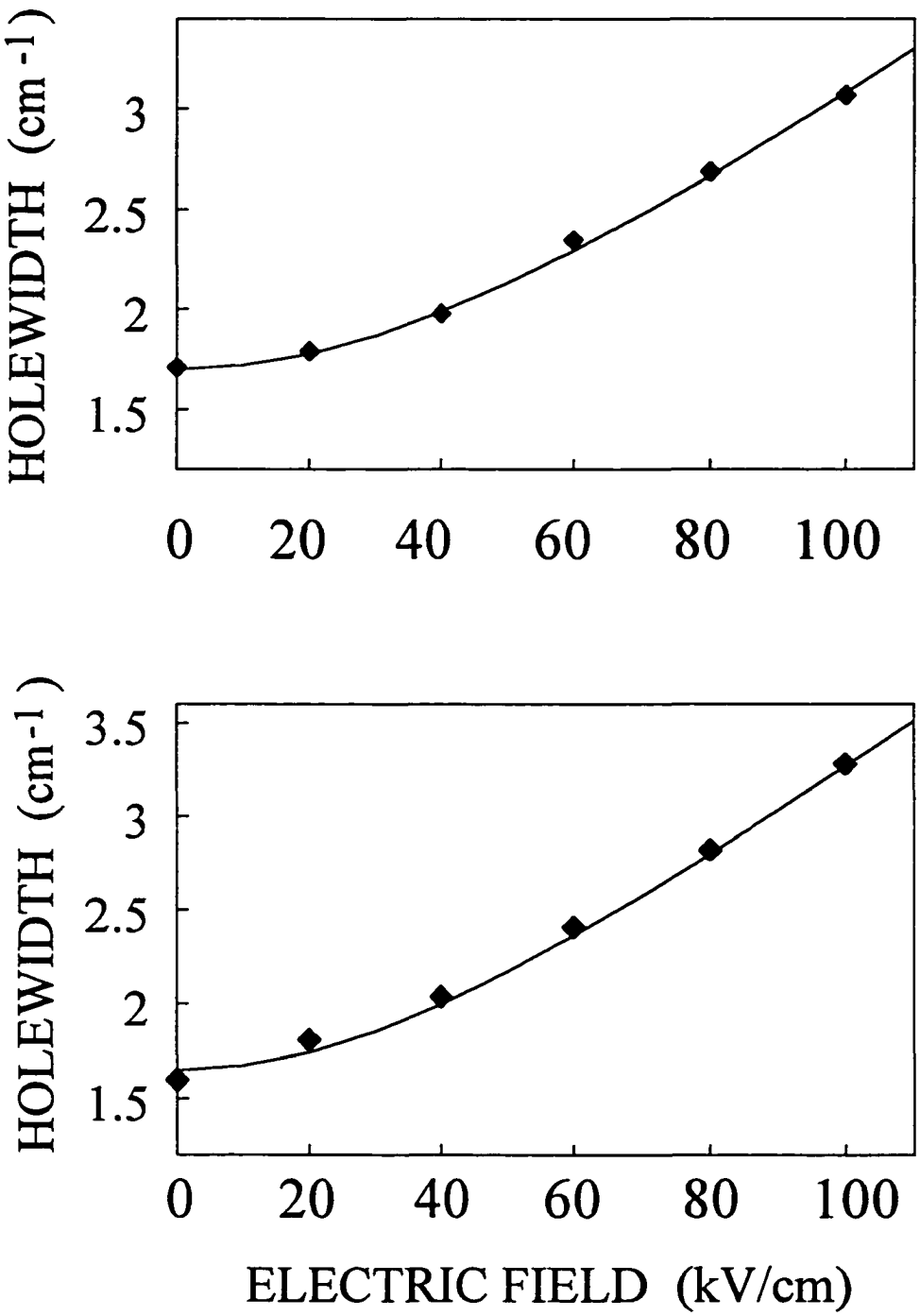
HOLEWIDTH (cm-1)
3
2.5
2
1.5
0
20
40
60
80
100
HOLEWIDTH (cm-1)
3.5
3
2.5
2
1.5
0
20
40
60
80
100
ELECTRIC FIELD (kV/cm)

Figure 5

CHAPTER 8. CONCLUSIONS

The results presented in this dissertation establish that non-photochemical hole burning spectroscopy combined with pressure and external electronic (Stark) fields is an powerful approach for the study of the Q_y-excited state electronic structures and energy transfer/relaxation dynamics of photosynthesis antenna complexes.

The high pressure data for the isolated LH2 complex or chromatophores from *Rps. acidophila* establish that the B800 → B850 energy transfer rate is resilient to significant pressure-induced changes in the B800-B850 energy gap, consistent with data reported earlier for the LH2 complex of *Rb. sphaeroides*. In addition, the energy transfer rate is also weakly dependent on temperature and mutation. All told, the B800-B850 energy gap can be varied between 450 and 1050 cm^{-1} without affecting the ~1 picosecond rate by more than a factor of 3. It was shown that the conventional Förster theory (which assumes the absence of inhomogeneous broadening of the Q_y-transition) based on spectral overlap between the B800 fluorescence origin band and the B850 absorption band is incorrect. The results of our theoretical calculations indicate that the Förster-like B800 → B850 transfer rate involves spectral overlap with weakly allowed BChl *a* modes which build on B850 which, with low frequency protein phonons, provide a quasi-continuum of final states. It is to be emphasized that the calculations involved no adjustable parameters.

Zero-phonon action spectroscopy was used to determine and characterize the lowest energy exciton level (B870) of the B850 ring of LH2 and of the B875 ring (B896) of the LH1 complex. (The results for B896 are not included in this dissertation.) Based on the structure for LH2, it was argued that the exciton level structure of the B850 ring of *Rps. acidophila* cannot be understood without taking into account energy disorder. A new theory based on symmetry-adapted basis defect patterns (BDP) was developed to provide for deeper insight and ease of computation in the study of the effects of disorder (diagonal or off-diagonal) on

cyclic arrays of coupled chlorophylls. The theory was used to explain the 200 cm^{-1} displacements of B870 below the B850 band maximum and B870's absorption intensity which is 3-5% of the total absorption intensity of the B850 ring. (The results are for *Rps. acidophila.*) It was found that in the absence of energy disorder, the average displacement of B870 is ~ 150 cm^{-1} at 4.2 K. The low temperature B850 absorption profile established that the B850 ring is in the weak energy disorder limit.

The BDP-based disorder calculations utilized a value of –320 cm^{-1} for the nearest dimer-dimer coupling, which differs by ~ 120 cm^{-1} from the value (–200 cm^{-1}) calculated using the room temperature X-ray structure of *Rps. acidophila.* The larger value of –320 cm^{-1} for the low temperature calculations was mandated by the T-dependence of the B850 absorption band which reveals that LH2 (isolated or in chromatophores) undergoes a quite subtle and non-denaturing structural change near 150 K. (This is also the case for the LH1 complex.) Theoretical analysis of the thermal broadening of the B850 band led to the conclusion that the nearest neighbor BChl *a* dimer-dimer coupling is about 40% larger for the low temperature structure. Comparison of the T-dependencies of the B850 band of *Rps. acidophila* and *Rb. sphaeroides* (LH2 structure unknown) indicates that the above coupling for the latter is about 20% weaker than for the former at all temperatures. It was suggested that the α, β-polypeptide pairs may be more loosely packed in *Rb. sphaeroides*. This is consistent with the pressure-dependent data obtained for the two LH2 complexes. It is interesting that the temperature dependencies for the B850 band of *Rps. acidophila* and *Rs. molischianum* are very similar since their LH2 complexes are, respectively, 9-mers and 8-mers of α, β-polypeptide pairs and there is only marginal sequence homology between the pairs of the two species. When the structure of the LH2 complex of *Rb. sphaeroides* becomes available, the suggestion that the α, β-pairs are more loosely packed in *Rb. sphaeroides*, which leads to a weakening in nearest neighbor BChl *a*-BChl *a* couplings, can be tested.

New data on the pressure dependencies of the B800 and B850 bands of LH2 and the B875 band of LH1 were reported for several species. In addition, the linear pressure shift rates for the B870 level of the B850 ring and B896 level of the B875 ring were determined. A theoretical model was introduced in order to understand why the linear pressure shifts for the B850 and B875 bands and the B870 and B896 exciton levels are ~ 4 to 6 times larger than the ~ –0.1 cm^{-1}/MPa shift rate of B800, which falls in the range of values observed for isolated chromophores in amorphous solids. The results of calculations with the model indicate that electron-exchange coupling, rather than electrostatic (Coulombic) coupling, between nearest BChl *a* neighbors of the B850 and B875 rings is primarily responsible for their unusually large pressure shifts. This assertion can be tested by electronic structure calculations since reasonable compressibility values are available.

Stark hole burning spectroscopy of bacterial and green algae antenna complexes was reported for the first time. The Stark data yield the dipole moment changes, $f \cdot \Delta\mu$, associated with the optical transitions from the ground electronic to excited Q_y-states. The dipole moment changes of B800 and B870 of LH2, B896 of LH1 and B825 of the FMO complex (*Cb. tepidum*) were determined. The values obtained fall in the range of ~0.5-1.2 D. Several conclusions were drawn. For the sake of brevity I mention only that: one cannot understand the Stark effect of the B850 and B875 rings without taking into account exciton localization effects produced by energy disorder and, therefore, the $f \cdot \Delta\mu$ values determined for B850 and B875 using classical Stark modulation spectroscopy are unreliable; the angle between $\Delta\underline{\mu}$ and the Q_y-transition dipole of BChl *a* in proteins is $\lesssim 15°$; and the protein-induced contribution to $\Delta\underline{\mu}$ is significant.

Understanding the excitation energy and electron transfer processes of photosynthetic complexes is a fascinating, challenging and important problem. A firm understanding of the processes is unattainable without a good understanding of the Chl Q_y-states. The candidate believes that her research has shown that the combination of spectral hole burning with

pressure and Stark fields are important new approaches for yielding data of very considerable importance to quantum chemists working on the excited state electronic structures of photosynthetic complexes.

APPENDIX

SYMMETRY ADAPTED BASIS DEFECT PATTERNS FOR ANALYSIS OF THE EFFECTS OF ENERGY DISORDER ON CYCLIC ARRAYS OF COUPLED CHROMOPHORES

A.1 Cyclic Arrays of Coupled Chromophores

Consider a molecule α in a cyclic (C_n) ring of n (≥ 3) identical chromophores undergoing an electronic transition to the state Ψ_α'. The *localized* wavefunction is given as

$$|\alpha\rangle = \Psi_\alpha' \prod_{\alpha=0(\beta\neq\alpha)}^{n-1} \Psi_\beta, \tag{A.1}$$

where Ψ_β is the ground state wavefunction for molecule β. If the interaction energy ($V_{\alpha\beta}$) between sites α and β is non-zero, the Hamiltonian for this cyclically coupled array in the absence of disorder is

$$H_0 = e\sum_{\alpha}^{n-1}|\alpha\rangle\langle\alpha| + \sum_{\alpha,\beta=0}^{n-1}{}' V_{\alpha\beta}|\alpha\rangle\langle\beta|, \tag{A.2}$$

where e is the excitation energy of the chromophore. The eigenfunctions of H_0 are wave-like and the excitation will no longer be localized at molecule α. The cyclic symmetry determines the delocalized wavefunctions to be [1]

$$|j\rangle = n^{-1/2}\sum_{\alpha} B^{j\alpha^*}|\alpha\rangle, \tag{A.3}$$

where $B = \exp(i2\pi/n)$. The factor of $n^{-1/2}$ holds when neglecting the overlap between chromophores. The quantum number $j = 0, 1, \ldots, (n\text{-}1)$ labels the 1-dimensional irreducible representations (reps) of the C_n group. Except for $j = 0$ and $n/2$ (n is even), each $|j\rangle$ has one degenerate partner, and together they give E-type reps. For example, when $n = 9$, the correspondence between quantum number j and group theoretical designation is j = 0 (A), $j = \{1, 8\}$ (E_1), $j = \{2, 7\}$ (E_2), $j = \{3, 6\}$ (E_3) and $j = \{4, 5\}$ (E_4). Or using another set of quantum numbers, the equivalent correspondence becomes $j = 0$ (A), $j = \{1, -1\}$ (E_1), $j = \{2, -2\}$ (E_2), $j = \{3, -3\}$ (E_3) and $j = \{4, -4\}$ (E_4). When n is even, there are two non-degenerate reps A ($j = 0$) and B ($j = n/2$).

In the nearest neighbor coupling approximation, the exciton energies are

$$E_j = e + 2V\cos(2\pi j/n), \tag{A.4}$$

where V is the nearest neighbor coupling energy.

In the presence of disorder, the total Hamiltonian becomes

$$H = H_0 + H_\lambda + H_\mathrm{v}, \tag{A.5}$$

where H_λ and H_v govern the diagonal and off-diagonal energy disorder, respectively, and are given as

$$H_\lambda = \sum_\alpha \lambda_\alpha |\alpha\rangle\langle\alpha| \tag{A.6}$$

$$H_\mathrm{v} = \sum_\alpha \mathrm{v}_\alpha (|\alpha\rangle\langle\alpha+1| + |\alpha+1\rangle\langle\alpha|). \tag{A.7}$$

To investigate how these two defect Hamiltonians couple with the zero-order delocalization levels it is convenient to express both in terms of the delocalized wavefunctions using

$$|\alpha\rangle = n^{-1/2} \sum_j B^{j\alpha} |j\rangle. \tag{A.8}$$

Eq. (A.6) becomes

$$H_\lambda = n^{-1} \sum_\alpha \sum_j \sum_k \lambda_\alpha B^{\alpha j} B^{\alpha k^*} |j\rangle\langle k|. \tag{A.9}$$

Thus, for H_λ the coupling between delocalized exciton levels r and s, *i.e.* the element in the row r and column s of the Hamiltonian matrix, is

$$\langle r|H_\lambda|s\rangle = n^{-1} \sum_\alpha \sum_j \sum_k \lambda_\alpha B^{\alpha j} B^{\alpha k^*} \delta_{jr} \delta_{ks} = n^{-1} \sum_\alpha \lambda_\alpha B^{\alpha(r-s)} \tag{A.10}$$

Similarly, for H_v we obtain

$$H_\mathrm{v} = n^{-1} \sum_\alpha \sum_j \sum_k \mathrm{v}_\alpha (B^{j\alpha} B^{k(\alpha+1)^*} + B^{j(\alpha+1)} B^{k\alpha^*}) |j\rangle\langle k|, \tag{A.11}$$

$$\langle r|H_\mathrm{v}|s\rangle = n^{-1} \sum_\alpha \mathrm{v}_\alpha B^{(r-s)\alpha} (B^{-s} + B^{r}). \tag{A.12}$$

A.2 Symmetry-Adapted Basis Defect Patterns (BDP)

With Eqs. (A.10) and (A.12), the Hamiltonian matrix can be constructed to calculate exciton level energies and oscillator strengths once the defect pattern λ_α and/or v_α at each chromophore α is determined. To systematically investigate the effects of energy disorder, symmetry adapted basis defect patterns (BDP) are introduced. The BDP transform like the irreducible representations of a C_n group. BDP may seem to have limited applications to real physical systems which exhibit random, rather than correlated, energy disorder. However, the usefulness of BDP will become apparent once one recognizes that any arbitrary defect pattern can be expressed as a superposition of the complete and orthogonal set of BDP, *vide infra*. Thus, one can examine the effects of each BDP on the ring exciton structure to determine which, if any, are of primary importance.

The procedure of generating the complete and orthogonal set of BDP for a C_n group is quite straightforward for those who are familiar with using projection operator technique to obtain π molecular orbitals of benzene or similar cyclic molecules [1, 2]. For brevity, the equations shown in the following are mainly for diagonal energy disorder. The corresponding equations for off-diagonal disorder can be obtained in a similar manner.

A.2.1 BDP for Diagonal Energy Disorder and Their Associated Selection Rules

The diagonal energy disorder at site α can be expressed as

$$\lambda_\alpha(e_{j,\pm}) = N_{j,\pm}\left[\cos\left(\frac{2\pi j\alpha}{n}\right) \pm \cos\left(\frac{2\pi j(\alpha-1)}{n}\right)\right], \tag{A.13}$$

for *e*-type patterns. (To avoid confusing BDP with exciton levels, lower case is used to indicate the symmetry of BDP.) The + and – signs denote the orthogonal partners of each degenerate pattern. $N_{j,\pm}$ is the normalization factor and is given as

$$N_{j,\pm}^{-2} = \sum_\alpha \left[\cos\left(\frac{2\pi j\alpha}{n}\right) \pm \cos\left(\frac{2\pi j(\alpha-1)}{n}\right)\right]^2. \tag{A.14}$$

Now one can define normalized basis defect vectors

$$\boldsymbol{D}_{j,\pm} = N_{j,\pm}(d^{\pm}_{j,0}, d^{\pm}_{j,1}, \ldots, d^{\pm}_{j,n-1}), \tag{A.15}$$

where the d-elements are given by the square-bracketed terms in Eq. (A.13). Figure 3 of Chapter 5 shows the normalized diagonal $e_{1,\pm}$ and $e_{2,\pm}$ BDP. The complete normalized coefficients of BDP for C_9 and C_8 groups are listed in Tables 1 and 2 of Chapter 6. Incorporation of the BDP into Eq. (A.10) leads to

$$\langle r|H_{\lambda}^{e_{j,\pm}}|s\rangle = \frac{\lambda_{j,\pm}N_{j,\pm}}{n}\sum_{\alpha}\left[\cos(\frac{2\pi j\alpha}{n}) \pm \cos(\frac{2\pi j(\alpha-1)}{n})\right]e^{i2\pi\alpha(r-s)/n}, \tag{A.16}$$

for $e_{j,\pm}$ BDP.

Before continuing to show the corresponding expressions for off-diagonal energy disorder, it is worthwhile to discuss first the *selection rule* associated with Eq. (A.16). For the diagonal elements of the coupling Hamiltonian, *i.e.* when $r = s$, we have

$$\begin{aligned}\langle r|H_{\lambda}^{e_{j,\pm}}|r\rangle &\propto \sum_{\alpha}\left[\left(B^{j\alpha} + B^{j\alpha^*}\right) \pm \left(B^{j(\alpha-1)} + B^{j(\alpha-1)^*}\right)\right] \\ &= \left(\frac{1-B^{jn}}{1-B^{j}} + \frac{1-B^{jn^*}}{1-B^{j^*}}\right) \pm \left[B^{-j}\left(\frac{1-B^{jn}}{1-B^{j}}\right) + B^{-j^*}\left(\frac{1-B^{jn^*}}{1-B^{j^*}}\right)\right]\end{aligned} \tag{A.17}$$

for any j. Since $B^{jn} = 1$, Eq. (A.17) equals zero. Furthermore, the off-diagonal elements are

$$\begin{aligned}\langle r|H_{\lambda}^{e_{j,\pm}}|s\rangle &\propto \sum_{\alpha}\left[\left(B^{j\alpha} + B^{j\alpha^*}\right) \pm \left(B^{j(\alpha-1)} + B^{j(\alpha-1)^*}\right)\right]B^{\alpha(r-s)} \\ &\propto \left(\frac{1-B^{(j+r-s)n}}{1-B^{j+r-s}} + \frac{1-B^{(j-r+s)n^*}}{1-B^{(j-r+s)^*}}\right) \\ &\pm \left[B^{-j}\left(\frac{1-B^{(j+r-s)n}}{1-B^{j+r-s}}\right) + B^{-j^*}\left(\frac{1-B^{(j-r+s)n^*}}{1-B^{(j-r+s)^*}}\right)\right]\end{aligned} \tag{A.18}$$

Again, $B^{[j\pm(r-s)]n} = 0$, since j, r and s are all integers. Care needs to be taken, however, when

$$r - s = \pm j, \tag{A.19}$$

which gives us the selection rule associates with Eq. (A.16). When $r - s = j$, the denominators of the second and the fourth terms of Eq. (A.18) are zero, though the

numerators of all four terms vanish. If $r-s=-j$, the first and the third terms have denominators of zero. That means in the presence of $e_{j,\pm}$ BDP exciton levels r and s will couple with each other if the condition $r-s=\pm j$ is met. It is not difficult to show that the above selection rule also applies to the non-degenerate a and b BDP which have non-vanishing coupling elements when

$$r-s=0 \tag{A.20}$$

and

$$r-s=\pm\frac{n}{2}, \tag{A.21}$$

respectively.

A.2.2 The Decomposition of Arbitrary Defect Patterns

Returning to Eq. (A.15), we define a non-singular matrix $\underline{\mathbf{D}}$ whose columns are the transposes of the row vectors defined by Eq. (A.15) plus the normalized BDP column vector associated with the a rep (n odd) or a and b reps (n even). If $\underline{\lambda}=(\lambda_0, \lambda_1,\ldots,\lambda_{n-1})$ is an arbitrarily chosen diagonal energy disorder pattern then

$$\underline{\mathbf{C}}^{\mathrm{T}}=\underline{\mathbf{D}}^{-1}\underline{\lambda}^{\mathrm{T}} \tag{A.22}$$

where $\underline{\mathbf{C}}=(C_0,C_1,\ldots,C_{n-1})$. The components of $\underline{\mathbf{C}}$ are the coefficients of the BDP basis vectors in the superposition that yield $\underline{\lambda}$. The beauty of Eq. (A.22) is that an arbitrary defect pattern can be decomposed into the superposition of BDP, which enables us to systematically investigate the effects of different BDP on the exciton level structure and spectrosopic properties of a C_n ring.

A.2.3 BDP for Off-Diagonal Energy Disorder and Their Associated Selection Rules

Following a procedure similar to that used in deriving Eq. (A.16), one obtains the corresponding expression for off-diagonal energy disorder

$$\langle r|H_{\mathrm{v}}^{e_{j,\pm}}|s\rangle=\frac{\mathrm{v}_{j,\pm}N_{j,\pm}}{n}\sum_{\alpha}\left[\cos\left(\frac{2\pi j\alpha}{n}\right)\pm\cos\left(\frac{2\pi j(\alpha-1)}{n}\right)\right]\times B^{\alpha(r-s)}\left(B^{-s}+B^{r}\right). \tag{A.23}$$

To visualize off-diagonal BDP on a cyclic ring, one can rotate the coefficients for diagonal BDP as shown in Figure 3 of Chapter 5 about the C_n axis by π/n to make them "bond-centered".

The aforementioned decomposition procedure, Eq. (A.22), also applies to patterns involving off-diagonal disorder or patterns involving both diagonal and off-diagonal disorder. The selection rule for diagonal energy disorder, Eq. (A.19), holds for off-diagonal disorder too, once one recognizes that the additional factor $(B^{-s} + B^{r})$ in Eq. (A.23) is independent of site number α and Eq. (A.23) can be simplified to Eq. (A.18). There is one exception, however, when applying the selection rule to b-type off-diagonal disorder. The factor $(B^{-s} + B^{r})$ will be zero when $r = 0$ and $s = n/2$, or *vice versa* (recall the selection rule for b BDP is $r - s = \pm n/2$, Eq. (A.21)). Therefore, the selection rules for b-type off-diagonal disorder are

$$r - s = \pm\frac{n}{2},\ r \neq 0 \text{ and } s \neq 0 \qquad \text{(A.24)}$$

A.2.4 Removal of Exciton Level Degeneracies as Predicted by Group Theory

Before ending this section, it is worthwhile to comment on the removal of exciton level degeneracies by BDP as predicted by group theory. The first order splitting of a degenerate exciton level r is determined by BDP of symmetry contained in the symmetric direct product $(E_r \times E_r)_+$. For a C_9 ring and r = 1-4 the symmetries of the BDP able to remove the degeneracies are e_2, e_4, e_3 and e_1, respectively. While for a C_8 ring and r = 1-3, those are e_2, b and e_2, respectively. However, a second-order mechanism for removal of degeneracy exists because of the off-diagonal coupling defined by Eqs. (A.16) and (A.23), as well as the associated selection rule, Eq. (A.19).

A.3 Application of BDP to Antenna Complexes of Purple Bacteria

Symmetry-adapted Basis defect patterns have been applied successfully to investigate spectroscopic properties of LH2 of C_8 and C_9 symmetry and LH1 of C_{16} from purple bacteria. Examples of using BDP to study the re-distribution of oscillator strengths and exciton level splitting can be found in Ref. [3] and Chapter 5 of this dissertation. The simulation of the B850 absorption band using $e_{1,-}$ and $e_{4,+}$ BDP [3] agreed well with experimental data. Another successful application is the simulation of the lowest exciton level, A, of B850 molecules using $e_{1,+}$ BDP with a half-Gaussian distribution for the disorder parameter λ_0(see Chapter 5). An important conclusion from these BDP studies is that of all BDP e_1 is the essential and necessary component in endowing the very weakly allowed A level with more intensity and while concurrently increasing the gap between A and E_1 levels. This effect is referred to as *hidden correlation* in Chapter 6. Our studies on random defects by expressing them as superpositions of BDP further suppose this point of view. The domination of e_1-type BDP over others gives us confidence for employing BDP to study spectroscopic properties with the convenience of fast and easy computation without losing the essential physics of the systems. More recently, as stimulated by our Stark hole burning results, the localization effects on exciton levels caused by BDP and random defect patterns was examined (see Chapter 6). Comparisons of effects of diagonal, off-diagonal, single-site and random defects on a C_n ring were discussed in Chapter 6.

A.4 REFERENCES

[1] Hochstrasser, R. M. *Molecular Aspects of Symmetry*, W. A. Benjamin, Inc: New York, 1966.

[2] Cotton, F. A. *Chemical Applications of Group Theory*, John Wiley & Sons, Inc., New York, 1971.

[3] Wu, H.-M.; Small, G. J. *Chem. Phys.* **1997**, 218, 225.

IMAGE EVALUATION
TEST TARGET (QA-3)

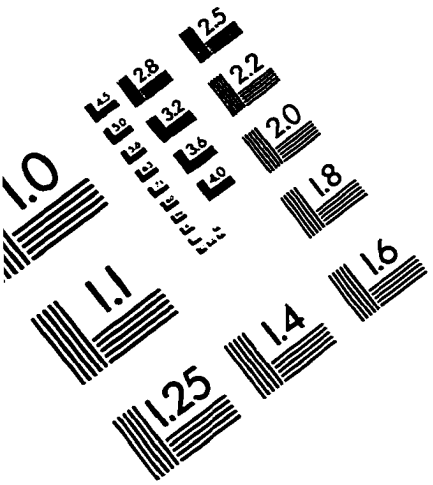

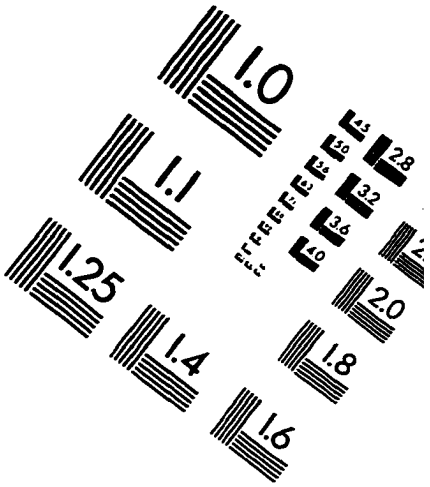

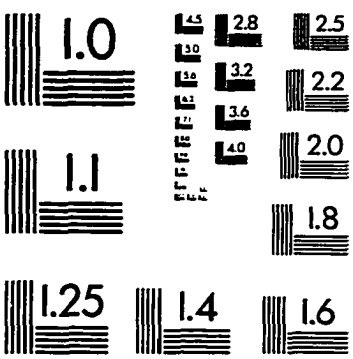

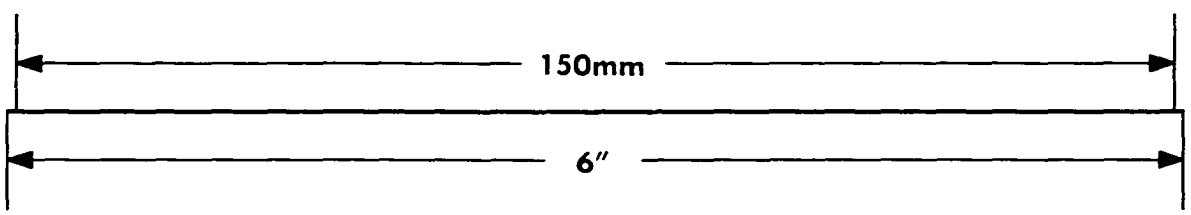

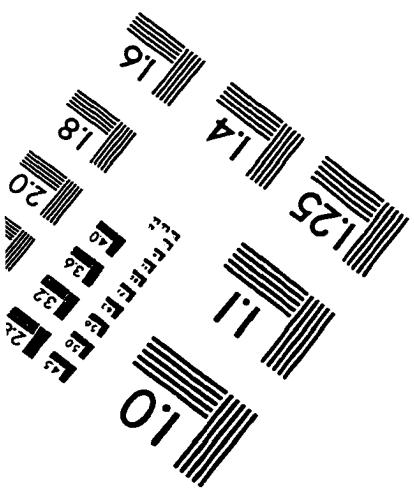

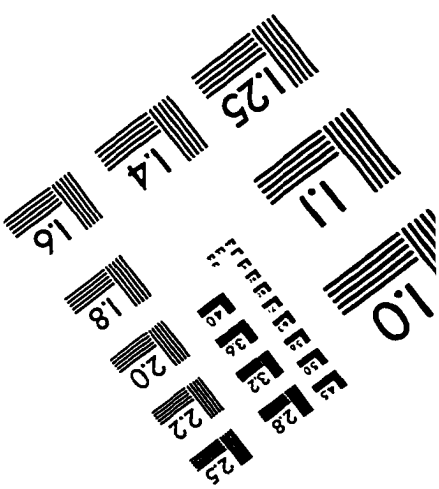

APPLIED IMAGE, Inc
1653 East Main Street
Rochester, NY 14609 USA
Phone: 716/482-0300
Fax: 716/288-5989